Structural analysis of concrete bridge decks: comparison between the Portuguese code (RSA) and the Eurocode road load models

Evaluation of the global and local effects

João Nuno Taborda Brás Robalo

Thesis to obtain the Master of Science Degree in

Civil Engineering

Examination Committee

Chairperson: Professor José Manuel Matos Noronha da Câmara

Supervisors: Professor Francisco Baptista Esteves Virtuoso

Professor Ricardo José de Figueiredo Mendes Vieira

Members of the Committee: Professor António Lopes Batista

Professor José Joaquim Costa Branco de Oliveira Pedro

June 2013

Aos meus pais e avó,
pilares fundamentais nesta
etapa da minha vida.

Acknowledgments

My acknowledgments and recognition to Professor Francisco Virtuoso for all the insight and experience shared regarding the analysis of structures and bridges in particular, which contributed a lot not only for the conception of this project, but also for my personal training as a structural engineer.

I would like to thank Professor Ricardo Vieira for all the support and orientation during this work, as well as for all the patience and dedication in the clarification of my countless questions.

I also want to thank all my teachers the knowledge shared with me during all these academic years.

At last but not least, I would like to thank my family and friends for all the friendship and unconditional support.

Abstract

A change in the Portuguese legislation regarding the definition of traffic loads to consider in bridge design will occur in near future. The current national code (RSA) [3] will be replaced by the Euro Norm EN1991-1-2 [2], which represents in general an increase of the design loads of bridges. The evaluation of the differences between the effects caused by both load codes in two-beam bridge decks (admitted as a slab supported by two rigid longitudinal beams, with two overhangs and one internal panel) was made in a local and global context.

For the local effects two semi-analytical methods were developed and calibrated using finite-element models, in order to evaluate the distributions of transverse moments in the deck slab (over the beams) due to wheel and knife-edge loads acting both on the overhangs and on the internal panel. The results of a finite element analysis considering, only for the RSA loads, a "clamped cantilever model" and ignoring the internal panel were also used in the comparison with the results due to the Eurocode. The transverse moments evaluated at the mid-span of the internal slab due to both load codes by using an analytical solution were also compared.

The longitudinal analysis was performed for bridge models with a different number of spans, deck widths and span lengths, in order to encompass in the analysis a wide range of practical cases; the maximum sagging and hogging bending moments and shear force were obtained by using the respective influence lines. The importance of the traffic live loads in the global analysis of bridges was proven meaningful through a comparison between the effects of these loads and the design loads (including the dead loads).

Several graphs were created by using the results of all these analyses, local and global, in order to provide an efficient and expeditious form of comparison between the effects caused by applying both codes in a wide range of bridges. To evaluate the applicability of those graphs, two real bridges were analyzed by using the semi-analytical methods and the results were then compared with the values extrapolated from the graphs.

Keywords: Bridge decks; Eurocode; RSA; Semi-analytical methods; Slab transverse moments; Global analysis

Resumo

Uma mudança na legislação portuguesa no que toca à definição das sobrecargas em pontes rodoviárias irá ocorrer num futuro próximo. O regulamento nacional ainda em vigor (RSA) [3] irá ser substituído pela Norma Europeia EN 1991-1-2 [2], o que representará um aumento das sobrecargas rodoviárias a considerar no projecto de pontes. A avaliação das diferenças entre os esforços obtidos devido à implementação dos dois regulamentos em modelos de tabuleiros de ponte bi-viga (admitidos como uma laje suportada por duas vigas rígidas, tendo duas partes em consola e um painel interior) foi feita tanto num contexto local como global.

Relativamente aos efeitos locais, dois métodos semi-analíticos foram desenvolvidos e calibrados utilizando modelos de elementos finitos de forma a poder obter as distribuições longitudinais de momentos flectores na direcção transversal da laje do tabuleiro (na zona sobre as vigas) devidos à acção de rodas de veículos e cargas de faca que actuem tanto nas consolas como no painel interior. Os resultados de uma análise em elementos finitos considerando, apenas para as sobrecargas definidas no RSA, um modelo de consola "rigidamente encastrada" e ignorando o painel interior foram também utilizados na comparação com os esforços devidos à implementação do Eurocódigo. Os momentos flectores transversais obtidos a meio vão da laje do painel interior para os dois códigos e utilizando uma solução analítica foram também comparados.

A análise longitudinal foi feita em modelos de pontes com diferente número de vãos, com várias larguras do tabuleiro e para vários comprimentos de vão de forma a englobar na análise um largo domínio de casos práticos; os momentos flectores e esforço transverso máximos foram obtidos através das respectivas linhas de influência. A grande importância das sobrecargas verticais na análise global de pontes rodoviárias foi demonstrada através da comparação entre os seus efeitos e os esforços devidos às cargas totais (incluindo as cargas permanentes).

Uma série de gráficos foi criada utilizando os resultados de todas estas análises, locais e globais, de forma a permitir uma comparação eficiente e expedita entre os esforços obtidos devido à aplicação dos dois regulamentos a um domínio abrangente de pontes reais. Para avaliar a aplicabilidade deste processo foram analisados dois casos específicos de pontes reais utilizando os métodos semi-analíticos, sendo os resultados então comparados com os valores extrapolados a partir dos gráficos obtidos anteriormente.

Palavras-chave: Tabuleiros de pontes; Eurocódigo; RSA; Métodos semi-analíticos; Momentos transversais de laje; Análise global

Contents

List of Figures

CHAPTER 1

1. Introduction

In the course of time, engineering sciences have evolved side by side with the knowledge and experience of the civil and structural engineers. The methods of design for the analysis of structures became more accurate, being the behavior of the constructions more easily predicted.

On the other hand, with the development of the interconnected societies and globalization, the moving of persons and needs between distant points increased, which means a need of constant improvement of the communication routes as a result of the increase of the traffic verified there. Hence, the transport infrastructures, e.g. road bridges, need to be designed in order to safely support the expected traffic loads. This fact is considered through the creation of updated regulations about the design of bridges under the action of these loads.

Approaching now the motivations and objectives of this work, it is interesting to mention O'Connor, 2000 [1]: "The steps leading to the introduction of new design loads and other major changes in codes of practice must include a comparison with older codes and some study of the performance and strength of existing structures."

The forthcoming of the implementation in Portugal of the European Norms for the design of structures (Eurocodes) [2] motivated a comparison, in a local and global context, between the effects of the current Portuguese load regulation (RSA - *Regulamento de Segurança e Acções para Estruturas de Edifícios e Pontes*) [3] and the effects of these Eurocodes regarding the traffic loads in road bridges. Thus, it was possible to do an evaluation of bridges already built in Portugal under the current regulation that will have to support the loads defined by these new European Norms. However, this comparison approached only the road bridges and taking into account only the road vertical loads.

In order to evaluate the local effects, the transverse bending moments in the deck slab were analyzed using semi-analytical methods which were calibrated based on the most important characteristics of the bridge decks. To obtain the transverse moments in the internal slab, another mathematical solution was used. For the analysis of the global effects, the influence lines of several bridge types were used to obtain the maximum bending moments and shear forces, due to both load codes [2] and [3].

Thus, in Chapter 2 is presented a brief historical review focused on the evolution of these regulations, both at national and international level, from the nineteenth century until nowadays, presenting an explanation regarding their development over time.

In Portugal, 2014 is expected to be the year when the Eurocodes become legislation, replacing the current regulations, RSA and REBAP (*Regulamento de Estruturas de Betão Armado e Pré-Esforçado*). Regarding the road bridges already built under the specifications of the RSA (regulation related to the traffic loads), this may mean that even well designed before, they can be insecure in 2014 since the Eurocode prescribes more and higher loads. The description of these two load codes, the RSA [3] and the EN 1991-2 [2], is also presented in Chapter 2. As referred above, a local and global comparative analysis of several bridge decks was made, under the action of the loads presented on both codes.

In order to simplify this analysis, the research for this work is focused on simplified methods for the analysis of bridge decks. Thus, the literature reviewed and related to these methods is presented in the third point of Chapter 2.

Focusing on the local analysis, the transverse moments in the deck slab were studied. The analysis of these moments due to uniformly distributed loads can be easily done by using a simple "beam model" with unit width. However, the analysis of these moments due to knife-edge or wheel loads is not that simple, being normally done with specific software using a finite element analysis. On the other hand, since this work encompasses the study of several load cases and bridge dimensions, it was found interesting, as referred before, the use of quicker and simpler methods. Thus, two semi-analytical methods were developed in Chapter 3 to calculate the distribution of these moments over the beams, caused by both cantilever and internal panel concentrated loads. These simplified methods were based on the ones described in the literature review of Chapter 2, and their applicability to knife-edge loads is also presented. The calibration of these methods was done after a careful study of the influence that several characteristics of the bridge deck have in these distributions of moments, neglecting the ones with irrelevant importance, and therefore simplifying the methods. Still on Chapter 3, a Timoshenko's solution [4] described also in the literature review is admitted and tested as another simplified method, but now for the calculation of the maximum transverse moments in the internal slab, verified in the mid-span and under the wheel loads.

In Chapter 4, using these simplified methods, several generic bridge decks were analyzed in order to compare the maximum transverse bending moments obtained, over the beams and at the mid span of the internal slab, due to the action of the RSA and the Eurocode. In order to represent this comparative analysis two charts were built for bridges with and without edge-stiffening (presence of structural jersey barriers in the overhangs), representing the relation between the moments due to the RSA and the ones due to the Eurocode in function of the deck width. Two other similar charts were produced, but now, in what concerns to RSA loads, were used the moments obtained in the supported end of the overhangs using a "clamped cantilever model", ignoring the flexibility of the internal panel. This was found with practical interest, since generally the design of this part of the deck is made considering this type of structural model, considering the overhang's supported end with infinite rotational restraint.

Finishing the chapter it is presented a last chart, representing the relation between the moments obtained in the mid-span of the internal slab due to both load codes, using Timoshenko's solution [4], in function of the internal span *S*.

The longitudinal analysis of several generic bridges with different deck widths, span lengths and number of spans is presented in Chapter 5. Several charts were defined representing the relation between the effects caused by the RSA [3] and by the Eurocode Load Model 1 [2]. These charts approach the sagging and hogging bending moments and shear force envelopes in function of the main span length. The analysis of these internal forces was performed using the respective influence lines and considering the lateral distribution of loads, focusing on the most loaded beam. The influence of the live loads (both RSA and Eurocode LM1) in the global analysis, in function of the central span length *L* is also presented in Chapter 5.

Finally, in Chapter 6 the results of the analysis of two real bridges are compared with the ones extrapolated from the charts of Chapter 4 and 5. For these two bridges the semi-analytical methods developed in Chapter 3 and Timoshenko's solution [4] were used to calculate the transverse moments in the deck slab. The respective influence lines were used to obtain the bending moments and shear force envelopes in the most loaded beam. In this way, by comparing these results with the ones obtained from the charts, the applicability of these to a wide range of bridges was evaluated when the purpose is a quick and approximated analysis of the differences between the effects caused by both load codes in study.

CHAPTER 2

2. Live Loads in Road Bridges – Literature Review

2.1 Historical Review of Bridge Codes

2.1.1 - Design philosophies of the codes and their international development

The design philosophies in which the bridge codes were based have been changing with the time, following the development of the structural and civil engineering and of the society itself, being the result an increase of the design traffic. This increase is generally considered in the evaluation of the traffic loads by a growth factor, as referred in [5], which predicts the traffic evolution for the respective design period.

The bridge design codes of the nineteenth century, by admitting the use of elastic linear models of structural analysis, adopted a verification of safety by considering upper bound estimates of the working loads. In addition, they used a *factor of safety* (Allowable Stress Design) which depends on the material, applied to its yield and ultimate stresses in order to create a safety margin in the material resistance. For example, some British codes used a uniformly distributed load together with an axle load which had been proposed by Jenkins in 1875, or the same but with a four-wheeled vehicle instead of the axle load, suggested by Unwin in the beginning of the twentieth century, as referred in [1].

Based on the evolution of the knowledge about the materials properties, the reduction imposed on these stresses by the *factor of safety* became smaller over the years. However, it's interesting to observe that bridge codes from the beginning of the twentieth Century had allowable stresses that varied with the nature of the loading, depending on the relation between the live loads and the dead loads [1]. The value of the *factor of safety* applied to the live loads took also into account effects like impact, fatigue and variability of the live load.

Back in the 40's, the using of plastic methods of structural analysis began when the emphasis changed from behavior at service loads to the ultimate limit state, giving the engineer the choice about how he wanted to design the structure, between the working loads model or this new collapse philosophy.

Then, in 1971 O'Connor [1] questioned the reasonableness of having to choose between these two philosophies, since for him the right way to design included the separated analysis at both working and ultimate loads, each of it with its own objectives. Thus, although some probabilistic concepts were already used in some regulations, with this thought emerged the possibility of using statistical methods of design with the emphasis on probability of failure, which have been used in the most recent bridge codes. According to O'Connor [1], the first edition of the *Ontario Highway Bridge Design Code* (1979) [6] was a pioneer in the use of this last concept for bridge design (Limit States Design), and influenced the development of many other codes in other countries. A particular feature of this code was the relation between the design loads and the legal limits of geometries and weights applied to trucks in Ontario, affecting also the traffic from other places which passed in Ontario roads. So, this method had two basic characteristics: it tried to consider all possible limit states and it was based on probabilistic methods. According to O'Connor [1], the simplest way to describe this method is considering two parameters: the load effect on some component of the structure and the resistance of that same component, and admitting that these two parameters are submitted to statistical variation. Thus, when the load effect exceeds the resistance, the component fails, and the engineer has to improve it in order to verify the structural safety.

The form and geometry of the live loads used in bridge design, represented generally by a uniformly distributed load and one or more major axle groups, as well as their origins, have been similar over the years. This means that new design codes are an improvement and calibration of the previous ones, essentially when there isn't a change of philosophy, which seems to have a trend towards the increase of the loads values over the years in most countries. Thus, the uniformly distributed load represents a sequence of lighter vehicles, and the concentrated loads represent the axle groups (heavy vehicles) that are important to model local effects in the deck slab. The calibration of these axle groups can be done with procedures leading directly from traffic surveys to a particular geometry, value and distribution of the loads, as explained by O'Connor in [1].

2.1.2 - Evolution of the Portuguese regulations

In Portugal, by the end of the nineteenth century, more specifically in 1897, a regulation for safety requirements already existed (*Regulamento para projectos, provas e vigilância das pontes metálicas*) as referred in [7], which supported the design and construction of steel bridges. As mentioned by Pipa [8], this regulation was updated in 1929 (*Regulamento de Pontes Metálicas*) with special attention on the railway and road traffic loads, and also later in 1958 by a Commission of the CSOP (*Conselho Superior de Obras Públicas*) which focused essentially on the definition of loads in road bridges, taking into account their transnational compatibilization.

In what concerns the concrete bridges, the regulation of 1935 (*Regulamento de Betão Armado*) included general rules about concrete buildings and bridges, including the definition of the loads used. Later in 1960, some modifications were made to reconcile the loads used in the design of concrete bridges with the ones introduced by the regulation for steel bridges (RPM) in 1958. In 1961 a single document was issued with all the considerations to take into account in the design of buildings and bridges. In this regulation (*Regulamento de*

Solicitações em Edifícios e Pontes) the probabilistic concepts were already introduced, being based on previous works made in LNEC (*Laboratório Nacional de Engenharia Civil*) [8].

The most recent Portuguese regulation (*Regulamento de Segurança e Acções para Estruturas de Edifícios e Pontes – RSA)* [3], which is still in use, was published in 1983 updating the previous one by an adjustment with the modern international trends of that time, following also the orientations of CEB (*Comité Européen du Betón*) [8].

2.2 Description of the codes in study

2.2.1 - The Portuguese code: *RSA*

The Portuguese regulation for the design of structures still in use was issued, as mentioned above, in 1983 and following the CEB trends and developments, corresponds to an approximation of the Portuguese regulation to the codes of other countries. It is an essential document that together with the REBAP (*Regulamento de Estruturas de Betão Armado e Pré-esforçado*) has established the rules for the safety verifications in structures, defining the loads to consider in a safety check procedure.

The RSA [3], in what concerns the road bridges, presents in the Chapter IX of its second part five types of loads, being their definition presented in five different articles:

- The article 41 states that one should consider the separate action of two different types of vertical traffic loads, whose values depend on the bridge class. The first (RSA-a) is a vehicle of three equidistant axles of two wheels each. The distance between axles is 1.5 m and between the two wheels of each axle is 2 m, being the load corresponding to each axle equal to 200 kN for bridges considered as Class I and equal to 100 kN for bridges of Class II. An illustration of the vehicle can be observed in Figure 2.1.

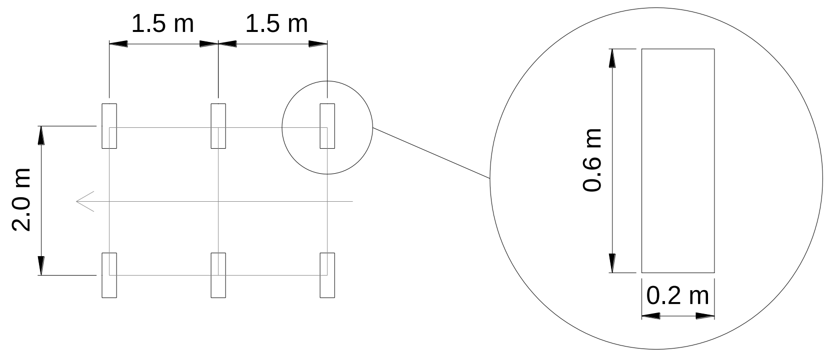

Figure 2.1 – Scheme of the RSA-a vehicle

The second type (RSA-b) is a uniformly distributed load q_1, together with a 'knife-edge' load q_2, uniformly distributed in the width of the carriageway. These traffic loads should be placed in the most unfavorable longitudinal and transverse location, and in the particular case of the vehicle, if we are dealing with a two way bridge, it should be placed in the both roadways if each of it has two or more traffic lanes. These loads depend on the bridge class, and the ones considered as Class I are expected to have intense and heavy traffic, being associated to the national and certain urban roads (q_1 = 4 kN/m^2 and q_2 = 50 kN/m), and the ones considered as Class II should support lighter traffic, like the major of the agricultural and forest roads (q_1 = 3 kN/m^2 and q_2 = 30 kN/m).

- The forty-second article refers to the centrifugal forces created in the curved bridges, taken into account as horizontal equivalent forces acting in the direction perpendicular to the bridge axis. These forces are applied at the pavement level to the vehicle and are obtained reducing the corresponding vertical loads by a coefficient β that depends on the maximum design speed for the respective curve (expressed in kilometers per hour), and multiplying them by another coefficient α dependent also on the maximum design speed and on the radius of curvature of the respective curve.
- The braking forces are represented in the article 43 as longitudinal 'knife-edge' loads, acting in parallel to the bridge axis and distributed in the width of the carriageway. Their values depend also on the class of the bridge.
- The article 44 indicates the actions on sidewalks, safety railings and curbs. For the first ones the engineer chooses the most unfavorable between a concentrated and a uniformly distributed load. About the actions on the safety railings of the bridge, the code recommend an horizontally distributed 'knife-edge' load at their superior level, and in the curbs we should just consider a concentrated horizontal load in the most unfavorable point.
- The last article (45) refers to the action of the wind on the vehicles.

This work focus only on article 41, which defines the vertical traffic loads on road bridges.

2.2.2 - The Eurocode: *EN 1991 – Part 2*

In 1975, the European Community decided to act in the field of construction, focusing on the elimination of technical obstacles between the Member States and on the harmonization of the technical features of their engineering regulations. Therefore, for fifteen years the responsible commission conducted the scientific development of the Eurocode program towards the establishment of a set of rules for the design of structures. The European Commission for Standardization compiled a set of rules into a final document consisting in ten parts, each of it concerning different parts of the design of structures, called European Standards (EN). The European Standard studied in this thesis is the EN 1991-2: *Traffic Loads on Bridges* [2], more specifically the Section 4, which deals with the definition of actions on road bridges. Thus, a brief description of this section is presented hereafter.

The Section 4 of the EN 1991-2 starts to present the surface of the deck divided into two different parts: the carriageway and the footways and cycle tracks (these last ones have their associated loads defined mostly in Section 5 of the same European Standard). The carriageway is divided into notional lanes and a remaining area, having a width dependent on the total width of the carriageway, as it can be seen in the Table 4.1 of Section 4 [2]. If the bridge is physically split into two independent decks (supported on independent piers) each deck has to be treated as a different carriageway. These notional lanes have to be numbered so that the effects of the traffic loads are the most unfavorable for the bridge deck, given that the lane which provides the most adverse effect is numbered Lane Number 1, the one giving the second most unfavorable effect is the Lane Number 2, and so on, as can be observed in Figure 2.1.

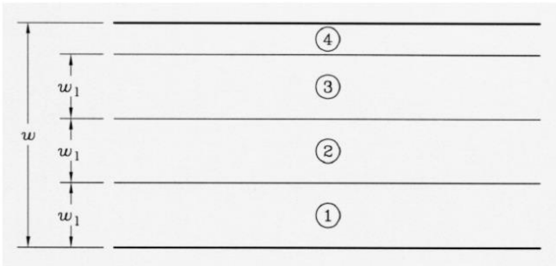

Key
w Carriageway width
w_1 Notional lane width
1 Notional Lane Nr. 1
2 Notional Lane Nr. 2
3 Notional Lane Nr. 3
4 Remaining area

Figure 2.2 - Example of the Lane Numbering taken from [2]

Hence, the loads should be applied on each notional lane and remaining area on such a length and longitudinally located in order to get the most unfavorable effect.

When relevant, the vertical load models, the horizontal forces and the pedestrian and cycle loads should be combined as shown in the Tables 4.4a and 4.4b of the EN [2], defining this way different groups of loads that should be considered as a characteristic (Table 4.4a) or frequent (Table 4.4b) action for combination with non-traffic loads. Note that the frequent value may be useful for the verification of some serviceability conditions, essentially in concrete structural elements.

The vertical loads that represent the road traffic effects associated with the limit state verifications are defined by four different load models (LM1 to LM4):

- The Load Model 1 (LM1) is generally the most demanding and consists of uniformly distributed loads together with four-wheeled vehicle loads represented by tandem-systems. This load model simulates most of the traffic of cars and lorries with appropriate reliability, being used for general and local effects. The referred tandem-systems have two axles separated by a distance of 1.2 m, being the distance between their two wheels of 2 m, and the contact surface of each wheel is a square of side 0.4 m. It is also important to mention that for local verifications half of the axle load is transmitted to each wheel and the tandem-systems should be applied at the most unfavorable location. Two tandem-systems in two adjacent notional lanes should be located as near as possible, but with a minimum distance between the longitudinal axis of the wheels stipulated on 0.5 m. For global effects, if the span length is bigger than 10 m, each tandem-system may be replaced in each lane by a pair of concentrated loads (one axle) with the same weight of the corresponding double-axle tandem-system. The values of these loads are obtained from the Table 4.2 of this EN, being the values of the adjustment factors given in the National Annex and selected depending on the expected traffic and on the different classes of roads (see (3) of point 4.3.2 of the present EN [2]). It should be referred that this is the only Load Model considered in the comparative analysis approached in this dissertation. This load model is illustrated in the example of Figure 2.3.

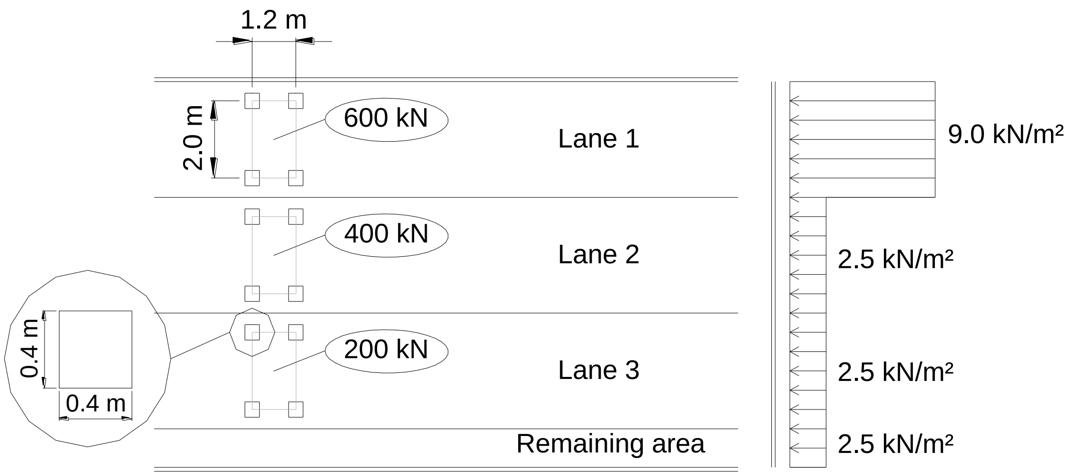

Figure 2.3 - Distribution of loads in an example of application of the Eurocode Load Model 1

- The Load Model 2 (LM2) is important essentially for the verification of short structural members not covered by the LM1. This model is represented by a single axle with the correspondent wheels separated by a 2m distance, having contact surfaces with dimensions 35 x 60 [cm^2]. The axle load is 400 kN, dynamic amplification included, and when relevant, only one wheel of 200 kN may be used. However, these load values are multiplied by a factor β_Q which represents the respective class of route [2].
- The third and fourth load models (LM3 and LM4) are usually adopted only when required by the client for a specific project. The LM3 stipulates that, when relevant, models of special vehicles should be defined by the respective National Annex and taken into account. The LM4 represents the crowd loading by a uniformly distributed load of 5.0 kN/m^2, only relevant in urban bridges and intended for general verification. It should be associated only with a transient design situation.

The horizontal loads to consider represent the braking and acceleration forces that shall be taken as longitudinal forces acting at the surface level of the carriageway. The corresponding characteristic values are calculated as a fraction of the total maximum vertical loads associated with the LM1 and acting on Lane Number 1, and depend on the length of the deck (or the part of it under consideration) and on the width of the Lane Number 1. These braking and acceleration forces, applied in opposite directions separately, are also limited to 900 kN, and should be located along the axis of any lane. However, the code refers that if the eccentricity effects are not significant, like in carriageways with small width, the force can be applied only along the axis of the carriageway. In what concerns the centrifugal force, its value depends on the total maximum weight of the tandem-systems defined in the LM1 and also on the horizontal radius of the carriageway centerline, if its value lies between 200m and 1500m. The formulas to obtain these values were derived for the normal speed of heavy vehicles, because individual cars don't create significant centrifugal effects. The direction of this force should be taken as normal to the axis of the bridge, acting at the finished carriageway level.

Finally, the Load Model for cycle tracks and footways in road bridges is represented by a uniformly distributed load and a concentrated load acting on a square surface with sides of 10cm. If the local and general verifications are distinguished, the concentrated load should be ignored for the general effects. The values of these loads are generally defined in the National Annex, but the EN provides recommended values that should be considered.

2.3 Literature Review: Simplified methods for the analysis of bridge decks

The bridge decks considered in this work are composed by a concrete slab supported by two longitudinal beams, having two overhangs and one internal panel. Two semi-analytical methods for the transverse analysis of the deck slab submitted to concentrated loads were developed, in order to allow an efficient procedure of the internal forces' evaluation within the scope of this thesis.

Hence, in the sequel, a brief review of the literature regarding simplified analytical and semi-analytical methods for the evaluation of transverse bending moments is presented.

The transverse moments in the bridge deck slabs evaluated in this work are due to three types of traffic loads: uniformly distributed loads, knife-edge loads and wheel loads.

The analysis of these bending moments due to uniformly distributed loads on the cantilever slab is relatively simple using a beam-model with a unit width. When acting on the internal panel this type of loads does not create any transverse moments in the part of the slab located over the beams provided that the torsional rigidity of the longitudinal beams is neglected.

On the other hand, the analysis of the effects caused by wheel or knife-edge loads cannot be performed in such a simple way due to the local structural behavior of the slab since its flexure is not cylindrical.

Thus, a research work was made in order to find simplified methods for the evaluation of transverse bending moments over the beams due to concentrated loads. A simplified formula to obtain the longitudinal distribution of transverse moments along the clamped end of the cantilever slab, with uniform thickness, due to a concentrated load was given in [9]:

$$m_y = -\frac{P}{\pi}\frac{1}{1+\left(\frac{x}{c}\right)^2} \tag{2.1}$$

where "c" represents the distance of the load from the clamped end, as can be observed in Figure 2.2.

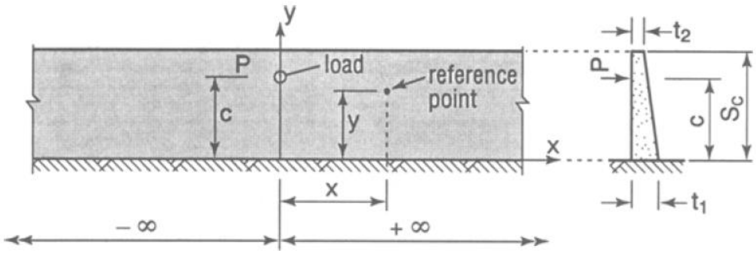

Figure 2.4 - Nomenclature used for cantilever slabs, taken from [10]

However, this method neglects the dimension of the cantilever span (S_c) and the position of the load in relation to the cantilever span length (c/S_c). Thus, it can be concluded that the results obtained are unrealistic estimates of the flexural moments along the cantilever support.

Timoshenko also presented in 1959 [4] a simplified solution using a sinusoidal function to obtain the flexural moments along the clamped end of a wide cantilever acted by a concentrated load.

$$m_y = -\frac{P}{\pi}\,cos^2(\varphi) \tag{2.2}$$

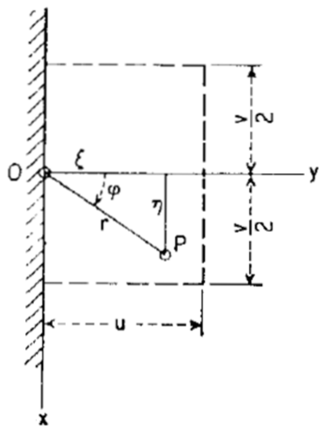

Figure 2.5 - Nomenclature for the analysis of cantilever slabs by Timoshenko, taken from [4], with the axis x and y changed from the original

This solution provides the value of m_y in the point O for any position of the load, which is considered through the angle φ. To obtain the longitudinal distribution of m_y in x this angle φ can be used in the same way, but now admitting a moving point O in the x-axis and the y-axis in the same x-coordinate of the load. However, also in this solution the size of the cantilever is not considered, leading to the same problem of the solution presented in [9] (Eq. (2.1)).

Sawko and Mills proposed in 1971 [11] a similar solution to the one given in [9] for cantilevers with constant thickness, but taking into account the cantilever span through the introduction of a coefficient A', which values depend on the ratio c/S_c as follows:

$$m_y = \frac{PA'}{\pi} \frac{1}{\cosh\left(\frac{A'x}{c}\right)} \tag{2.3}$$

The Equation (2.3) satisfies the essential equilibrium condition: the area under the distribution curve of transverse moments along the clamped end is equal to P x c, or by another words, the integration of this equation for the infinite domain results on the statically equivalent bending moment of a cantilever beam.

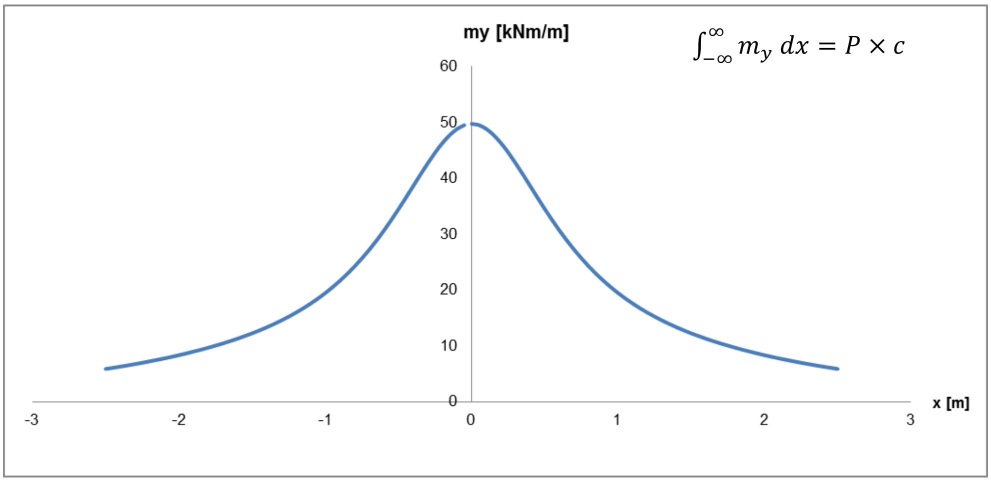

Figure 2.6 - Example of a distribution curve of transverse moments along the longitudinal direction due to a concentrated load acting on the cantilever slab

On the other hand, two other conditions more related to the form of the distribution curves are also satisfied: for a given load position, m_y has the maximum value for x = 0 and m_y tends to zero as *x* tends to infinite.

The values of A' were obtained by Sawko and Mills [11] from the peak values of the distributions of transverse moments given by Jaramillo (1950) and confirmed using a finite element analysis:

$$A' = \pi \frac{(m_y{}^{Jaramillo})_{x=0}}{P} \tag{2.4}$$

Bakht and Holland extended this solution in 1976 [12] to cantilevers with linearly varying thickness, an important feature of bridge deck's overhangs. The equation used is the same (2.3) and the method to obtain the values for A' is similar, but now using the peak values of the transverse moments obtained from the influence surfaces of Homberg and Ropers (1965), since they considered also the thickness variation in the cantilever slabs. The charts providing the value of the coefficient A' for different load positions and thickness variations in the cantilever slab and which were adapted for practical use in the *Ontario Highway Bridge Design Code* (1983) [6] can be observed in Figure 2.7.

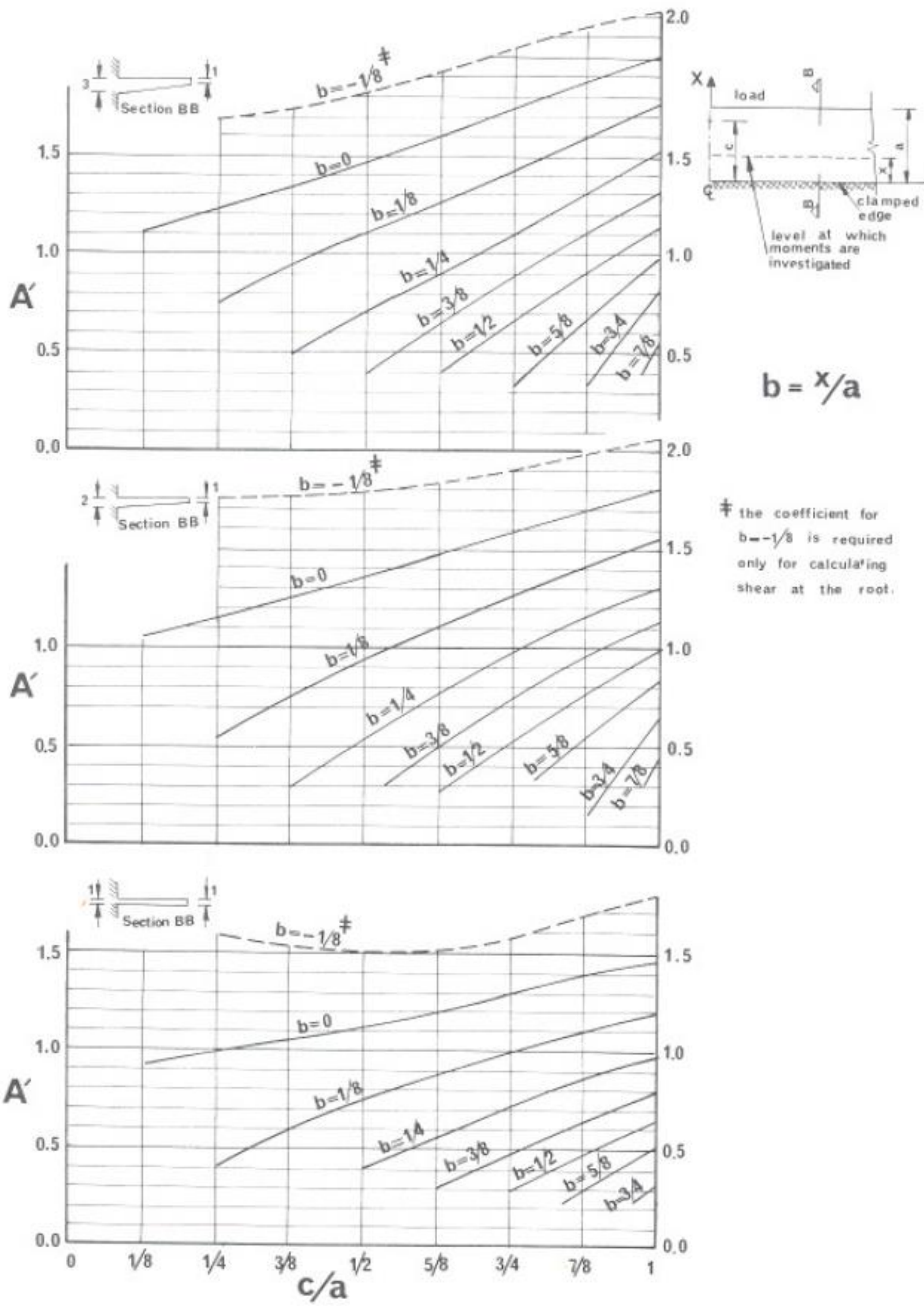

Figure 2.7 – Charts for the evaluation of the coefficient A' (Eq. (2.3)) taken form [12]

Both analyses and calibrations made by Sawko and Mills in [11] and by Bakht and Holland in [12] considered a Poisson's ratio equal to zero.

In 1990, Dilger *et. Al* also presented in [13] an extension of Bakht and Holland's solution to cantilever slabs in which the rotational restraint at the clamped end is finite, or by another words, considering the continuity of the deck slab over the beams and the flexibility of the internal panel.

Finally, in 1993 a solution was presented by Mufti *et. Al* in [10] using the same formulae, but now dependent on a coefficient B.

$$m_y = \frac{2PB}{\pi}\frac{1}{\cosh\left(\frac{2Bx}{c}\right)} \qquad ,B = \frac{A'}{2} \tag{2.5}$$

This coefficient B was calibrated for three thickness variation ratios of the cantilever slab (t_1/t_2 = 1, 2 and 3, as illustrated in Figure 2.5) by using a finite element analysis (Eq. (2.6)). Several relations between the cantilever span and the internal span and several positions of the load in the overhang were considered, as it can be observed in Figures 2.5 and 2.6.

$$B = \pi\frac{(m_y{}^{F.E.M.})_{x=0}}{2P} \tag{2.6}$$

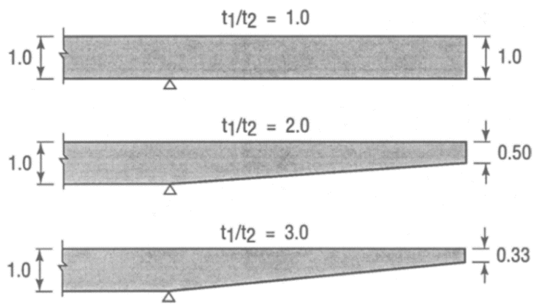

Figure 2.8 - Thickness variation ratios considered in [10]

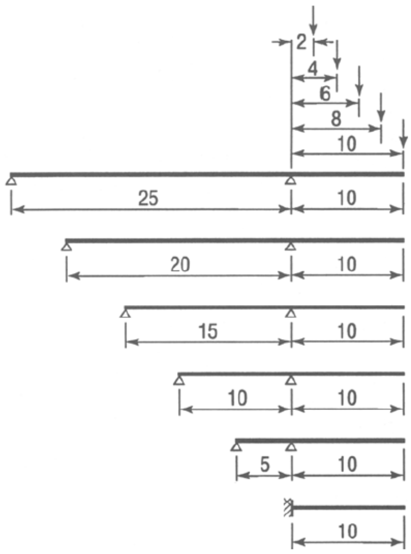

Figure 2.9 - Spans of the slabs analyzed in [10]

The values of B were calibrated for a Poisson's ratio equal to 0.2. However, it was found interesting to quote Mufti *et. Al* in [10]: "Through several analyses, it was found that the effect of increasing the Poisson's ratio from 0.0 to 0.2, on the values of B is indeed very small; it causes the largest value of B to increase by about 5%."

For edge-stiffened overhangs, with the presence of structural barriers (curbs) in the edge of the cantilever slab, Bakht presented in 1981 [14] some other charts for the calculation of different values of A', now for the use of his simplified method in cantilevers with an edge-beam. These new charts depend on the relation between the moment of inertia of the edge-beam's cross section ($I_{y,curb}$) and the moment of inertia of the cantilever slab transversal section $I'_{y,slab}$, obtained by the intersection between the cantilever slab and the *yz* plan to its middle surface, as can be observed in Figure 2.7.

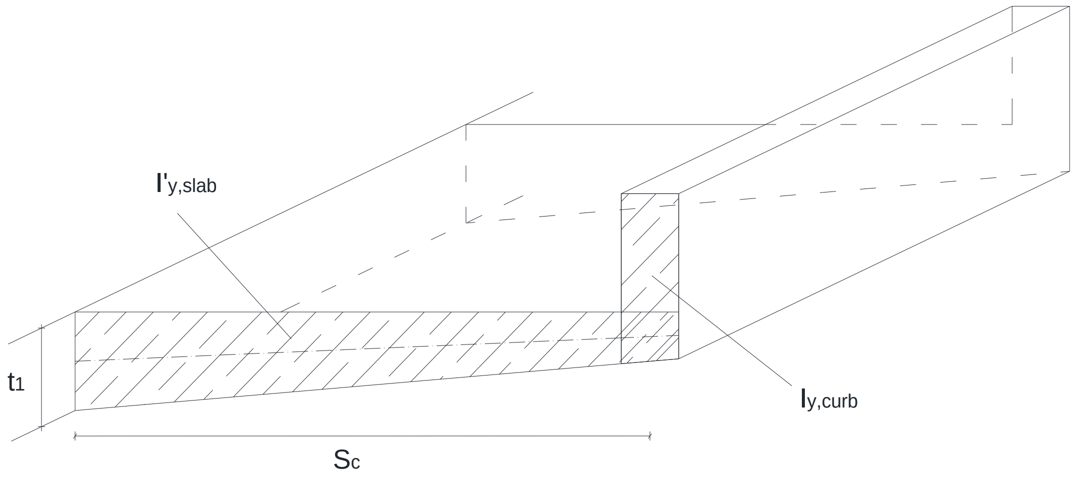

Figure 2.10 - Illustration representing the cross-sections associated with $I_{y,curb}$ and $I'_{y,slab}$

The new values for A' also depend on the thickness variation of the cantilever slab and on the relative position of the load (c/S_c), but the charts were only made for curbs located at the edge of the cantilever and for cantilevers with infinite rotational restraint in their longitudinal support.

Another feature of these simplified methods is that is possible to evaluate these transverse moments not only in the supported edge of the overhang, but also in any point of the cantilever slab between the clamped end and the load. However, since the objective of this work is only the calculation of the transverse moments over the beams, this characteristic of the methods was ignored.

For the calculation of the transverse moments due to concentrated loads applied in the internal panel it wasn't found any literature with similar solutions. However, it is developed in Chapter 3 of this work a similar solution for this load case.

CHAPTER 3

3. Structural Analysis of Bridge Deck Slabs

3.1 Introduction

This chapter is focused on the structural analysis of bridge decks composed by a concrete slab supported in two longitudinal beams. The deck slabs are therefore divided into three parts: two overhangs and one internal panel.

The loads transmitted by the vehicles to the pavement are defined in the codes as road traffic actions, being represented by different types of loads: uniformly distributed loads, knife-edge loads and wheel loads.

The behavior of the deck slab under these three types of loads is not the same and therefore it is analyzed using different methods.

For the uniformly distributed loads the process is simple since the deck slab bends in a cylindrical surface along most of its length. In fact, the structural behavior can be modeled by a beam of unit width.

The structural effect in the deck slab due to vehicle wheel loads cannot be evaluated with the same simplicity given the bidirectional curvature of the slab. In addition, concentrated loads have a local effect, with a decaying pattern, on the slab behavior.

Therefore, two methods for the evaluation of the transverse bending moments on the bridge deck slab are developed in this chapter. The methods are focused on obtaining the slab bending moments over the beams due to concentrated loads. An analytical solution proposed by Timoshenko in [4] is also presented to evaluate the transverse moments at the mid-span of the internal slab (between longitudinal beams).

The knife-edge loads, as it is demonstrated in this chapter, can be assumed as a group of concentrated loads or as a very thin and long wheel load, being analyzed with the same methods as the wheel loads.

The methods usually adopted for the elastic-linear analysis of slabs under wheel loads consist in: (i) analytical solutions through an approach of Fourier series, (ii) the Influence Surfaces Method, (iii) the Finite Element Method and (iv) equivalent “Beam-Models” with an effective width.

The analytical solution proposed by Timoshenko in [4] was developed to solve shells and plates acted by wheel loads under specific conditions, using mathematical tools as Fourier series. However, these solutions were developed only for certain types of slabs and boundary conditions, being their applicability to real structures limited.

The Influence Surfaces obtained by Pucher [15] are very useful tools for the calculation of the flexural moments caused by wheel loads in both directions. Several diagrams for different longitudinal boundary conditions and for different reference points (the ones where the flexural moments are calculated) are provided, being a method which doesn't need a computer or long mathematical calculations. However, this method ignores characteristics of the deck like the thickness variation in the slab or the influence of the stiffness of adjacent slab panels in the rotational restraint of the overhang's clamped end.

Moreover, for the calculation of internal forces due to wheel loads using influence surfaces, an integration on the wheel area has to be made. Since the influence surfaces are given as diagrams, this process has to be done using simplified and approximate integration methods, like the Simpson's Rule or Gauss Quadrature for numerical integration.

"*The Finite Element Method is the most powerful and versatile analytical method available at present because with a sufficiently large computer, the elastic behaviour of almost any structure can be analysed accurately*", by Hambly in [16]. This is the major reason why almost all the present structural analysis software are based on this method, including the one used to support this work, the SAP2000®. Nowadays the computer capacity is very large and all this software is made to provide the best results possible to the designer, being capable to reproduce all type of structures and to control the accuracy desired for the results by the mesh used.

On the other hand, the use of very detailed models with a high number of elements can cause a big time-expense for the analysis, and in some situations, it can turn a simple analysis into an unnecessary cumbersome process. Furthermore, the accuracy of the results also depends on the finite element type and on the capacity of the designer to distinguish and avoid singularities like, for example, modeling the wheel loads as uniformly distributed loads in the wheel areas instead as point loads for the calculation of the flexural moments under the load.

Therefore, the search for more efficiency influenced the engineers to consider alternative approximated methods that could provide quicker analyses of slabs under concentrated loads.

The "beam-model" proposed by Leonhardt and presented by Reis in [17], e.g. assumes the slabs, even for concentrated loads, under cylindrical bending. The process consists on considering the slab as a beam which width (effective width) is obtained in order to ensure a static equivalence between the beam's bending moment and the integral of a uniform distribution of transverse moments. This uniform distribution value is the peak of the real distribution of transverse moments and the corresponding effective width is calculated using different formulas depending on the source, which can be the codes for structural design of structures, like for example, the REBAP (*Regulamento para Estruturas de Betão Armado e Pré-Esforçado*). The simplicity associated with this method is, hence, the fact that having this effective width, which normally depends on the boundary conditions and span length, it's only needed the calculation of the beam bending moment due to a concentrated load to obtain the design transverse moments in the slab. However, the flexural moments depend on many parameters that are not usually taken into account in the definition of the effective width, which compromises the use of the method.

Therefore, other methods towards the calculation of the slab transverse moments over the beams are presented in this work. The semi-analytical methods presented in [10] and [14], which were slightly described in Chapter 2, represent methods with an already proved efficiency.

In this chapter some characteristics of the bridge decks regarding their influence on the distribution curves of the slab transverse moments due to cantilever loads are firstly evaluated in order to conclude which of them can be neglected when simplified methods are used: Poisson's ratio, relation between the cantilever span and the internal span (S_c/S), torsional and flexural rigidity of the beams, thickness variation in the cantilever slab (t_1/t_2), the presence of structural barriers in the cantilever slab (edge-stiffening) and their relative positioning in the overhang.

After this study and since the semi-analytical methods presented in [10] and [14] have some gaps and provide, for some cases, distributions of moments considerably different from the ones obtained by using a finite element analysis, a similar and improved method is developed and presented in this work.

Since these semi-analytical methods ([10] and [14]) consider only one coefficient A' (Equation (2.4)) or B' (Equation (2.6)), it was only possible the adaptation of the distributions to the ones obtained in a finite element analysis by one value, which was the peak value. The remaining distribution curve is then expected to be reliably represented by the hyperbolic cosine function.

The improvement presented in the new semi-analytical method consists in considering four coefficients instead of only one. This enables an adaptation of the distributions obtained by using this method to the ones obtained in a finite element analysis by more points, leading to a much reliable approximation.

This methodology was also extended for the application to the transverse bending moments over the beams due to loads acting on the internal panel. Since the overhangs introduce a rotational stiffness in the deck slab at the supported edge, it leads to the appearance of self-balanced flexural moments over the beams when concentrated loads are acting on the internal panel. The values of these transverse moments are not neglectable and should be added to the ones caused by loads in the cantilever, increasing the reinforcement needs.

Also for this case the following characteristics of the bridge deck were evaluated in the first place, in order to conclude which of them are important or neglectable: the torsional and flexural rigidity of the beams, the relation between the cantilever span and the internal span

(S_c/S), the thickness variations, both in the cantilever (t_1/t_2) and in the internal panel and the presence of edge-stiffening in the cantilever.

Hence, a similar semi-analytical method was then developed, also with four coefficients, to the evaluation of the distributions of the slab transverse moments over the beams due to internal panel loads.

The analytical solution proposed by Timoshenko and presented in [4] is also proposed as a simplified method for the calculation of the transverse moments in the mid-span of the internal slab. However, this method considers the internal panel as a simply supported plate in the longitudinal beams (these considered with zero torsional rigidity and infinite flexural stiffness), ignoring also the influence of the overhangs and of the thickness variation in the internal slab. The importance of these characteristics was then evaluated in order to verify the applicability of this method in the comparative analysis between the RSA [3] and the Eurocode [2].

3.2 Cantilever slabs under wheel loads

3.2.1 – Analysis of parameters affecting the structural behavior

The type of deck considered in this work is made by a slab supported by two beams or ribs, being divided into two overhangs and one internal panel, as illustrated in Figure 3.1.

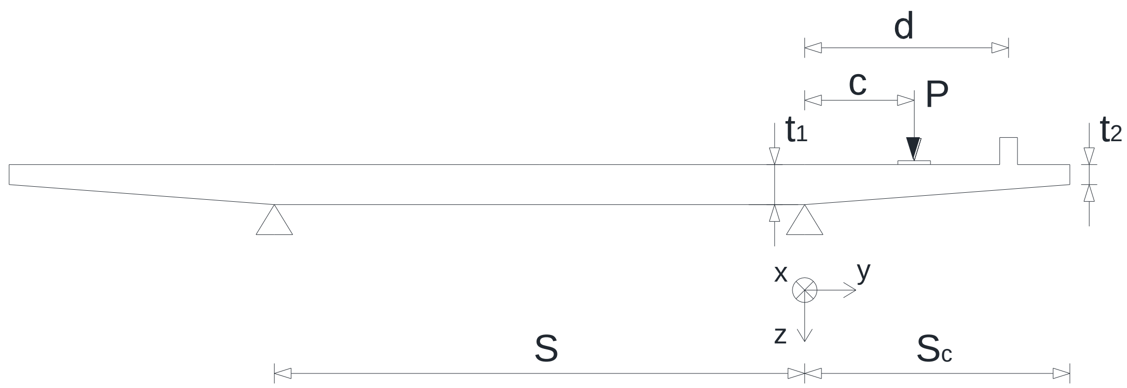

Figure 3.1 - Example of a bridge deck cross-section with the respective nomenclature

The overhangs have characteristics that influence the distribution of the transverse moments over the beams due to cantilever loads: (i) their span in the y-direction, S_c; (ii) the thickness variation, t_1/t_2; and (iii) the edge-stiffening in the cantilever caused by a structural barrier (curb), being important the distance of this curb from the clamped end of the overhang *d* and its relative stiffness, represented by a factor K' defined in the sequel.

The factor K' represents the relation between the longitudinal flexural stiffness of the curb ($I_{y,curb}$), which is assumed to include the "slab portion", and the flexural stiffness of the cantilever slab ($I_{y,slab}$), represented by the moment of inertia of a section with a thickness t_1 and a width S_c (Figure 3.2), being given by:

$$K' = \frac{I_{y,curb}}{I_{y,slab}} \tag{3.1}$$

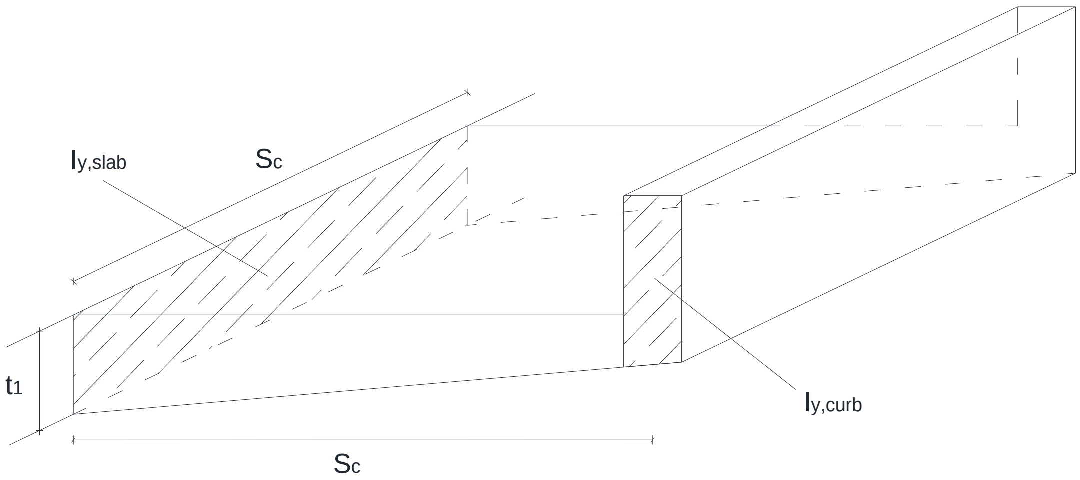

Figure 3.2 - Illustration representing the cross-sections associated with $I_{y,curb}$ and $I_{y,slab}$

Regarding the structural influence of the beams, the corresponding flexural and torsional stiffness, represented respectively by the moment of inertia (I_y) and by the factor K (Eq. (3.2)) are parameters to consider. The factor K relates the torsional rigidity of the longitudinal element with the flexural stiffness of the internal slab by considering a cross section with unit width and thickness t_1:

$$K = \frac{GJ}{L} \times \frac{S}{EI} \tag{3.2}$$

with:

S = transverse span of the internal panel;

I = moment of inertia of the slab's unit cross section:

$$I = \frac{{t_1}^3}{12} \tag{3.3}$$

L = length between points with rotational restraint;

J = torsional rigidity factor of the beam.

The wheel load position in the overhang, represented by *c* in Figure 3.1, is obviously important for the slab transverse moments obtained at the clamped end and the corresponding area is a parameter which importance is also evaluated in this section. In terms of the deck's material (concrete), the only parameter approached is the Poisson's ratio.

3.2.2 – Study of the influence of the bridge deck parameters

Towards the evaluation of the influence of the wheel loads areas, the peak value of the transverse moments over the beams was calculated for a concentrated load and the following load areas: 0.04 m^2, 0.16 m^2, 0.36 m^2, 0.64 m^2 and 1.00 m^2, for a load applied at $c/S_c = 2/3$ and considering three thickness variations in the cantilever slab (t_1/t_2 = 1, 2 and 3). The length of the cantilever (S_c) used in the finite element model was 3 m, being the support at the beam section considered clamped.

The relation between the maximum moments ($m_{y,máx}$) for the different wheel areas considered and the higher value of these maximum moments, corresponding to the concentrated load ($m_{y,máx}^{WLA=0}$) is presented in Figure 3.3. It can be concluded that considering the wheel loads as concentrated loads is conservative and the deviation from the real values is very small, being neglectable. Thus, all the other parameters in the sequel will be evaluated using concentrated loads instead of wheel loads.

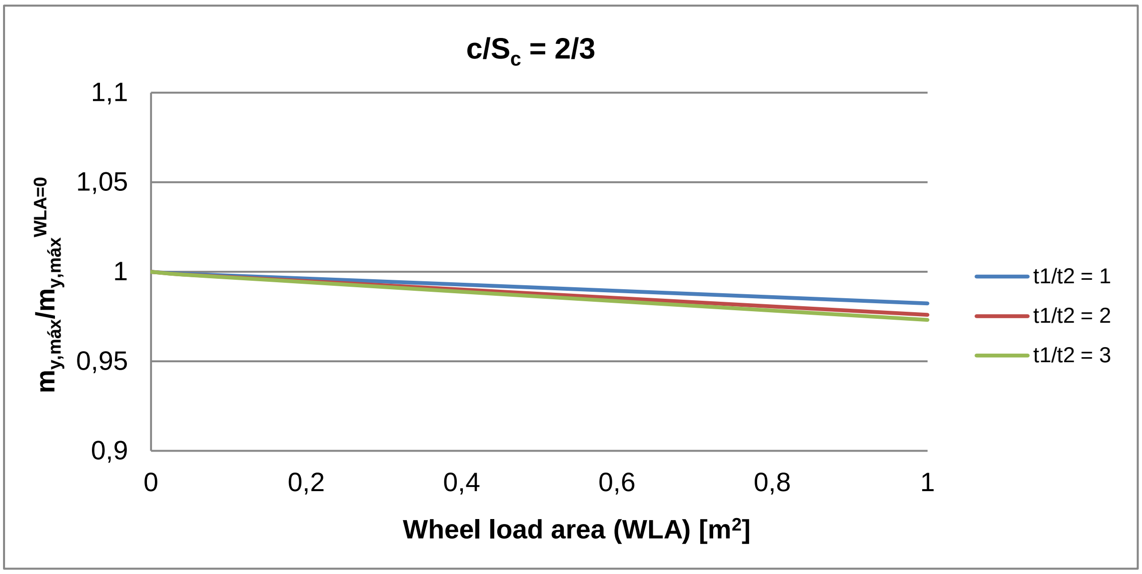

Figure 3.3 - Influence of the wheel load area on the maximum transverse moments for three cases of thickness variation in the cantilever slab (t_1/t_2)

The Poisson's effect was considered differently in the literature reviewed. In fact, the Poisson's ratio (ν) assumed different values in the different versions of Bakht's semi-analytical method. In [12] and [14] it was assumed ν = 0.0 in the calibration of the charts for the values of A' (Eq. (2.4)). However, in [10] it was admitted a Poisson's ratio equal to 0.2 in the development of the values for the coefficient B (Eq. (2.6)). Meanwhile in [10] it is referred that the effect on the values of B caused by considering ν = 0.2 instead of zero was very small.

Nevertheless, a finite element model of a cantilever slab was analyzed with the load acting on the edge, with and without thickness variation of the slab, evaluating the difference between the distributions of transverse moments at the clamped end of the overhang by considering ν = 0.0 or ν = 0.2. These distributions are presented in Figure 3.4.

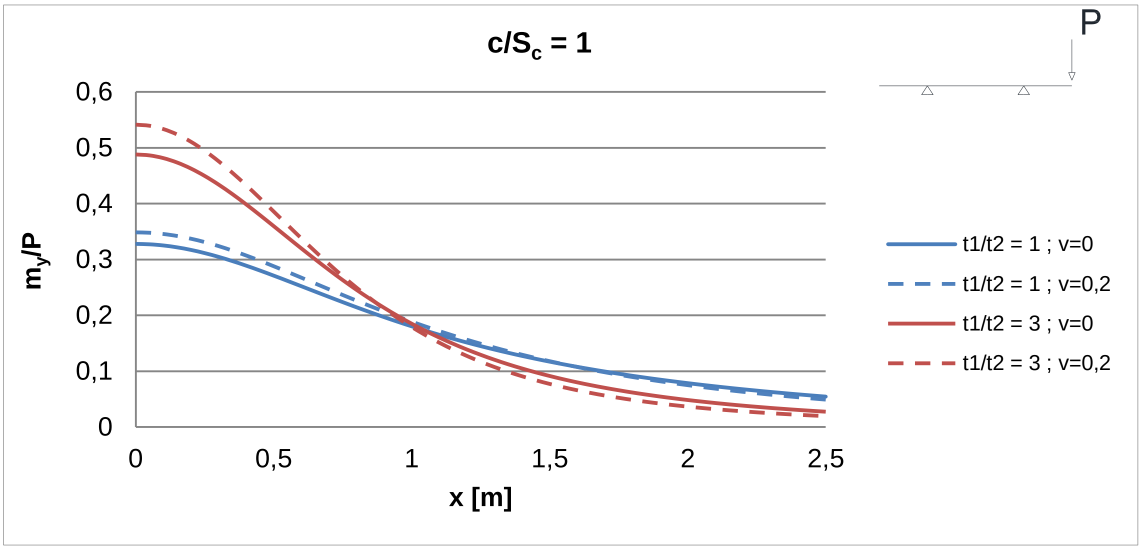

Figure 3.4 - Influence of the Poisson's ratio on the distributions of transverse bending moments

On the other hand, if the objective is to obtain flexural moments for design purposes, which means for the Ultimate Limit State, the concrete can be admitted as cracked and in that conditions the Poisson's ratio should be considered as zero, since the interaction between the two orthogonal directions is minimal. Thus, the effect of Poisson was neglected by assuming $\nu = 0$ on the study of the parameters that influence more or less the distributions of transverse moments in the deck slab.

Focusing on the size of the overhang (S_c), it is convenient to refer that the peak value of a distribution of moments, for a constant value of the ratio c/S_c (position of the load in the overhang) doesn't change with the variation of S_c. However, the value of the integration of the transverse moments along the longitudinal beams increases with S_c, since it has to be equal to P x c (Figure 2.4). Thus, this longitudinal distribution of transverse moments widens in order to guarantee the equilibrium, maintaining a constant peak value for that specific value of c/S_c.

Nevertheless, the value S_c has an indirect influence on other parameters (e.g. the ratio S_c/S, which represents the relation between the cantilever span and the internal panel length), as can be verified further on this section.

The rotational restraint at the supported edge of the overhangs depends essentially on the ratio S_c/S and on the torsional stiffness of the beam, being evaluated in the sequel.

This elastic degree of restraint only affects the shape of the distribution curves, remaining the area below their line equal to P x c (Figure 2.4), in order to verify the equilibrium conditions. In fact, the equilibrium conditions require that the resultant moment, in a cantilever, is only dependent of *c* (distance between the load and the clamped edge of the cantilever). If it is considered a constant value of *c* but variable values of c/S_c, the area below the distribution curves is the same but the shape of these distribution curves is different, being dependent on the value of the overhang length S_c.

Thus, the importance of the ratio S_c/S was evaluated by analyzing several finite element models with S_c = 3 m, considering: (i) three different load positions in the overhang (c/S_c = 1/3, 2/3 and 1), (ii) the thickness variation in the cantilever slab and (iii) the ratio S_c/S between three of the values used in the tables presented in [10] for Bakht's semi-analytical method: S_c/S = 0,4, 0,5 and 0,67. The results are presented in Figures 3.5 and 3.6, respectively for t_1/t_2 = 1 and t_1/t_2 = 2.

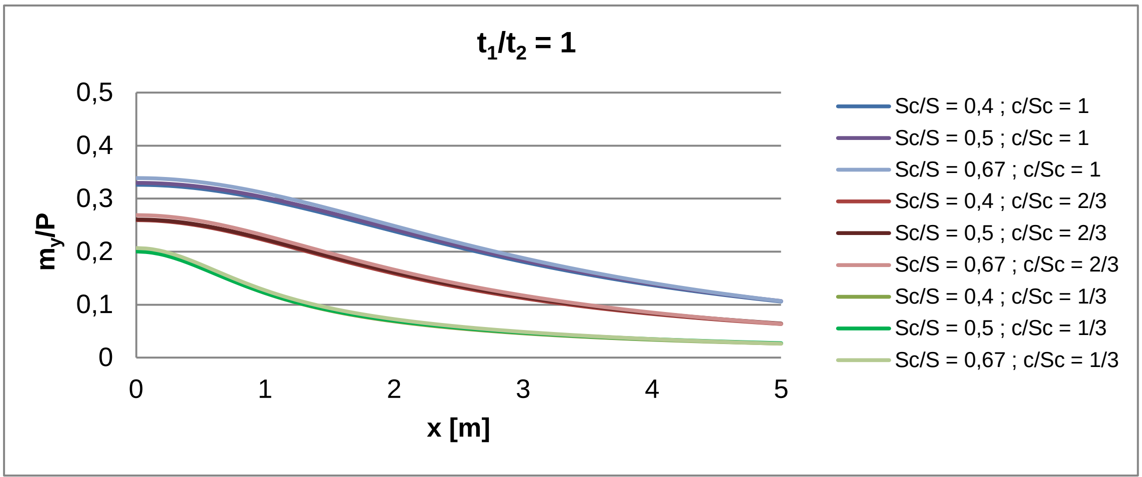

Figure 3.5 - Influence of the relation between the cantilever length and the internal span, for three load position cases and for a thickness variation ratio on the cantilever slab t_1/t_2 = 1

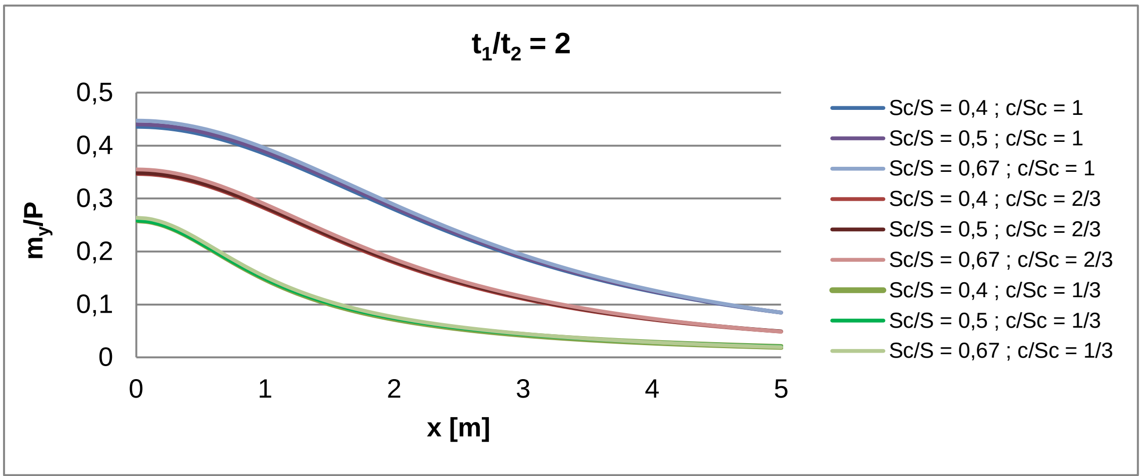

Figure 3.6 - Influence of the relation between the cantilever length and the internal span, for three load position cases and for a thickness variation ratio on the cantilever slab t_1/t_2 = 2

It can be observed in Figures 3.5 and 3.6 that the influence of the parameter S_c/S on the longitudinal distributions of transverse moments over the beams is very small, being verified that the corresponding peak value increases slightly with the ratio S_c/S.

However, it is convenient to evaluate this parameter when the difference is extreme, as for example, between the cases with S_c/S = 0.5 and the cases of clamped cantilevers (total rotational restraint), equivalent to $S_c/S = \infty$.

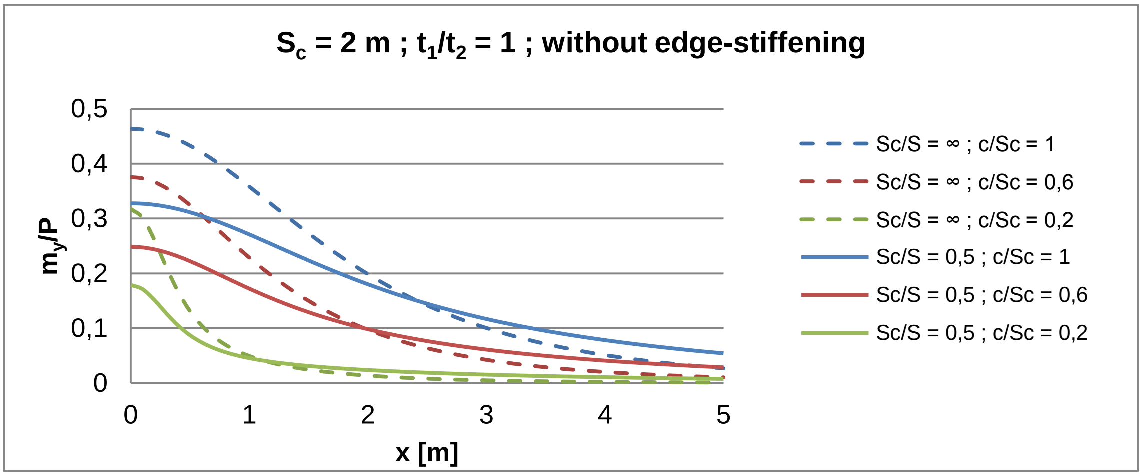

Figure 3.7 - Differences between the distributions of transverse moments obtained for three load positions considering a full fixed clamped end of the cantilever and considering a continuity of the deck slab to the internal panel with a ratio $S_c/S = 0.5$

A big difference between the values corresponding to much different ratios S_c/S (0.5 and ∞) is verified in Figure 3.7, which means that considering total rotational restraint at the cantilever support leads to an overdesign of the slab reinforcement at this part of the deck.

Since in the reality the bridge decks have finite values of S_c/S, and since the difference verified between cases with expected values in real bridges is neglectable (see Figures 3.5 and 3.6), the value considered further on was $S_c/S = 0.5$.

The effect of the torsional stiffness of the beams, represented by the factor K defined in Eq. (3.2) on the longitudinal distributions of the slab transversal bending moments at the cantilever support was evaluated. It was used a finite element model with $t_1/t_2 = 2$ and a load positioned on the edge of the overhang ($c/S_c = 1$). The results are presented in Figure 3.8.

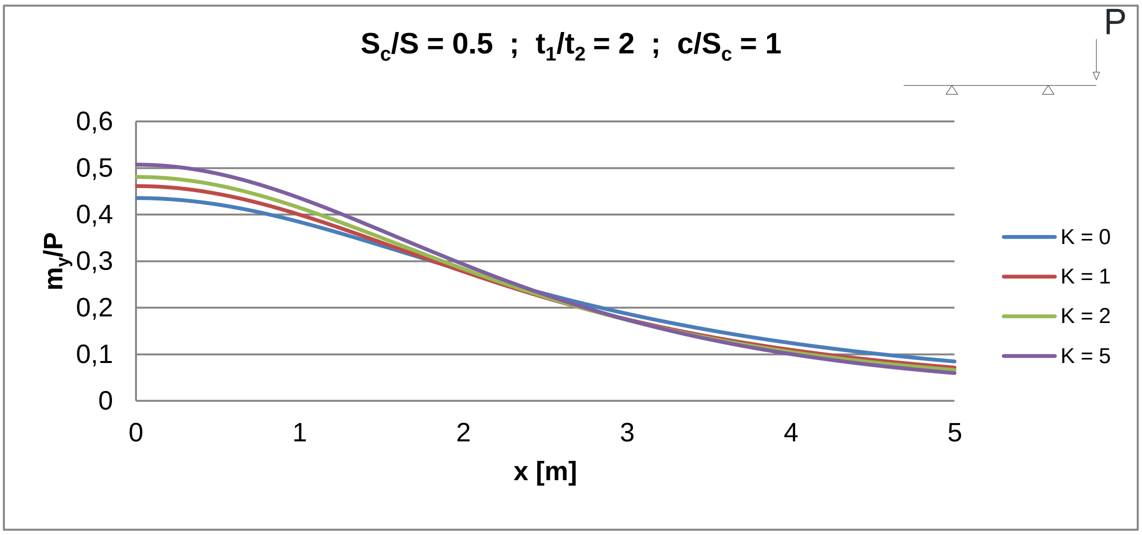

Figure 3.8 - Influence of the torsional stiffness of the beams on the distributions of transverse moments

It can be concluded that the peak value of the distributions of moments is, as expected, higher for a bigger torsional stiffness of the beam. However, this was an elastic-linear analysis, and in the design of bridges the torsional stiffness is reduced to take into account the cracking of the concrete. This, together with the fact that the beams aren't generally designed to resist to torsional forces led us to ignore this parameter by considering always the deck slab simply supported in the beams, with K = 0. Therefore, the rotational stiffness at the cantilever longitudinal support is only represented, from now on, by the ratio S_c/S.

In the previous analyses, the flexural stiffness of the longitudinal beams was considered infinite. However, it was found convenient to evaluate the influence of this parameter in the distributions of the slab transverse moments. Towards this evaluation, a finite element model of a continuous bridge, with span lengths of 30 m, S = 7.5 m and S_c = 3.0 m was defined. Simplifications due to symmetric considerations were adopted in the model definition (Figure 3.9).

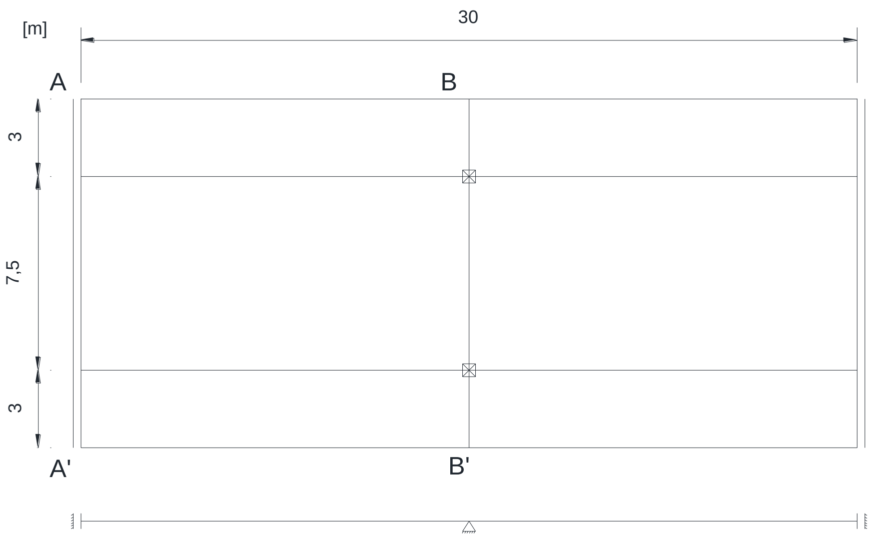

Figure 3.9 - Bridge deck model used to evaluate the influence of the flexural stiffness of the longitudinal beams

A typical cross-section of a bridge beam was considered (represented in Figure 3.10) in order to evaluate the influence of the beam flexural stiffness on the transverse bending moments of the deck slab. The moment of inertia of the cross-section represented in Figure 3.10 (I_y) was obtained (I_y = 0.9444 m^4), being also considered three other values for comparison purposes: 0.5Iy, 2.0Iy and ∞.

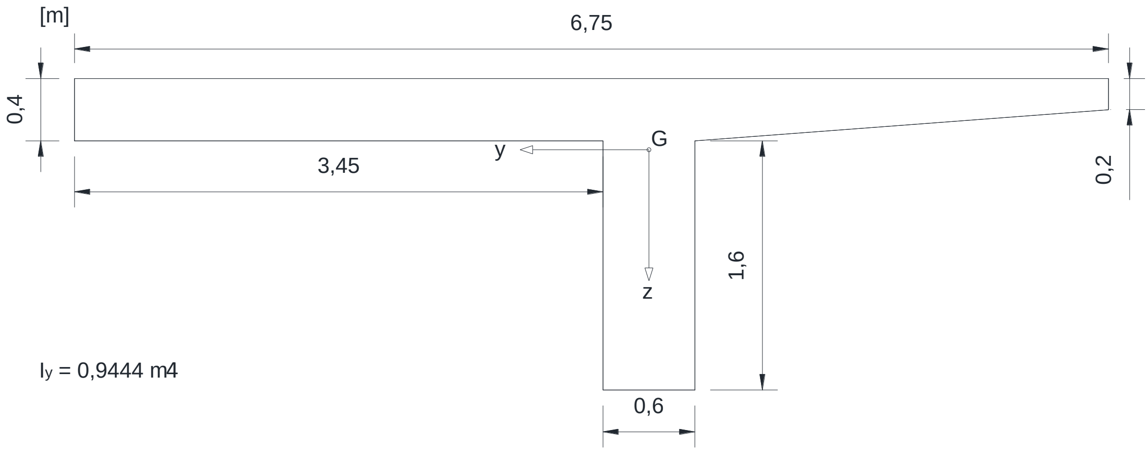

Figure 3.10 - Cross-section of the beam-type used to evaluate the influence of the flexural stiffness of the longitudinal beams on the transverse moments distributions, with the respective moment of inertia I_y

This comparison was made for the load acting on two different points of the bridge longitudinal length: (i) at the mid-span (section AA') and (ii) near the supports (section BB'), being the results presented in Figures 3.11 and 3.12.

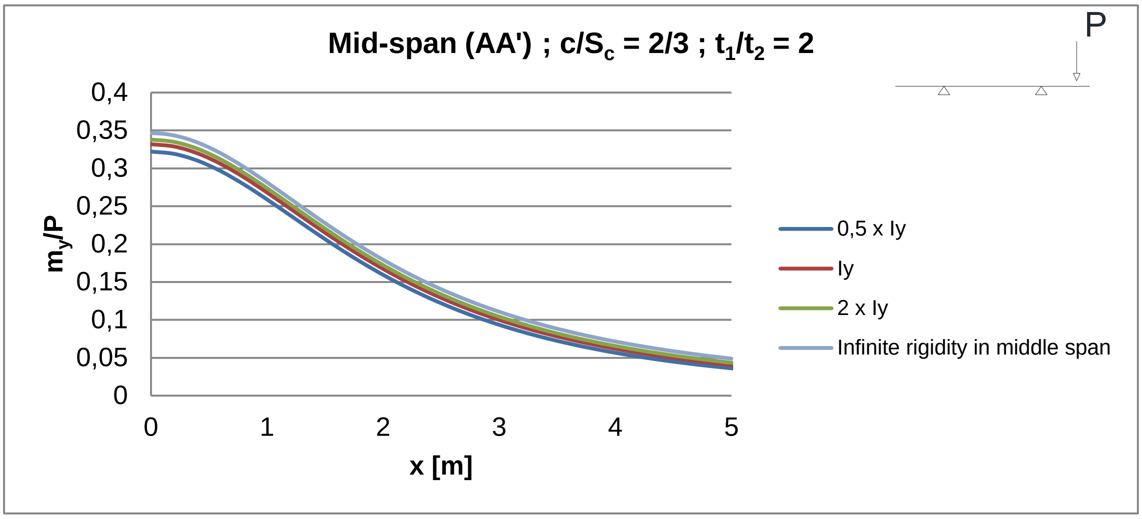

Figure 3.11 - Influence of the flexural stiffness of the beams at the mid-span of the bridge deck (Section AA' in Figure 3.9)

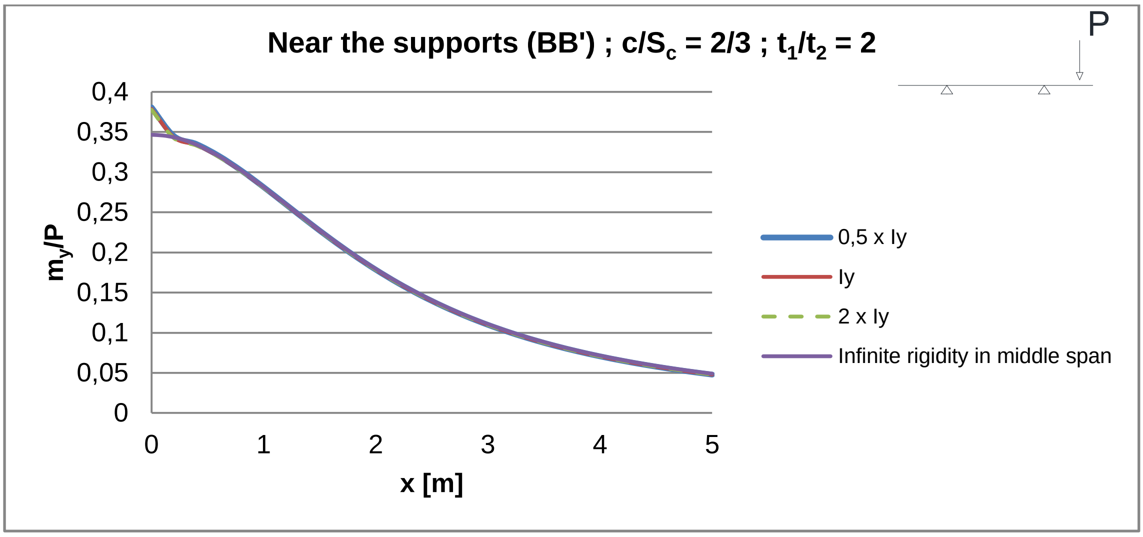

Figure 3.12 - Influence of the flexural stiffness of the beams on the transverse moments near the supports of the bridge deck (Section BB' in Figure 3.9)

It can be concluded from Figure 3.11 that in the most flexible part of the bridge, at the mid-span, the results obtained using infinite flexural stiffness for the beams are conservative, but with a minimum deviation from the finite values. In the zone near the piers, the most rigid part, as expected and verified in Figure 3.12, the difference between the results with rigid beams and the other values of stiffness is neglectable.

Nevertheless, if the beams are sufficiently resistant to support the bridge, the variations of the respective cross-sections (and consequently, the variations on their flexural stiffness) don't have a significant influence on the distribution of the slab transverse moments at the cantilever clamped end, being this parameter neglected. Thus, in further analyses the beams are also admitted to have an infinite flexural stiffness.

It was already verified in Figure 3.4 the influence of the thickness variations of the cantilever slab in the distributions of transverse moments. Nevertheless, it was made an analysis considering the five load positions and the three thickness variations considered in [10] for Bakht's semi-analytical method (c/S_c = 0.2, 0.4, 0.6, 0.8 and 1.0; t_1/t_2 = 1, 2 and 3). The comparison between the respective peak values of the transverse moments is presented in Figure 3.13.

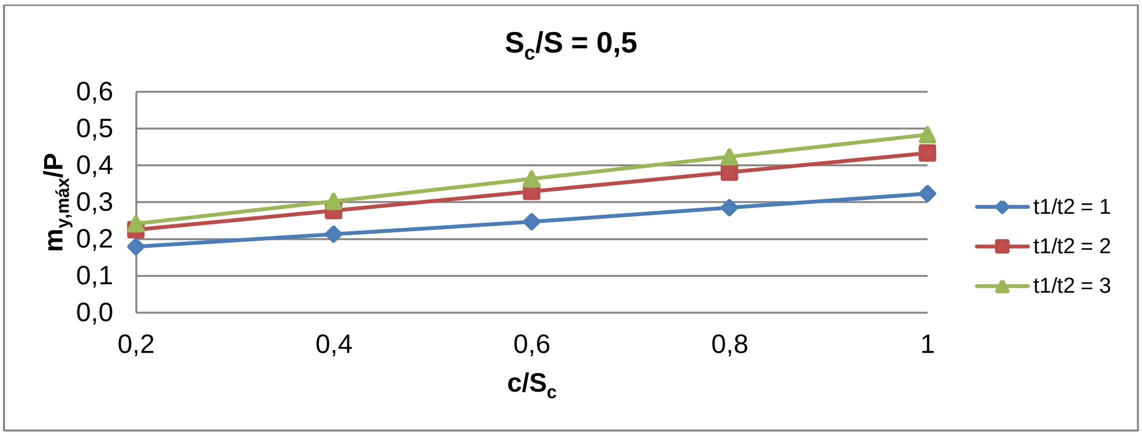

Figure 3.13 - Influence of the thickness variation on the peak values of the transverse moments m_y

It is confirmed by this analysis the important influence of the thickness variation on the cantilever slab, since the differences between the peak values for the different ratios t_1/t_2 = 1, 2 and 3 can reach 50%.

The edge-stiffening due to the presence of structural jersey barriers (curbs) in the overhang can affect the distributions of transverse moments. To assess this effect, two parameters were evaluated: (i) the relative flexural stiffness of the curb, represented by a factor K' defined in Eq. (3.1) and (ii) the position of the curb in the overhang, which is represented by the ratio d/S_c (*d* is represented in Figure 3.1).

The evaluation of the influence of having a curb in the edge of the overhang was made considering three different positions of the load (c/S_c = 1/3, 2/3 and 1) acting on a cantilever slab with constant thickness. The rectangular barrier used as curb in the finite element model was assumed to have 0,6 m depth and 0,35m width, which corresponds, considering S_c = 3 m and t_1 = 0.4 m, a value of K' = 0.394. The results of this analysis were compared with the distribution of moments for the same model but without the curb, being represented in Figure 3.14.

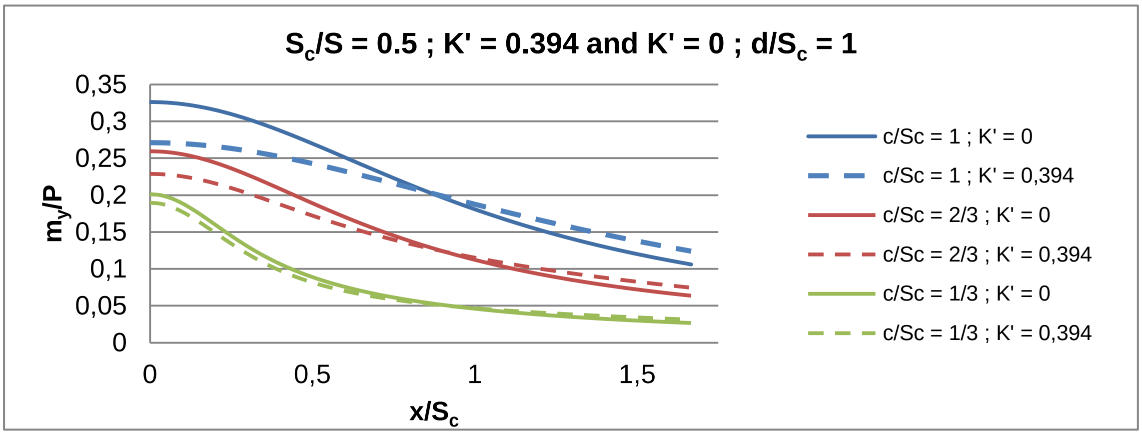

Figure 3.14 - Influence of the presence of edge-stiffening on the distributions of transverse bending moments

The presence of edge-stiffening in the overhangs decreases the peak values of the transverse moments over the beams, as it can be verified in Figure 3.14, widening the corresponding distribution along the x-axis.

To evaluate the influence of the curb positioning in the cantilever three positions of the load (c/S_c = 0.2, 0.4 and 0.6) and two positions of the curb (d/S_c = 1 (in the edge) and 2/3) were considered, being assumed a value K' = 1. The results can be observed in Figure 3.15.

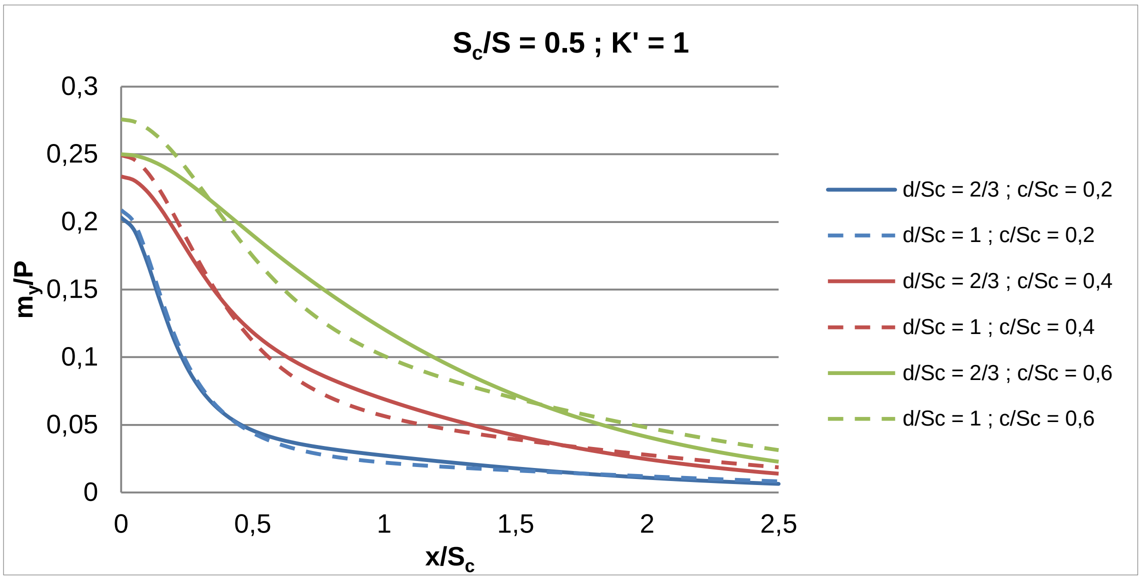

Figure 3.15 - Influence of the position of the curb in the distributions of transverse moments for three load positions

It can also be concluded from Figure 3.15 that the influence of the position of the curb decreases with the distance between it and the load, becoming almost neglectable for some load positions near the beam. However, for loads closer to the curb, this parameter is important. Thus, in this work both the stiffness and location of these curbs are considered important parameters.

3.2.3 – Comparison between the results obtained by adopting Bakht's semi-analytical method and by using a finite element analysis

After the identification of the most relevant parameters for the structural analysis of slab-beam decks, a comparison between the results obtained by using finite element models and the semi-analytical method presented in [10] (Eq. (2.5)) was performed.

Regarding the relation between the cantilever span and the internal span S_c/S, Mufti *et. al* assume in [10] different values of *B* for different relations S_c/S. However, in this comparative analysis only the cases with a ratio of S_c/S = 0.5 were considered.

The analyzed models had the following characteristics: (i) a cantilever span of 2 m without edge-stiffening, (ii) infinite flexural stiffness of the beams and zero torsional rigidity, (iii) three values of thickness variation (t_1/t_2 = 1, 2 and 3) and (iv) five positions of the load (c/S_c = 0.2, 0.4, 0.6, 0.8 and 1.0). Since the values of the coefficient *B*, tabled in [10], were calibrated for a Poisson's ratio of 0.2, the results of Bakht's method were compared with the results from the finite element analysis performed by using the software SAP2000® also considering ν = 0.2. The results are presented in Figures 3.16, 3.17 and 3.18.

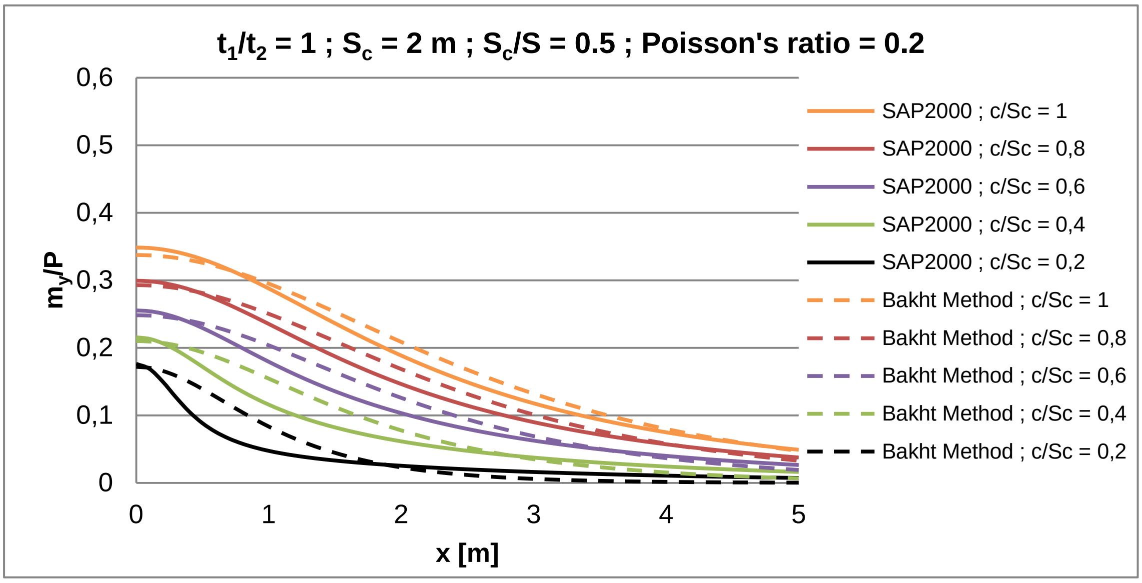

Figure 3.16 - Comparison between the results provided by Bakht's semi-analytical method [10] and by a finite element analysis for a thickness variation ratio t_1/t_2 = 1 and for five load positions

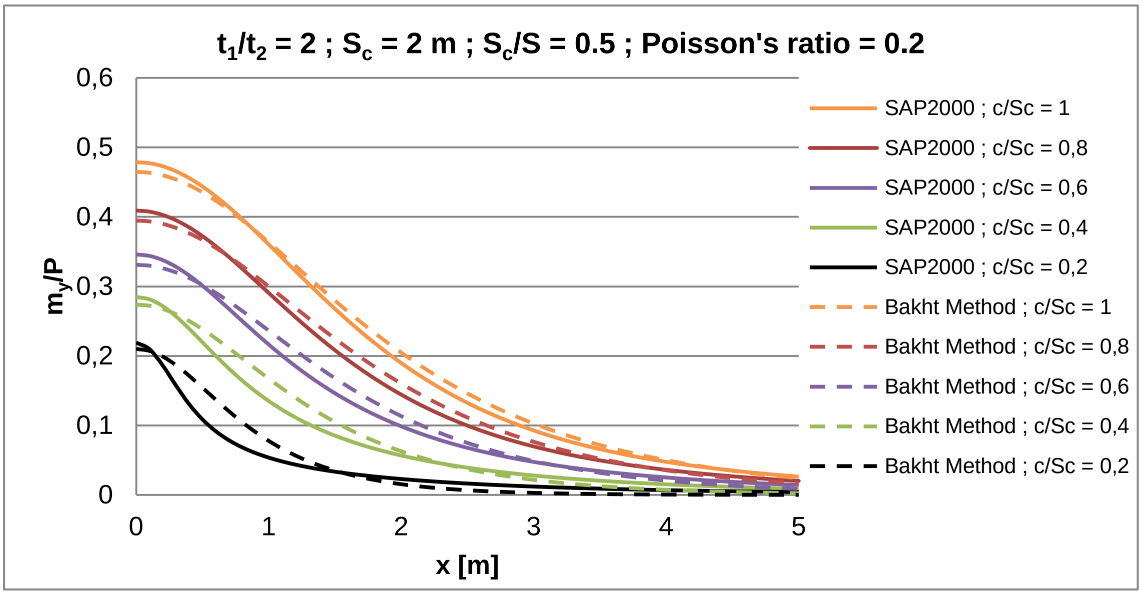

Figure 3.17 - Comparison between the results provided by Bakht's semi-analytical method [10] and by a finite element analysis for a thickness variation ratio t_1/t_2 = 2 and for five load positions

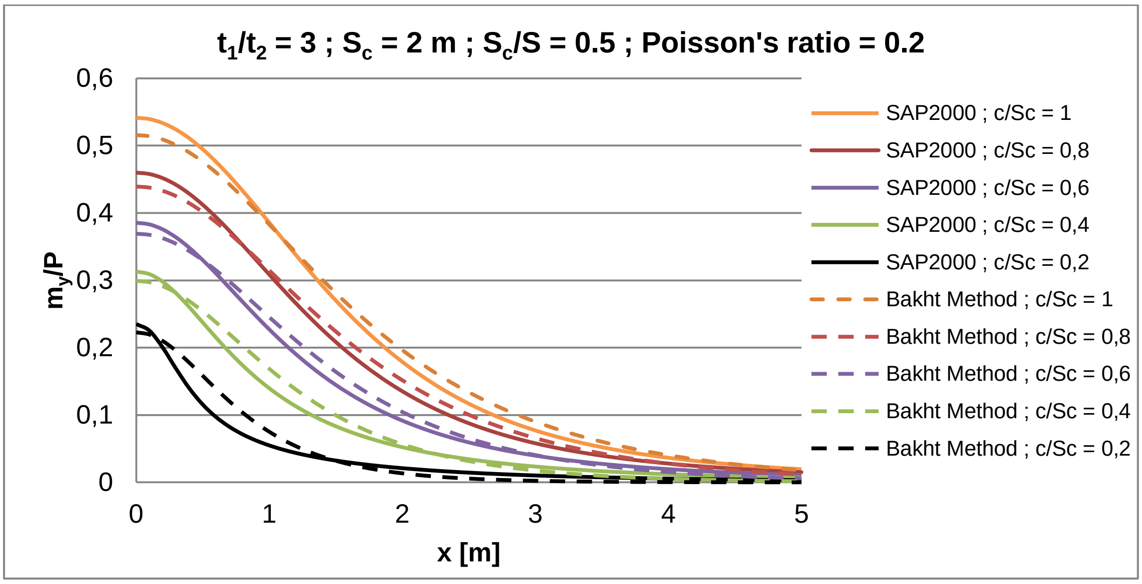

Figure 3.18 - Comparison between the results provided by Bakht's semi-analytical method [10] and by a finite element analysis for a thickness variation ratio t_1/t_2 = 3 and for five load positions

The transverse moments distributions along the x-axis obtained by Bakht's method [10] can be significantly different from the distributions obtained using a finite element analysis when the thickness variation of the cantilever is smaller and when the load is located closer to the longitudinal beam (see Figures 3.16, 3.17 and 3.18). Regarding the maximum values, the semi-analytical method [10] provides non-conservative results, although the difference to the values obtained from the finite element analysis is small.

In what concerns the edge-stiffened cantilevers, the results given by the simplified method presented by Bakht [14] (where it was considered ν = 0) were compared with the ones provided by a finite element analysis using a Poisson's ratio equal to zero. In the analyzed model an infinite rotational restraint at the cantilever support was considered, since the charts presented in [14] were calibrated for full fixed overhangs, without considering the influence of the internal panel's flexibility. The cantilever has constant thickness (t_1/t_2 = 1), a length S_c = 2m and a curb which dimensions result in a relation I_B/I_S = 1. The results were obtained for five positions of the load (c/S_c = 0.2, 0.4, 0.6, 0.8 and 1.0), being represented in Figure 3.19.

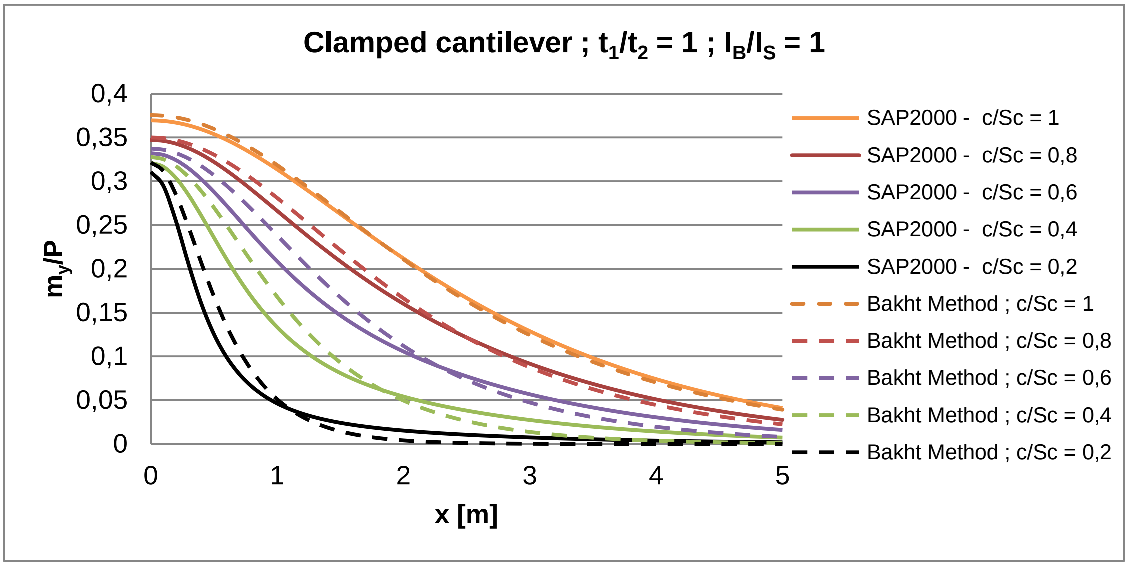

Figure 3.19 - Comparison between the results provided by Bakht's semi-analytical method [14] and by a finite element analysis for a thickness variation ratio $t_1/t_2 = 1$, for five load positions and for an edge-stiffening represented by the ratio $I_B/I_S = 1$

The method presented by Bakht [14] provides very good results for clamped edge-stiffened cantilevers (without considering the influence of the internal slab stiffness), in spite of the differences verified when the load is closer to the clamped edge of the overhang. However, as concluded in the previous section, the differences between the distributions of moments for full fixed cantilevers and for cantilevers considering the flexibility of internal slab, providing finite rotational restraint, is very significant (see Figure 3.7).

3.2.4 – Development of a new semi-analytical method to analyze the transverse moments over the beams due to cantilever loads

The Bakht methods [10] and [14] were only calibrated using the peak values obtained by accurate methods (Eq. (2.4) and Eq. (2.6)), expecting that the development of the curves given by the hyperbolic cosine function fit on the "real" ones.

However, some longitudinal patterns of the transverse moments are difficult to represent if only one coefficient (A' or B) is considered for adjusting the distribution curves, justifying the differences observed in Figures 3.16, 3.17 and 3.18 between the distribution curves provided by the Bakht method and by the finite element model analyses.

Therefore, in this thesis another solution is proposed for the distributions of transverse moments using hyperbolic cosine functions.

This solution, instead of using only one coefficient (A' or B, as in Bakht's method), depends on four coefficients: α, A, β and B, or α, A'', β and B'' as can be observed in Eq. (3.4) and Eq.

(3.5). This fact allows to have a more flexible approximation of the distribution curves, enhancing the evaluation of the transverse bending moments.

$$m_y = \alpha \frac{PA''c}{\pi} \frac{1}{\cosh(A''x)} + \beta \frac{PB''c}{\pi} \frac{1}{\cosh(B''x)} \tag{3.4}$$

The Eq. (3.4) was also adapted in order to consider non-dimensional axis for the distributions of transverse moments, leading to Eq. (3.5), in the form:

$$\frac{m_y}{P} = \alpha \frac{A}{\pi} \frac{1}{\cosh\left(\frac{\frac{A}{c}}{S_c}\left(\frac{x}{S_c}\right)\right)} + \beta \frac{B}{\pi} \frac{1}{\cosh\left(\frac{\frac{B}{c}}{S_c}\left(\frac{x}{S_c}\right)\right)} \quad , \qquad A = A''c \quad ; \quad B = B''c \tag{3.5}$$

This was possible since the widening of the distributions of transverse moments, in the x-direction, is only consequence of the increase of S_c.

The advantage of Eq. (3.5) is then to allow the evaluation of the transverse moments distribution curves independently of the absolute values of S_c and of the load P.

To sustain this fact two finite element models were tested: one with S_c = 3 m and the other with S_c = 6 m, having both a ratio c/S_c = 2/3 and a thickness variation t_1/t_2 = 2. The independence of the distributions from the absolute value of S_c, if the abscissas axis is considered non-dimensional (x/S_c), can be verified in Figure 3.20.

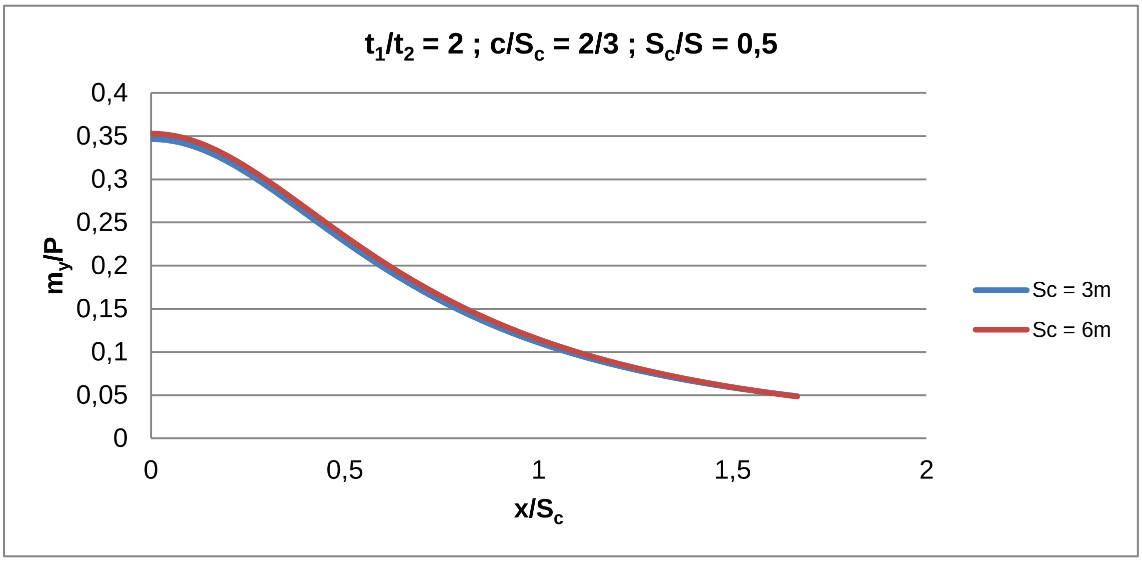

Figure 3.20 - Demonstration of the possibility to represent the distributions of transverse bending moments at the clamped end of the overhangs with a non-dimensional abscissas axis x/S_c

The calibration of this new semi-analytical method was made neglecting the Poisson effect since this is a model to analyze structures at the Ultimate Limit State, where the concrete is assumed to be cracked.

In order to obtain the condition which guarantees the equilibrium of the transverse moments distributions obtained by using Eq. (3.5), the following process was adopted:

$$\int \frac{\psi}{\pi \cosh(\psi x)} dx = \frac{2arctg(e^{\psi x})}{\pi} \tag{3.6}$$

$$arctan(e^{\infty}) = \frac{\pi}{2} \quad and \quad arctan(e^{0}) = \frac{\pi}{4}$$

From these equalities it can be concluded that:

$$\int_0^{\infty} \frac{P\psi c}{\pi \cosh(\psi x)}\, dx = \frac{Pc}{2} \tag{3.7}$$

And taking into account those results in Eq. (3.5) it is obtained:

$$\int_0^{\infty} m_y\, dx = \int_0^{\infty} \left(\alpha \frac{PAc}{\pi} \frac{1}{\cosh(Ax)} + \beta \frac{PBc}{\pi} \frac{1}{\cosh(Bx)} \right) dx = \alpha \frac{Pc}{2} + \beta \frac{Pc}{2} = (\alpha + \beta) \frac{Pc}{2} \tag{3.8}$$

Therefore, by considering the symmetry of the distribution curves in relation to the y-axis, the equilibrium is verified:

$$\int_{-\infty}^{\infty} m_y\, dx = (\alpha + \beta)\, Pc \tag{3.9}$$

Maintaining the condition α + β = 1, the area delimited by the longitudinal distribution curve of transverse bending moments is equal to P x c, verifying the cantilever equilibrium. Moreover, due to the local effect of the concentrated load, the transverse moments have the maximum value for *x* = 0 and the m_y distribution tends to zero when *x* tends to infinite, characteristics also represented by Eq. (3.5).

This new formula can then be more accurately adjusted to the solution obtained from the finite element analysis, since in the calibration process are considered three points of the finite element moment distribution instead of only one, as occurred in the calibration of the Bakht methods [10] and [14]. The fourth coefficient corresponds to the equilibrium condition α + β = 1. Therefore, the following four-equation system (Eq. (3.10) to Eq. (3.13) is obtained (with three of them non-linear, involving hyperbolic cosine functions).

$$\left(\frac{m_y}{P}\right)_i = \alpha \frac{A}{\pi} \frac{1}{\cosh\left(\frac{\frac{A}{c}}{S_c}\left(\frac{x}{S_c}\right)_i\right)} + \beta \frac{B}{\pi} \frac{1}{\cosh\left(\frac{\frac{B}{c}}{S_c}\left(\frac{x}{S_c}\right)_i\right)} \quad , i = 1, 2\ and\ 3 \qquad (3.10\ to\ 3.12)$$

$$\alpha + \beta = 1 \tag{3.13}$$

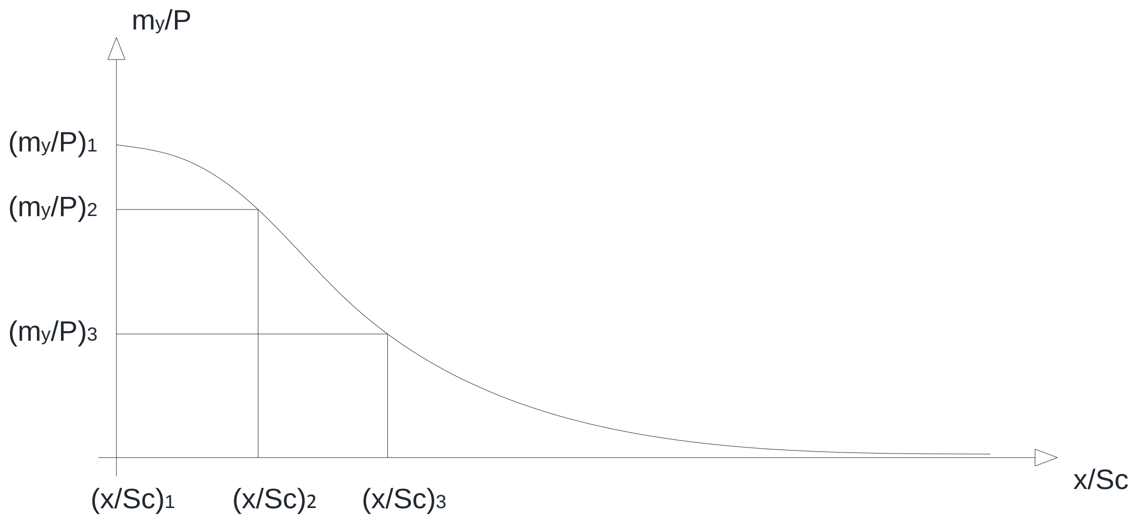

Figure 3.21 - Distribution-type of moments with the three points used in the calibration of the new method

Thus, the calibration process consists on the obtainment of the coefficients α, A, β and B by the solving of the non-linear equations system (Eq. (3.10) to Eq. (3.13)) by using the coordinates of three points taken from the distribution curves obtained in a finite element analysis, as exemplified in Figure 3.21.

This new method was calibrated for the following cases:

- t_1/t_2 = 1, 2 and 3 (thickness variation);
- c/S_c = 0.2, 0.4, 0.6, 0.8 and 1.0 (position of the load);
- K' = 0, 1 and 5 (edge-stiffening);
- d/S_c = 2/3 and 1 (position of the curb).

The values of these parameters for each case can be observed in the Tables 3.1, 3.2 and 3.3.

$t_1/t_2 = 1$						
d/S_c	K'	c/S_c	**α**	**A**	**β**	**B**
-	0	0.2	0.6772	0.1807	0.3228	1.3636
		0.4	0.6983	0.3296	0.3017	1.4581
		0.6	0.6085	0.3994	0.3915	1.3733
		0.8	0.5743	0.5053	0.4257	1.4345
		1.0	0.5334	0.6029	0.4666	1.5180
1	1	0.2	0.6807	0.1516	0.3193	1.3684
		0.4	0.7296	0.2912	0.2704	1.5002
		0.6	0.7947	0.4438	0.2053	1.6534
		0.8	0.8493	0.5971	0.1507	1.7364
		1.0	0.8509	0.1491	0.1491	1.4680
	5	0.2	0.6910	0.1227	0.3090	1.3912
		0.4	0.7471	0.2313	0.2529	1.5348
		0.6	0.8738	0.3944	0.1262	2.0002
		0.8	0.9551	0.5377	0.0449	2.6204
		1.0	0.8937	0.6707	0.1063	0.6708
2/3	1	0.2	0.7137	0.1692	0.2863	1.4367
		0.4	0.7912	0.3380	0.2088	1.5948
		0.6	0.7178	0.4386	0.2822	1.2635
	5	0.2	0.7383	0.1373	0.2617	1.4978
		0.4	0.8403	0.2877	0.1597	1.7137
		0.6	0.9481	0.4664	0.0519	1.8790

Table 3.1 – Table with the coefficients α, A, β and B for a thickness variation ratio $t_1/t_2 = 1$

$t_1/t_2 = 2$						
d/S_c	K'	c/S_c	**α**	**A**	**β**	**B**
-	0	0.2	0.5896	0.2381	0.4104	1.3440
		0.4	0.5561	0.4109	0.4439	1.4557
		0.6	0.4456	0.5080	0.5544	1.4698
		0.8	0.3615	0.6137	0.6385	1.5430
		1.0	0.2559	0.6624	0.7441	1.6252
1	1	0.2	0.5939	0.1810	0.4061	1.3506
		0.4	0.6086	0.3148	0.3914	1.5114
		0.6	0.6731	0.4750	0.3269	1.6723
		0.8	0.8691	0.7361	0.1309	2.0740
		1.0	0.8634	0.9324	0.1366	0.9354
	5	0.2	0.5905	0.1358	0.4095	1.3457
		0.4	0.6124	0.2233	0.3876	1.5160
		0.6	0.7146	0.3683	0.2854	1.7436
		0.8	0.8530	0.5210	0.1470	2.0396
		1.0	0.8585	0.6839	0.1415	0.7099
2/3	1	0.2	0.6655	0.2054	0.3345	1.4998
		0.4	0.7607	0.4243	0.2393	1.7173
		0.6	0.9634	0.7074	0.0366	2.8396
	5	0.2	0.6587	0.1441	0.3413	1.4572
		0.4	0.8087	0.3329	0.1913	1.8506
		0.6	0.9628	0.5325	0.0372	2.2598

Table 3.2 – Table with the coefficients α, A, β and B for a thickness variation ratio $t_1/t_2 = 2$

$t_1/t_2 = 3$						
d/S_c	K'	c/S_c	**α**	**A**	**β**	**B**
-	0	0.2	0.5561	0.2595	0.4439	1.3401
		0.4	0.4214	0.3802	0.5786	1.3730
		0.6	0.3733	0.5377	0.6267	1.5135
		0.8	0.2663	0.6207	0.7337	1.6002
		1.0	0.1471	0.5870	0.8529	1.6962
1	1	0.2	0.5466	0.1951	0.4534	1.3119
		0.4	0.5755	0.3313	0.4245	1.5658
		0.6	0.6675	0.5095	0.3325	1.8307
		0.8	0.8610	0.7480	0.1390	2.3683
		1.0	0.9723	0.9233	0.0277	1.0050
	5	0.2	0.5477	0.1436	0.4523	1.3295
		0.4	0.5712	0.2360	0.4288	1.5598
		0.6	0.6917	0.3851	0.3083	1.9010
		0.8	0.8615	0.5531	0.1385	2.4303
		1.0	0.9570	0.6816	0.0430	0.7002
2/3	1	0.2	0.6182	0.2092	0.3818	1.4349
		0.4	0.7275	0.4318	0.2725	1.7190
		0.6	0.9872	0.7778	0.0128	3.6444
	5	0.2	0.6254	0.1437	0.3746	1.4450
		0.4	0.7854	0.3346	0.2146	1.8938
		0.6	0.9628	0.5512	0.0372	2.2598

Table 3.3 – Table with the coefficients α, A, β and B for a thickness variation ratio $t_1/t_2 = 3$

Intermediate values for the coefficients α, A, β and B between those given in each table can be obtained by linear interpolation. However, the variation of the coefficients between different ratios $t_1/t_2 = 1$, 2 and 3 is undefined and can present a non-linear shape. If a better accuracy is sought, then the non-linear interpolation proposed by Mufti *et. Al* in [18] for a similar situation and presented in the sequel should be adopted.

Being *y* the unknown coefficient to obtain, and if the values of y corresponding to $t_1/t_2 = 1$, 2 and 3 are represented as y_1, y_2 and y_3, respectively, the interpolation formula is given as follows:

$$2y = y_1(3-x)(2-x) - 2y_2(3-x)(1-x) + y_3(1-x)(2-x) \tag{3.14}$$

where $t_1/t_2 = x$.

It should be noticed that for K' = 5, when the curb is located in the edge of the overhang, the values interpolated between $c/S_c = 0.8$ and $c/S_c = 1.0$ are not so better adjusted to the ones obtained from a finite element analysis. However, normally road bridges have safety areas or sidewalks on the edge of the overhangs that prevent the wheel loads to act on places in a distance from the clamped end of $0{,}8S_c$ to S_c, reducing the importance of this problem.

In order to demonstrate the enhancement on the accuracy provided by the proposed semi-analytical method, five transverse moment distributions obtained in a finite element analysis (by using the software SAP2000®) were compared with the distributions provided by the application of Eq. (3.5).

In the models analyzed, three didn't have edge-stiffening, for the thickness variation cases on the cantilever slab given by t_1/t_2 = 1, 2 and 3, and two had edge-stiffening, one with the curb located on the edge (d/S_c = 1), with K' = 1 and t_1/t_2 = 2, and the other considering d/S_c = 2/3, K' = 5 and t_1/t_2 = 3. From the results presented in Figures 3.22 to 3.26 it can be verified that a very good agreement is obtained.

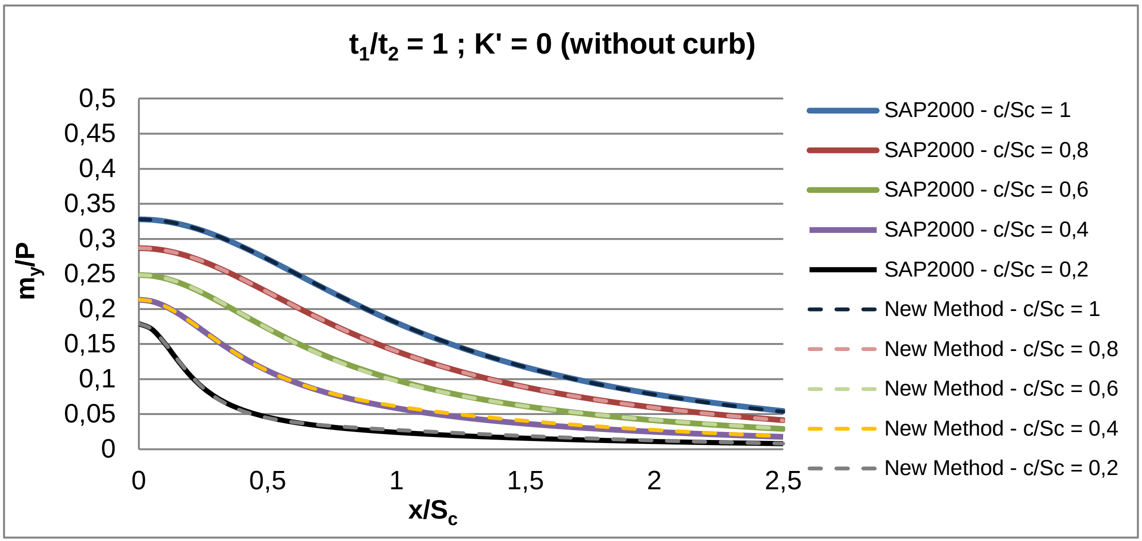

Figure 3.22 - Comparison between the results provided by the new semi-analytical method and by a finite element analysis for a thickness variation ratio t_1/t_2 = 1 and for five load positions, without edge-stiffening

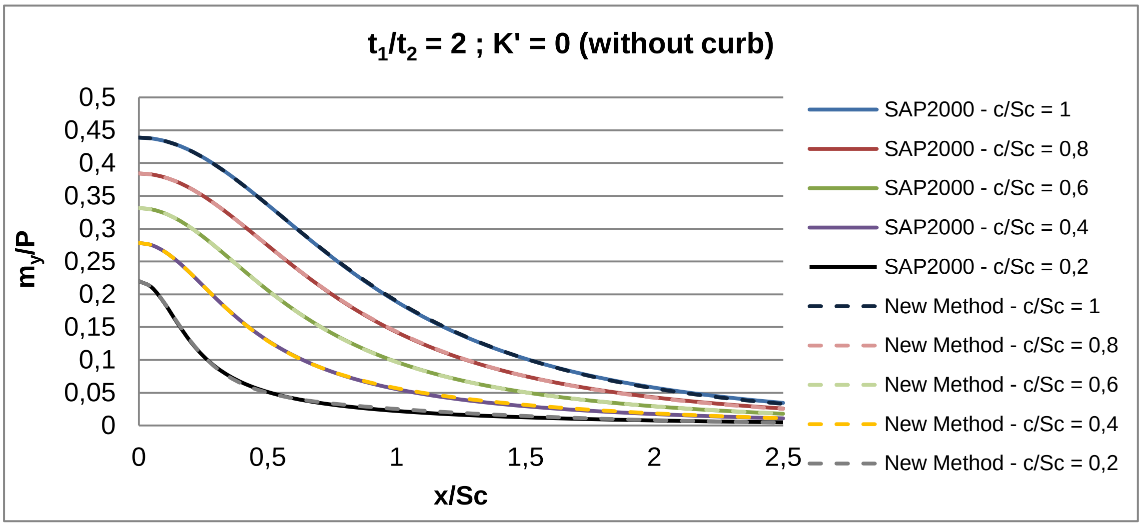

Figure 3.23 - Comparison between the results provided by the new semi-analytical method and by a finite element analysis for a thickness variation ratio t_1/t_2 = 2 and for five load positions, without edge-stiffening

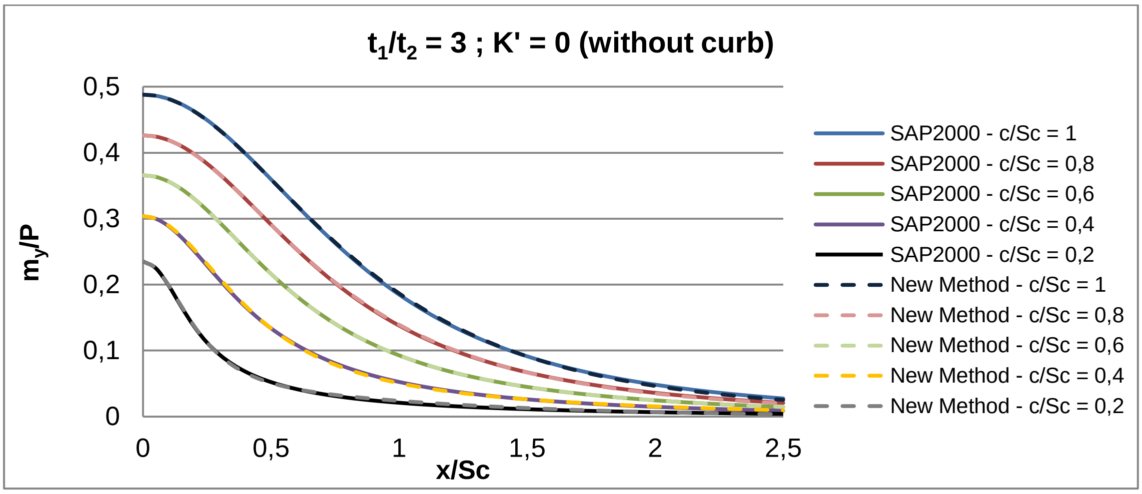

Figure 3.24 - Comparison between the results provided by the new semi-analytical method and by a finite element analysis for a thickness variation ratio $t_1/t_2 = 3$ and for five load positions, without edge-stiffening

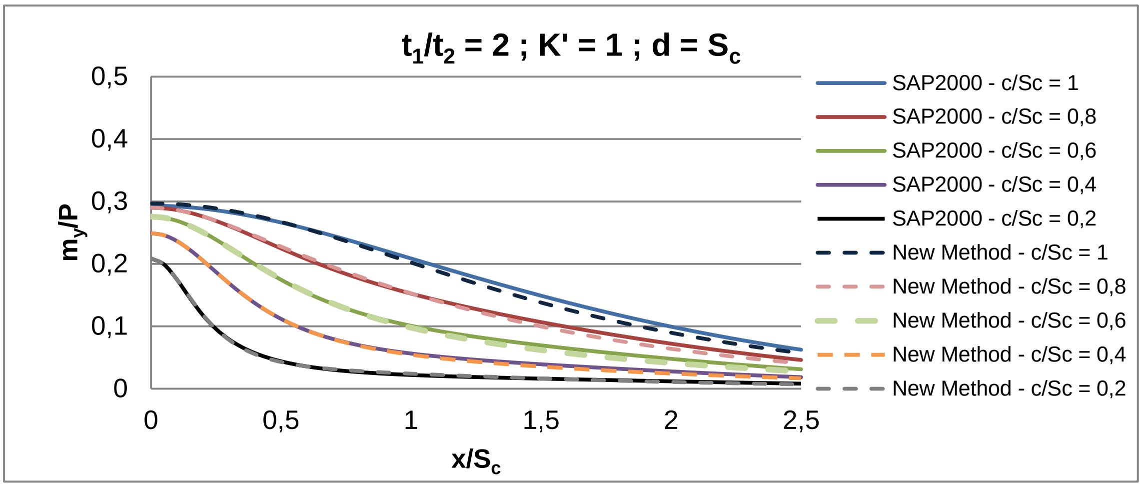

Figure 3.25 - Comparison between the results provided by the new semi-analytical method and by a finite element analysis for a thickness variation ratio $t_1/t_2 = 2$ and for five load positions, with a curb located at the edge of the cantilever and a factor K' = 1

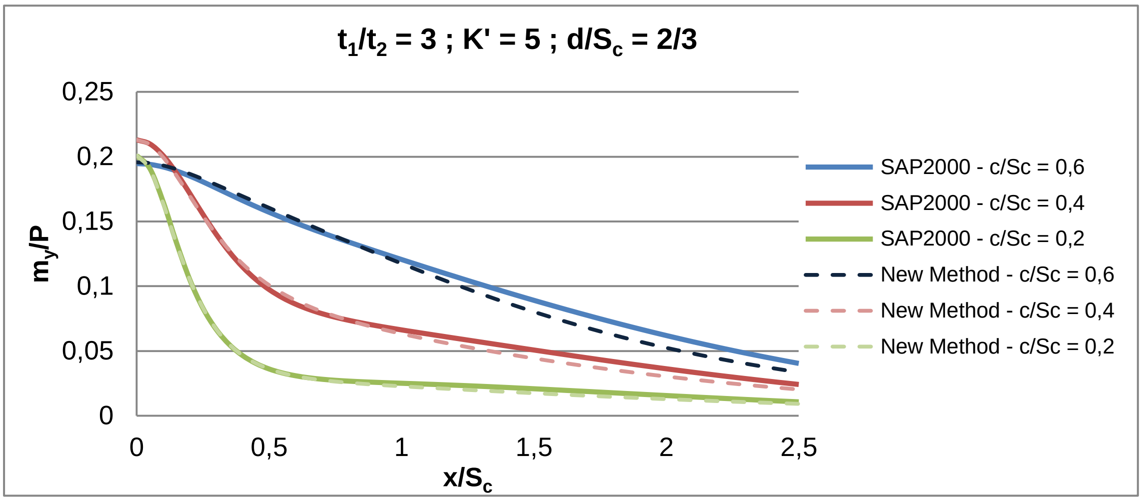

Figure 3.26 - Comparison between the results provided by the new semi-analytical method and by a finite element analysis for a thickness variation ratio $t_1/t_2 = 3$ and for five load positions, with a curb located at a distance d = 2/3 of S_c from the clamped end and corresponding to a factor K' = 5

This new semi-analytical method (Eq. (3.5)), by considering more coefficients than Bakht methods presented in [10] and in [14] (four instead of one), allows to have a better adjustment of the transverse moments distribution curves to the ones obtained from a finite element analysis, providing better solutions.

3.2.5 – Application of the new method to the analysis of knife-edge loads

It was not found in the literature research anything about simplified methods to analyze the slab transverse moments due to knife-edge loads. Therefore, it was proposed the use of a group of equivalent concentrated loads in order to be possible the application of the semi-analytical method represented by Eq. (3.5).

This equivalence was evaluated by performing a finite element analysis: two clamped cantilever models with t_1/t_2 = 1 and 2, both with S_c = 3 m and admitting a full fixed support for the overhangs were acted by: (i) a knife-edge load of 100 kN/m and by (ii) five equivalent concentrated loads of 60 kN, as illustrated in Figure 3.27. The distributions of transverse moments obtained are presented in Figure 3.28.

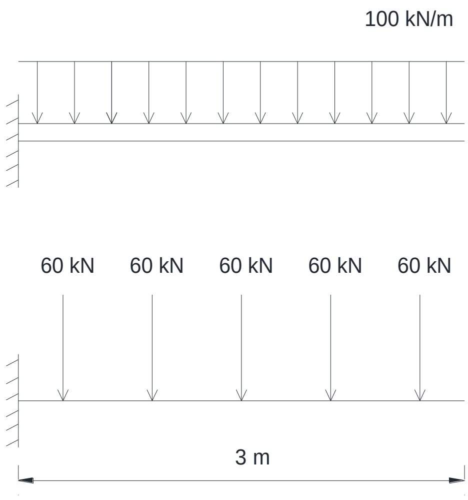

Figure 3.27 - Knife-edge load and the equivalent group of five concentrated loads acting on a clamped cantilever

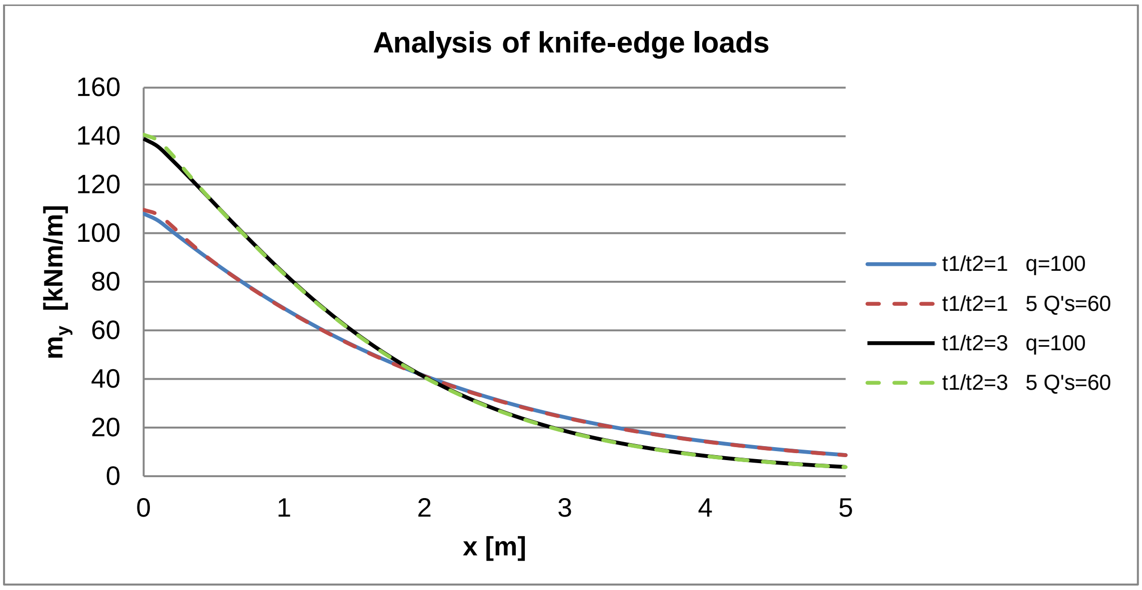

Figure 3.28 - Comparison between the distributions of transverse moments caused by a knife-edge load and by five equivalent concentrated loads

The distributions of m_y for the knife-edge load and for the five concentrated loads are very similar for both cases of t_1/t_2, as can be observed in Figure 3.28. Therefore, the transverse moments along the support of a cantilever caused by knife-edge loads can be evaluated by using the semi-analytical method presented in the previous section (Eq. (3.5)) by admitting an equivalent group of concentrated loads.

3.3 Internal panels under wheel loads

3.3.1 – Presentation of the studied parameters and respective nomenclature

The analysis of the bridge concrete slab due to wheel loads acting on the internal panel is presented in this section. The transverse bending moments at the mid-span of the internal panel of the bridge deck are evaluated using an analytical method and the moments along the longitudinal supports of the slab are evaluated using a semi-analytical method, developed in this chapter and similar to the one presented in section 3.2 (Eq. (3.5)) for cantilever loads.

In addition to the parameters already identified in section 3.2 regarding the cantilever behavior, the thickness variation of the internal slab through the introduction of brackets and the loading area of the vehicle wheels were also considered for the evaluation of the transverse moments.

The two parameters evaluated regarding the thickness variation of the internal slab through the introduction of brackets correspond to: (i) the length of the bracket compared with the internal span (c'/S) and the relation between thicknesses (t_1/t_3). A cross-section type is represented in Figure 3.29.

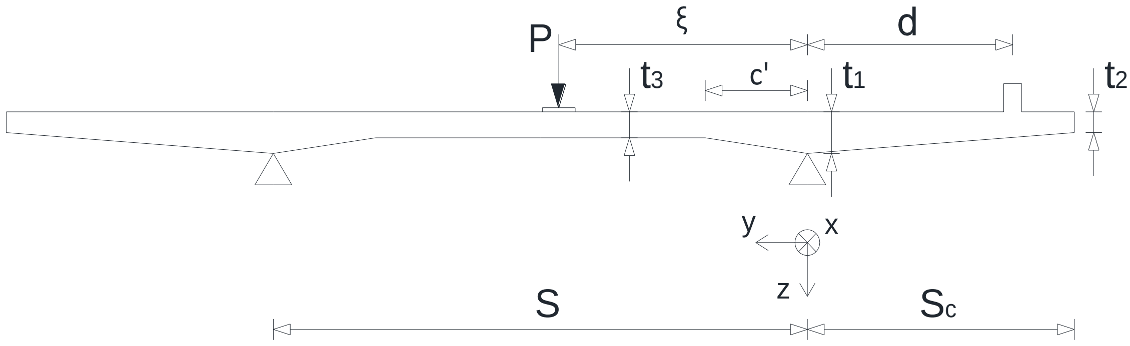

Figure 3.29 - Bridge deck cross-section type with the respective nomenclature

In the analyses the Poisson effect was neglected since the concrete was assumed as cracked.

The influence of the loading area was evaluated considering a uniform load distributed in an area of *u* x *v* (Figure 3.30), which represents the action of a vehicle wheel.

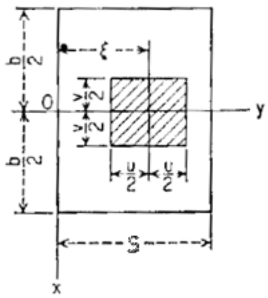

Figure 3.30 - Nomenclature for the use of Timoshenko's solution (Figure adapted from [4], with the axis x and y switched from the original)

3.3.2 – Evaluation of the relevant parameters for the analysis of transverse moments in the internal slab

The transverse moments at the mid-span of the internal slab are evaluated in this section. Although the significant importance of the longitudinal moments, as can be observed by comparing the Figures 3.31 and 3.32, these bending moments were not studied in this work.

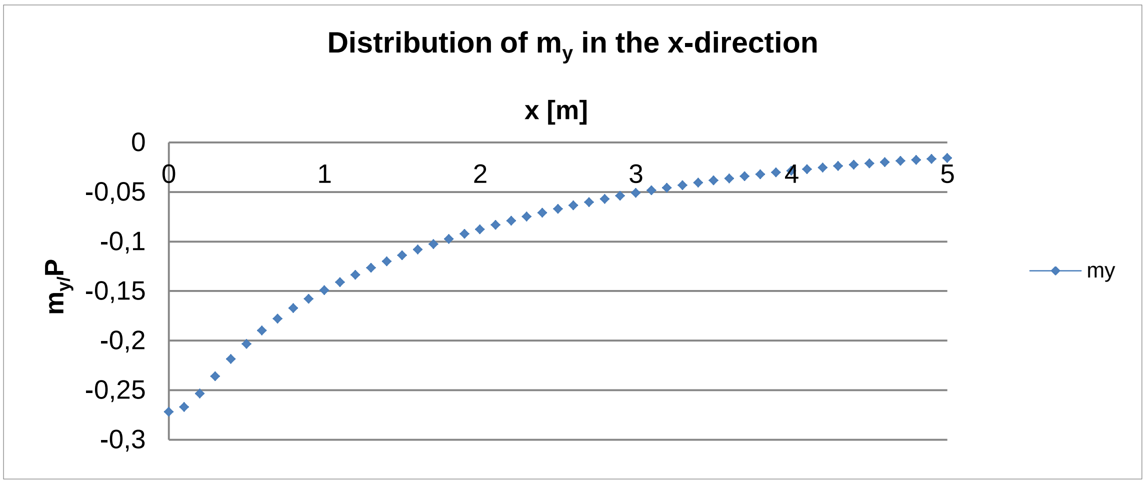

Figure 3.31 - Distribution of transverse moments m_y at the mid-span of the internal panel

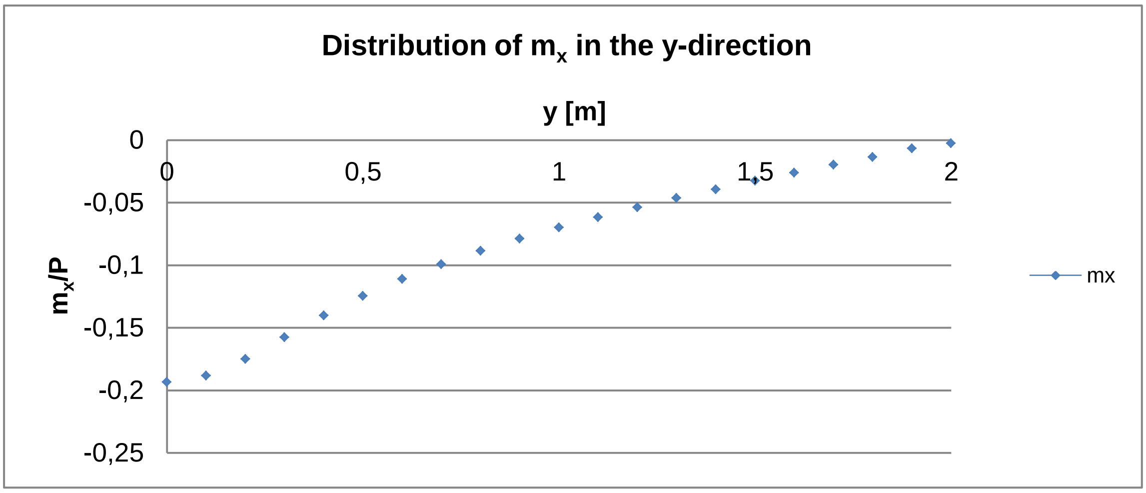

Figure 3.32 - Distribution of longitudinal moments m_x at the mid-span of the internal panel

The proposed analytical method for the analysis of the transverse moments in the internal slab due to vehicle loads is a solution presented by Timoshenko in [4], as follows:

For the calculation of the bending moments in any point of the slab for which $|x| \geq v/2$, we have the following expression:

$$m_y = \frac{qS}{\pi^2}\sum_{m=1}^{\infty}\frac{1}{m^2}\sin\left(\frac{m\pi\xi}{S}\right)\sin\left(\frac{m\pi u}{2S}\right)\sin\left(\frac{m\pi y}{S}\right)\left\{\left[\frac{2S}{m\pi}+(1-\nu)\left(x-\frac{v}{2}\right)\right]e^{-\frac{m\pi(2x-v)}{2S}} - \left[\frac{2S}{m\pi}+(1-\nu)\left(x+\frac{v}{2}\right)\right]e^{-\frac{m\pi(2x+v)}{2S}}\right\} \tag{3.15}$$

Now, to obtain the moments in the points of the plate for which *x* = 0, the following expression should be used:

$$m_y = \frac{4qS^2}{\pi^3}\sum_{m=1}^{\infty}\frac{1}{m^3}\sin\left(\frac{m\pi\xi}{S}\right)\sin\left(\frac{m\pi u}{2S}\right)\sin\left(\frac{m\pi y}{S}\right)\left\{1-\left[1+(1-\nu)\frac{m\pi v}{4S}\right]e^{-\frac{m\pi v}{2S}}\right\} \tag{3.16}$$

It should be noticed that Timoshenko's solution [4], represented by Equations (3.15) and (3.16) and used in the comparative analysis between the RSA [3] and the Eurocode [2] regarding the transverse moments in the internal slab, does not take into account the major of the parameters studied. However, the loading dimensions (*u* x *v*) and the internal panel length in the transverse direction (*S*) are considered.

Regarding the transverse bending moments in the internal slab, the torsional stiffness of the beams was the first parameter evaluated, being represented by a coefficient K, the same used for cantilever loads (Eq. 3.2).

A cross-section of a bridge with a longitudinal span length L = 24 m, with the geometry represented in Figure 3.29 but without the overhangs and with S = 4 m was analyzed using a finite element model.

The distributions of transverse moments were calculated at the sections y = S/2 and y = S/4 corresponding to the load positions ξ/S = 0.5 and ξ/S = 0.25, respectively by a finite element model. The analyses considered the cases with K = 0, neglecting the torsional stiffness of the beam, and with K = 0.5, 1.0 and 2.0.

The bending moment distributions obtained through this analysis are presented in Figures 3.33 and 3.34.

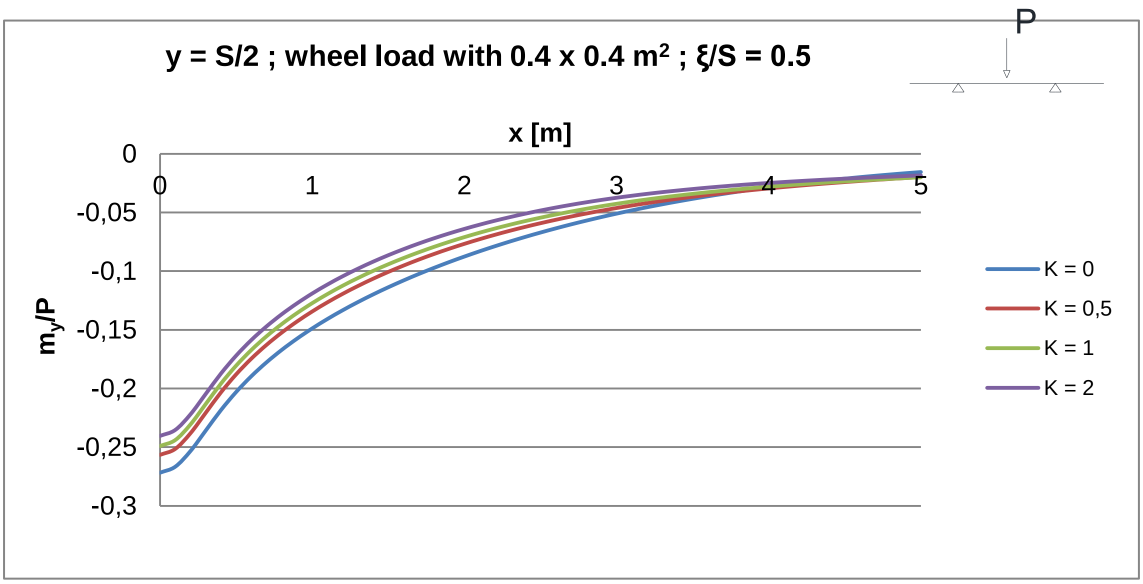

Figure 3.33 - Influence of the torsional stiffness of the longitudinal beams on the distributions of transverse moments for a load position ratio ξ/S = 0.5

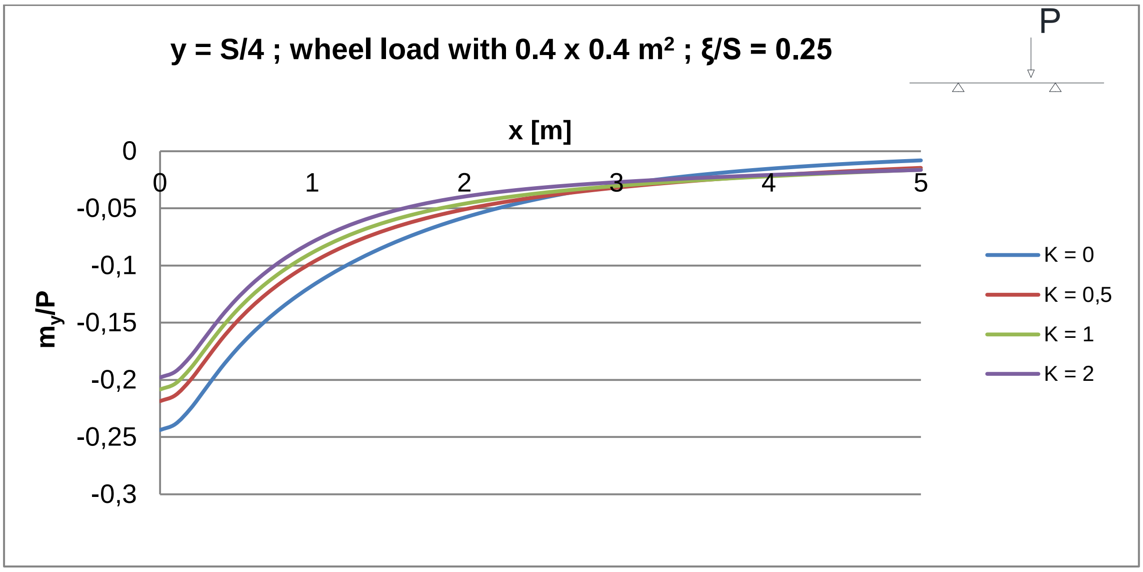

Figure 3.34 - Influence of the torsional stiffness of the longitudinal beams on the distributions of transverse moments for a load position ratio ξ/S = 0.25

From the Figures 3.33 and 3.34 it can be concluded that the beam torsional stiffness doesn't have a significant influence on the distribution of transverse bending moments in the slab, and that for K = 0 (which is the assumption adopted in the Timoshenko solution [4]) the results are, as expected, always conservative.

Towards the evaluation of the influence on the distributions of moments of the flexural stiffness of the beams where the deck slab is supported, the bridge model represented in Figures 3.9 and 3.10 was analyzed. This bridge model consists on a multi-span continuous bridge with span lengths L = 30 m, with an overhang length S_c = 3 m and with an internal span S = 7.5 m. The moment of inertia of the longitudinal beam taken as reference is $I_y = 0.9444\ m^4$ (Figure 3.10), being the distributions of the flexural moments in the internal panel obtained through a finite element analysis also by adopting different longitudinal stiffness: for 2.0Iy, for 0.5Iy and for approximately infinite rigidity.

It was considered a wheel load with 0.4 x 0.4 m^2 acting at the mid-span of the bridge and with a transversal positioning corresponding to ξ/S = 0.5. The results are presented in Figure 3.35.

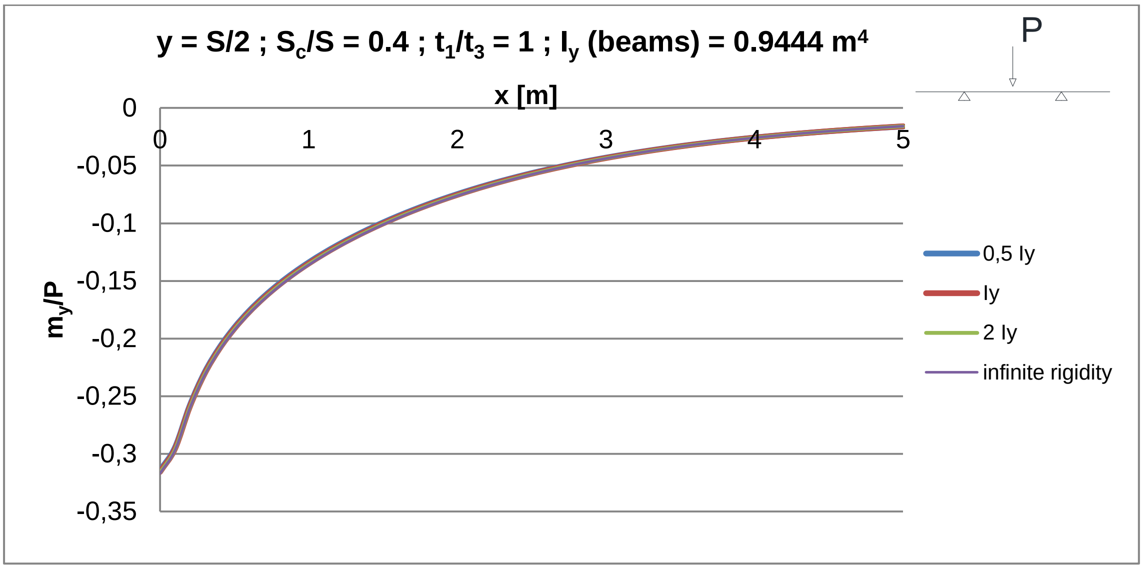

Figure 3.35 - Influence of the flexural stiffness of the longitudinal beams on the distributions of transverse moments for a load position ratio ξ/S = 0.5

As it can be observed in Figure 3.35, the influence of the longitudinal flexural stiffness of the beams in distributions of transverse moments on the internal slab is practically none.

The overhangs can contribute for the stiffness of the internal panel in the transverse direction. The structural influence of the overhangs was then evaluated through the analysis of a finite element model representing a bridge deck with S = 4 m submitted to a wheel load with 0.4 x 0.4 m^2. This load was considered as acting on the transverse positions ξ/S = 0.5 and ξ/S = 0.25. It can be concluded from Figures 3.36 and 3.37 that this parameter is not relevant for the transverse moments in the internal slab.

The Timoshenko's solution [4] was also represented in Figures 3.36 and 3.37, in order to verify that it corresponds to an appropriate approximation of the values obtained from the finite element analysis. However, it should be noticed that Timoshenko presents a solution divided into two parts (see Eq. (3.15) and Eq. (3.16)): the first one corresponds to the moments under the center of the load area, and the second one represents the distribution of m_y outside the load area. This fact means that the transverse moments between the center of the loading area and its boundary are not provided by Timoshenko's solution [4].

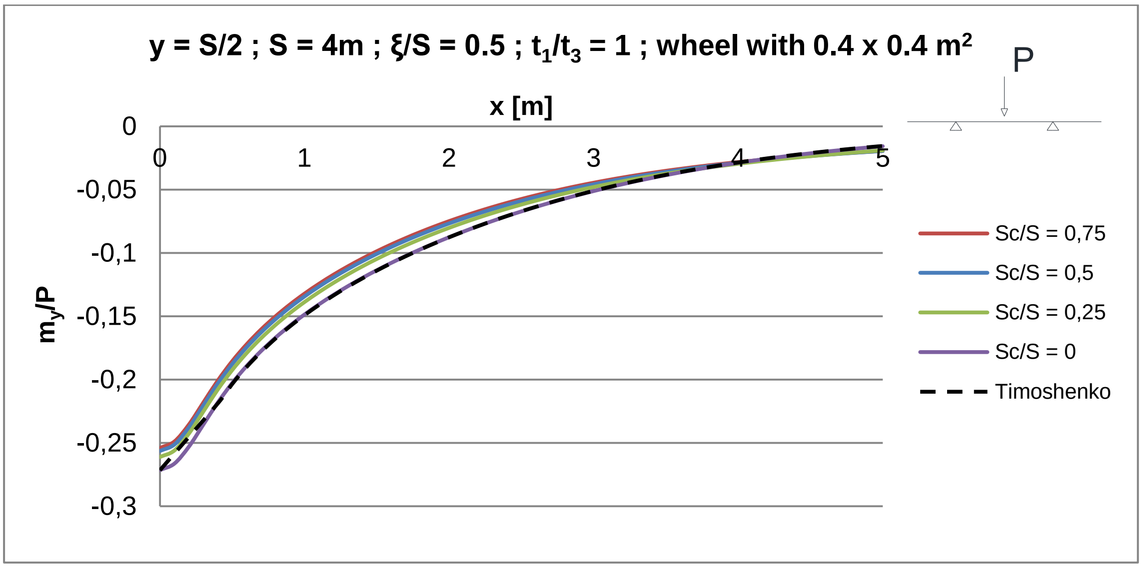

Figure 3.36 - Influence of the relation between the cantilever length and the internal span (S_c/S) on the distributions of transverse moments for a load position ratio ξ/S = 0.5

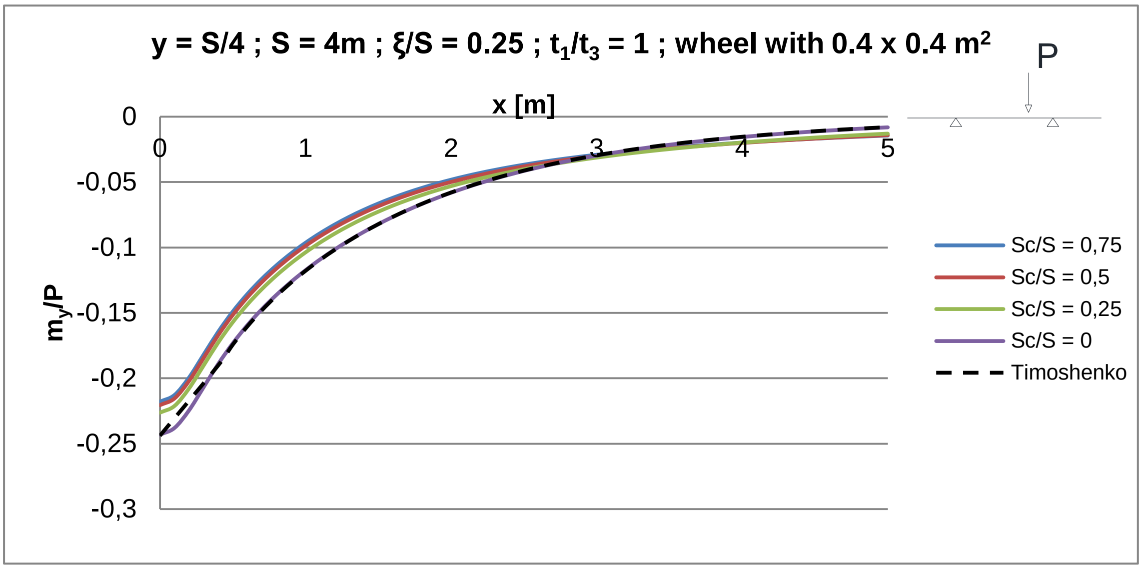

Figure 3.37 - Influence of the relation between the cantilever length and the internal span (S_c/S) on the distributions of transverse moments for a load position ratio ξ/S = 0.25

Since the cantilevers introduce minimal effects on the transverse moments in the internal slab, the effects of their thickness variation or even the existence of curbs was disregarded. Hence, the corresponding influence was not evaluated for this type of flexural moments.

Regarding the thickness variation verified in the internal panels, normally in the form of brackets, there are two distinct parameters to evaluate: the relation t_1/t_3, which represents the difference of thicknesses, and the relation c'/S, which represents the length of the brackets in comparison with the internal span.

In order to evaluate the influence of the bracket length through the relation c'/S, the analysis of the internal slab was performed by admitting a thickness variation for the bracket corresponding to t_1/t_3 = 2. The internal slab was modeled through a simply supported model since it was already considered that the structural influence of the cantilevers and of the torsional stiffness of the beams can be neglected.

The bridge model has a deck slab with 30 m length and 4 m width, acted by a wheel load with 0.4 x 0.4 m^2 at the mid-span, for the following four ratios c'/S: 0, 0.2, 0.25 and 0.33. The results can be observed in Figure 3.38.

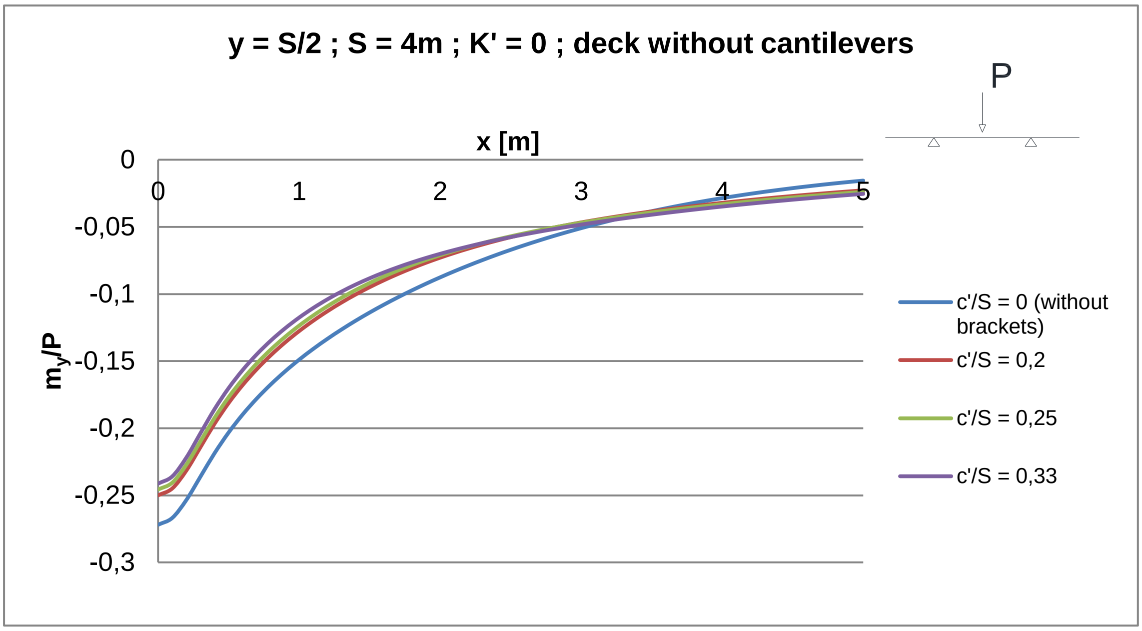

Figure 3.38 - Influence of the length of the brackets related with the internal span (c'/S) on the distributions of transverse moments for a load position ratio ξ/S = 0.5

It is verified that this parameter can be conservatively disregarded. In fact, the difference from the peak values of m_y/P both for c'/S = 0.00 and c'/S = 0.33 is approximately 12% in this case.

To evaluate the relevance of the thickness variation along the bracket through the ratio t_1/t_3, the beam-slab deck was analyzed considering the wheel load positioned at ξ/S = 0.5 and ξ/S = 0.25 for a bracket length corresponding to c'/S = 0.25. The analysis was performed through the finite element method by considering three sets of thickness variations t_1/t_3: 1.0, 1.5 and 2.0. The results of this analysis are presented together with Timoshenko's solution [4] in Figure 3.39 and 3.40.

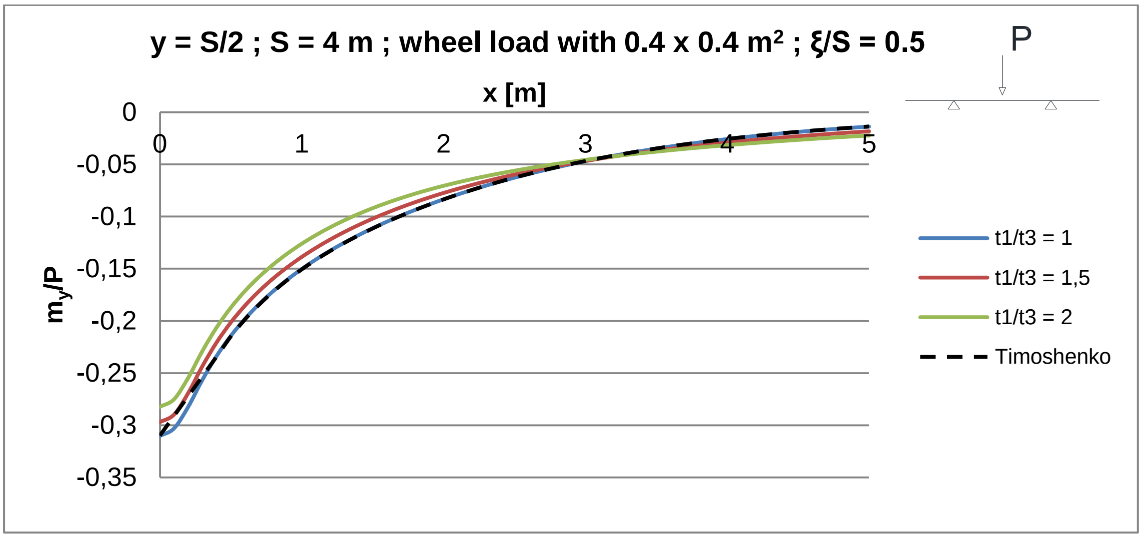

Figure 3.39 - Influence of the thickness variation of the brackets at the internal slab (t_1/t_3) on the distributions of transverse moments for a load position ratio ξ/S = 0.5

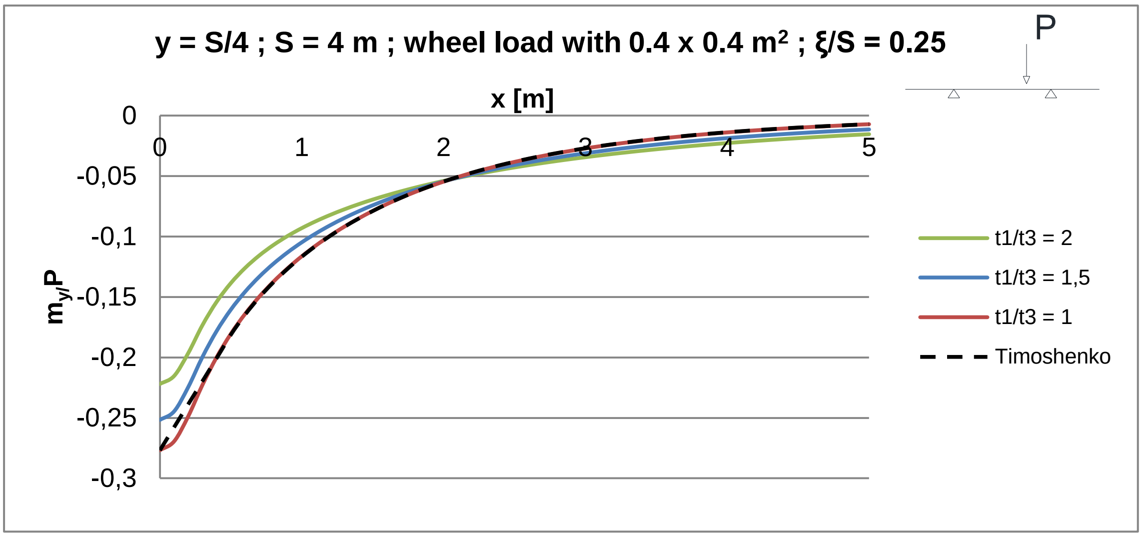

Figure 3.40 - Influence of the thickness variation of the brackets at the internal slab (t_1/t_3) on the distributions of transverse moments for a load position ratio ξ/S = 0.25

It can also be observed from Figures 3.39 and 3.40 that admitting a constant thickness for the internal slab is conservative for the domain of the *x*-axis closer to zero (near the load). For loads closer to the beams the influence of this parameter is more relevant and the assumption of t_1/t_3 = 1 for all cases can become too conservative, being the difference between the maximum values for t_1/t_3 = 1 and t_1/t_3 = 2 approximately 25% for the load case with ξ/S = 0.25. However, Timoshenko's solution [4] neglects those parameters and it was verified that the use of Eq. (3.15) and Eq. (3.16) for the analysis of transversal moments due to vehicle loads in the internal slab provides always conservative results.

3.3.3 – Application of Timoshenko's solution in cases with knife-edge loads

The analysis of the internal slab submitted to knife-edge loads can be performed through the solution presented by Timoshenko (Eq. (3.15) and Eq. (3.16)) [4]. In fact, the loading area dimensions (u and v) can be set as u = S (the overall width of the deck) and $v = t_3$, which corresponds to reference the load to the slab middle surface.

A bridge deck with a span length of 30 m and a cross-section with a width of 4 m and a thickness of 40 cm subjected to a knife-edge load p = 100 kN/m was analyzed both through a finite element model and by using Timoshenko's analytical solution. The results are presented in Figure 3.41 in terms of transverse bending moment distributions. A good agreement can be verified between the results obtained.

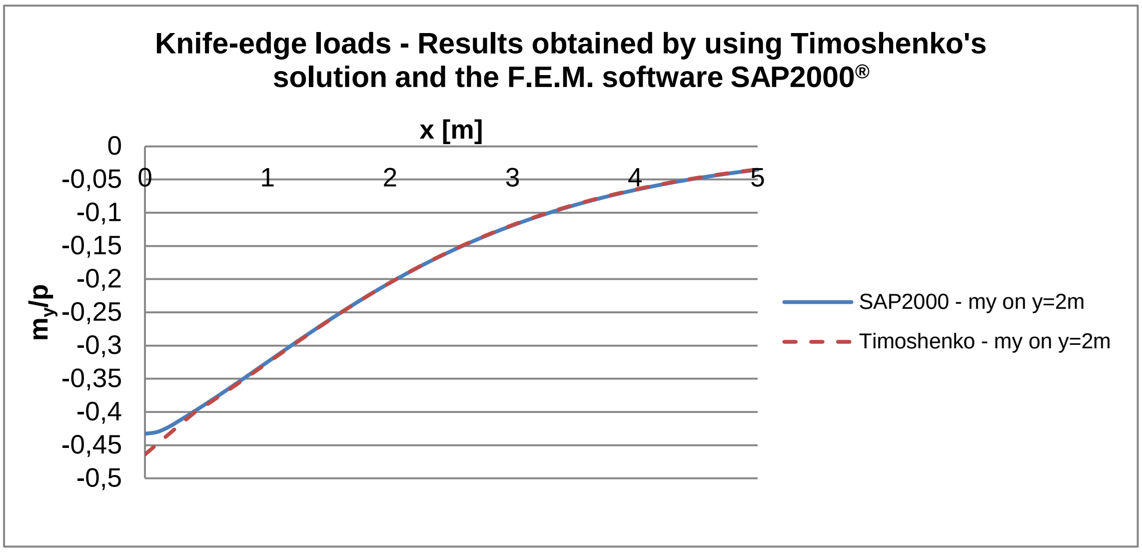

Figure 3.41 - Comparison between the distributions of transverse moments due to a knife-edge load obtained through a finite element analysis and by using Timoshenko's solution [4]

3.3.4 – Evaluation of the parameters related with the transverse moments over the beams due to internal panel loads

The parameters analyzed that can have an influence on the longitudinal distribution of the slab transverse bending moments over the beams are: (i) the loading area size, (ii) the torsional stiffness of the beams, (iii) the longitudinal flexural stiffness of the beams, (iv) the stiffness of the slab considered indirectly through the ratio S_c/S, (v) the thickness variation of the cantilever slab, (vi) the edge stiffening and the position of the respective curbs in the overhangs and (vii) the thickness variation in the internal slab through the form of brackets.

To evaluate the influence of the loading area on the transverse moments obtained over the longitudinal supports of the deck slab, some analyses of a finite element model with a geometry corresponding to $S_c/S = 0.5$, $t_1/t_2 = 2$ and different relations t_1/t_3 were made.

The analyses consisted on having several wheel loads with different areas acting on the mid-span of the internal panel (ξ/S = 0.5), providing therefore the respective maximum values for these moments.

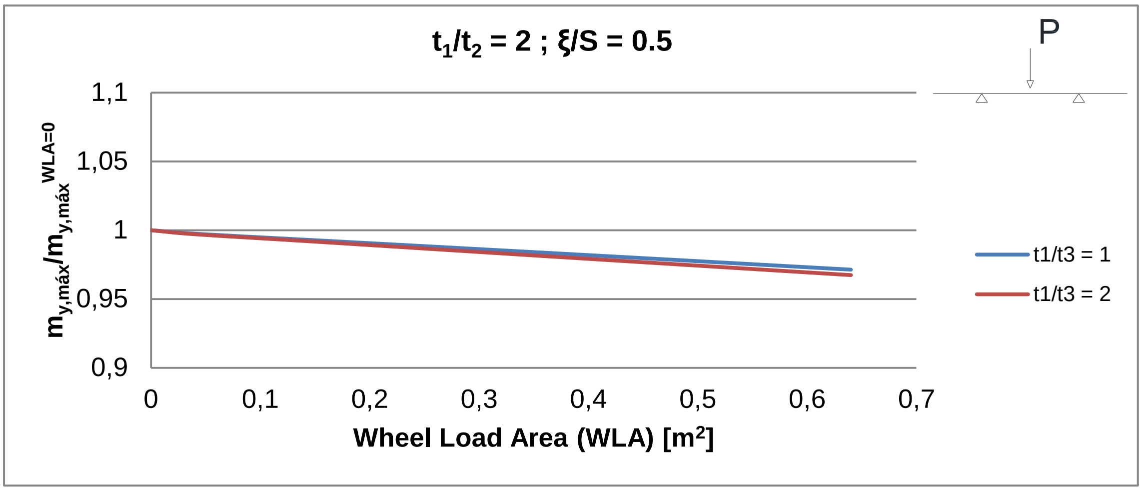

Figure 3.42 - Influence of the wheel load area on the maximum transverse moments for two cases of thickness variation in the brackets of the internal slab (t_1/t_3)

In Figure 3.42 the relation between the maximum moments ($m_{y,máx}$) for the different wheel areas considered and the higher value of these maximum moments ($m_{y,máx}^{WLA=0}$), corresponding to a concentrated load, is represented. It can be observed that the load dimensions do not influence significantly these peak values. Therefore, point loads instead of loads distributed in a wheel area were conservatively used in the following analyses.

The torsional stiffness of the beams, already referred regarding the cantilever loads in section 3.2, was neglected due to the following facts: (i) the beams are usually not designed to resist to torsional forces and (ii) the concrete is considered as cracked, which reduces drastically the torsional stiffness of a concrete beam.

For the evaluation of the influence of the longitudinal beam's flexural stiffness on the transverse moments over the beams due to internal panel loads, the bridge model represented in Figures 3.9 and 3.10 was adopted. It was admitted a ratio $S_c/S = 0.4$, constant thickness in the internal slab and the following values for the moment of inertia of the longitudinal beams, taking as reference $I_y = 0.9444$ m4: $0.5I_y$, I_y, $2.0I_y$ and infinite stiffness. The results are presented in Figure 3.43.

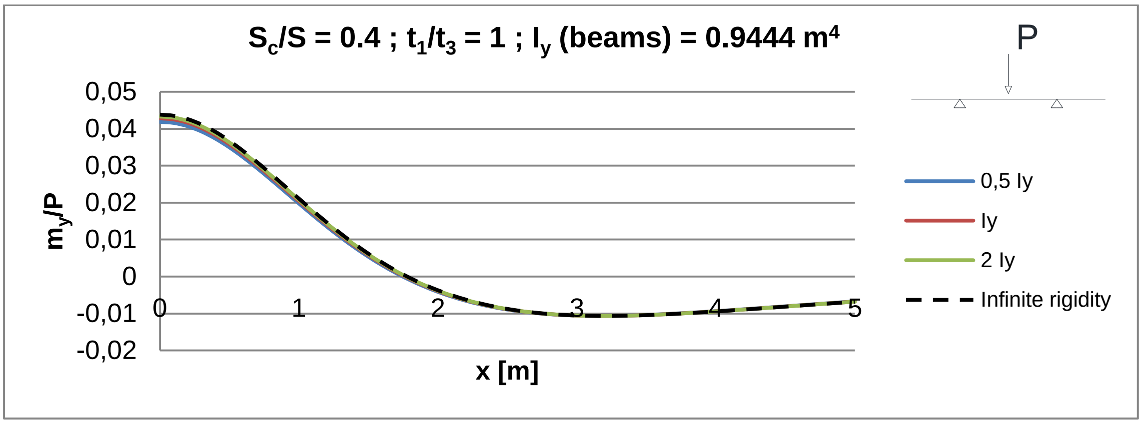

Figure 3.43 - Influence of the flexural stiffness of the longitudinal beams on the distributions of transverse moments for a load position ratio ξ/S = 0.5

As it can be observed in Figure 3.43, the influence of the beam flexural stiffness can be ignored for the evaluation of the slab transverse moments over the longitudinal supports of the deck slab, since the differences between the distributions of Figure 3.43 are neglectable. This flexural stiffness was then admitted as infinite in the sequel.

As previously referred, since the torsional rigidity of the beams is disregarded, the reason for the appearance of transverse moments over the beams is the existence of overhangs.

Therefore, an evaluation of the overhang characteristics influence on the slab structural behavior was performed by considering: (i) the length of the overhangs through the ratio S_c/S, (ii) the thickness variation of the cantilever slab and (iii) the existence of curbs (edge-stiffening).

In order to evaluate the influence of the overhang length, three solutions corresponding to ratios of S_c/S = 0.5, 0.25 and 0.125, here with a fixed internal panel length S = 4 m and a constant thickness were analyzed through a finite element analysis. The three distributions of transverse moments obtained in this analysis are presented in Figure 3.44.

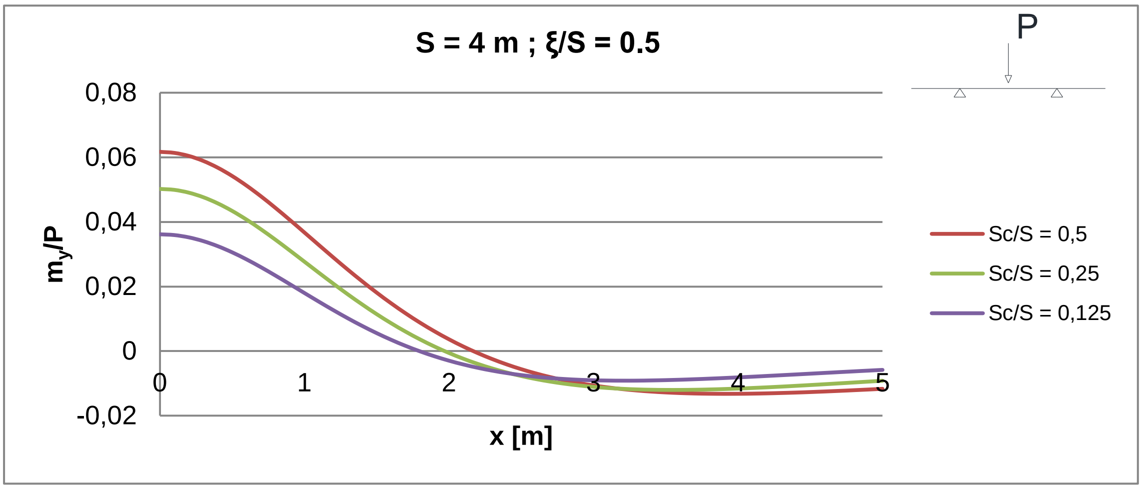

Figure 3.44 - Influence of the relation between the cantilever length and the internal span (S_c/S) on the distributions of transverse moments for a load position ratio ξ/S = 0.5

The stiffness introduced by the cantilever increases with its length compared to the internal panel span. As a consequence, the transverse moments created by the same load at the same position also increase, requiring more reinforcement in this zone of the deck slab, being the ratio S_c/S an essential parameter for the analysis of these internal forces.

In order to evaluate the importance of the thickness variation in the cantilever slab, three finite element models with a relation $S_c/S = 0.5$ for S = 4 m were analyzed, corresponding to three different thickness variations of the cantilevers: t_1/t_2 = 1, 2 and 3, respectively. The results of this analysis are presented in Figure 3.45.

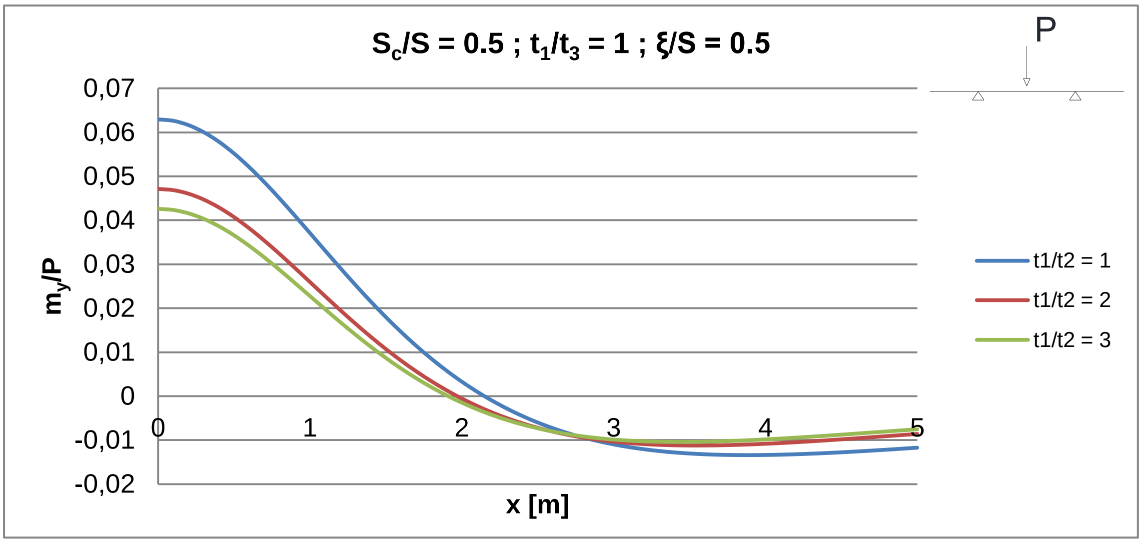

Figure 3.45 - Influence of the thickness variation of the cantilever slab (t_1/t_2) on the distributions of transverse moments for a load position ratio ξ/S = 0.5

It can be observed in Figure 3.45 that the transverse moments that appear over the beams are smaller for greater thickness variations of the cantilever slab, being the differences observed significant.

For the evaluation of the edge-stiffening effect, similar finite element models considering a ratio S_c/S = 0.5 with S = 4 m were analyzed, but now only with t_1/t_2 = 1; the solution without curbs was compared with two solutions where the cantilever has an edge-beam corresponding to K' = 1 and K' = 5 (Eq. (3.1)). The distributions of transverse moments obtained by applying the load on ξ/S = 0.25 and on ξ/S = 0.5 are represented in Figure 3.46.

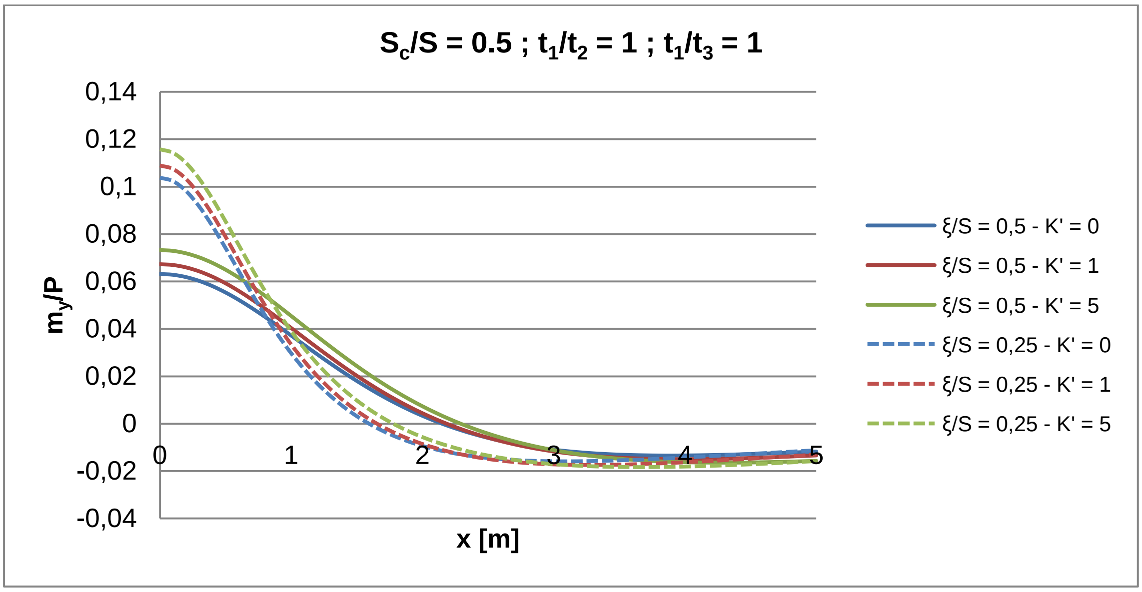

Figure 3.46 - Influence of edge-stiffening on the distributions of transverse moments for two load positions

The influence of the curbs and the respective flexural stiffness represents a small variation for both load cases considered as it is shown in Figure 3.46, but it is non-conservative to neglect this effect; thus, this parameter should also be taken into account in the analysis of edge-stiffened bridge decks.

In order to simplify the evaluation of the transverse bending moments over the longitudinal supports through a semi-analytical method, some ideas to reduce the important parameters were analyzed.

In what concerns the edge-stiffening in the overhangs, Mufti *et Al*. [10] refer that the calculation of hogging moments in the internal panel due to cantilever loads could be done by replacing the edge-beam for an extra length of the cantilever with the same flexural stiffness. However, for the calculation of the flexural moments over the beams due to internal panel loads, this simplification can be non-conservative, since it considers the stiffness distant from the clamped end of the cantilever. On the other hand, for certain types of curbs this simplification can lead to very high values of cantilever lengths, and consequently, to very high values of S_c/S, which means that this could complicate the method instead of simplify it.

In order to consider the thickness variation of the cantilever in the developed method an “equivalent” cantilever of uniform thickness (with equivalent moment of inertia in the transverse section) was adopted. Since the constant thickness equivalent cantilever has always a smaller length S_c than the one with a varying thickness, the resultant longitudinal stiffness is closer to the supported edge of the overhang, being expected to provide conservative and approximate values of transverse moments.

This simplification was then evaluated through the analysis of several finite element models to compare the distributions of moments obtained by using the varying thickness overhangs and the equivalent ones with constant thickness. The results are presented in Figures 3.47 to 3.52.

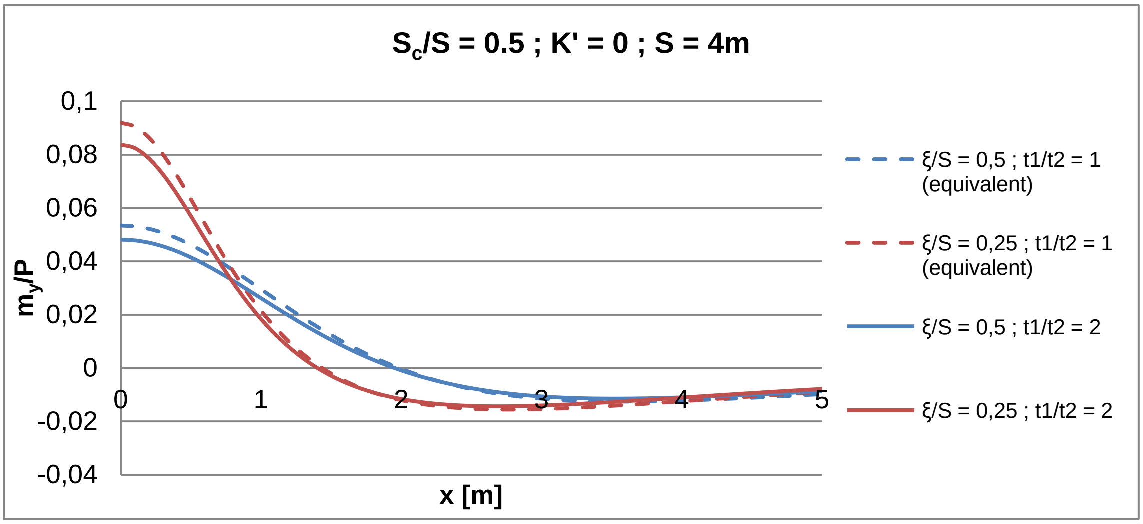

Figure 3.47 - Comparison between the distributions of transverse moments obtained by considering a thickness variation of the cantilever slab $t_1/t_2 = 2$ and by considering an equivalent cantilever slab with uniform thickness for two load positions, without edge-stiffening and with a cantilever length of 2 m

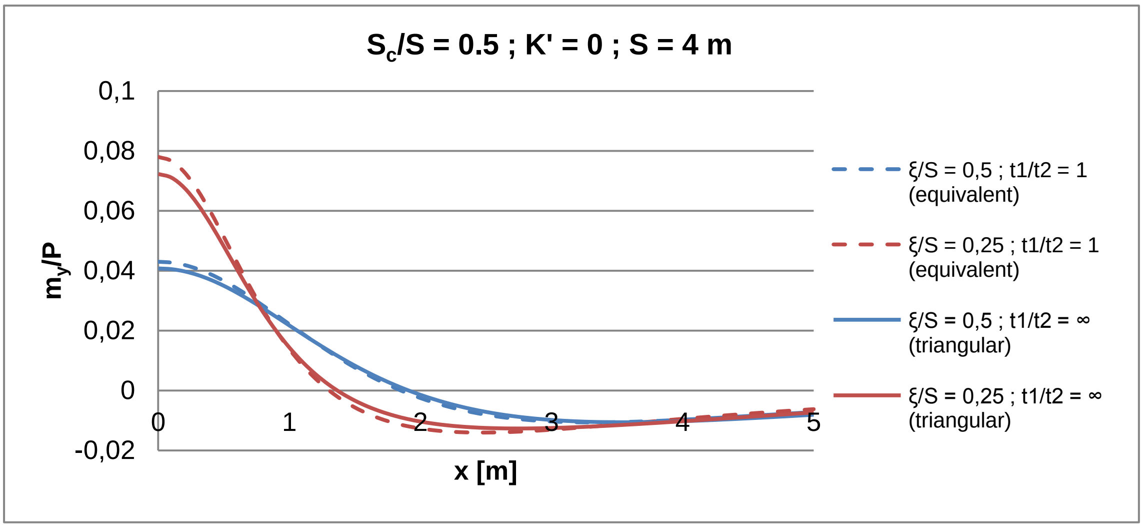

Figure 3.48 - Comparison between the distributions of transverse moments obtained by considering a thickness variation of the cantilever slab $t_1/t_2 = \infty$ (triangular) and by considering an equivalent cantilever slab with uniform thickness for two load positions, without edge-stiffening and with a cantilever length of 2 m

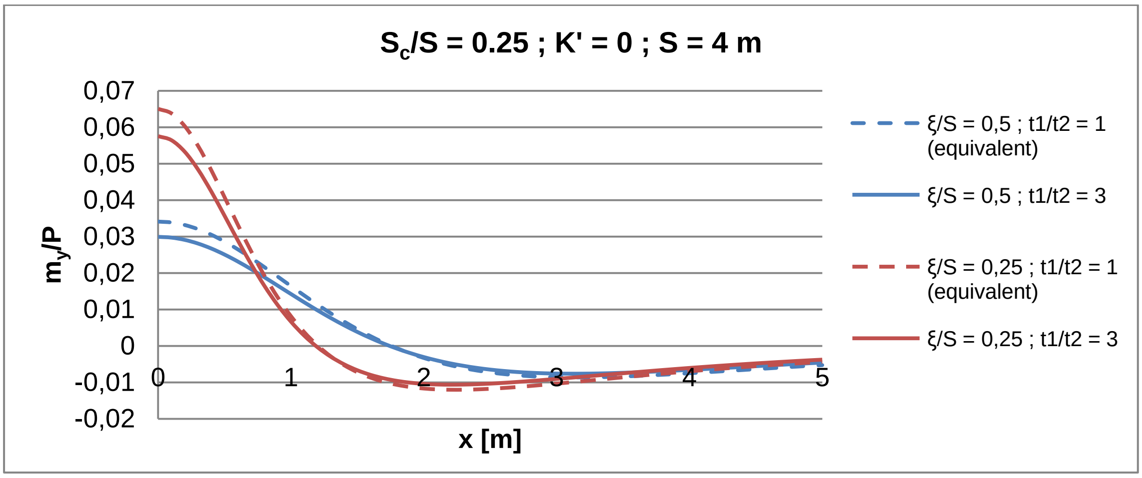

Figure 3.49 - Comparison between the distributions of transverse moments obtained by considering a thickness variation of the cantilever slab t_1/t_2 = 3 and by considering an equivalent cantilever slab with uniform thickness for two load positions, without edge-stiffening and with a cantilever length of 1 m

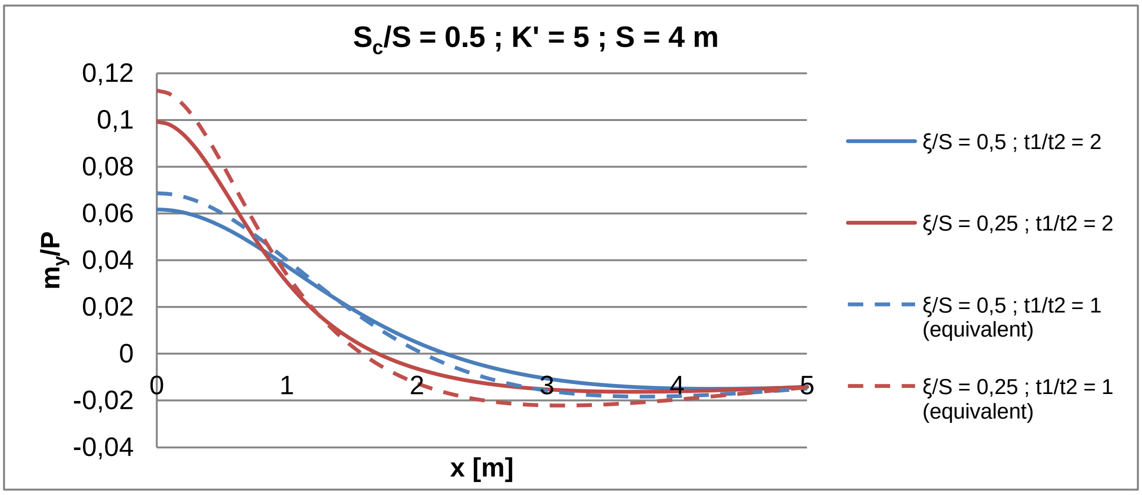

Figure 3.50 - Comparison between the distributions of transverse moments obtained by considering a thickness variation of the cantilever slab t_1/t_2 = 2 and by considering an equivalent cantilever slab with uniform thickness for two load positions, with edge-stiffening (K' = 5) and a cantilever length of 2 m

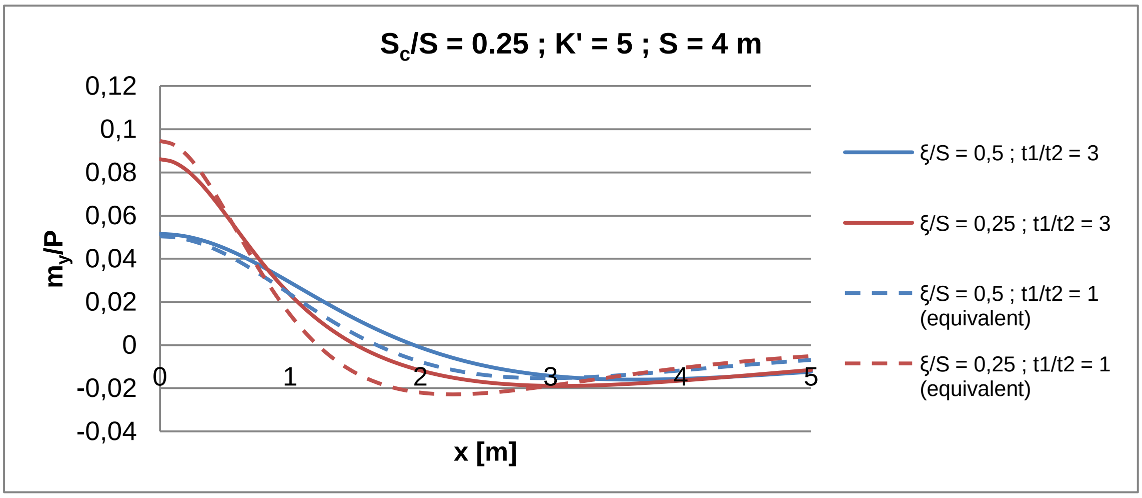

Figure 3.51 - Comparison between the distributions of transverse moments obtained by considering a thickness variation of the cantilever slab t_1/t_2 = 3 and by considering an equivalent cantilever slab with uniform thickness for two load positions, with edge-stiffening (K' = 5) and a cantilever length of 1 m

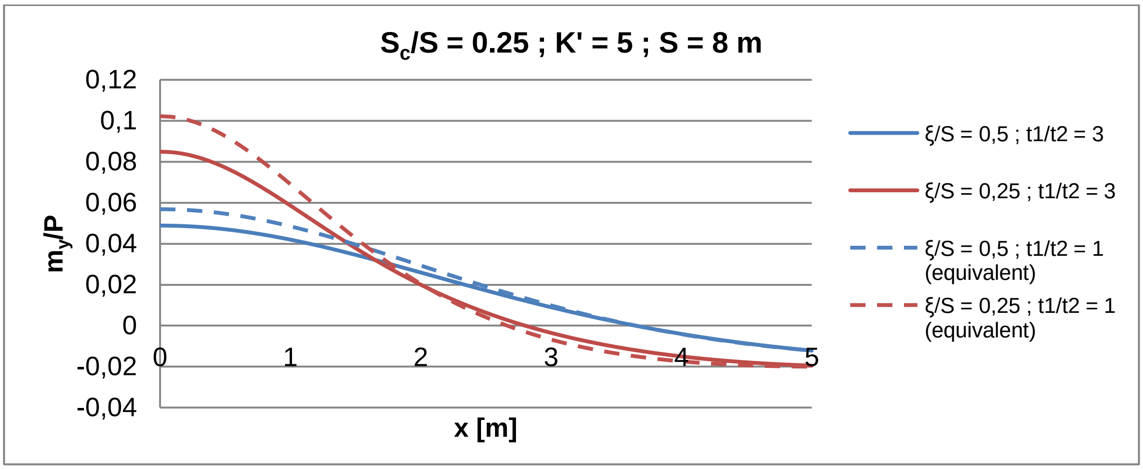

Figure 3.52 - Comparison between the distributions of transverse moments obtained by considering a thickness variation of the cantilever slab t_1/t_2 = 3 and by considering an equivalent cantilever slab with uniform thickness for two load positions, with edge-stiffening (K' = 5) and a cantilever length of 2 m

As it can be observed in Figures 3.50 to 3.52, when this simplification is applied on edge-stiffened cantilevers the results are not so good, since the moments distribution curves differ more in these cases. In fact, for smaller cantilevers (less than 1m span, as can be observed in the case of Figure 3.51), the results can even become non-conservative.

Nevertheless, this simplification was adopted to take into account the thickness variation in the cantilever slab in the evaluation of transverse moments over the beams due to internal panel loads.

The influence of the position of the curbs in the cantilever structural behavior can be observed in Figure 3.53, where the distributions of transverse moments caused by a point load acting on ξ/S = 0.25 and on ξ/S = 0.5 are represented for different positions of the curb in the overhang. A finite element model with S_c/S = 0.5 and a constant thickness in all the deck slab was used in the analysis. The curb, corresponding to a factor K' = 5, was positioned at three different positions: d/S_c = 1.00, 0.75 and 0.50.

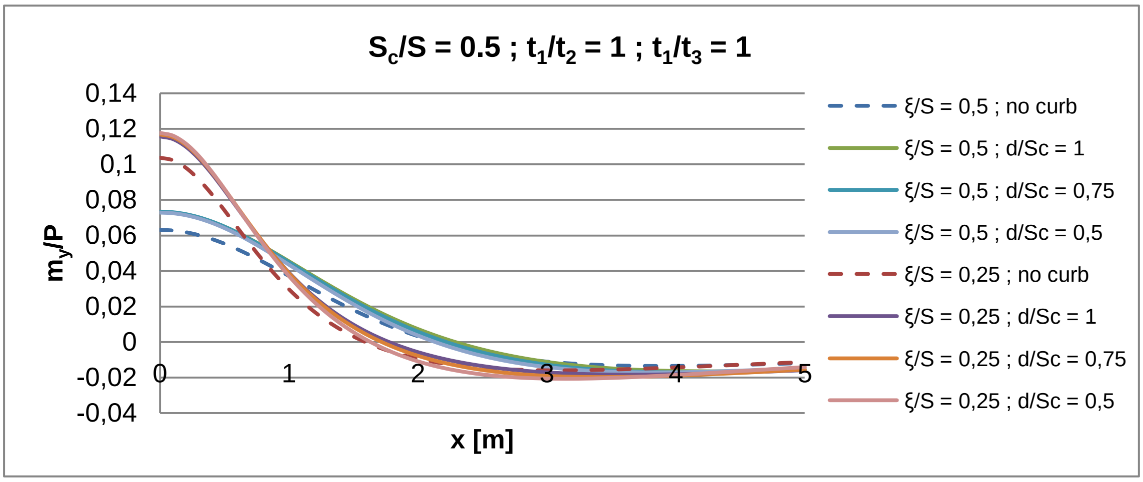

Figure 3.53 - Influence of the position of the curb at the cantilever slab (d/S_c) on the distributions of transverse moments due to internal panel loads

It can be observed in Figure 3.53 that only the case without curb corresponds to a different moment distribution, whereas the position of the curb has a small influence on the distributions of transverse moments over the beams due to internal panel loads. Thus, this parameter can be neglected in further analysis, being always considered in the edge (d/S_c = 1).

In what concerns the influence of the thickness variation in the internal slab, through the introduction of brackets, two parameters were evaluated: the thickness variation ratio (t_1/t_3) and the relation between the length of the bracket and the internal span (c'/S). The analyses were performed in finite element models considering a ratio S_c/S = 0.5 and t_1/t_2 = 1. The results are presented in Figures 3.54 and 3.55.

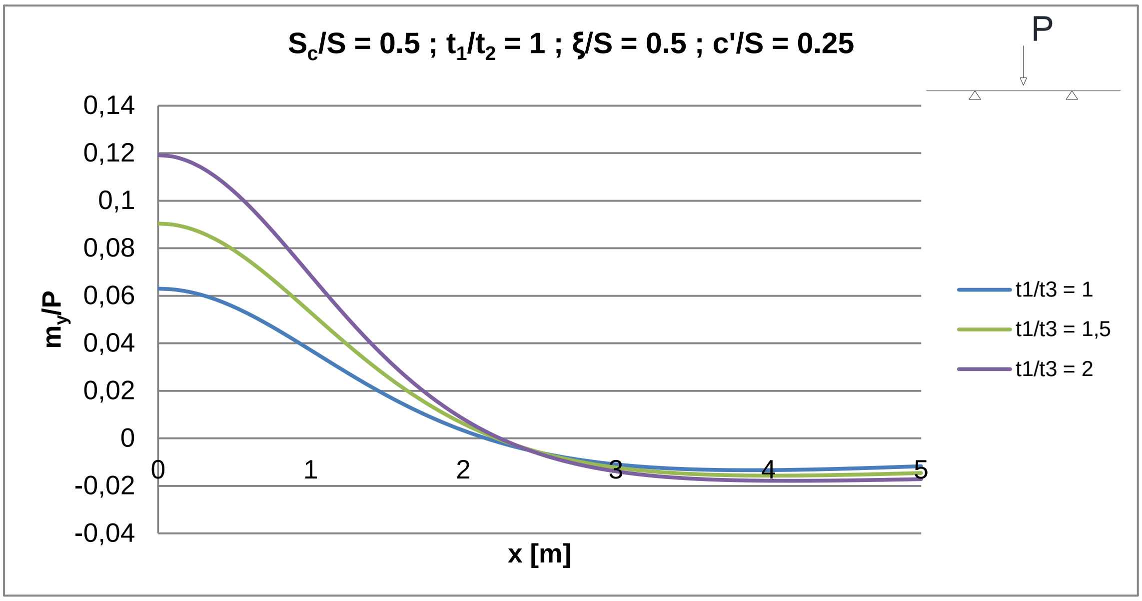

Figure 3.54 - Influence of the thickness variation of the brackets (internal slab) on the distributions of transverse moments due to internal panel loads

It can be concluded from Figure 3.54 that the influence of the bracket thickness variation is crucial. In fact, in the case of the variation of the ratio t_1/t_3 from 1 to 2, the increase of the peak value is around 100%.

The influence of the brackets length compared with the internal span was analyzed by considering a thickness variation ratio t_1/t_3 = 2, being the results presented in Figure 3.55.

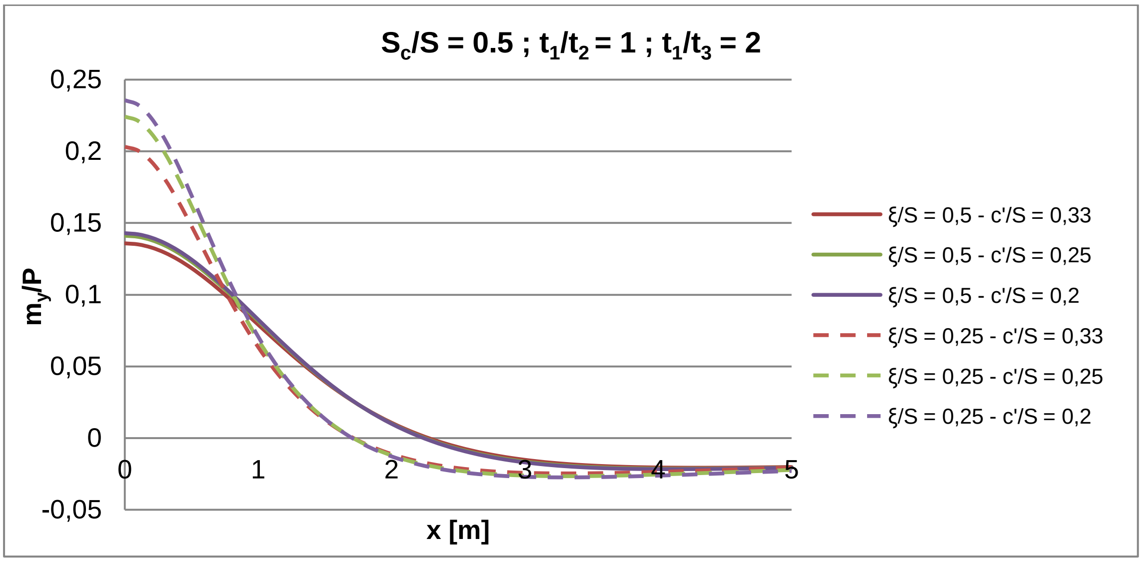

Figure 3.55 - Influence of the thickness variation of the brackets (internal slab) on the distributions of transverse moments due to internal panel loads

For the position of the load on ξ/S = 0.25 some differences in the peak values can be observed. In the sequel it was considered c'/S = 0.2 as representative, since it is conservative and it is not probable to have smaller brackets on bridge decks, being the influence of the relative length of the brackets disregarded in further analysis.

3.3.5 – Development of a semi-analytical method to analyze transverse moments over the beams due to internal panel loads

Timoshenko presents in [4] an approximated and conservative analytical solution using Fourier series to obtain the distributions of flexural moments, in both directions *x* and *y*, in the internal slab. However, to obtain the distribution of transverse moments over the beams due to loads acting on the internal panel it was not found a satisfactory simplified solution in the literature reviewed. Therefore, a method similar to the one presented for cantilever loads (Eq. (3.5)) was developed by considering a moment distribution given as follows:

$$\frac{m_y}{P} = \alpha' \frac{A'}{\pi} \frac{1}{\cosh\left(A'\left(\frac{x}{S}\right)\right)} + \beta' \frac{B'}{\pi} \frac{1}{\cosh\left(B'\left(\frac{x}{S}\right)\right)} \tag{3.17}$$

This equation provides the distributions of transverse moments with both axis non-dimensional, using the relation x/S for the abscissas axis. In order to evaluate this assumption, a finite element analysis was performed by using two finite element models with the same relation $S_c/S = 0.25$, the same position of the load, but for different values of span length: S = 4 m and S = 6 m. The transverse moments distribution curves obtained in both models and the respective similarity are presented in Figure 3.56.

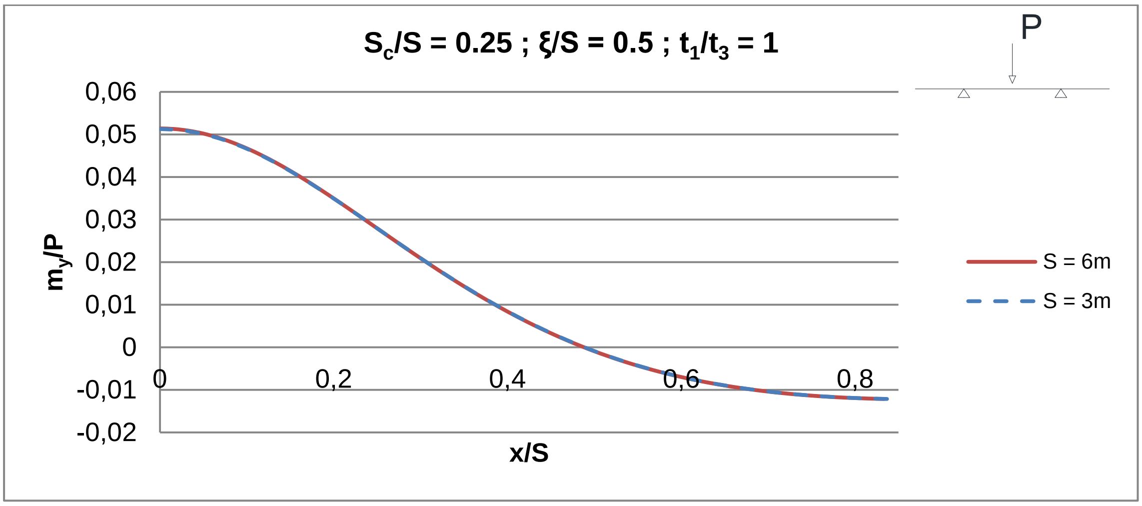

Figure 3.56 - Demonstration of the possibility to represent the distributions of transverse bending moments over the beams due to internal panel loads with a non-dimensional abscissas axis x/S

The important difference from this method to the one adopted for the analysis of cantilevers is that in order to verify the equilibrium conditions, the integration of this function in the infinite domain has to be null. In fact, since the torsional stiffness of the longitudinal beams was neglected, the resisting bending moments along the internal panel longitudinal boundaries result null, which corresponds to self-equilibrated distributions of transverse bending moments.

Taking into account that:

$$\int \frac{\psi}{\pi \cosh(\psi x)} dx = \frac{2arctg(e^{\psi x})}{\pi} \tag{3.18}$$

$$arctan(e^{\infty}) = \frac{\pi}{2} \quad and \quad arctan(e^{0}) = \frac{\pi}{4}$$

Is obtained:

$$\int_0^{\infty} \frac{P\psi}{\pi \cosh(\psi x)} \, dx = \frac{P}{2} \tag{3.19}$$

and as a consequence:

$$\int_0^{\infty} m_y \, dx = \int_0^{\infty} \alpha' \frac{A'}{\pi} \frac{P}{\cosh\left(A'\left(\frac{x}{S}\right)\right)} + \beta' \frac{B'}{\pi} \frac{P}{\cosh\left(B'\left(\frac{x}{S}\right)\right)} \, dx = \frac{P\,(\alpha' + \beta')}{2} \tag{3.20}$$

Therefore, by considering the symmetry of the distribution curves in relation to the y-axis, the equilibrium is verified if:

$$\int_{-\infty}^{\infty} m_y \, dx = P\,(\alpha' + \beta') = 0 \tag{3.21}$$

Hence, in order to verify the equilibrium, the condition α' = -β' has to be assured. Moreover, by considering the solution given by Eq. (3.17) the distribution of m_y has a maximum value for x = 0 and tends to zero as the distance from the load increases.

Therefore, in the calibration process of this method three points of the distributions obtained in the finite element analyses (see Figure 3.57) were used together with the condition α' = -β' to obtain the coefficients α', β', A' and B' (presented in Tables 3.4 and 3.5).

The process consisted on the solving of a four-equation system with three non-linear equations with hyperbolic cosine functions and the other representing the condition α' = -β', as follows.

$$\left(\frac{m_y}{P}\right)_i = \alpha' \frac{A'}{\pi} \frac{1}{\cosh\left(A'\left(\frac{x}{S}\right)_i\right)} + \beta' \frac{B'}{\pi} \frac{1}{\cosh\left(B'\left(\frac{x}{S}\right)_i\right)} \quad , i = 1, 2 \; and \; 3 \qquad (3.22 \; to \; 3.24)$$

$$\alpha' = -\beta' \qquad (3.25)$$

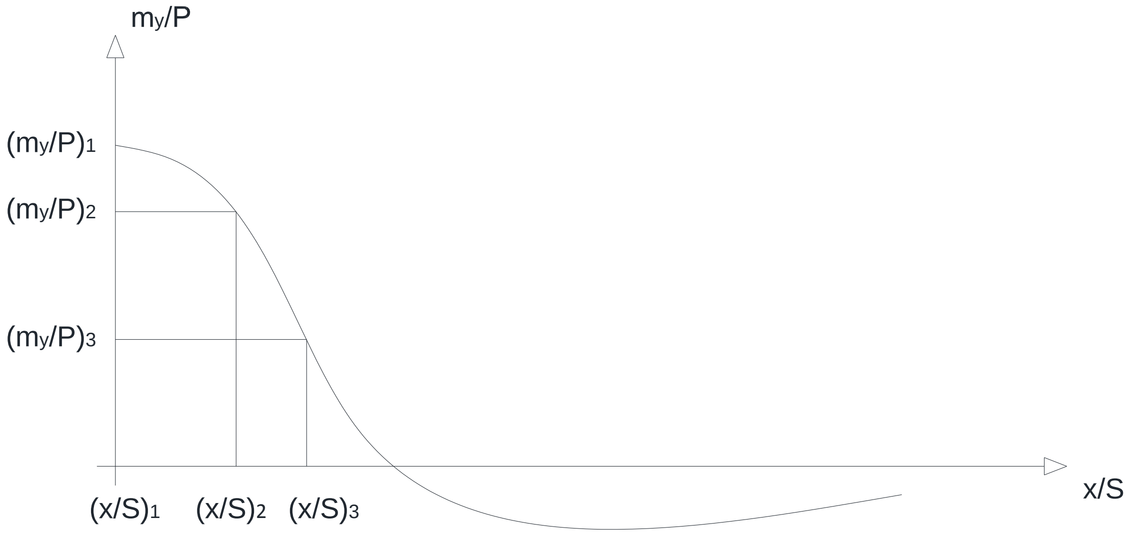

Figure 3.57 - Distribution-type of transverse bending moments due to an internal panel concentrated load with the three points used in the calibration of the semi-analytical method

The semi-analytical method represented by Eq. (3.17) was then calibrated for the best adjustment possible to the results provided by the finite element analysis. The parameters of the bridge deck for which the coefficients were obtained are:

- K' = 0 (without edge-stiffening) and 5 (maximum realistic value for K' with the curb placed on the edge of the overhang);
- S_c/S = 0.125, 0.25, 0.5;
- t_1/t_3 = 1.0 (constant thickness in the internal panel), 1.5 and 2.0 (brackets with c'/S = 0.2);
- ξ/S = 0.25, 0.5, 0.75.

Regarding the position of the load in the internal panel, it should be noticed that theoretically the closer the load is to the beams the higher will be the peak value of these transverse moments. This can also be observed, for example, in the influence surfaces of Pucher [15], for which the much closer the point load gets to the reference point, the higher is the peak value of the transverse moments, leading to a singularity.

This behavior was not considered in the proposed method, but it does not compromise its applicability. In fact, loads located in a distance from the beams smaller than t_1 are transmitted directly to the beams and hence do not cause the appearance of transverse moments in the deck slab. On the other hand, the dimensions of the wheels also gain substantial importance for those load positions. Thus, it becomes incorrect to consider wheel loads as concentrated loads in that domain of the internal panel.

Therefore, in this work it is assumed that for loads acting between $\xi/S = t_1/S$ and $\xi/S = 0.25$ it is acceptable to use the values tabled for $\xi/S = 0.25$ as an approximation, since the increase of the peak value is relatively small. Loads acting between $\xi/S = 0.75$ and $\xi/S = 1$ are not considered because the transverse moments due to loads in these positions are neglectable.

The values for α', β', A' and B' for the cases without edge-stiffening (K' = 0) and with edge-stiffening (K' = 5) are presented in Tables 3.4 and 3.5, respectively.

K’	S_c/S	t_1/t_3 (brackets)	ξ/S	**α'**	**A’**	**β'**	**B’**
0	0.125	1.0	0.25	0.0522	6.3418	-0.0522	2.1801
			0.5	0.1189	3.1736	-0.1189	2.1989
			0.75	0.0976	2.5056	-0.0976	1.9877
		1.5	0.25	0.0733	6.8687	-0.0733	1.5867
			0.5	0.1300	3.4743	-0.1300	1.8014
			0.75	0.1703	2.3059	-0.1703	1.8240
		2.0	0.25	0.0950	7.0141	-0.0950	1.3574
			0.5	0.1367	3.7462	-0.1367	1.5010
			0.75	0.0653	2.7359	-0.0653	1.2035
	0.25	1.0	0.25	0.0709	5.8378	-0.0709	1.8860
			0.5	0.1175	3.1788	-0.1175	1.8072
			0.75	0.0878	2.5147	-0.0878	1.6987
		1.5	0.25	0.0917	6.5401	-0.0917	1.2535
			0.5	0.1132	3.7438	-0.1132	1.1968
			0.75	0.0691	2.7232	-0.0691	1.1535
		2.0	0.25	0.1151	6.7569	-0.1151	1.0477
			0.5	0.1290	4.0000	-0.1290	0.9607
			0.75	0.0594	2.9213	-0.0594	0.8133
	0.5	1.0	0.25	0.0718	5.8790	-0.0718	1.3399
			0.5	0.1026	3.2944	-0.1026	1.3602
			0.75	0.0974	2.3616	-0.0974	1.4607
		1.5	0.25	0.1062	6.2195	-0.1062	1.0288
			0.5	0.1287	3.6534	-0.1287	1.0067
			0.75	0.0713	2.7341	-0.0713	0.9494
		2.0	0.25	0.1331	6.4124	-0.1331	0.8947
			0.5	0.1483	3.8792	-0.1483	0.8493
			0.75	0.0638	2.8997	-0.0638	0.7115

Table 3.4 - Table with the coefficients α’, A’, β’ and B’ for cases without edge-stiffening (K’ = 0) and considering a ratio c’/S = 0.2

K’	S_c/S	t_1/t_3 (brackets)	ξ/S	**α'**	**A’**	**β'**	**B’**
5	0.125	1.0	0.25	0.0762	5.9620	-0.0762	2.5115
			0.5	0.1323	3.3546	-0.1323	2.2945
			0.75	0.0976	2.6055	-0.0976	2.0023
		1.5	0.25	0.1121	6.2039	-0.1121	2.1357
			0.5	0.2723	3.1770	-0.2723	2.2495
			0.75	0.1703	2.4059	-0.1703	1.8654
		2.0	0.25	0.1258	6.6365	-0.1258	1.7018
			0.5	0.1626	3.7075	-0.1626	1.6191
			0.75	0.0711	2.8099	-0.0711	1.2641
	0.25	1.0	0.25	0.0890	5.5457	-0.0890	1.8207
			0.5	0.1309	3.1761	-0.1309	1.6779
			0.75	0.0901	2.4947	-0.0901	1.5579
		1.5	0.25	0.1349	5.7895	-0.1349	1.5310
			0.5	0.1658	3.4621	-0.1658	1.4084
			0.75	0.0857	2.6815	-0.0857	1.2295
		2.0	0.25	0.1412	6.4499	-0.1412	1.1815
			0.5	0.1583	3.8375	-0.1583	1.1198
			0.75	0.0683	2.9140	-0.0683	0.9373
	0.5	1.0	0.25	0.0760	5.8171	-0.0760	1.0354
			0.5	0.1455	3.0047	-0.1455	1.4229
			0.75	0.1491	2.1814	-0.1491	1.4500
		1.5	0.25	0.1221	6.0015	-0.1221	0.9349
			0.5	0.1589	3.4502	-0.1589	1.0433
			0.75	0.0796	2.6972	-0.0796	0.9408
		2.0	0.25	0.1483	6.2823	-0.1483	0.8649
			0.5	0.1668	3.7619	-0.1668	0.8958
			0.75	0.0651	2.9596	-0.0651	0.7199

Table 3.5 - Table with the coefficients α’, A’, β’ and B’ for cases with edge-stiffening (K’ = 5) and considering a ratio c’/S = 0.2

For brackets with different thickness variations from the ones considered in calibration, for load positions between ξ/S = 0.25 and ξ/S = 0.75 different from the ones presented in the tables and for values of K’ between 0 and 5 a linear interpolation between the values for α’, β’, A’ and B’ presented in Tables 3.4 and 3.5 is acceptable as an element of a simplified method. However, the variations between the different values of the tables are undefined and for a better accuracy in the results an interpolation formulae based on a parametric study of those variations should be developed and adopted.

In order to evaluate the accuracy of the results obtained by the proposed method (Eq. (3.17)) a comparison with the transverse moments distributions obtained from the finite element analysis was performed.

Four cases were considered for this comparison: three cases without edge-stiffening, corresponding to three different relations between the cantilever length and the internal panel span S_c/S = 0.125, 0.25 and 0.5. The existence of thickness variation in the internal slab in the form of brackets with t_1/t_3 = 2 was considered. The fourth case corresponds to an example considering the edge-stiffening through a K' = 5, with uniform thickness in the internal slab (t_1/t_3 = 1) and a ratio S_c/S = 0.25.

The results are presented in Figures 3.58 to 3.61.

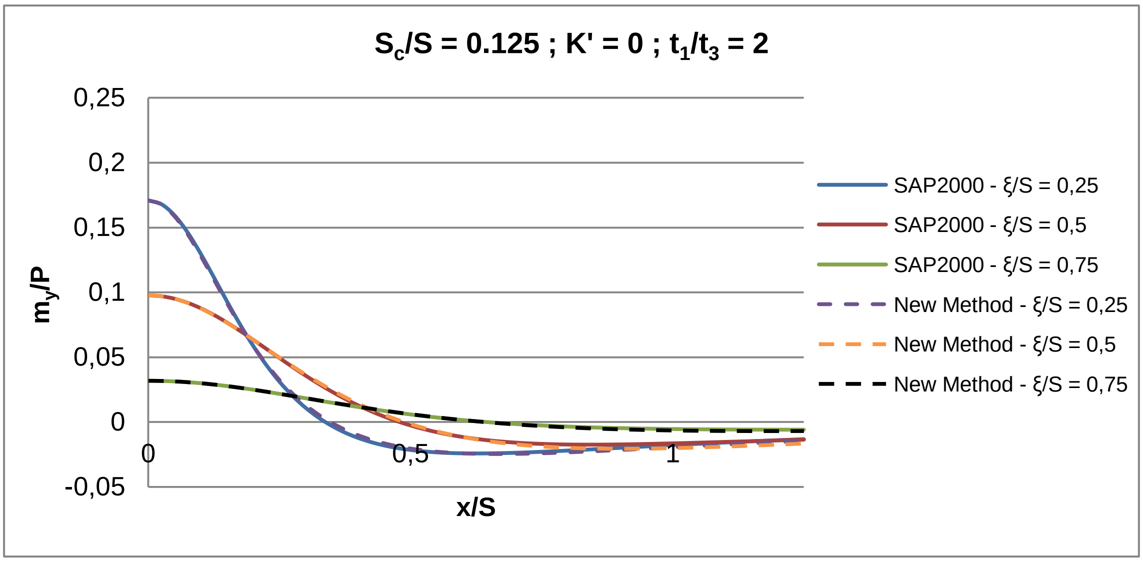

Figure 3.58 - Comparison between the results provided by the semi-analytical method and by a finite element analysis for a deck without edge-stiffening considering a ratio S_c/S = 0.125 and a ratio t_1/t_3 = 2

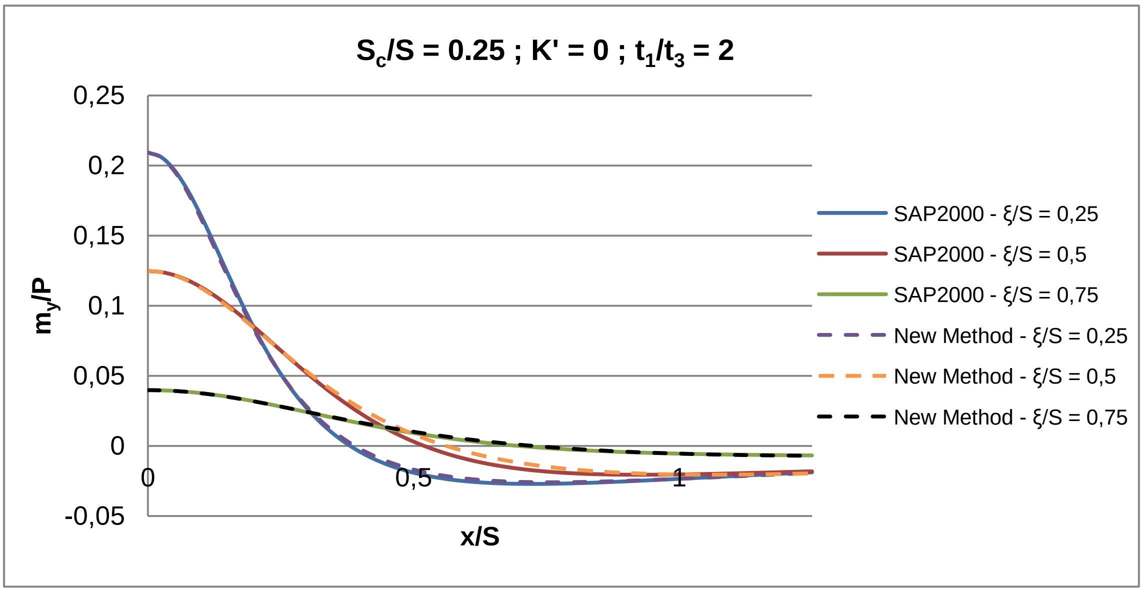

Figure 3.59 - Comparison between the results provided by the semi-analytical method and by a finite element analysis for a deck without edge-stiffening considering a ratio S_c/S = 0.25 and a ratio t_1/t_3 = 2

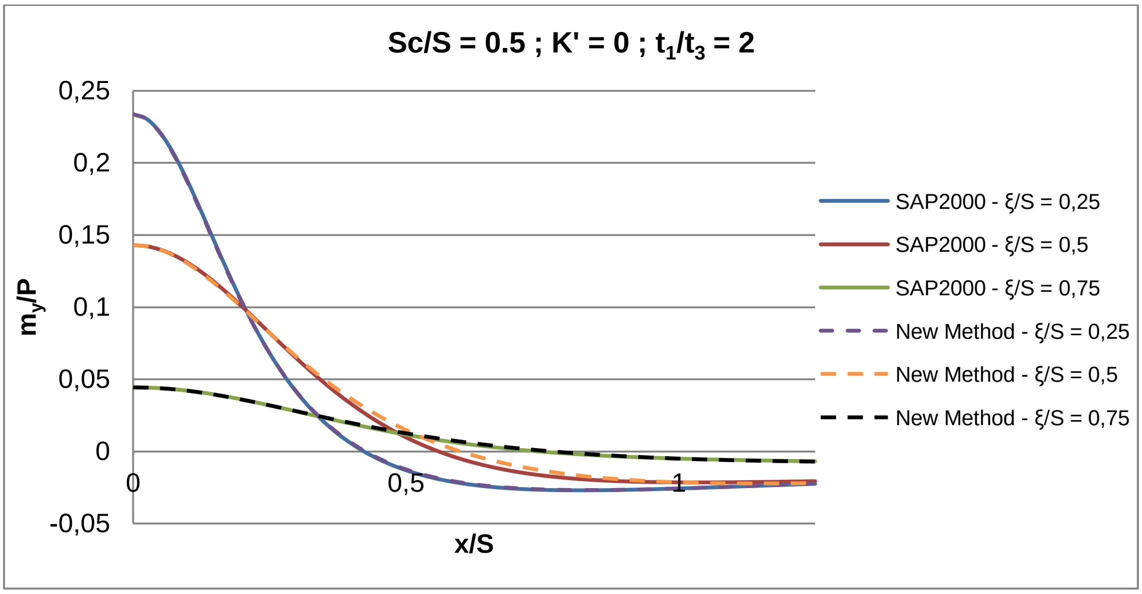

Figure 3.60 - Comparison between the results provided by the semi-analytical method and by a finite element analysis for a deck without edge-stiffening considering a ratio $S_c/S = 0.5$ and a ratio $t_1/t_3 = 2$

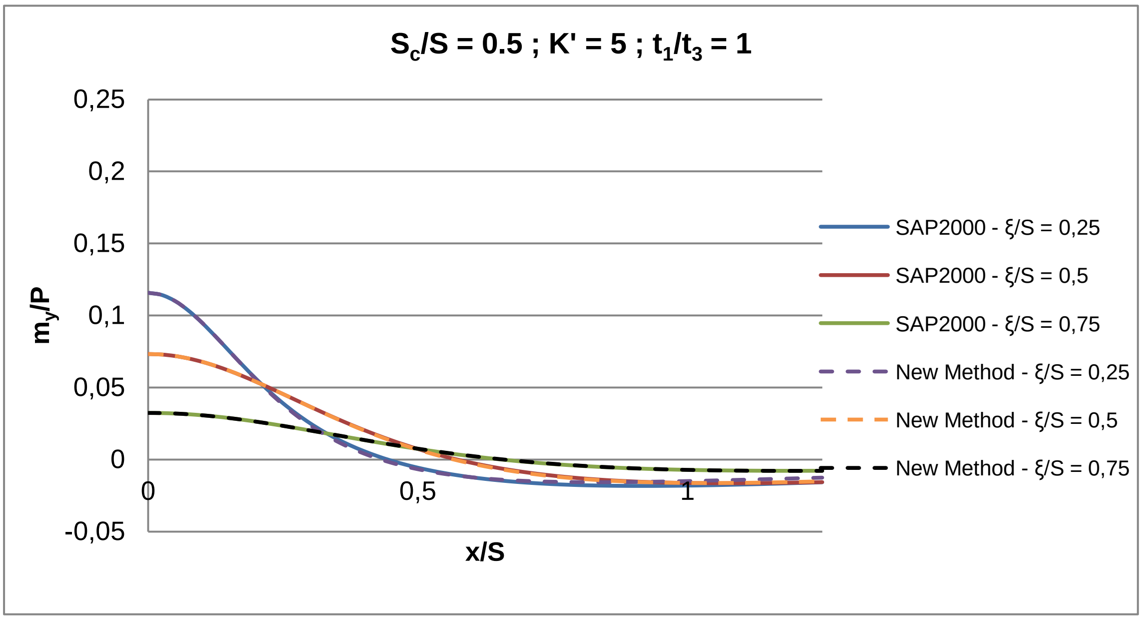

Figure 3.61 - Comparison between the results provided by the semi-analytical method and by a finite element analysis for a deck slab with edge-stiffening (K' = 5) considering a ratio $S_c/S = 0.5$ and a ratio $t_1/t_3 = 1$

3.3.6 - Analysis of knife-edge loads

The analysis of transverse bending moments in the bridge deck due to knife-edge loads acting on the internal panel is proposed by using equivalent concentrated loads with the same resultant load.

In order to demonstrate the equivalence between the use of a knife-edge load and the use of equivalent concentrated loads, the transverse moments due to both load cases represented in

Figure 3.62 (a knife-edge load of 100 kN/m uniformly distributed along the internal panel's width and, being S = 4 m, five equivalent concentrated loads of 80 kN) were evaluated using a finite element analysis. The finite element model used is illustrated in Figure 3.62 and it was admitted a ratio $S_c/S = 0.5$, a constant thickness of the cantilever slab and it was considered the existence of brackets with $t_1/t_3 = 2$ in the internal slab.

The comparison between both distributions of transverse moments obtained is presented in Figure 3.63.

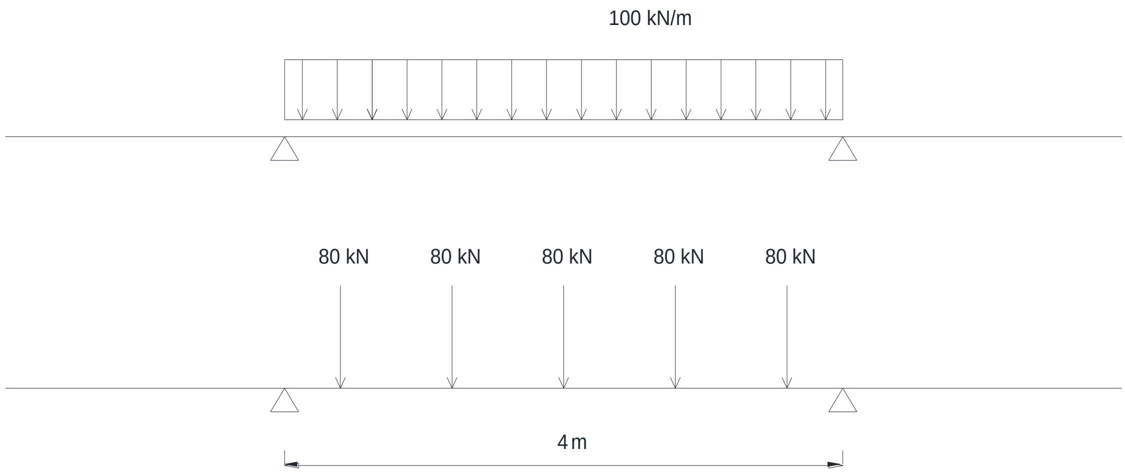

Figure 3.62 - Knife-edge load and the equivalent group of five concentrated loads acting on the internal panel of a bridge deck slab

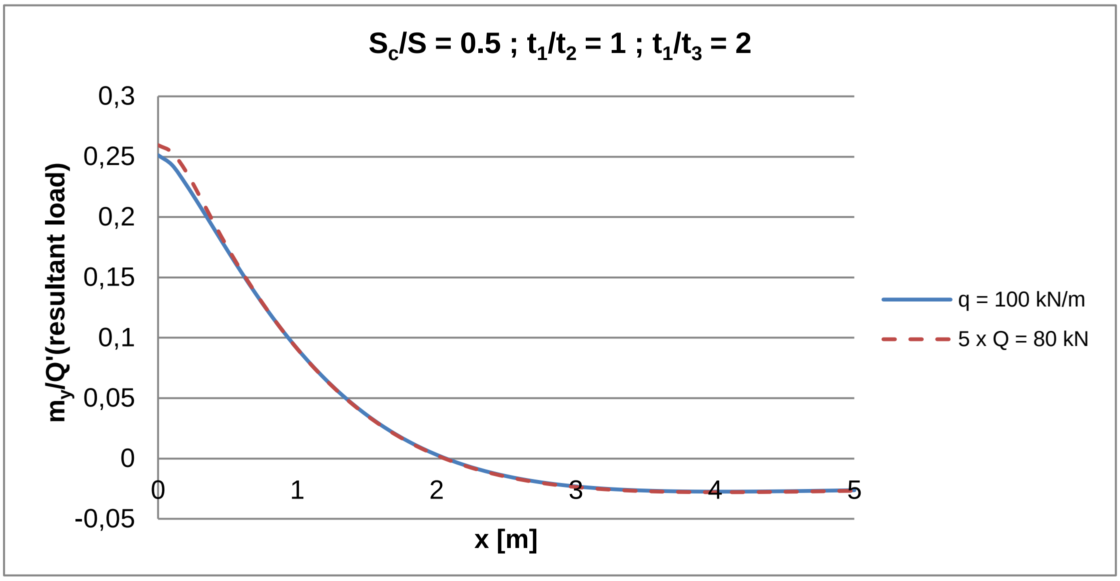

Figure 3.63 - Comparison between the distributions of transverse moments caused by a knife-edge load and by five equivalent concentrated loads

It can be concluded that the analysis of transverse bending moments over the beams due to knife-edge loads acting on the internal panel can be performed by using equivalent concentrated loads, since both distribution curves obtained using a knife-edge load and using five equivalent loads are very similar, as it can be observed in Figure 3.63. Therefore, the use of the semi-analytical method represented by Eq. (3.17) in the analysis of transverse moments due to knife-edge loads acting on the internal panel is admitted by using equivalent concentrated loads.

3.4 Chapter Conclusions

The most important characteristics of the bridge deck influencing the distributions of slab transverse moments due to wheel loads were evaluated. Based on the obtained results it was possible to develop and calibrate semi-analytical methods for the analysis of the deck slab regarding the transverse moments over the beams.

The slab transverse moments can be due to loads acting on the overhang and/or on the internal panel. Hence, a separate analysis was considered for each of those load cases.

For the cantilever loads it was verified that the dimensions of the loading area are not important. Thus, they were always admitted conservatively as point loads.

In the analysis of cantilever loads it was also considered a constant value of $S_c/S = 0.5$, since the variation of this characteristic does not provide important differences on the results. However, the difference between the distributions obtained by consdering $S_c/S = 0.5$ and $S_c/S = \infty$ (full fixed cantilever) was found very significant. The flexural and torsional stiffness of the longitudinal beams were also neglected, being those admitted with null torsional stiffness and infinite flexural stiffness.

For edge-stiffened overhangs two parameters were considered as important: the flexural stiffness of the curb (structural barrier) related to the flexural stiffness of the slab and the position of the curb in the overhang.

The existent methods to evaluate the distributions of transverse moments due to concentrated loads acting on the cantilever slab (presented in Chapter 2) have a limited applicability. Hence, a new semi-analytical method was developed by extending previous expressions for the distributions of moments through the introduction of additional coefficients; the coefficients were defined in order to accurately adjust the corresponding distributions of transverse moments to the ones obtained from a finite element analysis.

The method allows to consider several other aspects with an adequate accuracy such as the effect of knife-edge loads by considering an equivalent group of concentrated loads.

The semi-analytical method was also extended for the analysis of transverse moments in the deck slab over the longitudinal beams due to wheel loads acting on the internal panel. The dimensions of the loads and the flexural and torsional stiffness of the longitudinal beams were considered neglectable. Since these moments are due to the presence of overhangs in the deck slab, the ratio between the cantilever span and the internal span (S_c/S), the overhang slab thickness variation (t_1/t_2) and the existence of curbs have a significant influence on the moment distributions.

In what concerns the characteristics of the internal slab, the ratio t_1/t_3, representing the thickness variation in the form of brackets, has a significant influence. On the other hand, the ratio c'/S representing the relative length of the brackets was disregarded, being always considered c'/S = 0.2.

This method is also applicable to the evaluation of the transverse moments due to knife-edge loads acting on the internal panel by the use of an equivalent group of concentrated loads.

The Timoshenko's solution [4] (Eq. (3.15 and Eq. (3.16)) was considered for the evaluation of the transverse moments under the loads in the internal slab. This solution does not consider thickness variations neither the presence of overhangs nor the flexural and torsional stiffness of the beams, parameters that could reduce these transverse moments. However, it was found that the influence of all these parameters is not very significant and that the results provided by Timoshenko's solution are conservative.

CHAPTER 4

4. Transverse analysis of bridge decks: Comparison between the RSA and the Eurocode LM1

4.1 Introduction

In Chapter 3 two semi-analytical methods for the evaluation of transverse bending moments in bridge decks have been proposed (Eq. (3.5) and Eq. (3.17)).

In this chapter those semi-analytical methods are applied to the analysis of bridge decks submitted to the loads specified in (i) the Portuguese code (RSA) [3] and in (ii) EN 1991-2 (Load Model 1) [2]. The objective is to perform a comparative analysis between the transverse moments obtained from the application of both codes.

As a result of this comparative analysis several charts were obtained, allowing to easily evaluate the relation between the transverse moments obtained due to each load code.

It is also presented a comparison between the transverse moments obtained due to the RSA by adopting a “clamped cantilever model” (neglecting the internal panel) and the moments due to the Eurocode LM1 evaluated by using the developed methods (Eq. (3.5) and Eq. (3.17)) This analysis provided additional charts that are presented for the evaluation of bridge decks designed according with the RSA by using “clamped cantilever models”.

With the same objectives, Timoshenko’s solution [4] (Eq. (3.15) and Eq. (3.16)) was also used to make a comparative graph between the transverse moments at the mid-span of the internal panel due to both codes [2] and [3].

4.2 Analysis models

The distributions of transverse moments due to the load models corresponding to each code were obtained for five bridge deck cross-sections. A cross-section geometry corresponding to a slab beam was considered, admitting widths of 8 m, 12 m, 16 m, 18 m and 20 m and setting the cantilever length by $S_c/S = 0.5$. A sidewalk located on the edge of the cantilevers, which width was admitted approximately equal to $S_c/3$, was also considered in the deck models.

The consideration of the intermediate case with *b* = 18 m has the objective of representing in a better way the entering of the second line of the vehicles wheels in the cantilever analysis (both for Eurocode [2] and RSA [3]).

For the analysis of the overhangs the following three options of thickness variation were considered: t_1/t_2 = 1, 2 and 3. To evaluate the edge-stiffening effect, a curb was considered at 2/3 of the cantilever length (d/S_c = 2/3, see Figure 3.1). The dimensions of this curb are the same for the five different deck widths: 0.35 m width and 0.7 m depth, including the cantilever slab's part. For the calculation of the factor K', which relates the flexural stiffness of the curb with the transverse flexural stiffness of the cantilever slab (as described in Chapter 3 – Eq. (3.1)), it was considered as a criterion that the thickness value over the beams is given by Eq. (4.1). The values of K' for the five cases are presented in Table 4.1.

$$t_1 = 0.1 + \frac{S_c}{10} \ [m] \tag{4.1}$$

b [m]	S_c [m]	t_1 [m]	d [m]	K'
8	2	0,3	1,3	2,223
12	3	0,4	2	0,625
16	4	0,5	2,7	0,24
18	4,5	0,55	3	0,16
20	5	0,6	3,3	0,111

Table 4.1 – Characteristics of the five bridge deck cross-sections studied and corresponding value of K'

In a first analysis a constant thickness was considered in the internal panel for all cases. Afterwards it was admitted the presence of brackets with a relation t_1/t_3 = 2 for the deck widths *b* = 16 m, 18 m and 20 m, in order to include in this analysis the effect of having a thickness variation in the internal panel.

To analyze and compare the transverse moments at the mid-span of the internal panel these parameters were not considered, since Timoshenko's solution (Eq. (3.15) and Eq. (3.16)) [4] was adopted.

In the bridge deck models considered in the analysis of the transverse moments at the mid-span of the internal slab the overhangs were not considered since the analysis method used (Timoshenko's solution) neglects them. The transverse spans considered were: S = 4 m, 6 m, 8 m and 10 m. These spans were chosen since admitting a relation S_c/S = 0.5, the cases of bridge decks cross-sections which widths are b = 8 m, 12 m, 16 m and 20 m have internal panel transverse lengths equal to 4 m, 6 m, 8 m and 10 m, respectively.

For the calculation of these flexural moments it was used a null Poisson's ratio, in order to be consistent with the analysis of the slab transverse moments over the beams.

In what concerns the positioning of the loads, and for all load cases, it was considered as criterion for the evaluation of the transverse moments over the beams to position the loads as much as possible for one side of the deck. The result of this positioning is an increase of the number of loads acting on the overhangs and on a bigger distance *c* of the loads from the clamped edge, which results on higher transverse moments.

For the calculation of the transverse bending moments due to the Eurocode LM1 at the mid-span of the internal panel, using Timoshenko's solution [4], the positioning of loads can be observed in Figures 4.1, 4.2, 4.3 and 4.4 for the internal spans S = 4 m, 6 m, 8 m and 10 m, respectively.

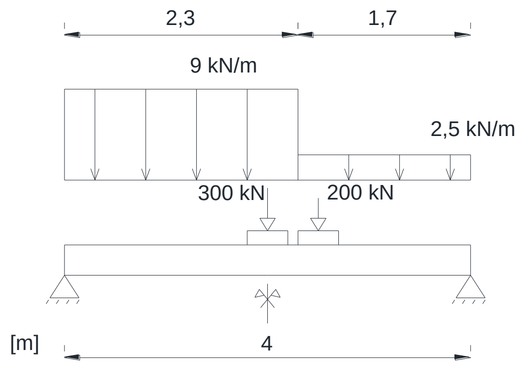

Figure 4.1 - Disposition of the Eurocode LM1 loads on the internal panel for S = 4 m

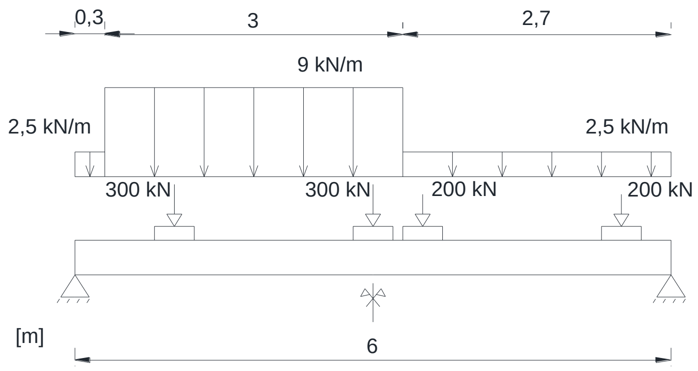

Figure 4.2 - Disposition of the Eurocode LM1 loads on the internal panel for S = 6 m

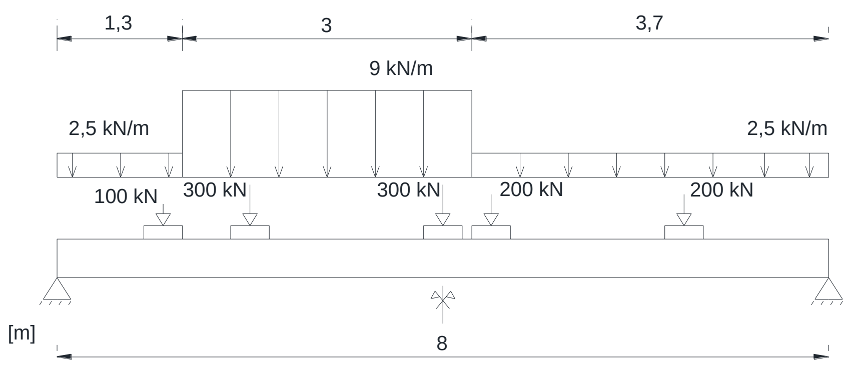

Figure 4.3 - Disposition of the Eurocode LM1 loads on the internal panel for S = 8 m

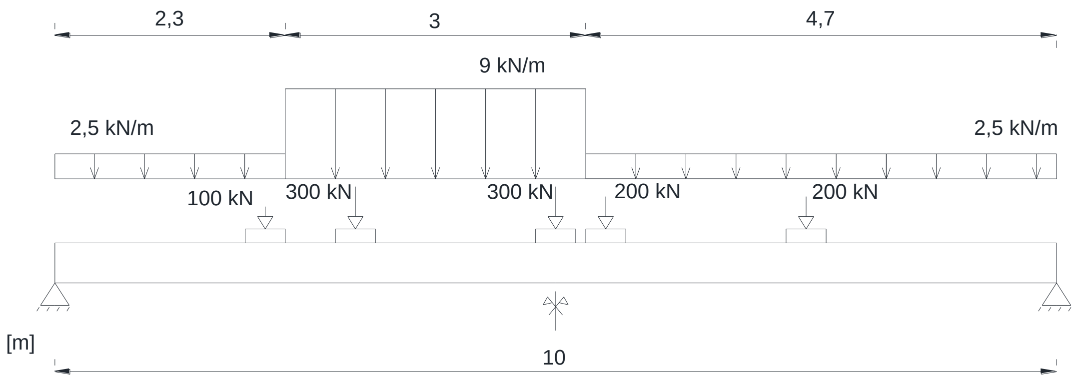

Figure 4.4 - Disposition of the Eurocode LM1 loads on the internal panel for S = 10 m

As referred in the point 2.2.1 of Chapter 2, the Portuguese code RSA [3] is divided into two vertical load models: (i) the RSA-a, corresponding to a six-wheels vehicle and (ii) the RSA-b, represented by an uniformly distributed load plus a knife-edge load.

For the evaluation of the transverse moments at the mid-span of the internal slab due to the RSA loads, a comparison between the effects of the RSA-a and RSA-b was firstly made. For the RSA-a, the vehicle was placed in two different positions: (i) with its axis coincident with the mid-span line and (ii) with the center of one line of wheels positioned in the mid-span. Hence, the position giving the most unfavorable effect was adopted. Therefore, the transverse moments corresponding to the most unfavorable RSA load case were compared with the ones due to the Eurocode Load Model 1.

4.3 Comparison of results: RSA versus Eurocode LM1

In this section the results of several comparative analyses between the transverse moments obtained in the deck slab due to the RSA [3] and due to the Eurocode LM1 [2] are presented.

Beginning with the slab transverse bending moments along the longitudinal supports, the relation between the results obtained for the RSA and for the Eurocode LM1 using the semi-analytical methods developed in Chapter 3 (Eq.(3.5) and Eq. (3.17)) was evaluated. The position of the loads considered was described in section 4.2 and the results are presented in Figures 4.5 and 4.6 for the analyses without considering edge-stiffening and considering a curb located at d/S_c = 2/3, respectively.

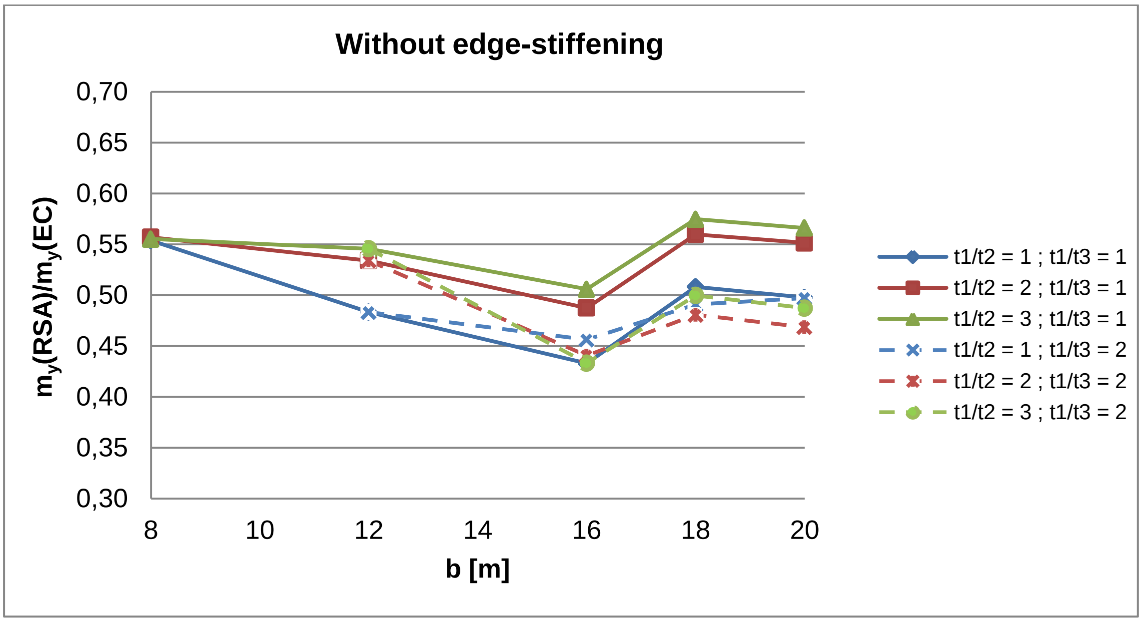

Figure 4.5 - Relation between the transverse moments m_y obtained using both load codes in study, without considering edge-stiffening and considering the influence of the flexibility of the internal slab

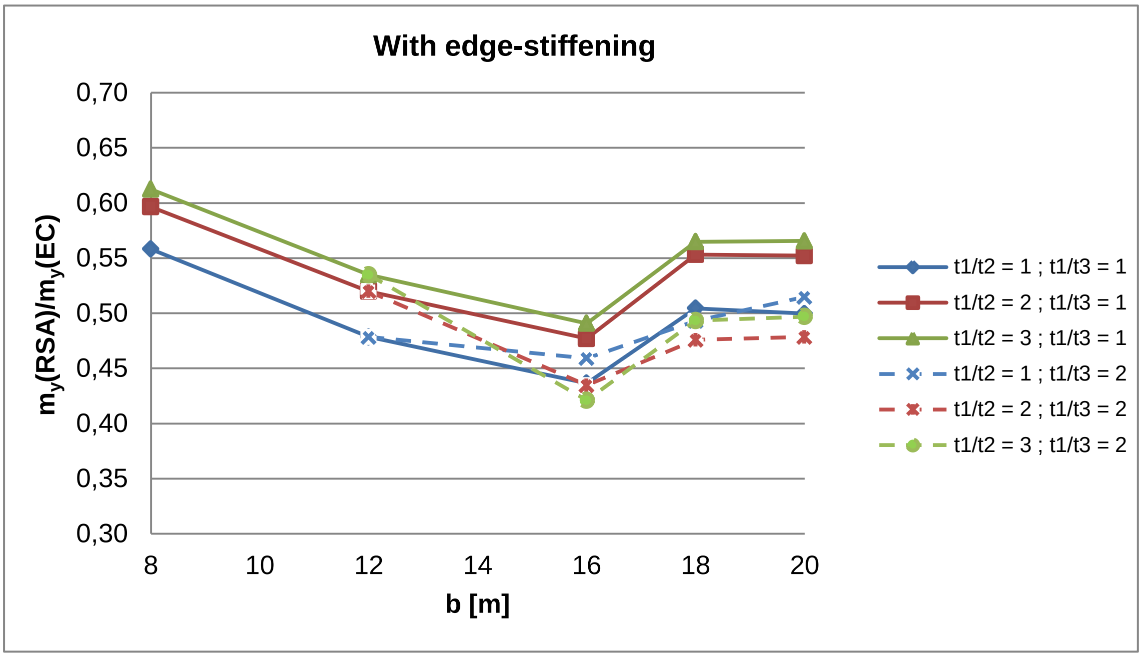

Figure 4.6 - Relation between the transverse moments m_y obtained using both load codes in study, considering edge-stiffening and considering the influence of the flexibility of the internal slab

A sudden variation in the graphs of Figures 4.5 and 4.6 can be observed between the cases with *b* = 16m and 18m, caused by the "entrance" of the second line of wheels in the cantilever slab. Although the entrance of the wheels occurred for both load codes, the Eurocode LM1 also includes an important uniformly distributed load on the cantilever and wheels on the internal panel, which increases the transverse moments produced over the beams. This means that for RSA-a (vehicle wheel loads), which provided in the majority of cases more unfavorable effects than RSA-b (uniformly distributed load plus knife-edge load), the entrance of wheels on the overhangs represents a bigger increase on the moments produced than for the Eurocode LM1, justifying the sudden variation verified in the graphs of Figures 4.5 and 4.6.

However, for the domain of values between b = 16 m and b = 18 m, the results for $m_{(RSA)}/m_{(EC)}$ obtained using Figures 4.5 and 4.6 can be slightly different from the ones obtained using accurate analysis methods because for values of *b* between 16 m and 18 m the wheels are near or over the longitudinal beams.

In the analyses the wheel loads in these positions (in a distance equal or smaller than t_1 from the beams) were neglected by admitting that the load would go directly to the support, not creating significant transverse moments.

This uncertainty for values of *b* between 16 m and 18 m also occurs because were used semi-analytical methods that have certain limitations in what concerns the load positions near the supports, being used some approximations described in Chapter 3 for this kind of situations, especially for loads acting on the internal panel.

This situation occurs for values of *b* between 16 m and 18 m because the models analyzed had a relation between the cantilever length and the internal span S_c/S = 0.5 and sidewalks with a length equal to $S_c/3$ in the edge of the overhangs. For smaller ratios S_c/S the uncertainty of the relation $m_{y(RSA)}/m_{y(EC)}$ would occur for bigger values of *b* and when there are no sidewalks in the bridge deck this would occur for smaller values of *b.*

It can be also observed in Figures 4.5 and 4.6 that generally the existence of brackets corresponds to a reduction of the relation $m_{y(RSA)}/m_{y(EC),}$ except for cantilevers with uniform thickness (t_1/t_2 = 1). This exception occurs because the RSA-b becomes more unfavorable than the RSA-a. In fact, the moments due to the knife-edge load (RSA-b) acting on the internal panel are increased by the introduction of brackets.

The evolution of the relation $m_{y(RSA)}/m_{y(EC)}$ with the deck width for t_1/t_2 = 1 and considering brackets (t_1/t_3 = 2) is very different from the one without brackets, having more subtle variations and being almost linear between b= 16 m and b = 20 m because, being the RSA-b the conditioning load model, the sudden variation which occurs for the cases with t_1/t_3 = 1 is not expected. However, the reason why only for t_1/t_2 = 1 the RSA-b is more unfavorable than the RSA-a when *b* = 18 m and 20 m is the simultaneous decrease of the importance of the internal panel's loads and increase of the importance of the cantilever loads when the ratio t_1/t_2 increases.

It was decided to provide in Figures 4.7 and 4.8 the same graphs presented in Figures 4.5 and 4.6, but now with the results obtained without considering the RSA-b load model, in order to be possible the comparison between the four graphs (Figures 4.5, 4.6, 4.7 and 4.8) and an easier analysis of the effect of having two RSA load models, since it affected, in some cases, the development of the graphs of Figures 4.5 and 4.6.

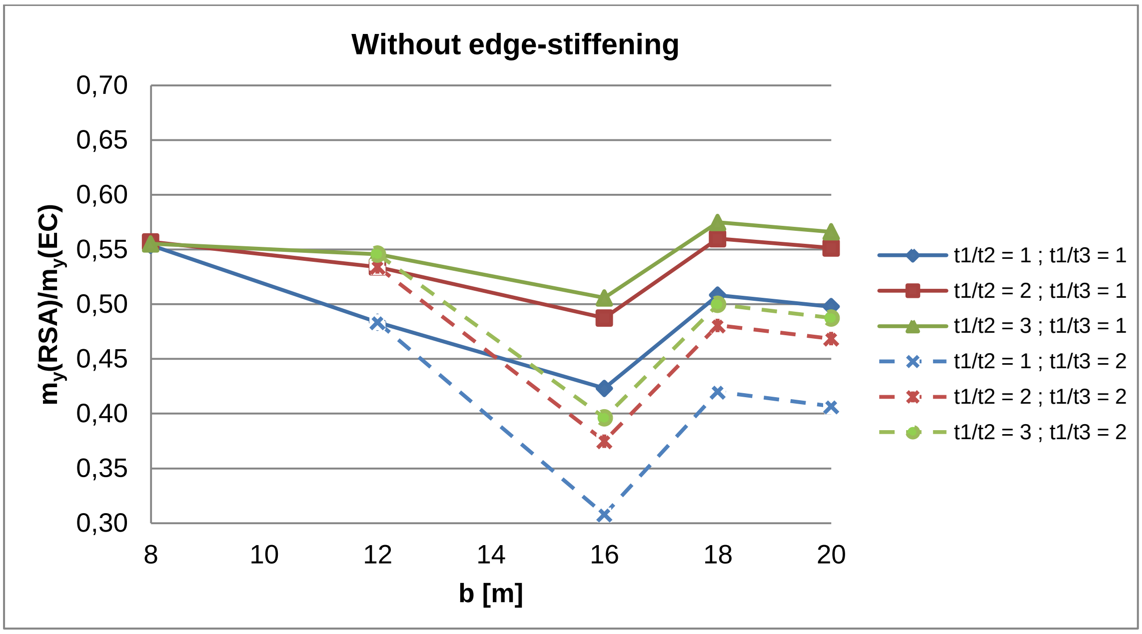

Figure 4.7 - Relation between the transverse moments m_y obtained using both load codes in study, without considering edge-stiffening, considering the influence of the flexibility of the internal slab and without considering the RSA-b load model

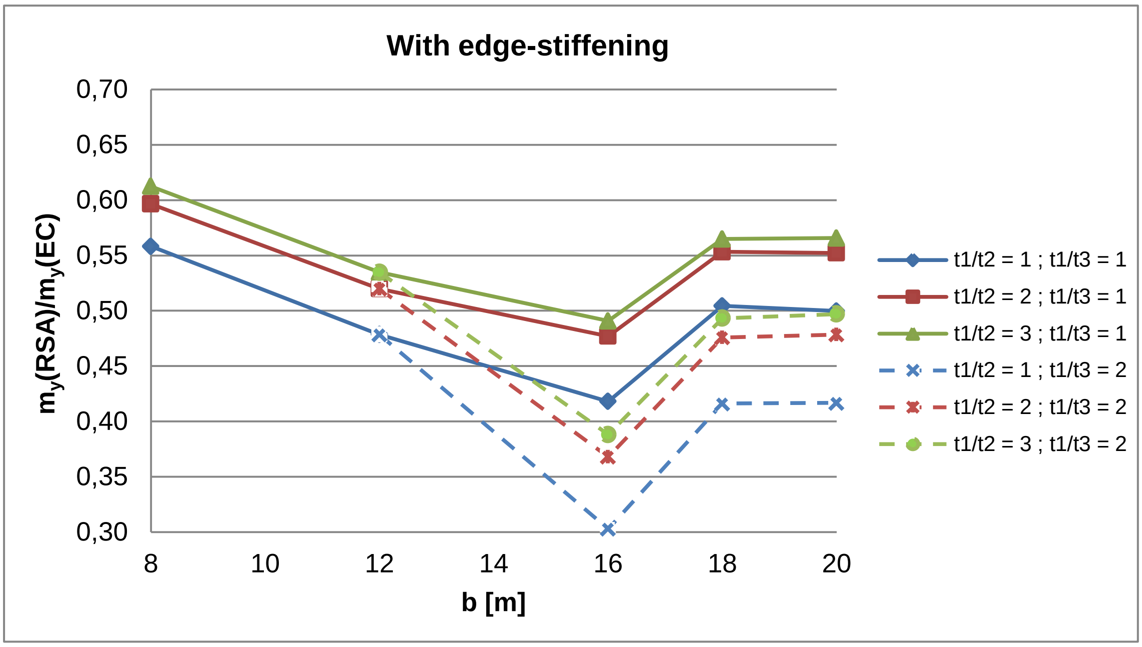

Figure 4.8 - Relation between the transverse moments m_y obtained using both load codes in study, considering edge-stiffening, considering the influence of the flexibility of the internal slab and without considering the RSA-b load model

The variation of the graphs values for the cases considering brackets with t_1/t_3 = 2 (Figures 4.7 and 4.8) is similar to the one for the cases considering constant thickness in the internal panel (t_1/t_3 = 1) when the RSA-b load model is not considered. However, due to the increase of the bending moments caused by the vehicles of the Eurocode LM1 [2] acting on the internal panel when brackets are considered, it is observed a general reduction of $m_{y(RSA)}/m_{y(EC)}$.

After the comparative analysis using the semi-analytical methods for both load codes in study (RSA and Eurocode LM1) it was found interesting to evaluate the transverse bending moments due to the RSA using a “clamped cantilever model”, in order to represent the design of bridges already built in Portugal. By considering the cantilevers clamped (by neglecting the internal slab), the corresponding moments (due to loads acting on the overhang) are higher than the ones obtained by considering the influence of the internal panel flexibility, as can be verified in Figure 3.6. On the other hand, this model doesn’t take into account the RSA loads acting on the internal panel, which for the RSA-a only matters for very small decks, but which for RSA-b is very important.

The analysis using this “clamped cantilever model” was performed with the finite element software SAP2000®, since the semi-analytical methods presented on Chapter 3 were not calibrated for “clamped cantilevers”. The graphs with the results of this comparative analysis are presented in Figures 4.9 and 4.10.

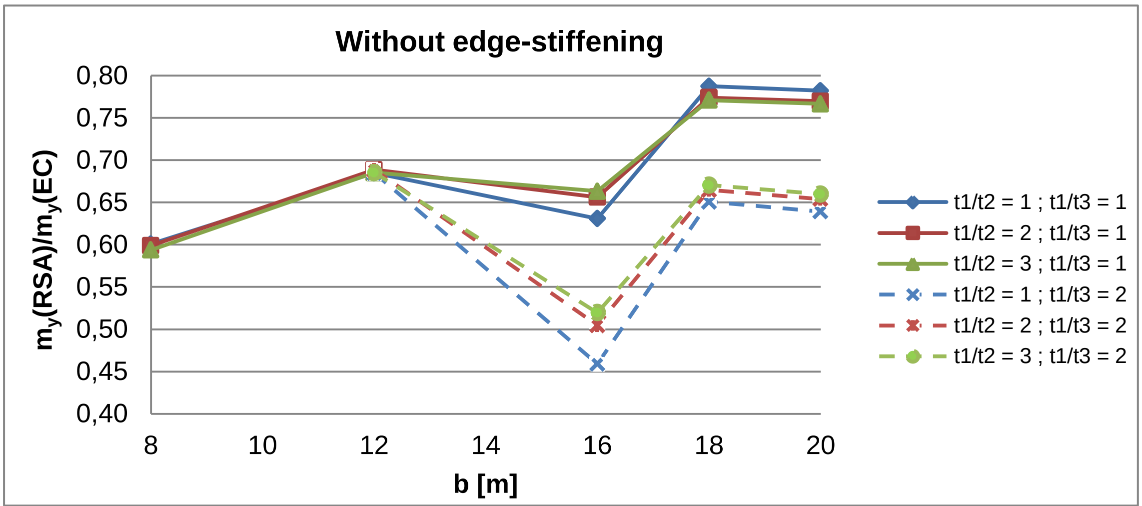

Figure 4.9 - Relation between the transverse moments m_y obtained using both load codes in study, without considering edge-stiffening and considering a “clamped cantilever model” for the RSA loads

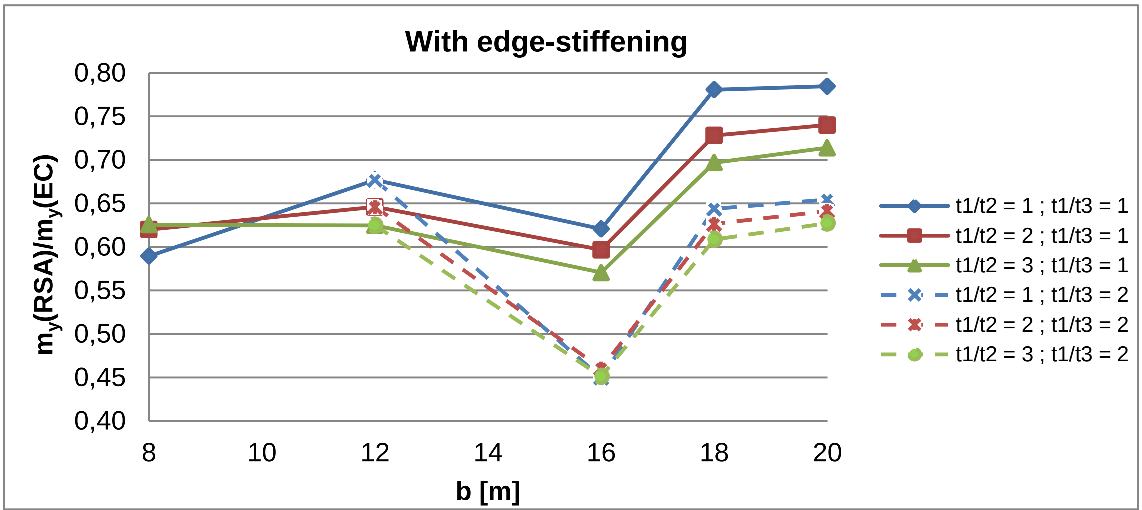

Figure 4.10 - Relation between the transverse moments m_y obtained using both load codes in study, considering edge-stiffening and considering a “clamped cantilever model” for the RSA loads

The graphs of Figures 4.9 and 4.10 allow to conclude that the use of a “clamped cantilever model” for the RSA loads increases the relation $m_{y(RSA)}/m_{y(EC)}$ essentially for higher values of *b*, since the effect of the cantilever loads is increased by the higher stiffness at the cantilever support.

It can also be observed in Figure 4.9 (without considering edge-stiffening) that, for b = 16 m, the relation $m_{y(RSA)}/m_{y(EC)}$ is higher for a bigger variation of the cantilever thickness, being the opposite for b = 18 m and b = 20 m. This type of situation can be explained by the passage of internal panel’s loads to the cantilever when *b* increases. In fact, the moments caused by cantilever loads increase with the ratio t_1/t_2, while for internal panel loads occurs the opposite.

The reduction of the relation $m_{y(RSA)}/m_{y(EC)}$ observed in Figures 4.9 and 4.10 is bigger for smaller values of t_1/t_2 (thickness variation in the cantilever slab) when considering the existence of brackets. This is justified by the fact that to smaller values of t_1/t_2 correspond higher moments due to internal panel loads.

In order to demonstrate the importance of the internal panel loads, the results obtained when neglecting them and using the semi-analytical method of Chapter 3 for the analysis of the cantilever loads are represented in Figures 4.11 and 4.12.

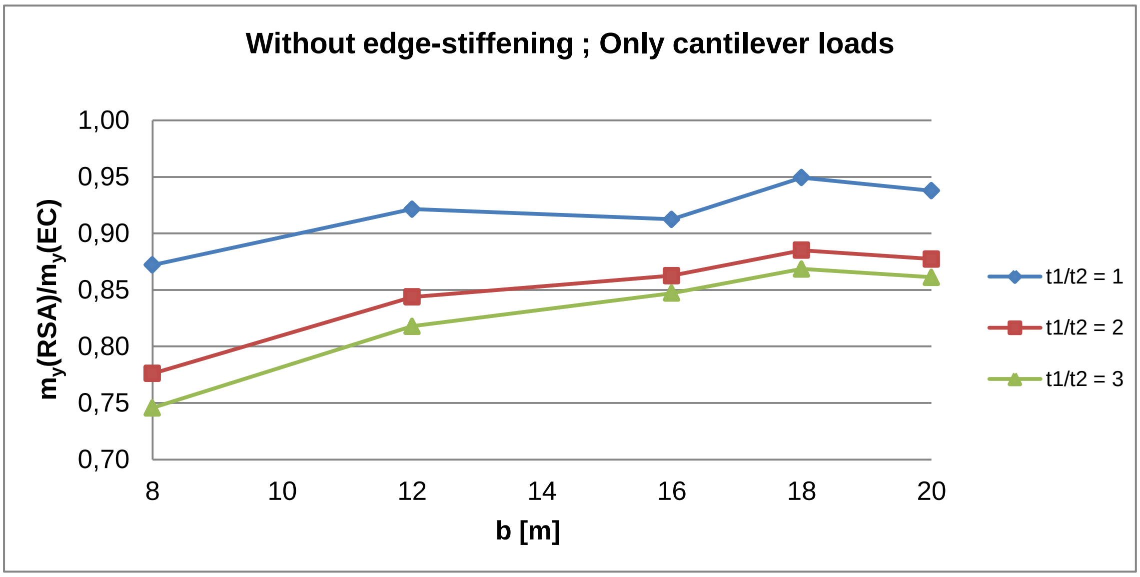

Figure 4.11 - Relation between the transverse moments m_y obtained using both load codes in study, without considering edge-stiffening and considering a “clamped cantilever model” for the RSA loads

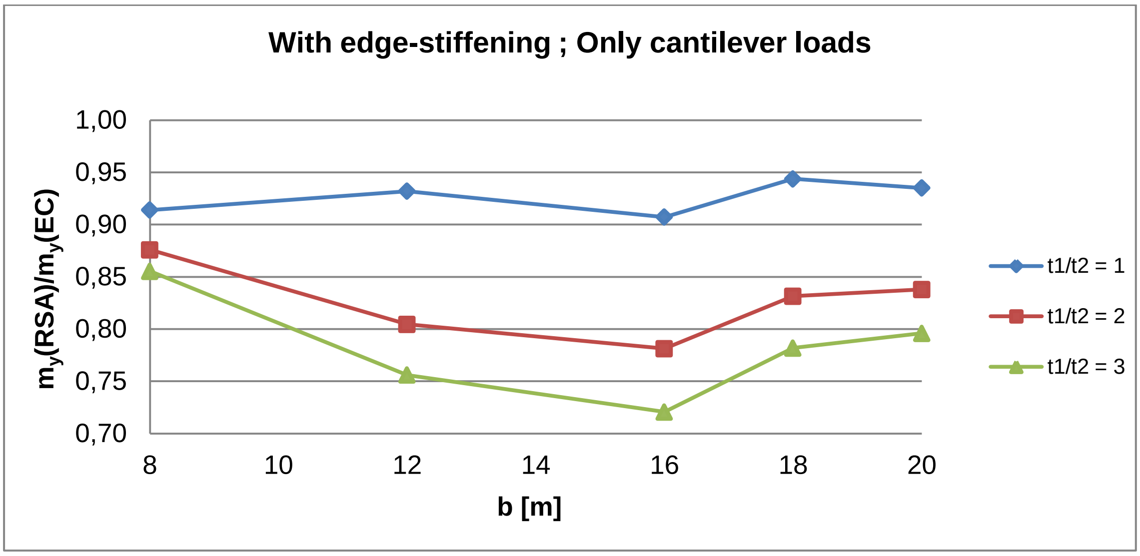

Figure 4.12 - Relation between the transverse moments m_y obtained using both load codes in study, considering edge-stiffening and considering a "clamped cantilever model" for the RSA loads

From the observation of the Figures 4.11 and 4.12 and comparing with the Figures 4.5 and 4.6, an increase of the values of $m_{y(RSA)}/m_{y(EC)}$ when the internal panel loads are neglected is verified. This fact occurs because the Eurocode LM1 considers more vehicles than the RSA-a, being some of them acting on the internal panel.

It can also be verified in Figures 4.11 and 4.12 that the relation $m_{(RSA)}/m_{(EC)}$ decreases with the increase of t_1/t_2, in opposition to what is observed in Figures 4.5 and 4.6. This difference occurs because, regarding the results illustrated in Figures 4.5 and 4.6, the Eurocode LM1 considers more loads acting on the internal panel and the moments due to these loads are higher for bigger values of t_1/t_2. Thus, the consideration of the internal panel loads in the analysis reduces more the relation $m_{y(RSA)}/m_{y(EC)}$ for cases with $t_1/t_2 = 1$ than with $t_1/t_2 = 2$ and even more than with $t_1/t_2 = 3$.

A significant influence of the internal panel loads in what concerns the design of bridges to these transverse moments was verified.

For the transverse moments at the mid-span of the internal panel an analysis was made considering the load positions described in section 4.2 (for the Eurocode LM1 are represented in Figures 4.1 to 4.4).

For the calculation of the loading areas in relation with the middle surface of the internal panel, a thickness $t_3 = 0.3$ m was admitted for the cases with $S = 4$ m and S = 6 m, and a thickness $t_3 = 0.35$ m for the cases with S = 8 m and S = 10 m.

The comparison between the transverse moments due to the loadings from both load codes and evaluated using Timoshenko's solution (Eq. (3.15) and Eq. (3.16)) [4] is represented in Figure 4.13.

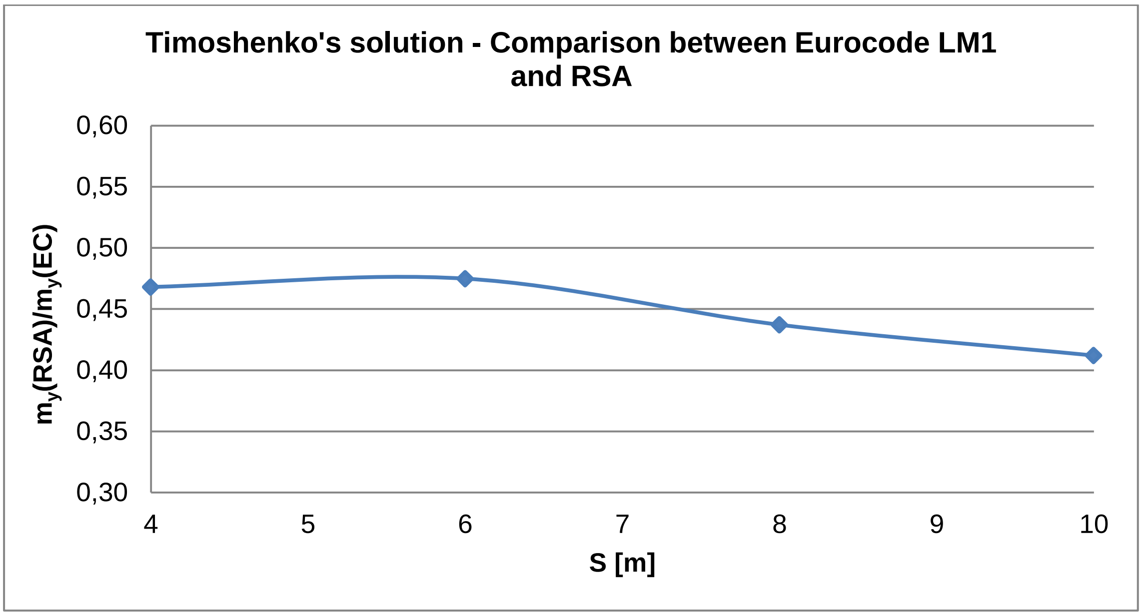

Figure 4.13 - Relation between the transverse moments at the mid-span of the internal slab obtained using both load codes in study using Timoshenko's solution [4]

For all values of the internal span S, the RSA load model which caused higher transverse moments was the RSA-a considering the vehicle with one line of wheels in the mid-span of the internal panel.

The development of the relation $m_{y(RSA)}/m_{y(EC)}$ presented in Figure 4.13 with the increase of *S* can be briefly explained with the fact that for S = 4 m only one line of vehicles is considered (since the distance between wheels is 2 m, the second line of wheels is located exactly over the beam), but for S > 4 m the two lines of wheels of the RSA-a load model fit in the internal panel when one of them is located at the mid-span line. With the increase of *S,* the relative position of the second line of wheels gets more centralized in the internal panel, producing bigger moments at the mid-span.

For the Eurocode LM1 the same situation occurs for the main vehicle, but its effect is smaller than for RSA because of the existence of more than one vehicle, which means that two wheels can be at a distance from each other of 0.5m, as can be observed in the Figures 4.1 to 4.4, and also because of the existence of distributed loads in addition to the vehicles.

Therefore, with the increase of *S*, besides the main vehicle, the Eurocode LM1 considers acting on the internal panel slab two more vehicles in addition to the natural increase of the distributed loads. This naturally leads to a progressive reduction of the relation between the moments produced by the RSA and Eurocode LM1 loads.

It is also expected that for larger decks the RSA-b loads become more unfavorable since they increase with *S,* and also the relation $m_{y(RSA)}/m_{y(EC)}$ is expected to stabilize for bigger values of *S*. However, internal panels with a length *S* bigger than 10 m are uncommon for this type of structural solution.

4.4 Chapter conclusions

The values for the transverse moments obtained by applying the Eurocode Load Model 1 are bigger than the ones due to the RSA. In fact, by observing the Figures 4.5 and 4.6 it can be verified that the relation $m_{y(RSA)}/m_{y(EC)}$, where m_y represents the slab transverse bending moments over the beams evaluated using the semi-analytical methods developed in Chapter 3, has values between more than 0.4 and around 0.6, with or without considering the existence of edge-stiffening.

When the “clamped cantilever model” was used for RSA loads, the values for the relation $m_{y(RSA)}/m_{y(EC)}$ increased and presented bigger variations along the *b* axis, being within the range 0.45 – 0.8, as can be observed in Figures 4.9 and 4.10.

In this analysis (considering the “clamped cantilever model” for the evaluation of the RSA loads) a significant difference between the values of $m_{y(RSA)}/m_{y(EC)}$ considering or not the existence of brackets was also noticed. This demonstrates the relevant influence of the brackets in the transverse moments caused by loads acting on the internal panel (in this case, the Eurocode loads).

The importance of the internal panel loads can be confirmed with a comparison between the Figures 4.5 and 4.6, considering the transverse moments caused by internal panel loads (that are much more important for the Eurocode LM1 than for the RSA) and the Figures 4.11 and 4.12, where only the cantilever loads were taken into account. The semi-analytical method (Eq. (3.5)) developed in Chapter 3 was used in this analysis to evaluate the transverse moments due to both codes.

Finally, by the observation of Figure 4.13 it can be concluded that the transverse moments in the mid-span of the internal panel due to the RSA are about 40% to 50% of those caused by the Eurocode LM1, which enhances the difference between both load codes.

CHAPTER 5

5. Longitudinal analysis of bridge decks: Comparison between the RSA and the Eurocode LM1

5.1 Introduction

This chapter is focused on the longitudinal analysis of bridge decks submitted to traffic loads.

Several bridge models were analyzed considering a different number of spans, different span lengths and different deck widths, in order to evaluate the differences between the use of the RSA and the Eurocode LM1 in a global structural analysis of bridge decks.

Regarding the bridge global analysis, the relevance of the live loads, represented by the RSA and Eurocode LM1, in comparison with the dead loads was evaluated considering the characteristic values of the actions.

The bending moments and the shear force in the bridge deck were defined and evaluated by making use of the respective influence lines, being defined the corresponding envelopes.

5.2 Analysis models

Four types of simply supported continuous bridges were analyzed; one, two, three and five spans were considered, having the central span lengths *L* equal to 20, 25, 30, 35, 40, 45 and 50 meters. For the quantification of the loads (represented by the RSA and the Eurocode LM1) four different deck widths were considered: b = 8m, 12m, 16m and 20m.

The analyses of the bridge deck models were made considering the deck simply supported on two beams or ribs. The lateral distribution of the loads to both beams was performed using the Courbon's Method presented in [19], which neglects the torsional stiffness of the longitudinal beams and the transverse flexibility of the deck. The flexural stiffness of the beams that support the rigid deck slab is represented by K_1 and K_2 (see Figure 5.1), respectively. Therefore, the loading supported by each beam depends on the position of the load *e* and on the relative stiffness of the beams K_1 and K_2, as represented in Eq. (5.1). Only the most loaded beam was analyzed.

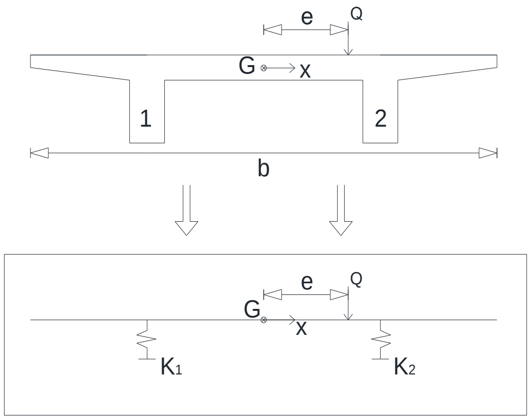

Figure 5.1 - Scheme of the Courbon's method for the lateral distribution of loads

The load distributed to the beam *i* is given by:

$$F_i = \frac{K_i}{\sum K_i} Q + \frac{K_i x_i}{\sum K_i {x_i}^2} Qe \tag{5.1}$$

For reading guidance, the models considered in the global analysis are schematically represented in Figures 5.2, 5.3 and 5.4, identifying the loading patterns and the cross-sections considered (A and B for the bending moments and C for the shear force).

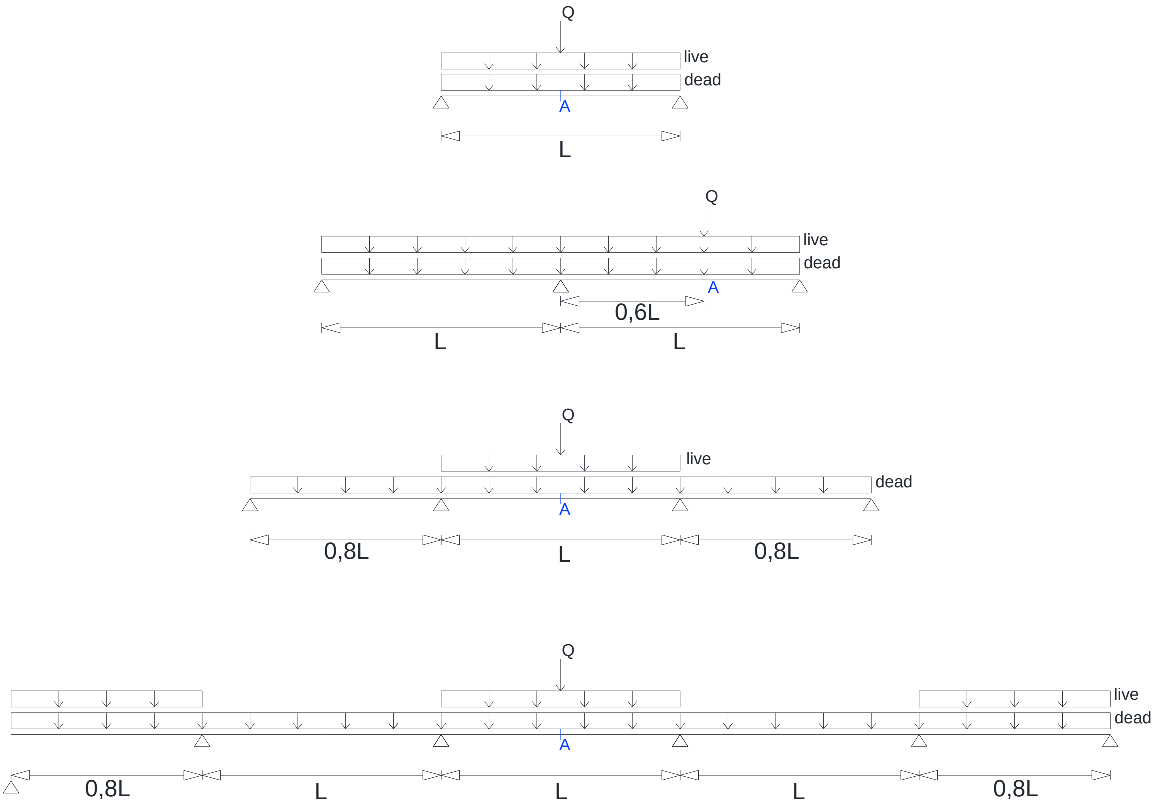

Figure 5.2 - Bridge models, loading patterns and cross-sections A for the evaluation of the sagging moments (M+)

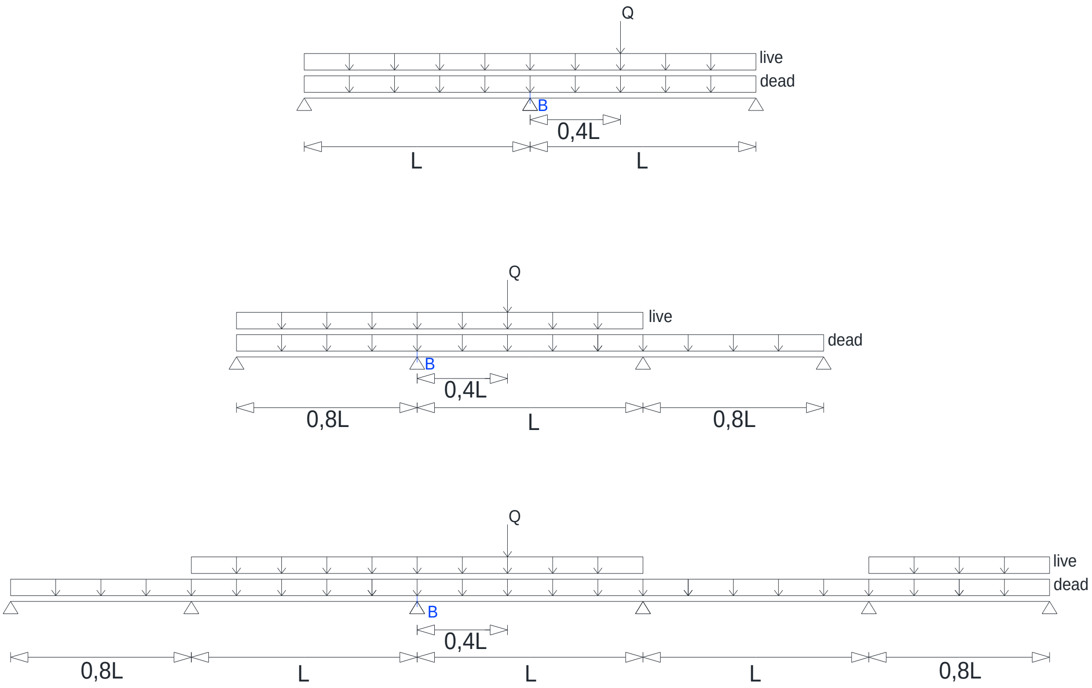

Figure 5.3 - Bridge models, loading patterns and cross-sections B for the evaluation of the hogging moments (M-)

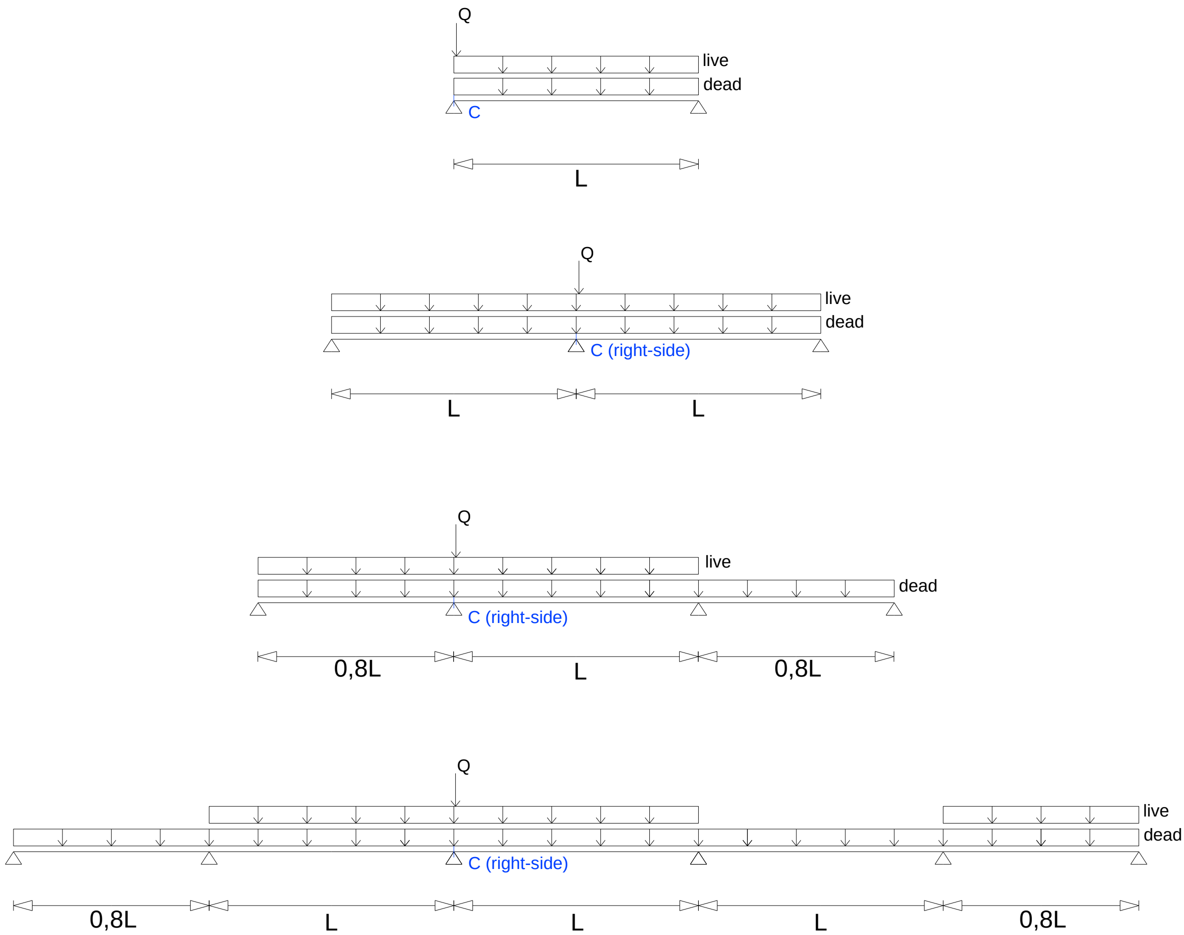

Figure 5.4 - Bridge models, loading patterns and cross-sections C for the evaluation of the shear force (V)

The cross-sections of the bridge decks have the slab-beam geometry represented in Figure 5.5, being admitted a relation $S_c/S = 0.5$ and a sidewalk's width of 1 m in both cantilever edges. For both RSA and Eurocode LM1, the vehicles were considered through one concentrated load (Q) in the longitudinal analysis, as represented in Figures 5.2, 5.3 and 5.4.

The sidewalk part is not considered to be loaded regarding the position of the loads along the deck width. On the other hand, it was considered the loading pattern which concentrates the most of the load in one side, leading to the most unfavorable situation for one of the longitudinal beams, when considered the lateral distribution of loads (Eq. (5.1)).

As an example of the loading patterns considered, it is represented in Figure 5.5 the case with *b* = 12 m acted by the Eurocode LM1 where it is taken into account the most unfavorable load distribution for the left beam.

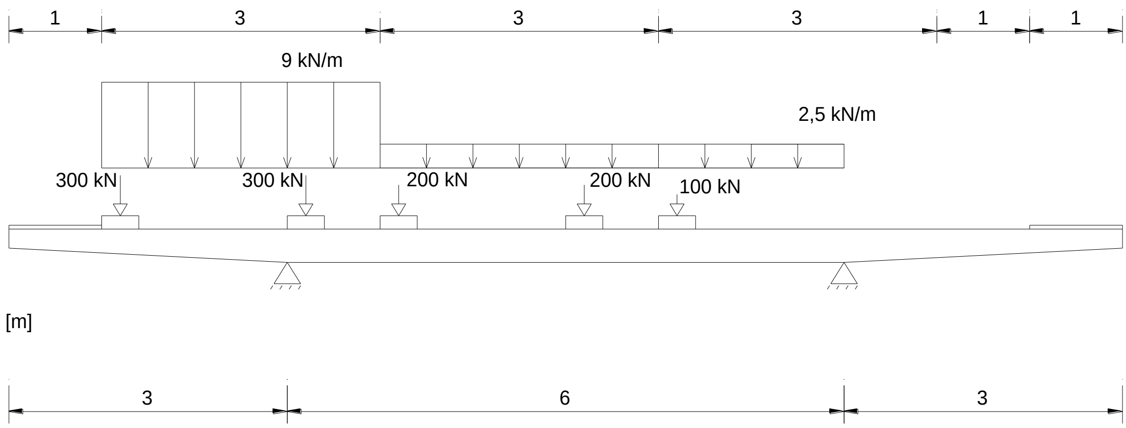

Figure 5.5 - Cross-section and lateral loading pattern for the case *b* = 12 m subjected to the Eurocode LM1

5.3 Comparison of results: RSA versus Eurocode LM1

A comparison between the internal forces (longitudinal bending moments and shear forces) obtained by applying the Eurocode LM1 and the RSA was performed for each of the four structural systems of bridges represented in Figures 5.2, 5.3 and 5.4.

The results are presented for each of the corresponding most-unfavorable cross-section:

(i) Cross-section A for sagging bending moments (Figure 5.2);
(ii) Cross-section B for hogging bending moments (Figure 5.3);
(iii) Cross-section C for the shear force (Figure 5.4).

Four cross-section widths (b = 8 m, 12 m, 16 m and 20 m) and a set of central span lengths *L* within the range 20 m – 50 m were considered for each internal force and structural system.

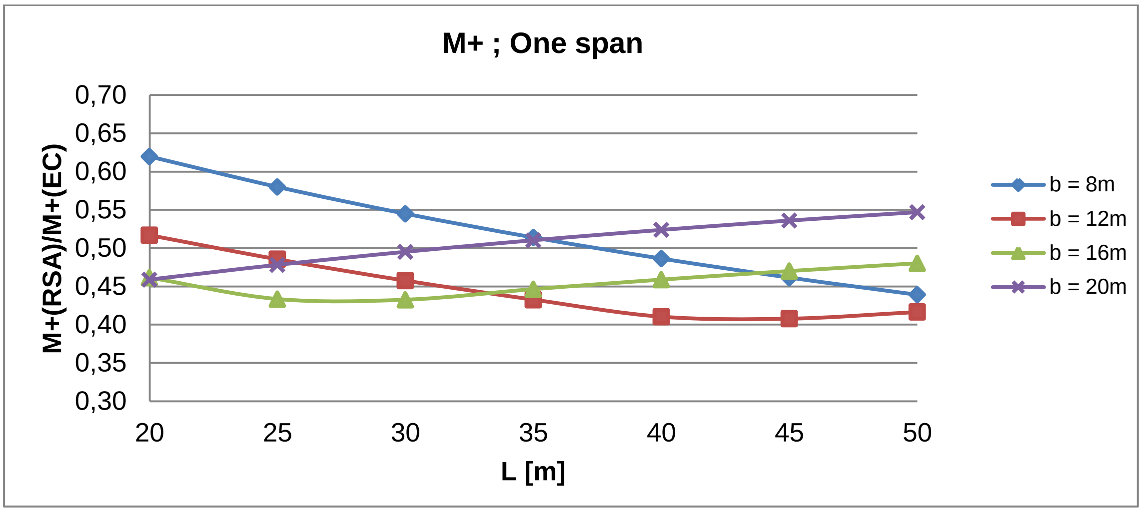

Figure 5.6 - Relation between the longitudinal sagging bending moments M+ at cross-section A obtained using the RSA and using the Eurocode LM1 at bridges with one span

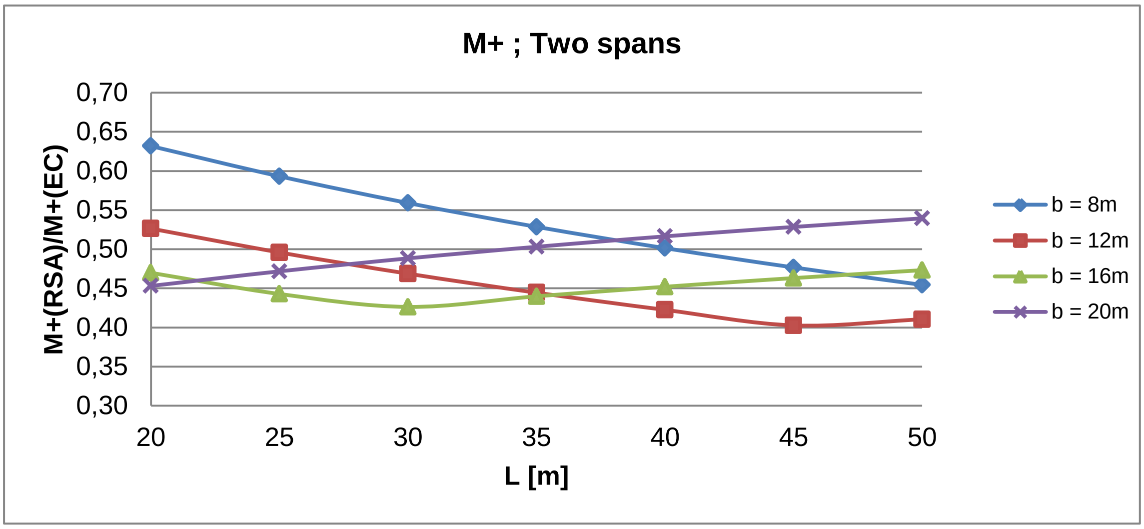

Figure 5.7 - Relation between the longitudinal sagging bending moments M+ at cross-section A obtained using the RSA and using the Eurocode LM1 at bridges with two spans

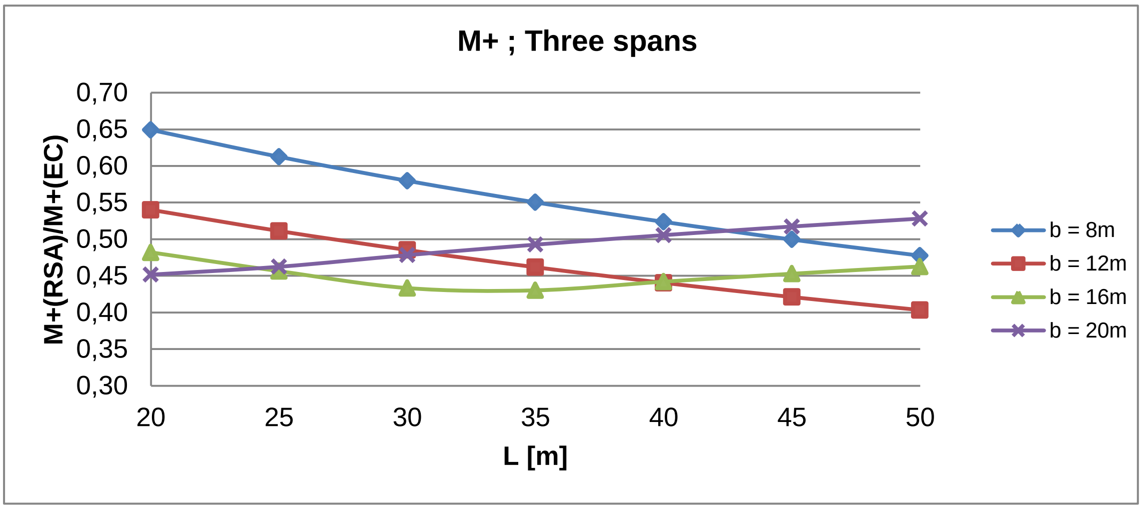

Figure 5.8 - Relation between the longitudinal sagging bending moments M+ at cross-section A obtained using the RSA and using the Eurocode LM1 at bridges with three spans

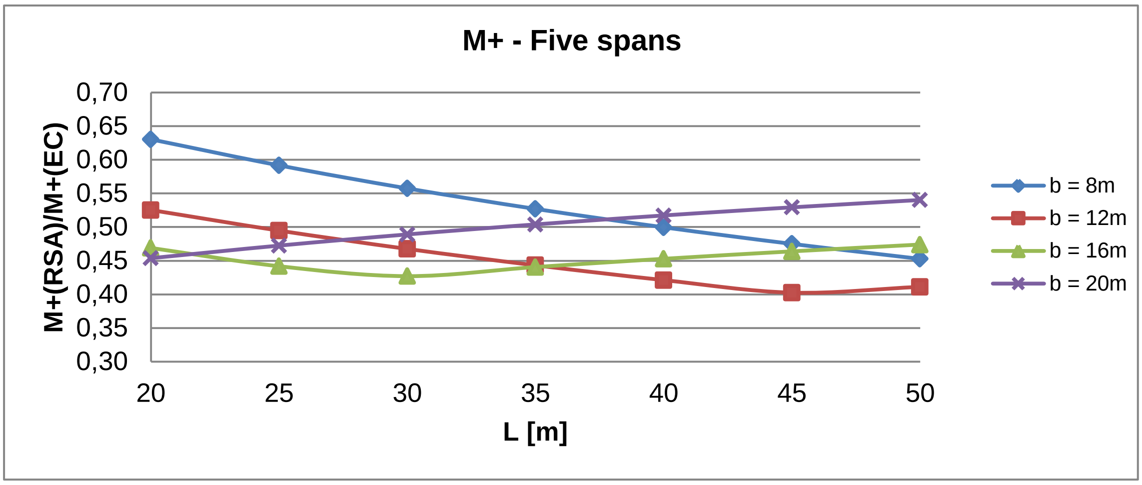

Figure 5.9 - Relation between the longitudinal sagging bending moments M+ at cross-section A obtained using the RSA and using the Eurocode LM1 at bridges with four spans

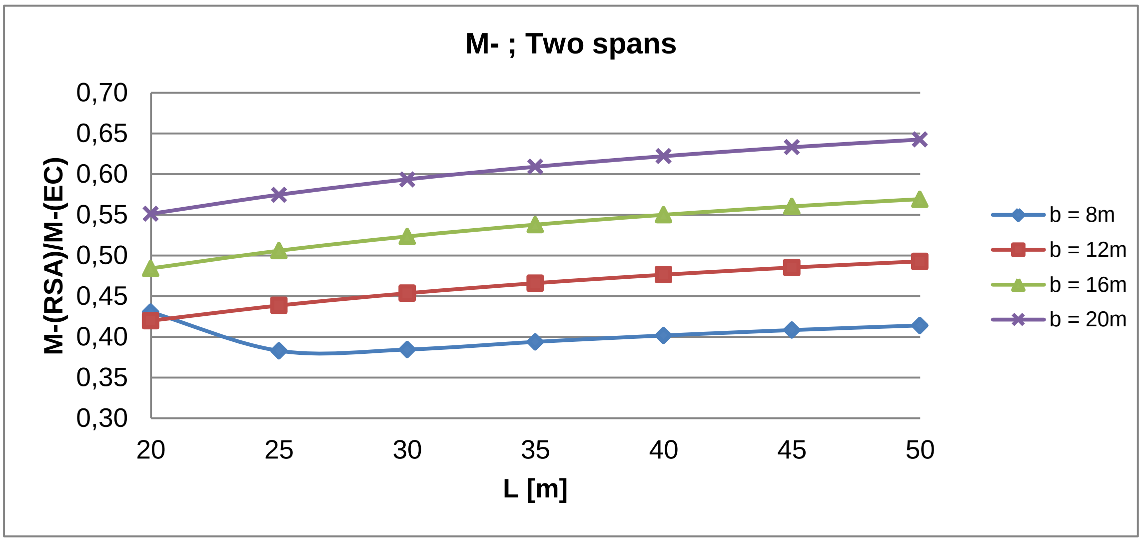

Figure 5.10 - Relation between the longitudinal hogging bending moments M- at cross-section B obtained using the RSA and using the Eurocode LM1 at bridges with two spans

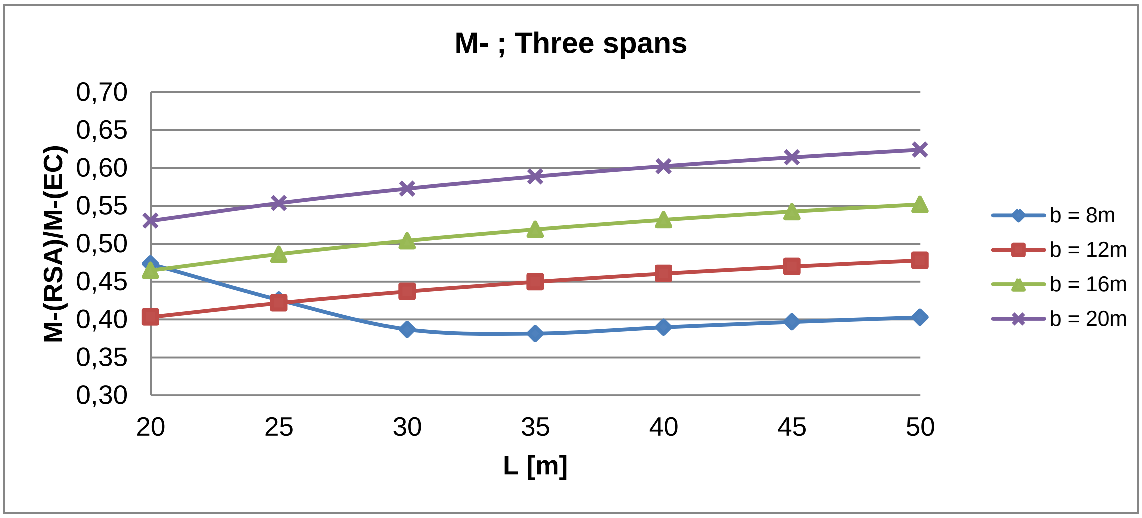

Figure 5.11 - Relation between the longitudinal hogging bending moments M- at cross-section B obtained using the RSA and using the Eurocode LM1 at bridges with three spans

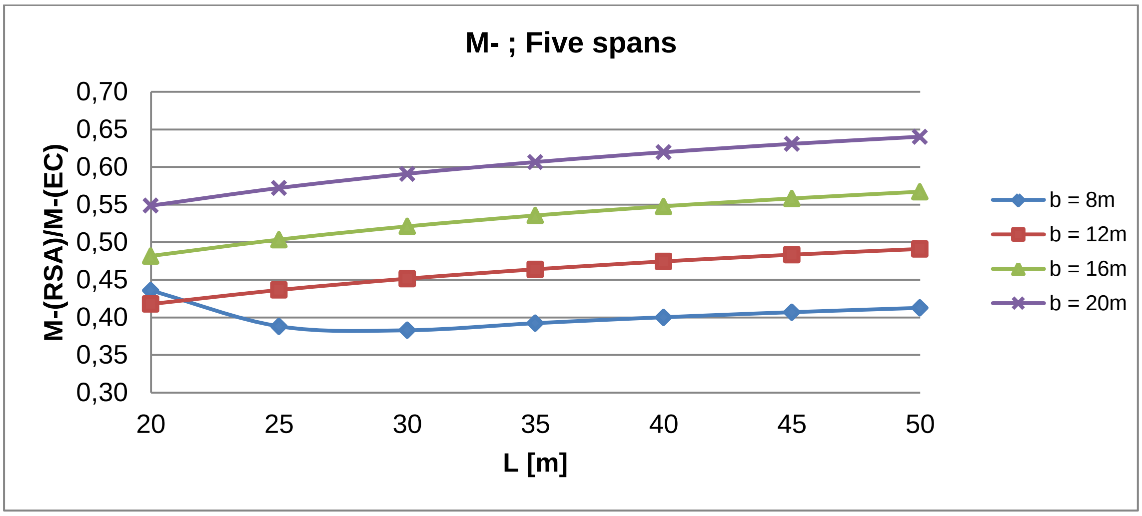

Figure 5.12 - Relation between the longitudinal hogging bending moments M- at cross-section B obtained using the RSA and using the Eurocode LM1 at bridges with five spans

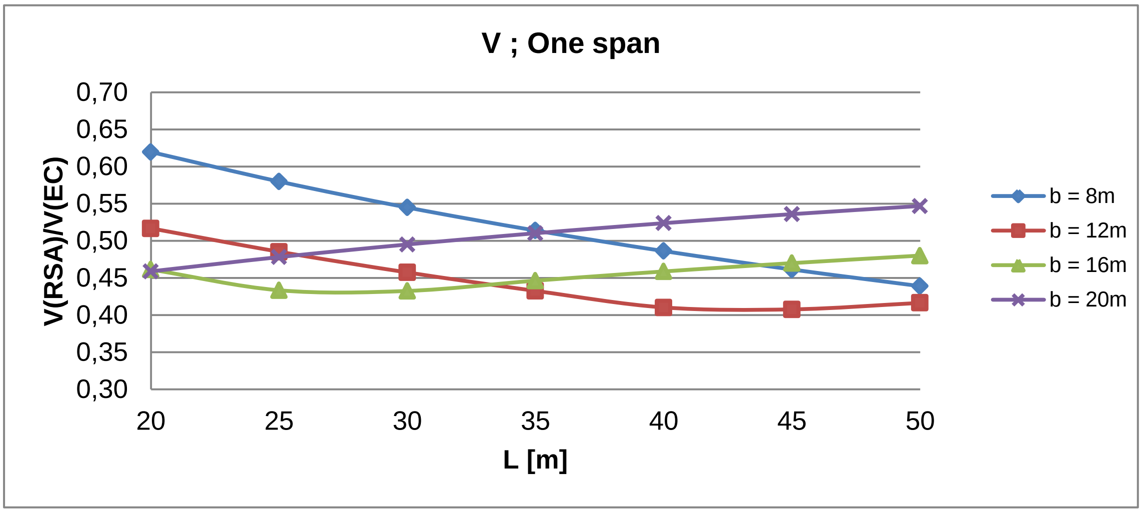

Figure 5.13 - Relation between the shear forces V at cross-section C obtained using the RSA and using the Eurocode LM1 at bridges with one span

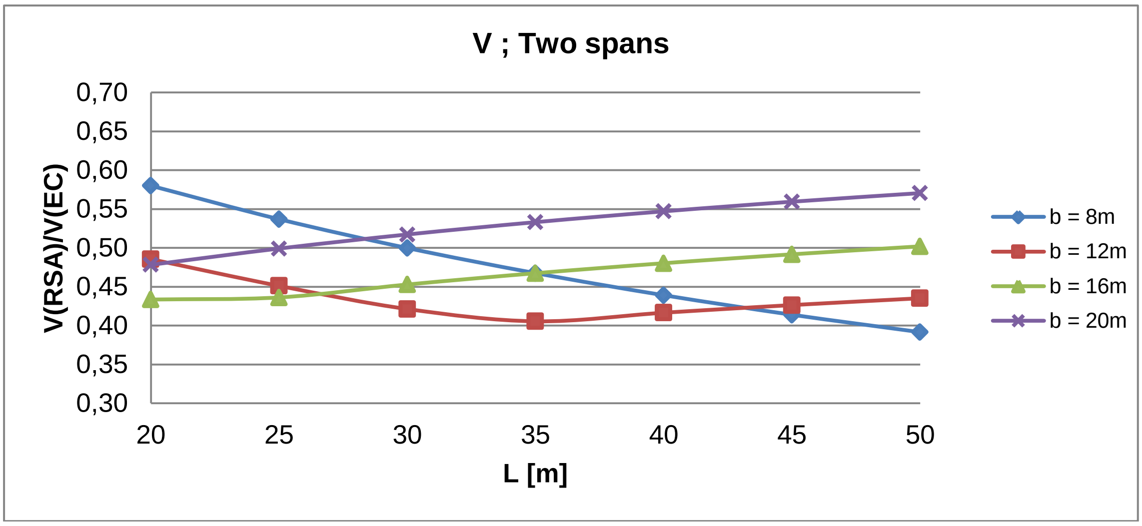

Figure 5.14 - Relation between the shear forces V at cross-section C obtained using the RSA and using the Eurocode LM1 at bridges with two spans

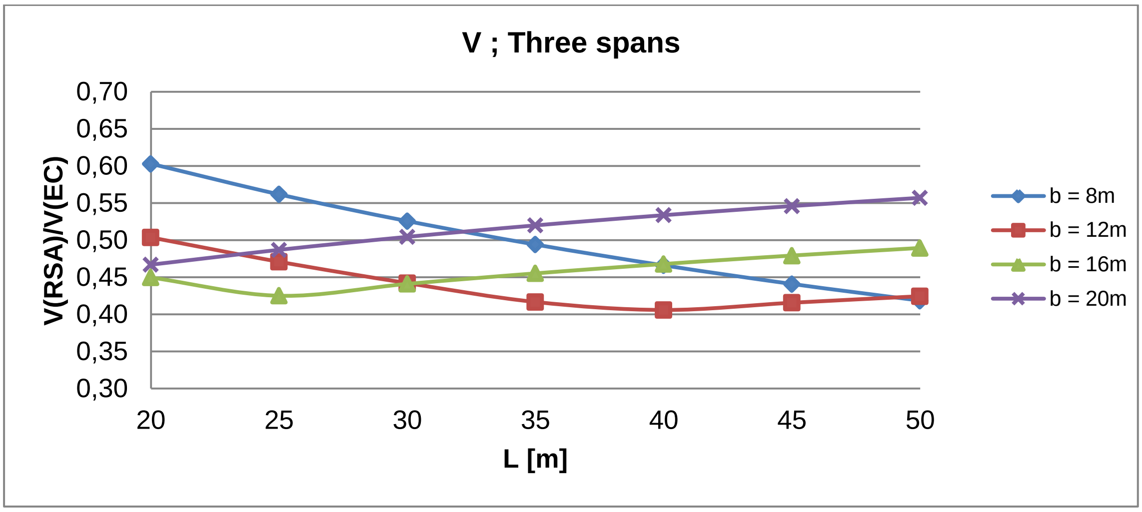

Figure 5.15 - Relation between the shear forces V at cross-section C obtained using the RSA and using the Eurocode LM1 at bridges with three spans

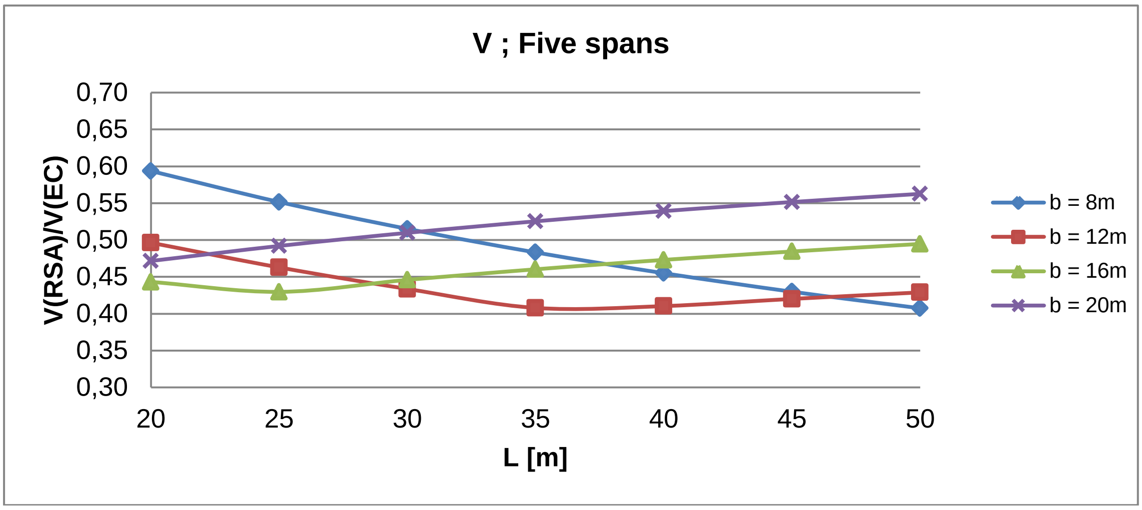

Figure 5.16 - Relation between the shear forces V at cross-section C obtained using the RSA and using the Eurocode LM1 at bridges with five spans

As described in Chapter 2, the RSA is divided into two load models regarding the vertical traffic loads: (i) the RSA-a, a six-wheel vehicle and (ii) the RSA-b, a uniformly distributed load plus a knife-edge load.

It can be verified in Figures 5.6 to 5.16 that the relation between the internal forces due to the RSA and the ones due to the Eurocode LM1 decreases with *L* when the RSA-a is more unfavorable than the RSA-b. This occurs because the Eurocode LM1 considers vehicles and uniformly distributed loads that increase with the span, contrary to the RSA-a which only considers one vehicle. However, when the RSA-b load case becomes more unfavorable than the RSA-a (for larger spans, since it considers a knife-edge load and also a uniformly distributed load), the tendency changes and tends to stabilize since the vehicle loads tend to loose importance with the increase of *L*.

It can also be verified that for larger deck widths the RSA-b becomes more unfavorable than the RSA-a with a smaller increase of the bridge span, since the loads of the RSA-b, contrary to the vehicle of RSA-a, increase with the deck width.

It was also verified in Figures 5.6 to 5.16 that for all the internal forces evaluated (bending moments and shear force) the relation between their maximum values lies between the 35% and the 65%, which demonstrates that the Eurocode LM1 is significantly more demanding than the RSA regarding the longitudinal analysis of bridge decks.

5.4 Evaluation of the importance of the traffic live loads

The contribution of the traffic live loads to the global analysis of a bridge is evaluated in this section by comparing the internal forces (sagging and hogging bending moments and shear force) due to the live loads defined according to the RSA and to the Eurocode LM1 with the ones due to the design loads (including the same traffic live loads and also the dead loads).

Four widths for the bridge cross-sections were considered: *b* = 8 m, 12 m, 16 m and 20 m.

The bridge deck dead weight was evaluated for the values of *b* considered by an equivalent thickness of the deck slab. This equivalent thickness was obtained for a characteristic span length through a formulae proposed by Virtuoso [20] and represented graphically in Figure 5.17.

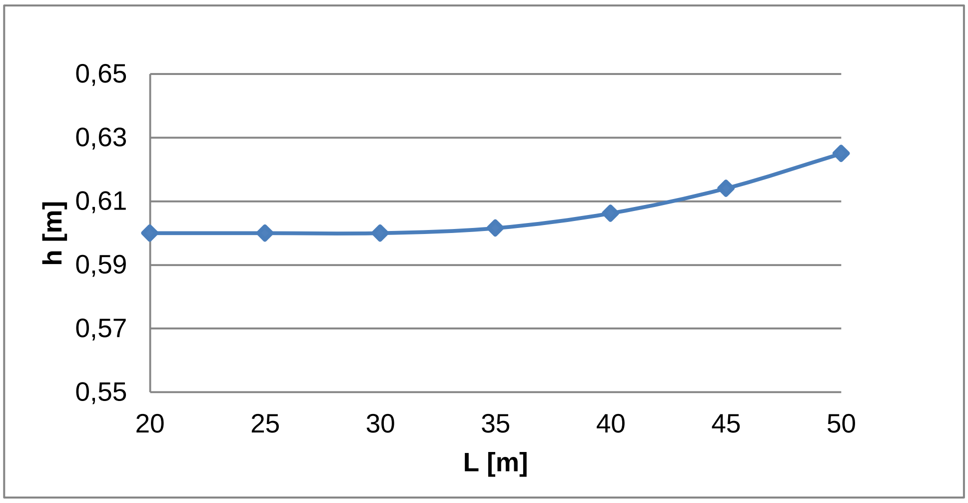

Figure 5.17 - Graph for the obtainment of an equivalent deck slab thickness for a characteristic span length *L* [20]

As it can be observed in Figure 5.17, it was assumed that the equivalent thickness has a constant value of 0,6 m for L ≤ 30 m, whereas for L > 30 m the following relation is taken into account:

$$h = 0{,}6 + (L - 30)^2 \times 6{,}25 \times 10^{-5} \quad [m] \tag{5.2}$$

By considering a superimposed dead load of 40 kN/m uniformly distributed in the entire bridge deck (associated with non-structural elements), the dead load supported by each beam is given by:

$$dead\ load = \frac{h \times b \times 25}{2} + \frac{40}{2} \quad [kN/m] \tag{5.3}$$

The internal forces due to the dead loads were obtained by using the corresponding influence lines, since this analysis is focused on the most unfavorable beam by considering the lateral distribution of loads. By taking into account the symmetry of the deck, half of the bridge dead load was considered on each beam. The results regarding the sagging bending moments can be observed in Figures 5.18 to 5.21, the ones corresponding to the hogging bending moments are represented in Figures 5.22 to 5.24 and in what concerns the shear force, the results are presented in Figures 5.25 to 5.28.

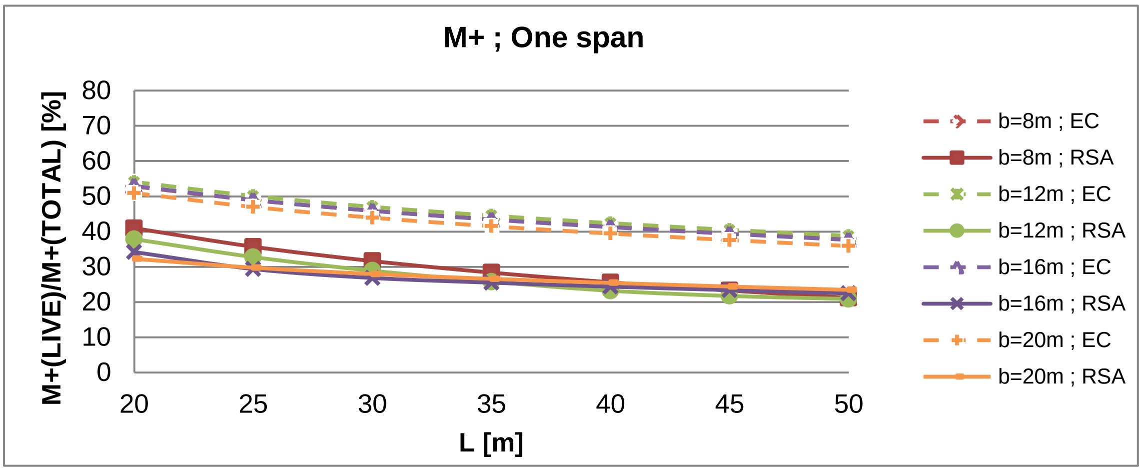

Figure 5.18 - Relation between the longitudinal sagging bending moments M+ at cross-section A obtained using the live loads and using all design loads at bridges with one span

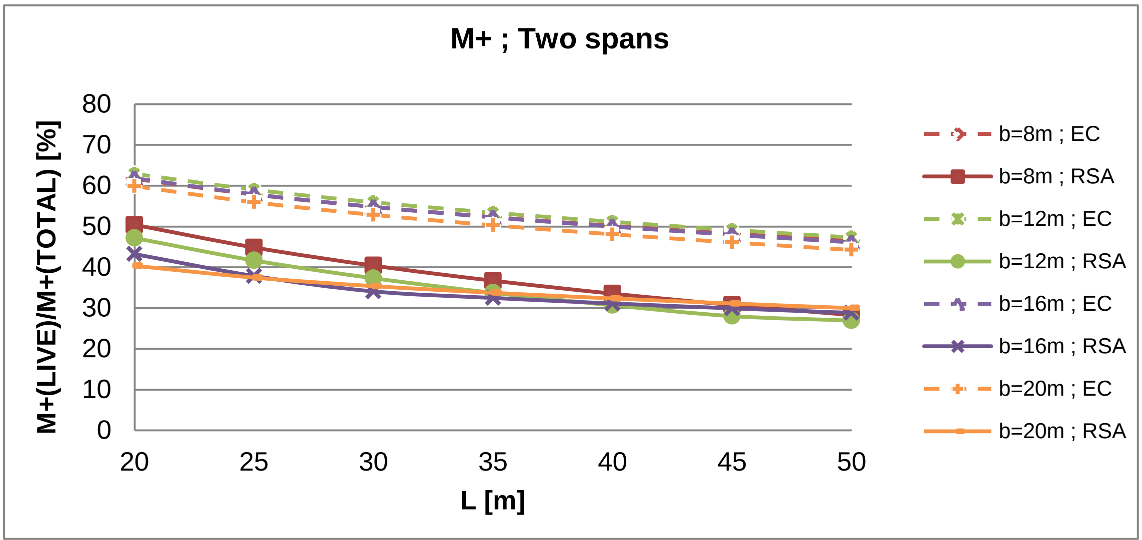

Figure 5.19 - Relation between the longitudinal sagging bending moments M+ at cross-section A obtained using the live loads and using all design loads at bridges with two spans

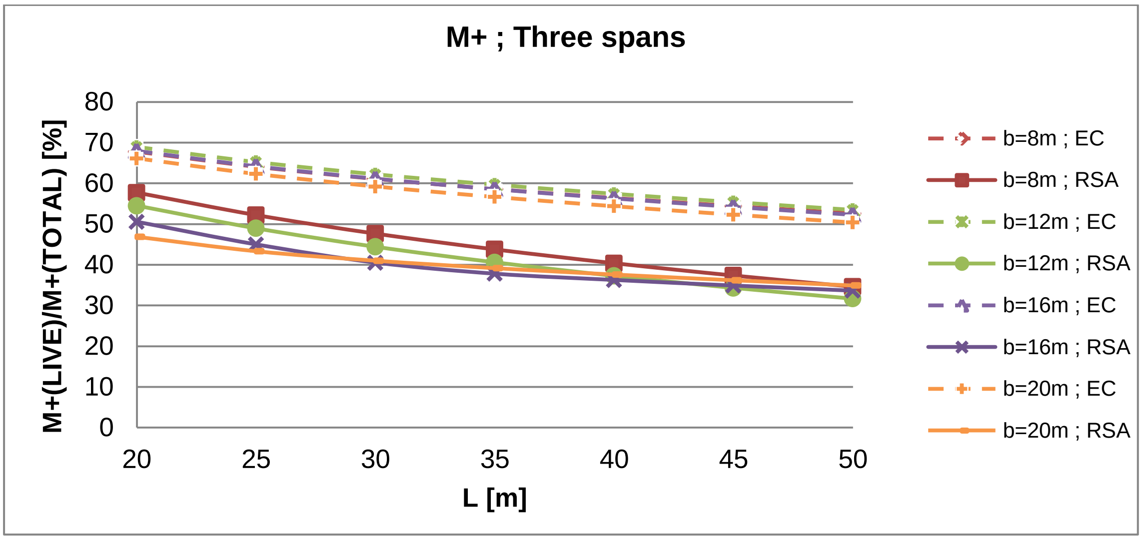

Figure 5.20 - Relation between the longitudinal sagging bending moments M+ at cross-section A obtained using the live loads and using all design loads at bridges with three spans

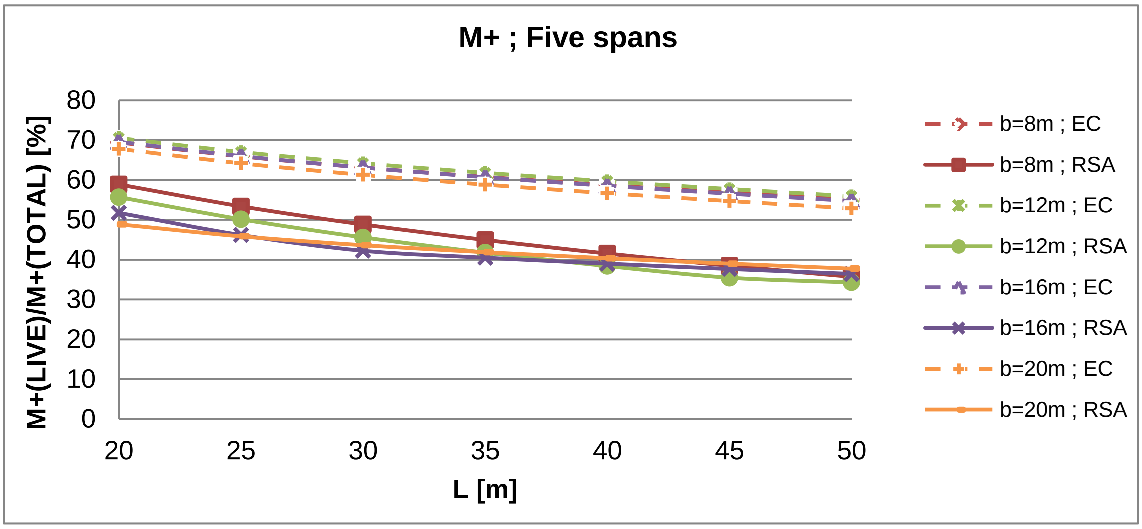

Figure 5.21 - Relation between the longitudinal sagging bending moments M+ at cross-section A obtained using the live loads and using all design loads at bridges with four spans

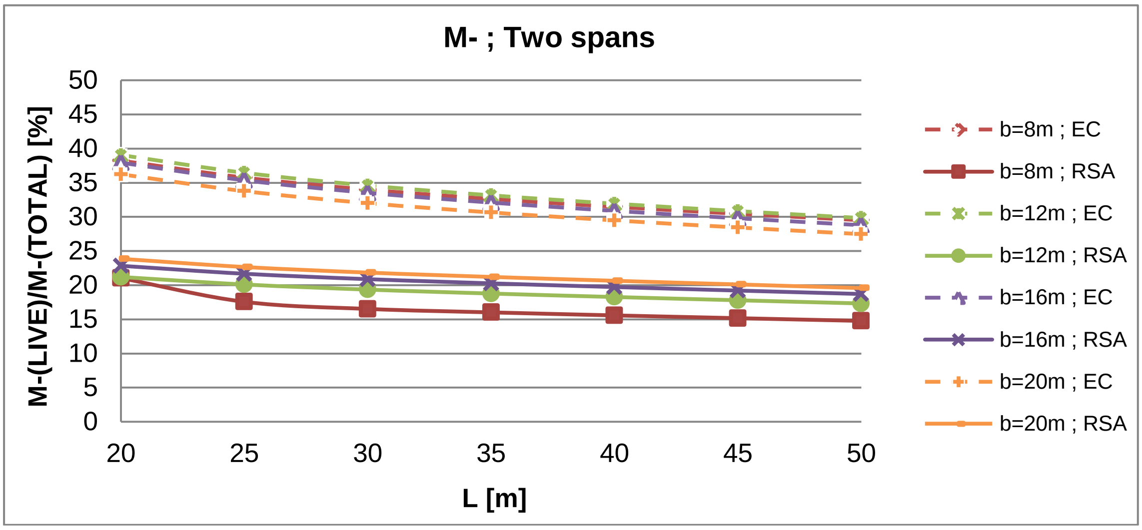

Figure 5.22 - Relation between the longitudinal hogging bending moments M- at cross-section B obtained using the live loads and using all design loads at bridges with two spans

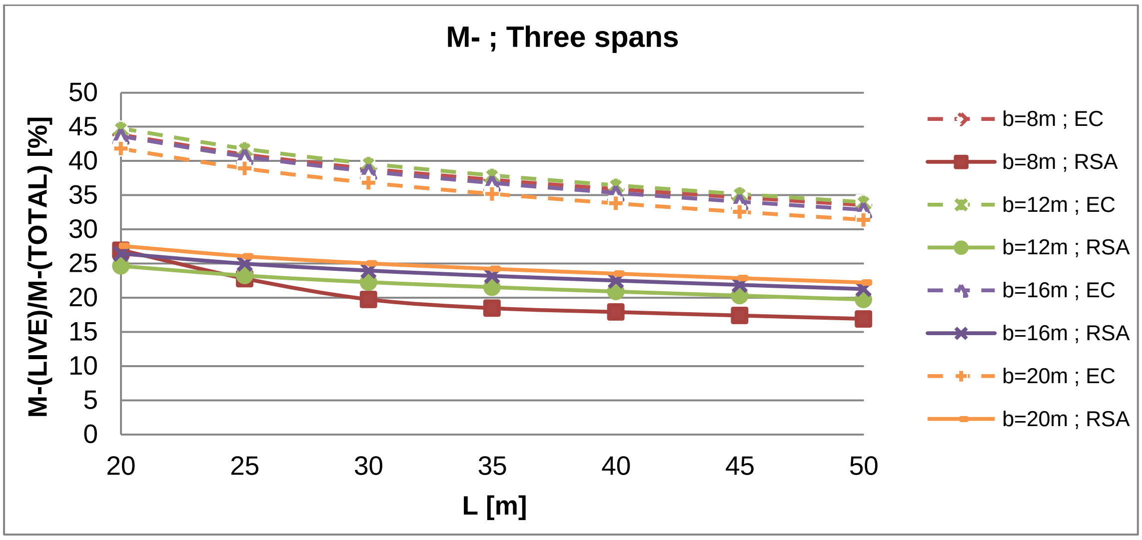

Figure 5.23 - Relation between the longitudinal hogging bending moments M- at cross-section B obtained using the live loads and using all design loads at bridges with three spans

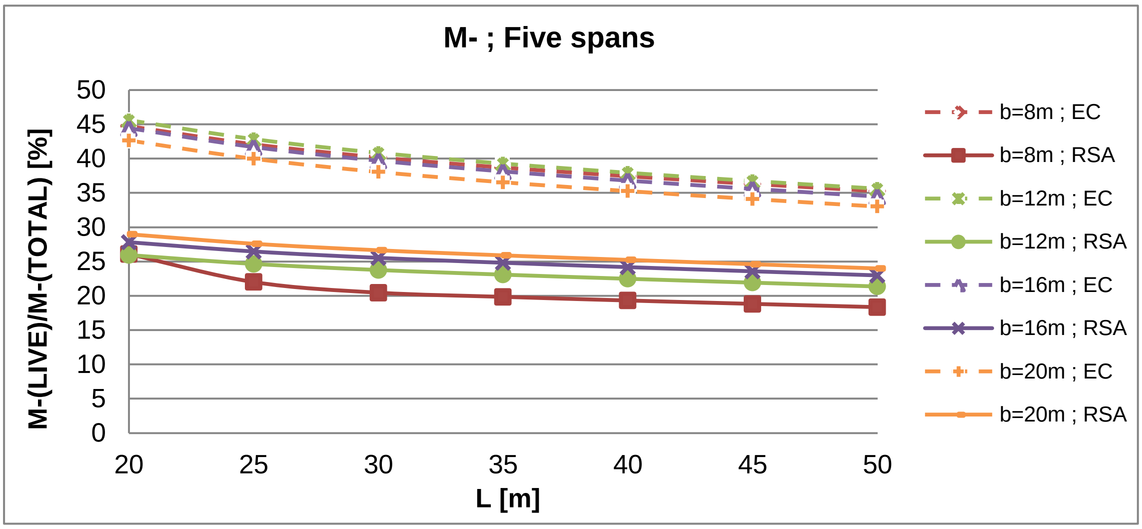

Figure 5.24 - Relation between the longitudinal hogging bending moments M- at cross-section B obtained using the live loads and using all design loads at bridges with five spans

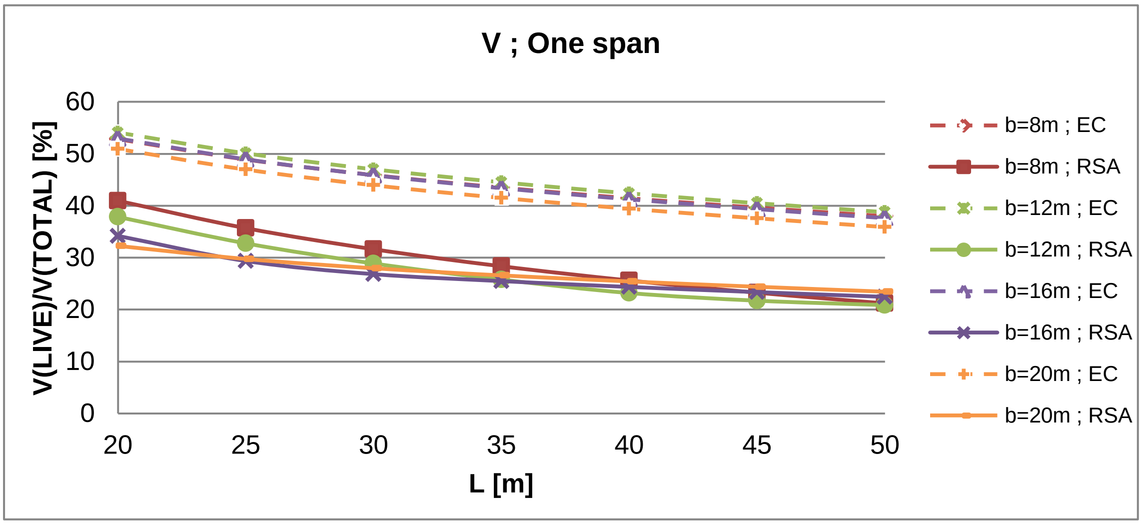

Figure 5.25 - Relation between the shear forces at cross-section C obtained using the live loads and using all design loads at bridges with one span

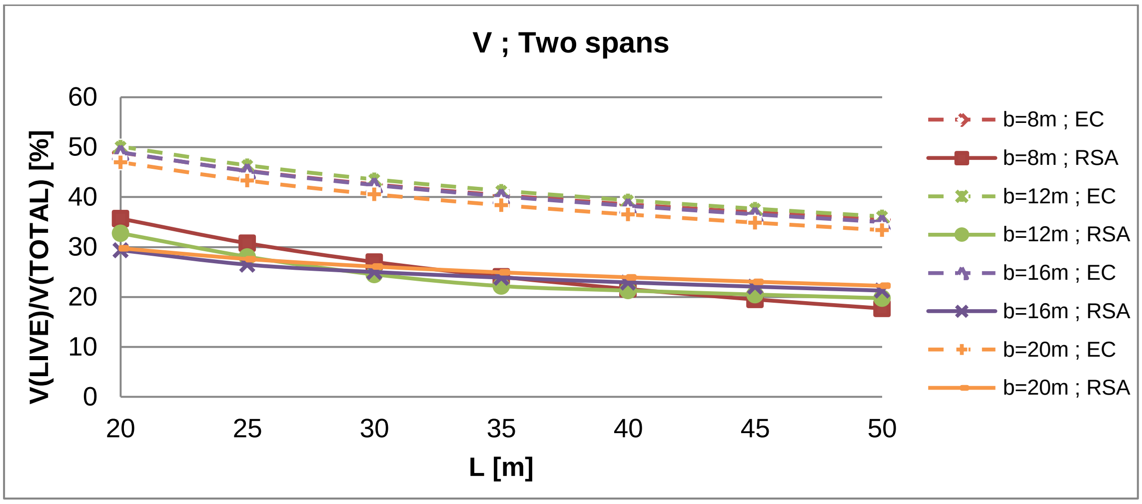

Figure 5.26 - Relation between the shear forces at cross-section C obtained using the live loads and using all design loads at bridges with two spans

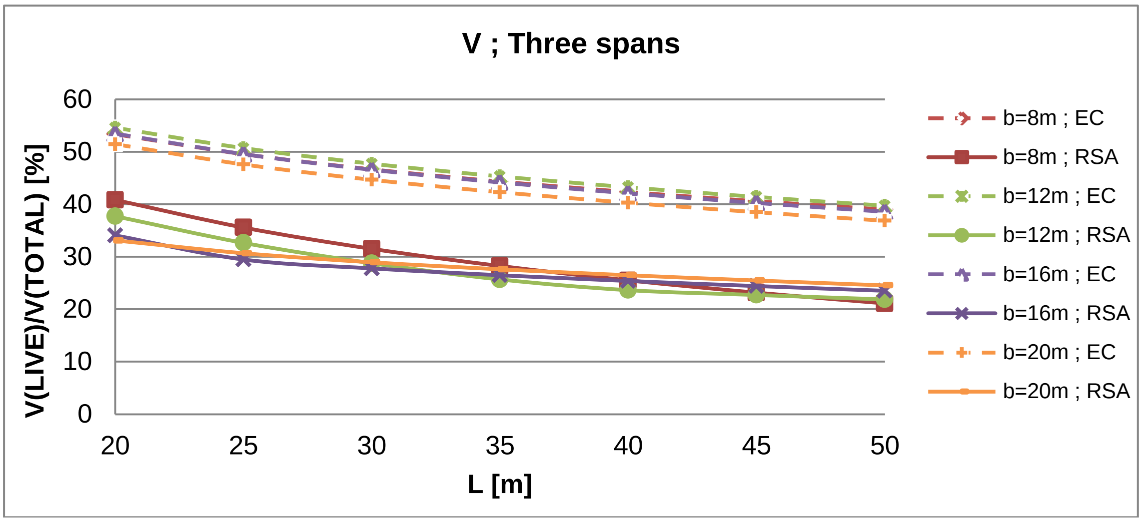

Figure 5.27 - Relation between the shear forces at cross-section C obtained using the live loads and using all design loads at bridges with three spans

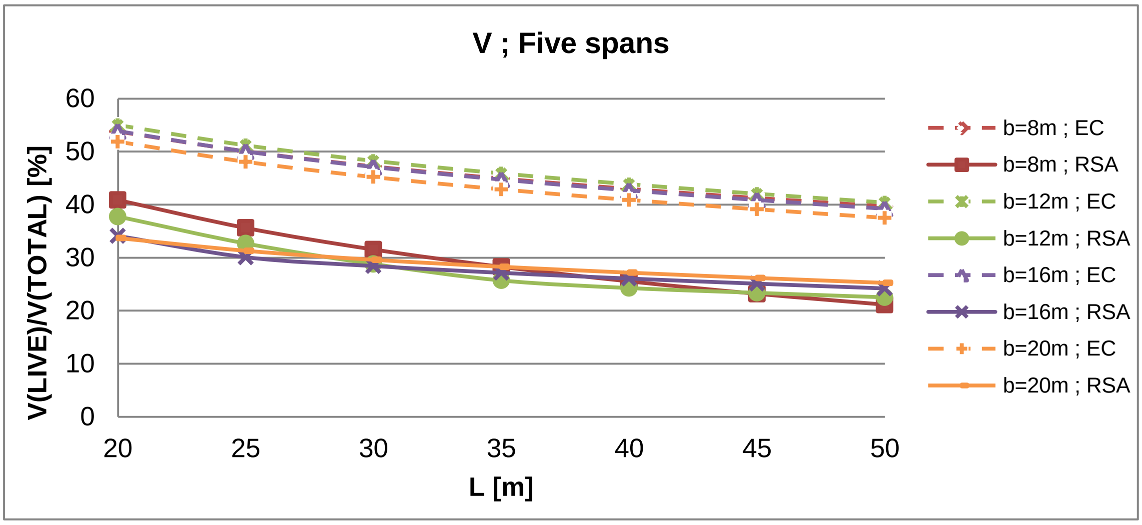

Figure 5.28 - Relation between the shear forces at cross-section C obtained using the live loads and using all design loads at bridges with five spans

From the values obtained for the bending moments and shear forces represented in Figures 5.18 to 5.28, it can be concluded that the relevance of the live loads on the global analysis decreases for longer spans *L*.

However, this relevance of the live loads is expected to become constant for higher values of *L*, since the concentrated loads (vehicles or knife-edge loads) of the live load models do not increase with the span as occurs with the dead loads and with the uniformly distributed loads. Therefore, this relevance of the live loads tends to a value for which these concentrated loads have almost no effect and which is expected to be constant.

Regarding the influence of the deck width on the variation of the values of Figures 5.18 to 5.28 corresponding to the Eurocode LM1 (EC), it has two contradictory effects since the superimposed dead load is independent of *b*, being the same for all deck widths (40 kN/m): (i) due to the different loads acting on the different lanes in the Eurocode LM1, it is expected that the relation between the live loads and the dead loads increases for smaller deck widths, since only the higher loads fit in the road width; (ii) since the superimposed dead load does not increase with the deck width its influence in the relation between the live loads and the dead loads is higher also for smaller decks.

Therefore, the relation between the live loads and the design loads increases with *b* until a certain value of the deck width from which that relation starts to decrease. This value of *b* depends on the value of the superimposed dead load, and for the cases analyzed, with a superimposed dead load of 40 kN/m, the relation between the effects of the live loads and the ones due to the design loads increase between b = 8 m and b = 12 m, decreasing thenceforth to b = 20 m. This fact justifies the coincidence of the values corresponding to b = 8 m and b = 16 m in the Figures 5.18 to 5.28, in what concerns the influence of the Eurocode LM1 on the design loads.

The live loads become more important when the number of spans is increased. However, for bridges with more than five spans the difference becomes irrelevant. Regarding the shear force V, both live load cases (Eurocode LM1 and RSA) maintain their importance except for the case with two spans, where their influence in the total shear force is slightly smaller.

Another feature of the curves presented in the graphs corresponding to the RSA is that they represent the relation between the effects of the most unfavorable RSA load case and the total loads.

Thus, being the RSA-a more unfavorable only for smaller values of *b* and *L* , it can be verified a reducing in the slope of the graph curves when the RSA-b becomes more unfavorable. As an example, it can be observed that for M- (Figures 5.22 to 5.24), only for *b* = 8 m this change occurs in the domain of values of *L* considered (20 m – 50 m), being the RSA-b almost always more unfavorable.

Another interesting fact verified in Figures 5.18 to 5.28 and regarding the RSA is that when the RSA-a is more unfavorable, the relation between the internal forces due to live loads and due to the design loads is bigger for smaller values of *b*. However, when the RSA-b becomes more unfavorable the relevance of the live loads is bigger for higher values of *b*.

This situation can be justified with the fact that, consisting only on uniformly distributed loads in the deck width, the values of the RSA-b loads increase directly with *b* as occurs with the self-weight. On the other hand, the RSA-a consists in only one vehicle and the load values don't increase with *b*, although the load transmitted to the most unfavorable beam, which depends also on the relative position of the vehicle in the deck width, increases with *b*.

As a global conclusion, it can be observed that the difference between the importance of both load codes in the total effects is significant, corresponding to a relevant difference between the effects caused by the RSA and by the Eurocode LM1.

5.4 Conclusions

It can be concluded from this chapter that in a longitudinal analysis of bridges, as occurred also in the transverse analysis, the values of the internal forces obtained according to the Eurocode LM1 are significantly higher than the ones obtained using the RSA.

The values for the longitudinal bending moments (in hogging and sagging regions) and for the shear force obtained according to the RSA are between 35% and 60% of those obtained by applying the Eurocode LM1, as verified in Figures 5.6 to 5.16.

The contribution of the live loads to the bridge global analysis, by comparison with the design loads, was verified in Figures 5.18 to 5.28 to be within the following ranges:

(i) M+ (EC-LM1): 35% - 70%;
M+ (RSA): 20% - 60%;

(ii) M- (EC-LM1): 27% - 45%;
M- (RSA): 15% - 30%;

(iii) V (EC-LM1): 35% - 55%;
V (RSA): 18% - 40%.

Thus, it can be inferred that regarding the relevance of the live loads when compared with the dead loads, the live loads are more important for the evaluation of the sagging moments M+ and shear forces V than of the hogging moments M-. However, the importance of the live loads for the global analysis of bridge decks was verified.

CHAPTER 6

6. Example of comparison between the RSA and the Eurocode LM1 - application to two real bridges

6.1 Introduction

A comparison between the results of the transverse and longitudinal analyses of bridges for the loads defined according to the RSA [3] and to the Eurocode Load Model 1 [2] was presented in Chapters 4 and 5, for bridges with a slab-beam cross-section, namely:

(i) The distributions of slab transverse bending moments over the beams were obtained by adopting the semi-analytical methods developed in Chapter 3 (Eq. (3.5) and Eq. (3.17)) and considering several relevant parameters: the relation between the cantilever span and the internal span (S_c/S), the relative position of the loads on the overhang (c/S_c) and on the internal panel (c'/S), the thickness variation of the cantilever slab (t_1/t_2) and of the internal slab (t_1/t_3), the existence and relative position (d/S_c) of structural curbs (edge-stiffening) and the relation between their stiffness and the transverse flexural stiffness of the cantilever slab (represented by the factor K' defined in Eq. (3.1));

(ii) The transverse moments in the internal slab were evaluated by adopting Timoshenko's solution [4] presented in Chapter 3 (Eq (3.15) and Eq. (3.16));

(iii) The comparison between the sagging and hogging bending moments (M+ and M-, respectively) and shear force (V) due to both codes and obtained in the longitudinal beams of bridges with different deck widths and different number of spans was made;

(iv) The relative influence of the live loads on the design loads, in terms of the global bridge analysis, is presented for several bridge structural systems and for both codes.

In the present chapter the results of the previous analyses are applied to the local and global analysis of two real bridges with different cross-section dimensions and structural systems: (i) the Bridge 1, a continuum bridge with thirteen spans (the eleven central spans with a length of 40 m and the two extreme spans with a length equal to 32 m) and a cross-section geometry represented in Figure 6.1 and (ii) the Bridge 2, a continuum bridge with three spans (the central span with 31 m and the extreme spans with 14,5 m) and a cross-section illustrated in Figure 6.2.

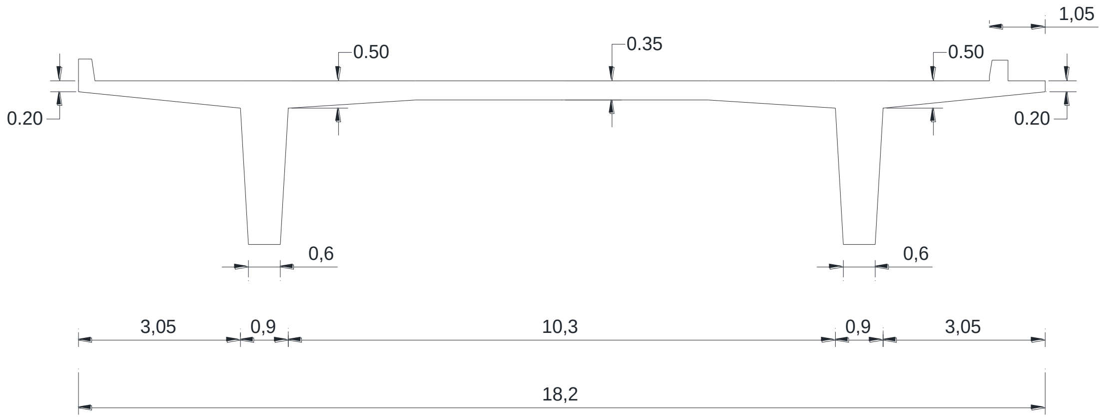

Figure 6.1 - Cross-section geometry of Bridge 1

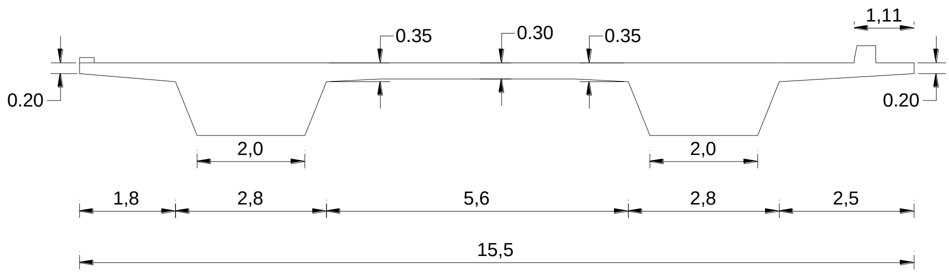

Figure 6.2 - Cross-section geometry of Bridge 2

Each cross-section has two different overhangs since they have curbs with different dimensions and with an unsymmetrical position on the cantilever slab. Thus, the transverse bending moments at the cantilever supports (over the beams) obtained according to both codes (RSA and Eurocode LM1) are presented for each side of the bridge deck.

The longitudinal bending moments and shear force at the most unfavorable beam of each bridge 1 and 2 were also evaluated in order to compare them with the results represented in the graphs of Figures 5.6 to 5.16 and of Figures 5.18 to 5.28.

For all the analyses of both bridges 1 and 2 the results are graphically represented.

6.2 Transverse analysis

The parameters with a relevant influence on the bridge structural behavior were defined in order to use the semi-analytical methods (Eq. (3.5) and Eq. (3.17)) and Timoshenko's solution (Eq. (3.15) and Eq. (3.16)) in the transverse analyses.

The parameters considered for the effect of the cantilever loads are: (i) the thickness variation t_1/t_2, (ii) the location of the curb (edge-stiffening), represented as the distance *d* of the curb from the overhang support, and (iii) the factor K' representing its relative stiffness.

For the loads acting on the internal panel the relevant characteristics are: (i) the thickness variation of the brackets t_1/t_3, (ii) the relation between the cantilever length and the internal span S_c/S (when the cantilever slabs have a varying thickness an equivalent value of S_c is calculated in order to consider that variation) and (iii), if exists, the curb's relative stiffness factor K'.

Since Timoshenko's solution [4] and the developed methods neglect the flexibility of the bridge longitudinal beams, the slabs of the models cross-sections are admitted rigidly supported by the beams as represented in Figures 6.3 and 6.4. By doing so, for the slab analysis the beams thicknesses were not considered, as well as the loads acting on them since they are directly resisted by the longitudinal beams and don't create any transverse moments in the deck slab. However, the positioning of the traffic loads in the analyzed model is defined taking into account the deck real width (including the beams thicknesses). The cross-sections of the models considered in the transverse analysis of bridges 1 and 2 are illustrated in Figures 6.3 and 6.4, respectively.

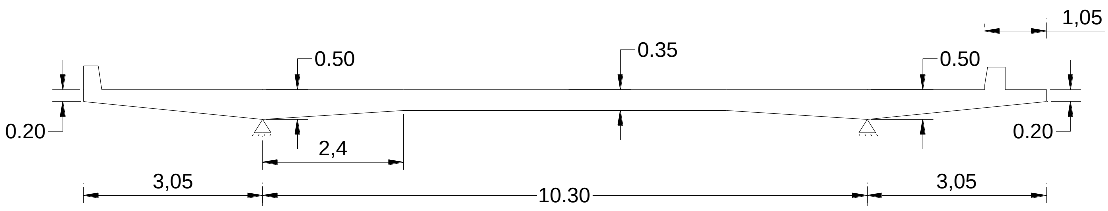

Figure 6.3 - Cross-section geometry of the model for Bridge 1, neglecting the beams widths

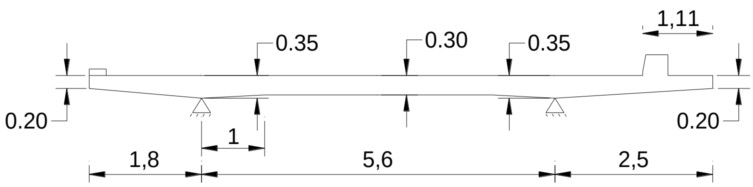

Figure 6.4 - Cross-section geometry of the model for Bridge 2, neglecting the beams widths

The characteristics of each bridge deck are described in Table 6.1:

Bridge	Side	t_1/t_2 (cantilever)	d/S_c	K'	t_1/t_3 (brackets)	S_c/S
1	left	2,50	1	0,161	1,430	0,138
	right	2,50	2/3	0,273	1,430	0,138
2	left	1,75	-	0	1,167	0,177
	right	1,75	2/3	0,658	1,167	0,248

Table 6.1 – Characteristics of bridge models 1 and 2

It can be verified in Figure 6.4 and in Table 6.1 that the curb presented in the left side of the Bridge 2 is a non-structural curb, which means that it was not considered as edge-stiffening in the analyses. On the other hand, the curb presented on the right side of Bridge 2 and both curbs of Bridge 1 are considered as structural.

The transverse bending moments were obtained by applying the developed semi-analytical methods (Eq. (3.5) and Eq. (3.17)) presented in Chapter 3 and Timoshenko's solution [4] (Eq. (3.15) and Eq. (3.16)) by considering the values of the parameters presented in Table 6.1 and adopting the same criterion for the positioning of loads used in Chapter 4.

It should be noticed that due to the characteristics of the cross-section of Bridge 1 some approximations were considered in the analysis of the left side:

(i) The respective curb is located at the cantilever edge while the graphs presented in Chapter 4 concerning the transverse analysis (Figures 4.5 to 4.12) were developed for cases with $d/S_c = 2/3$ (with the curb located at 2/3 of the cantilever length), and as it was demonstrated in Chapter 3 (Figure 3.15) the position of the curb in the overhang has a considerable influence on the results;

(ii) By considering the criterion defined for the loads located close to the beams, which is the neglecting of the loads acting at a distance from the longitudinal supports of the deck slab equal or smaller than the slab thickness t_1, it was verified, as illustrated in Figures 6.5 and 6.6, that the second line of wheels of the RSA-a vehicle was neglected, while the second line of wheels of the Eurocode LM1 main vehicle was considered. This situation is due to the difference in the wheels dimensions of both codes, and it leads to an high reduction of the ratio $m_{y(RSA)}/m_{y(EC)}$ which may not represent the reality, but which is a consequence of the method and criterion used.

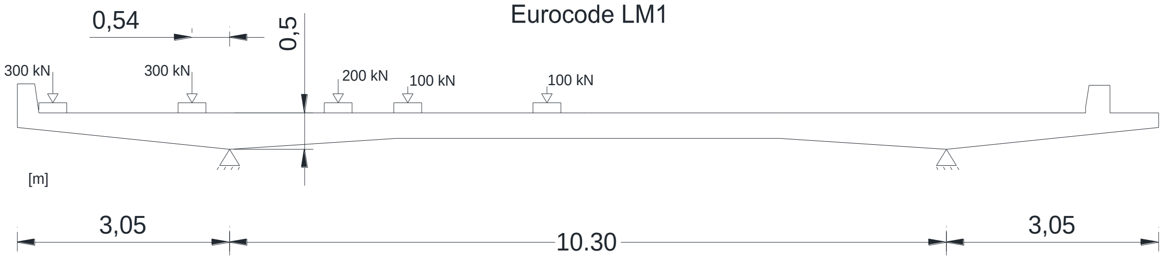

Figure 6.5 - Consideration of the second line of wheels of the Eurocode LM1 main vehicle (Bridge 1)

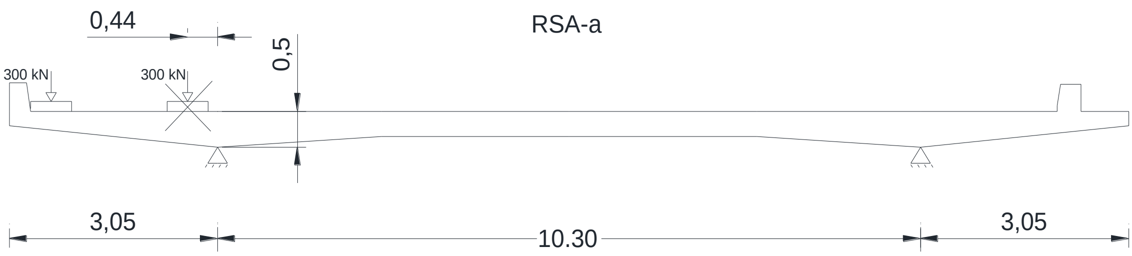

Figure 6.6 - Neglecting of the second line of wheels of the RSA-a vehicle (Bridge 1)

It should also be noticed that the value of $m_{y(RSA)}/m_{y(EC)}$ corresponding to the right side of Bridge 1 was obtained without considering the second line of wheels on the cantilever (of both codes, RSA and Eurocode LM1), as it was expected for the corresponding width *b*. This is explained with the fact that the graphs presented in Chapter 4 concerning the transverse analysis (Figures 4.5 to 4.12) were developed for a relation of spans S_c/S = 0.5, which is not the value corresponding to Bridge 1.

The results obtained for the slab transverse moments over both longitudinal beams of both Bridges 1 and 2 are presented in Table 6.2 and plotted in Figures 6.5 and 6.6.

		Transverse bending moments over the beams		
		$m_{y(RSA)}$ [kNm/m]	$m_{y(EC)}$ [kNm/m]	$m_{y(RSA)}/m_{y(EC)}$
Bridge 1	Left side	96,87	217,72	0,445
	Right side	72,50	159,18	0,455
Bridge 2	Left side	62,14	127,27	0,488
	Right side	52,37	107,45	0,487

Table 6.2 – Results for the transverse moments over the beams for both sides of both bridges, evaluated using the developed semi-analytical methods (Eq. (3.5) and Eq. (3.17))

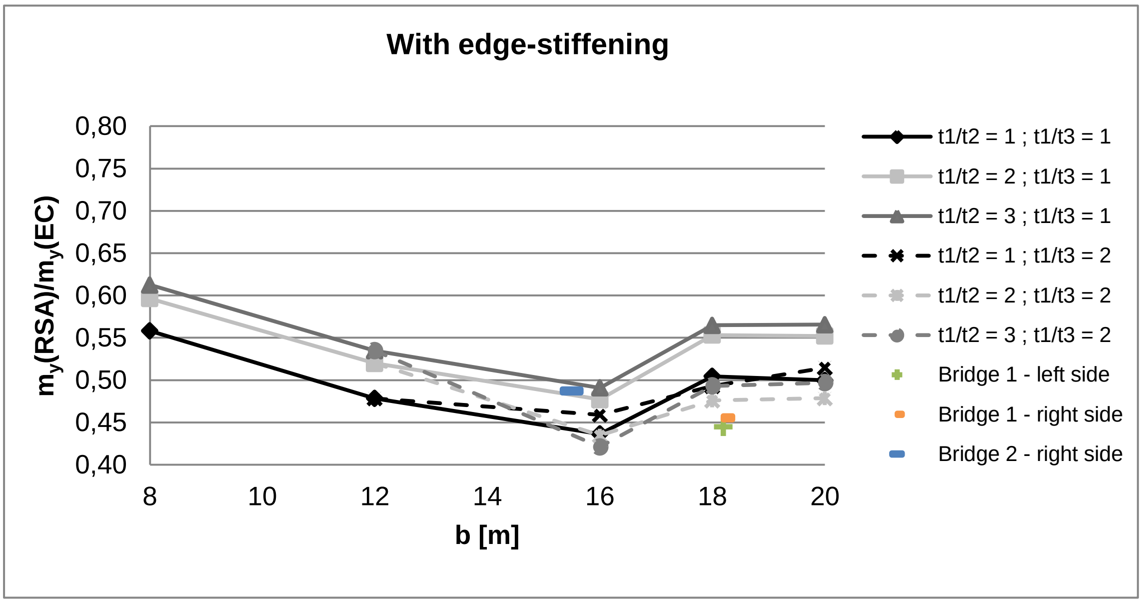

Figure 6.7 - Results corresponding to both sides of Bridge 1 and the right side of Bridge 2 represented in the graph of Fig. 4.6

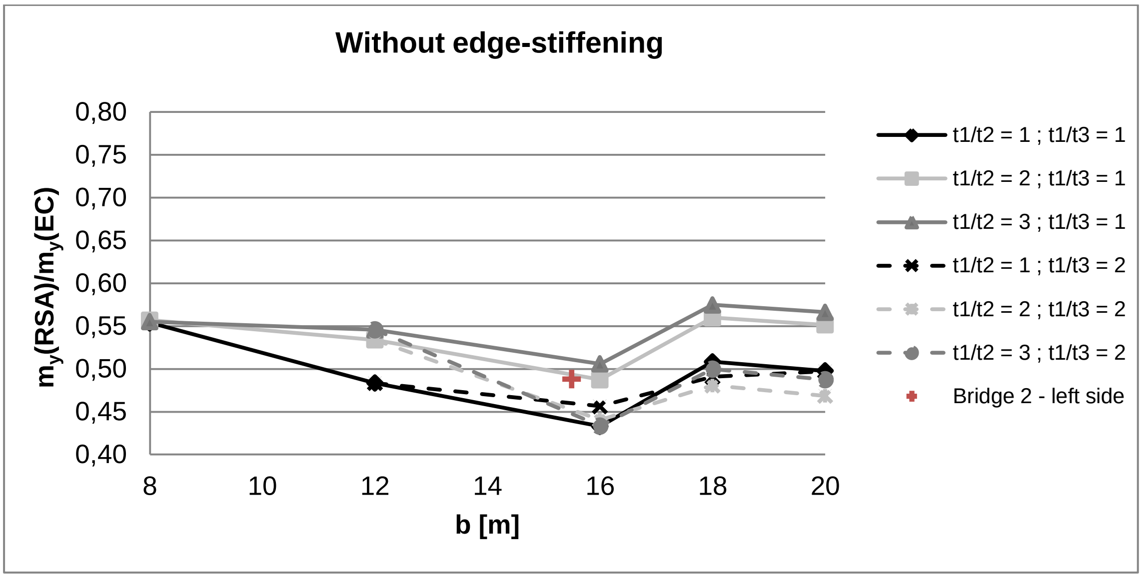

Figure 6.8 - Results corresponding to the left side of Bridge 2 represented in the graph of Fig. 4.5

The results obtained for Bridge 2 and plotted in Figures 6.7 and 6.8 fit within the results represented in the corresponding graphs. For the results corresponding to Bridge 1, due to the approximations assumed and described previously, the results don't fit so well with the corresponding values in the graphs of Figure 6.7. However, the differences verified are not much significant and it can be inferred that the developed graphs are suitable for a quick comparative analysis of this type of bridge decks regarding the RSA and the Eurocode LM1, even for the cases where certain approximations have to be assumed as occurred for Bridge 1.

The transverse bending moments at the mid-span of the internal panel obtained by using Timoshenko's solution [4] are presented for both bridges in Table 6.3.

The results were also plotted in the graph of Figure 6.9, where a comparison between the values of m_y obtained by applying the RSA and the Eurocode LM1 was made. However, all the results obtained neglected the effect of the cantilevers and other parameters that could reduce these moments.

	Transverse bending moments at the mid-span of the internal panel		
	$m_{y(RSA)}$ [kNm/m]	$m_{y(EC)}$ [kNm/m]	$m_{y(RSA)}/m_{y(EC)}$
Bridge 1	100,78	238,85	0,422
Bridge 2	64,49	133,06	0,485

Table 6.3 – Results for the transverse moments at the mid-span of the internal panel, evaluated using Timoshenko's solution [4]

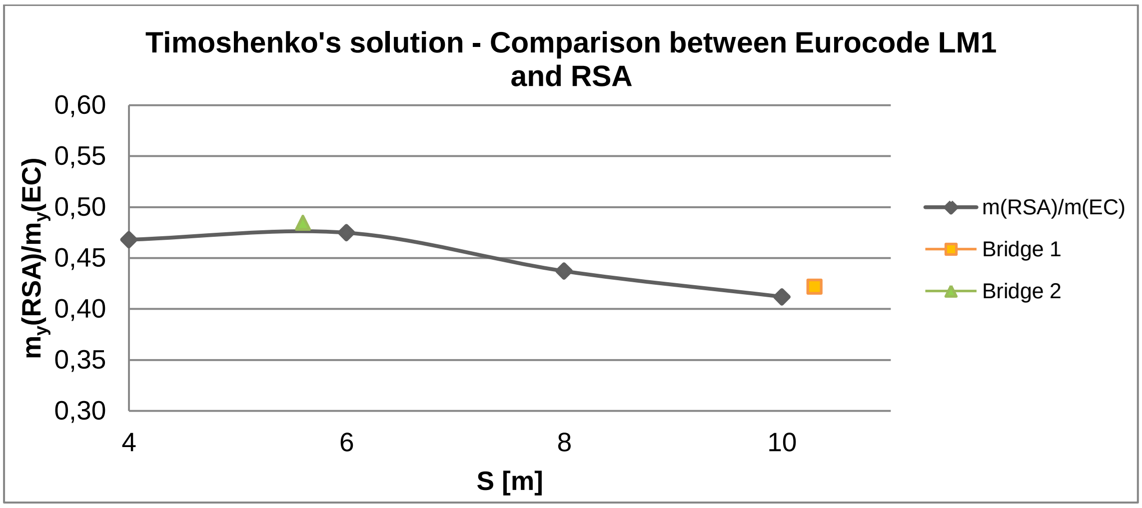

Figure 6.9 - Results for the transverse moments at the internal slab represented in the graph of Fig. 4.13

Since it was current practice in a simplified design to consider the cantilever clamped, i.e., neglecting the influence of the internal panel flexibility, a finite element analysis considering the overhangs of both bridges clamped when acted by the RSA was also performed. The approximations adopted previously for the use of Eq. (3.5) and Eq. (3.17) (see p.104 of this work) were maintained in this finite element analysis. The transverse moments due to Eurocode LM1 used in these new comparisons are the ones represented in Tables 6.2 and 6.3, obtained by using the developed semi-analytical methods (Eq. (3.5) and Eq. (3.17)).

The results obtained are plotted in Figures 6.10 and 6.11.

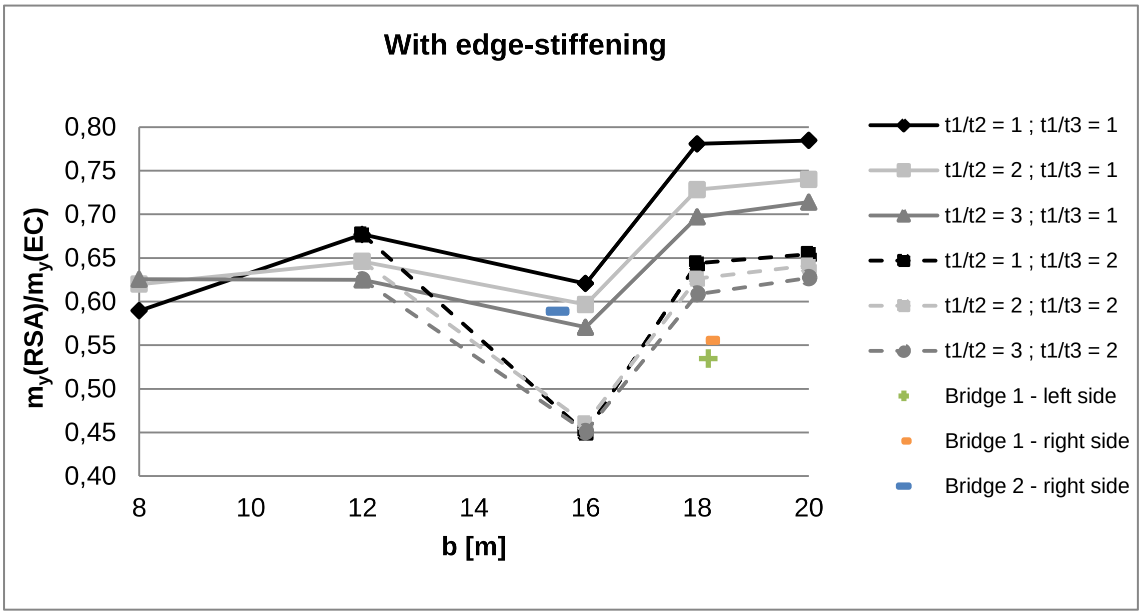

Figure 6.10 - Results corresponding to both sides of Bridge 1 and the right side of Bridge 2 represented in the graph of Fig. 4.10

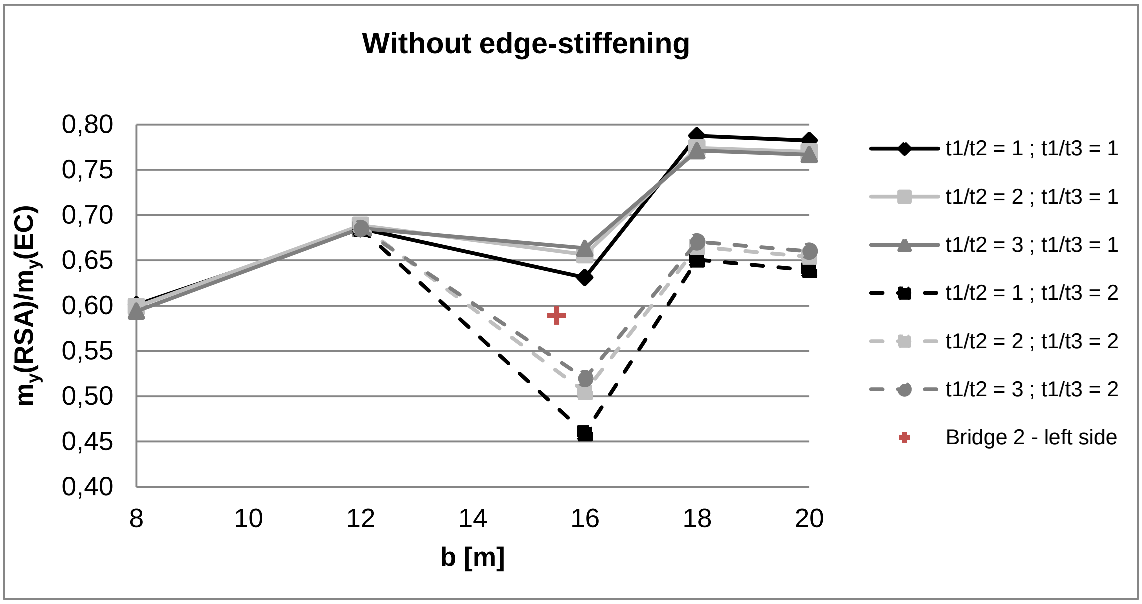

Figure 6.11 - Results corresponding to the left side of Bridge 2 represented in the graph of Fig. 4.9

It can be verified that the results obtained for Bridge 2 in this comparative analysis between the RSA and the Eurocode LM1 (considering the overhangs rigidly clamped for the analysis of the transverse moments due to the RSA) are close to the ones expected by extrapolation from the graphs of Figures 6.10 and 6.11. For Bridge 1 the results don't fit so well in the ones represented in the graphs of Figure 6.10 due to the approximations admitted (see p. 104 of this dissertation), but do not differ much from the expected ones.

6.3 Longitudinal analysis

The comparison between the effects due to both load codes (RSA and Eurocode LM1) was also performed for the longitudinal analysis of Bridges 1 (Figure 6.1) and 2 (Figure 6.2) by using the influence lines adopted in Chapter 5.

Although the bridge 1 has thirteen spans, it was used as an approximation the influence lines of a five-span bridge, since the analysis is focused on the central span and the values of the influence lines for the central span tend to stabilize as the number of spans increases.

The results with the comparison between the values of the bending moments (M+ and M-) and shear force (V) obtained according with the RSA and with the Eurocode LM1 are presented in Tables 6.4 and 6.5 and plotted in Figures 6.12, 6.14 and 6.16 for Bridge 1 and in Figures 6.11, 6.15 and 6.17 for Bridge 2.

	Bridge 1				
	b [m]	L [m]	max(EC)	max(RSA)	RSA/EC
M+ [kNm]	18.2	40	13926	7659	0.550
M- [kNm]	18.2	40	11835	7732	0.653
V [kN]	18.2	40	2240	1282	0.572

Table 6.4 – Results of the longitudinal analysis using the RSA and the Eurocode on Bridge 1

	Bridge 2				
	b [m]	L [m]	max(EC)	max(RSA)	RSA/EC
M+ [kNm]	15.5	31	7922	3416	0.431
M- [kNm]	15.5	31	6567	3159	0.481
V [kN]	15.5	31	1807	814	0.450

Table 6.5 – Results of the longitudinal analysis using the RSA and the Eurocode on Bridge 2

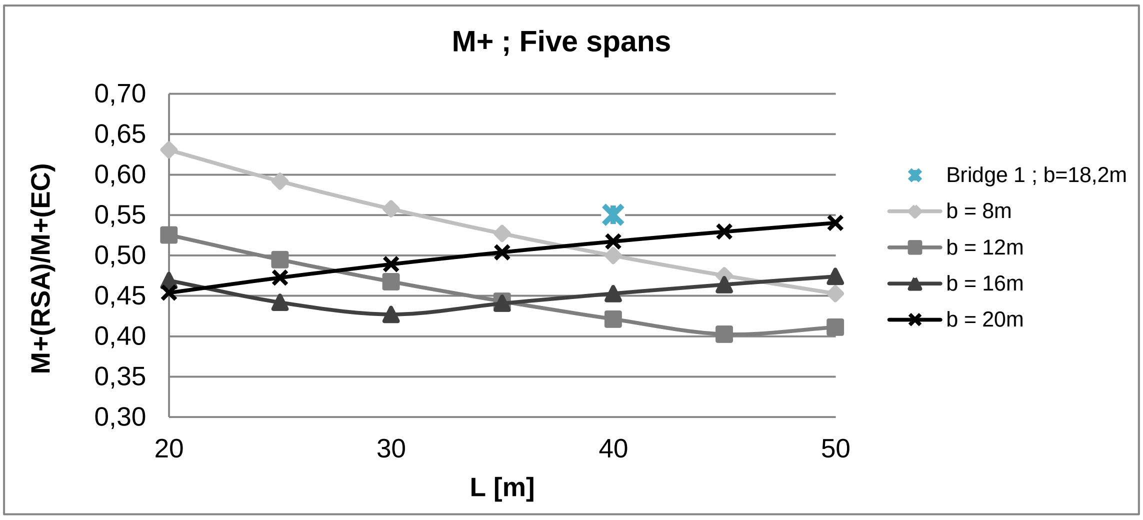

Figure 6.12 - Relation between the sagging moments M+ caused by both load codes on the most loaded beam of Bridge 1 and represented in the graph of Fig. 5.9

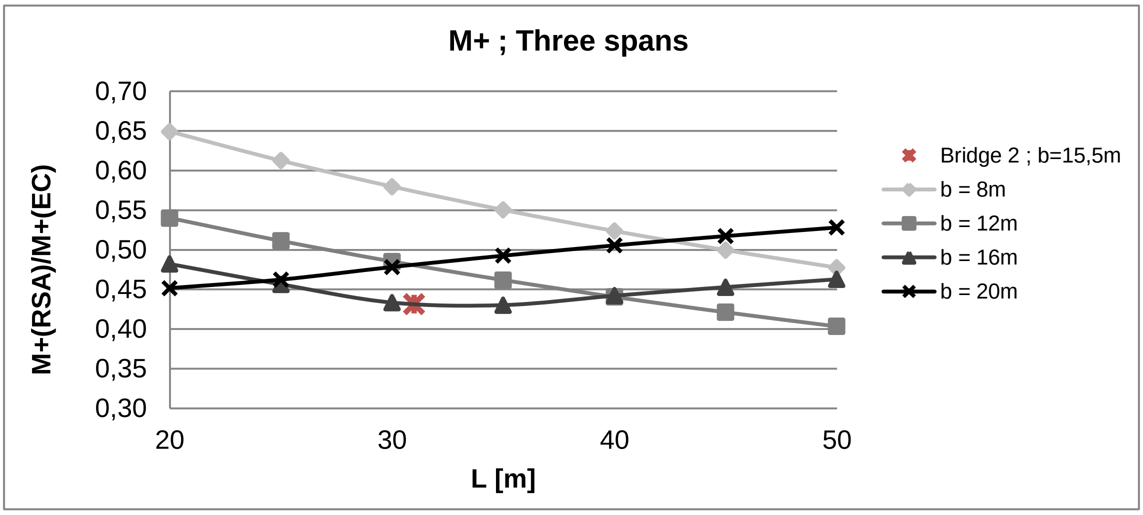

Figure 6.13 - Relation between the sagging moments M+ caused by both load codes on the most loaded beam of Bridge 2 and represented in the graph of Fig. 5.8

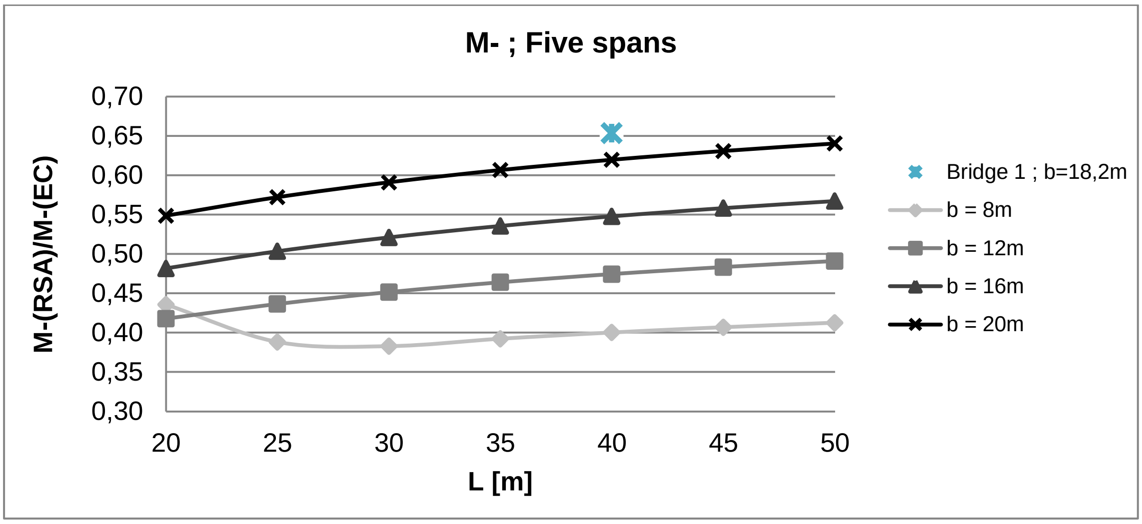

Figure 6.14 - Relation between the hogging moments M- caused by both load codes on the most loaded beam of Bridge 1 and represented in the graph of Fig. 5.12

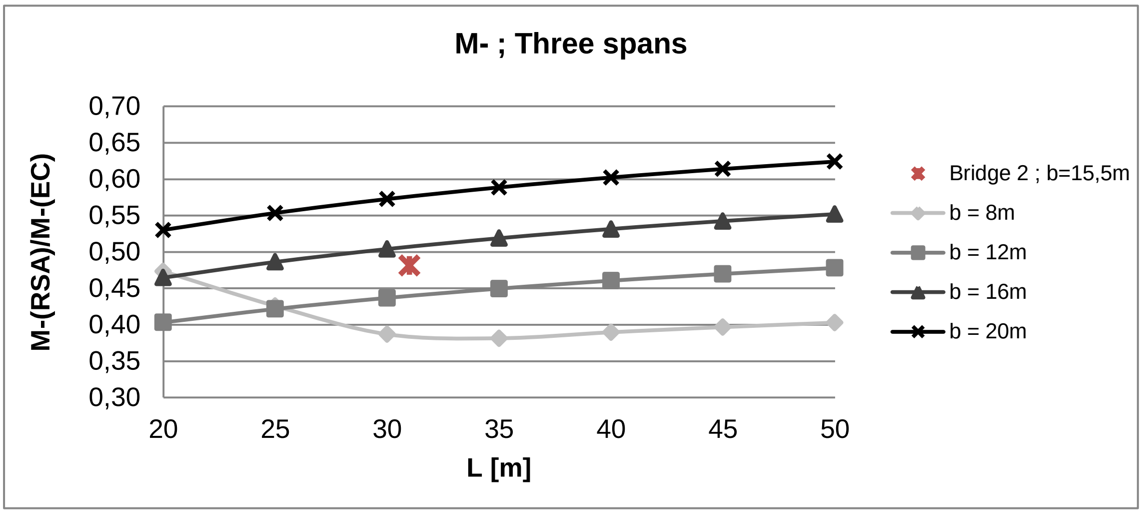

Figure 6.15 - Relation between the hogging moments M- caused by both load codes on the most loaded beam of Bridge 2 and represented in the graph of Fig. 5.11

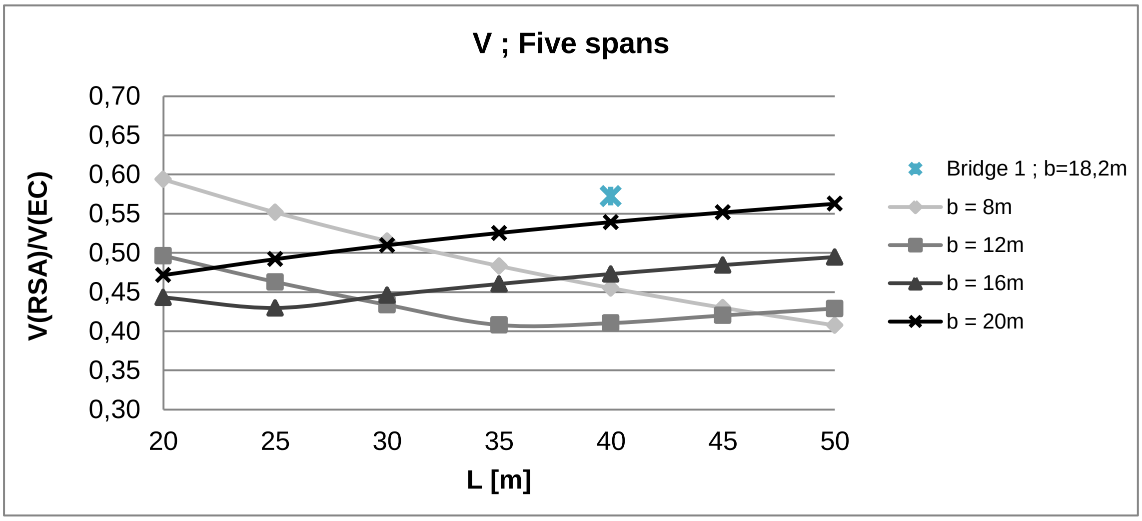

Figure 6.16 - Relation between the shear forces V caused by both load codes on the most loaded beam of Bridge 1 and represented in the graph of Fig. 5.16

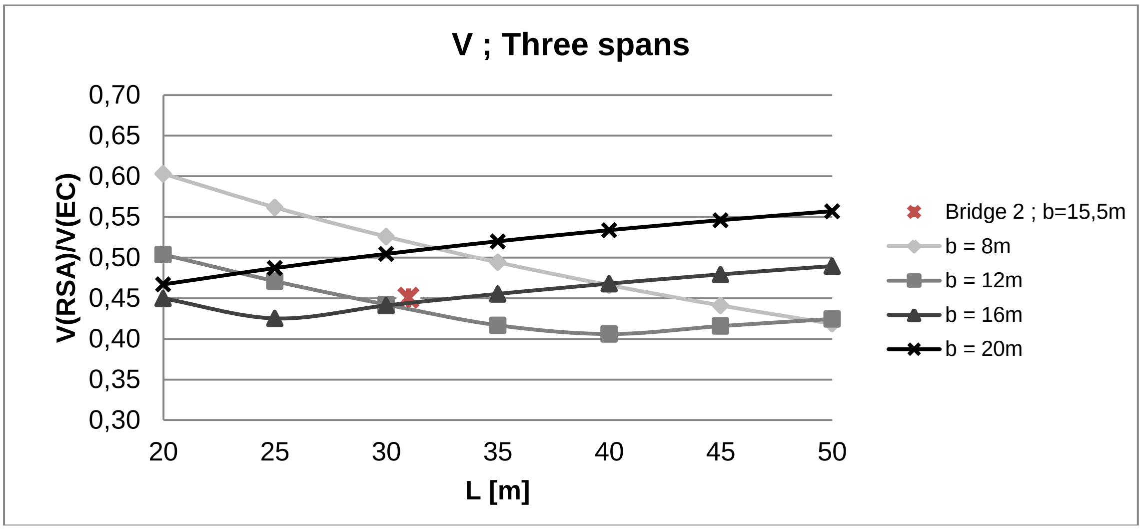

Figure 6.17 - Relation between the shear forces V caused by both load codes on the most loaded beam of Bridge 2 and represented in the graph of Fig. 5.15

The relation between the internal forces obtained by applying the RSA and the Eurocode LM1 can be evaluated through the results presented in Figures 6.12 to 6.17 since the results obtained fit in the ones provided by the graphs.

However, for the Bridge 1 the relation between the internal forces due to the RSA and due to the Eurocode LM1 is higher than what is expected for b = 18.2 m and L = 40 m. This fact can be explained with the following differences between the models of bridges used in Chapter 5 and the model used to analyze the Bridge 1.

(i) Bridge 1 has a relation between the overhang length and the internal slab S_c/S smaller than 0.5, which is the value adopted in the bridge models in Chapter 5;

(ii) In opposition to the models presented in Chapter 5, the Bridge 1 is transversely non-symmetrical. The most unfavorable beam for Bridge 1 is the left one, corresponding to a side where the cantilever has no sidewalk and the curb is on the edge of the overhang (d/S_c = 1), while the bridge models used in Chapter 5 considered sidewalks widths of 1 m in both overhangs.

Although these differences have been verified, their influence on the results is not much significant and the deviation between the results obtained and the ones expected is small. Therefore, the extrapolation from the values of Figures 5.6 to 5.16 for a comparison between the RSA and the Eurocode LM1 in practical cases is admitted as an approximated method.

In what concerns the percentage of the total internal forces caused in both Bridges 1 and 2 by the traffic loads, the results, as can be observed in Tables 6.6 and 6.7 and in Figures 6.18 to 6.23, are also as expected considering the graphs developed in Chapter 5 (Figures 5.18 to 5.28).

	Bridge 1 - left side (with lateral distribution of loads)						
	A [m^2]	L [m]	max(EC)	max(RSA)	max(dead loads)	EC/TOTAL	RSA/TOTAL
M+ [kNm]	5.55	40	13926	7659	10500	0.570	0.422
M- [kNm]	5.55	40	11835	7732	21240	0.358	0.267
V [kN]	5.55	40	2240	1282	3187	0.413	0.287

Table 6.6 – Results of the longitudinal analysis using the live loads and the dead loads on Bridge 1

	Bridge 2 - left side (with lateral distribution of loads)						
	A [m^2]	L [m]	max(EC)	max(RSA)	max(dead loads)	EC/TOTAL	RSA/TOTAL
M+ [kNm]	4.735	31	7922	3416	5664	0.583	0.376
M- [kNm]	4.735	31	6567	3159	10821	0.378	0.226
V [kN]	4.735	31	1807	814	2141	0.458	0.275

Table 6.7 – Results of the longitudinal analysis using the live loads and the dead loads on Bridge 2

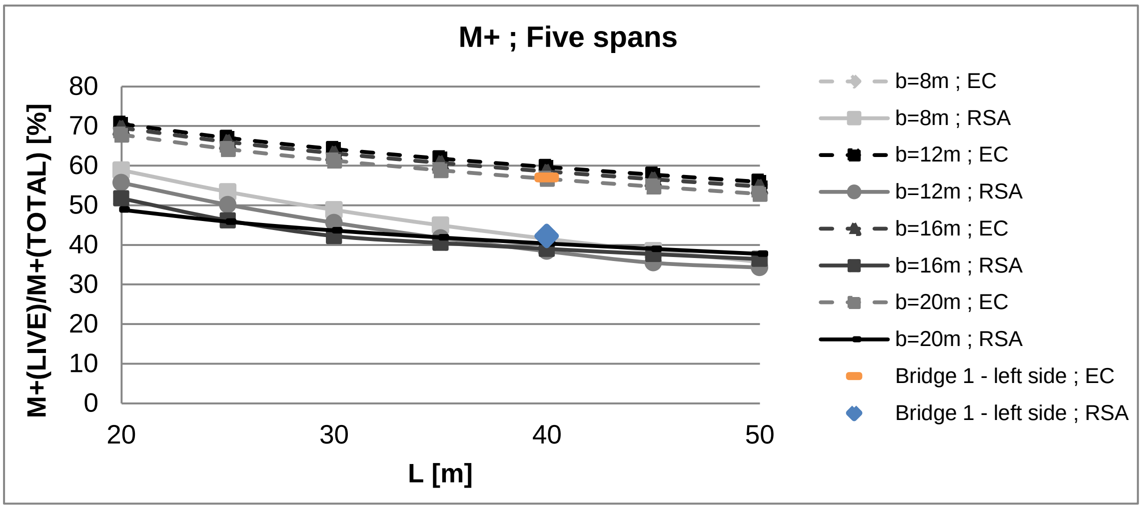

Figure 6.18 - Relation between the sagging moments M+ caused by the live loads and design loads on the most loaded beam of Bridge 1 and represented in the graph of Fig. 5.21

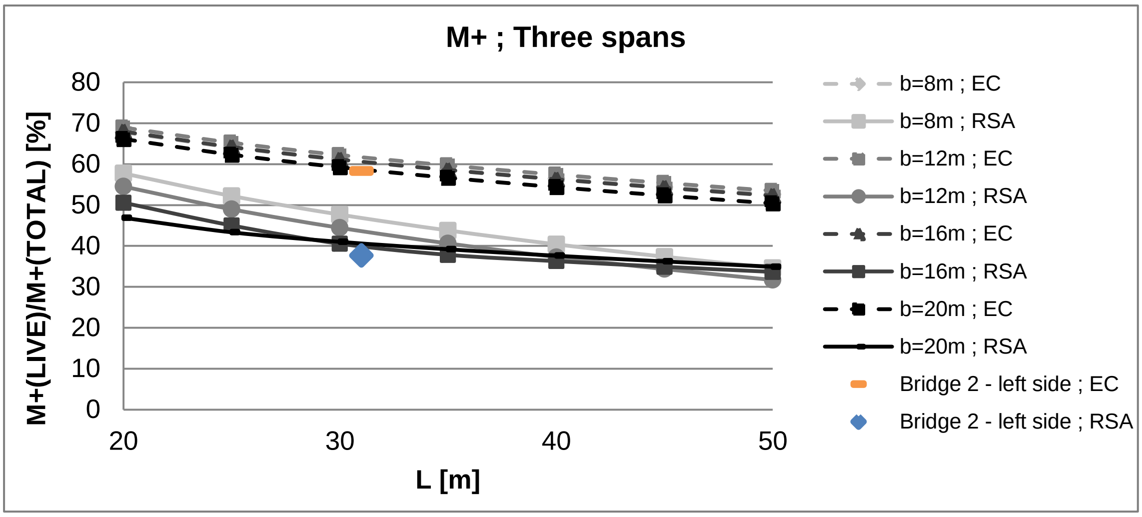

Figure 6.19 - Relation between the sagging moments M+ caused by the live loads and design loads on the most loaded beam of Bridge 2 and represented in the graph of Fig. 5.20

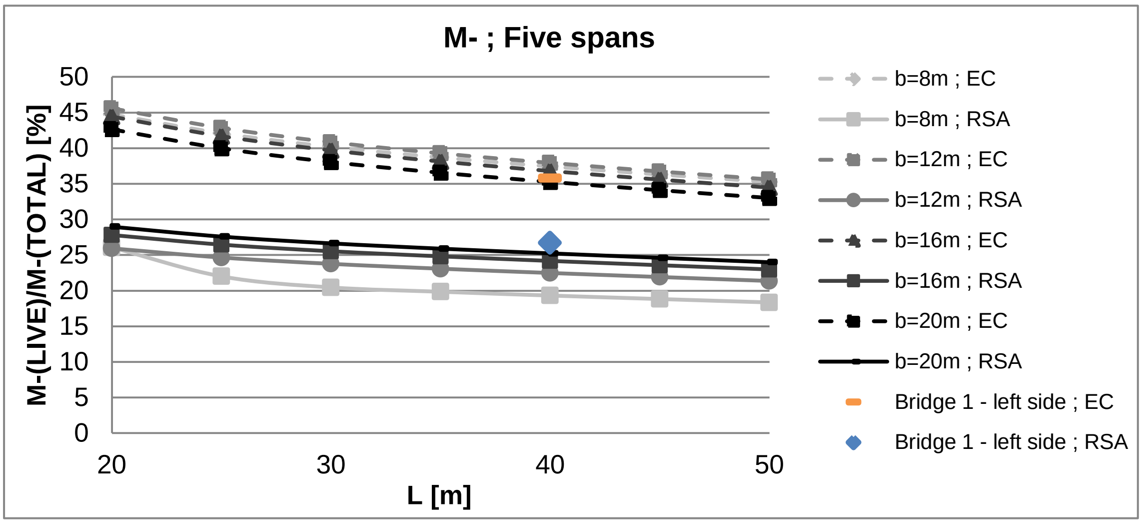

Figure 6.20 - Relation between the hogging moments M- caused by the live loads and design loads on the most loaded beam of Bridge 1 and represented in the graph of Fig. 5.24

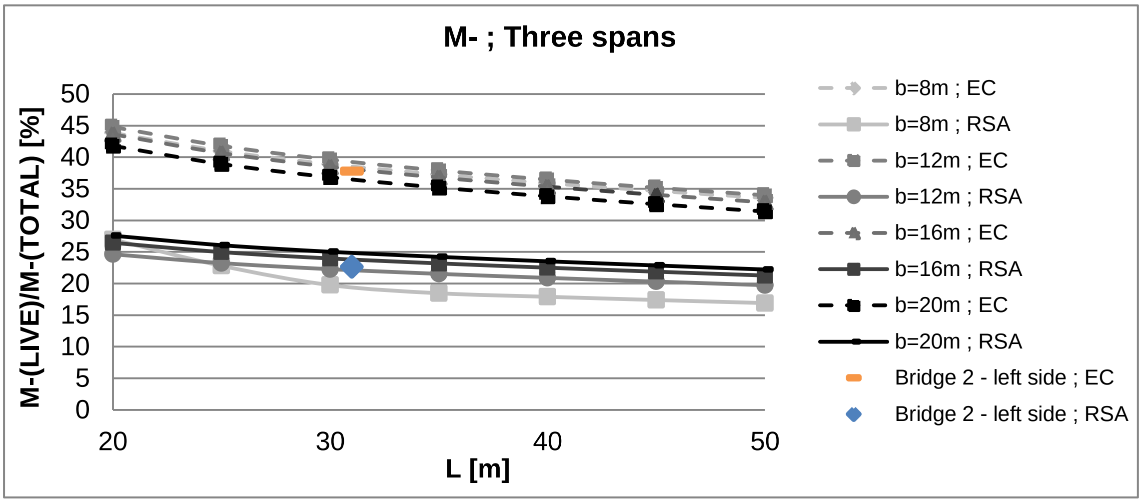

Figure 6.21 - Relation between the hogging moments M- caused by the live loads and design loads on the most loaded beam of Bridge 2 and represented in the graph of Fig. 5.23

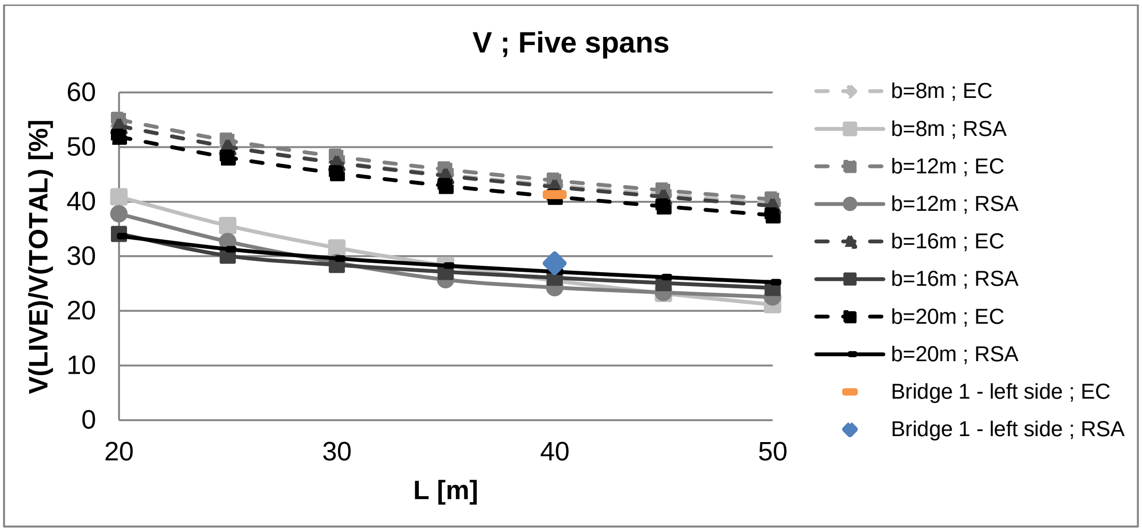

Figure 6.22 - Relation between the shear forces V caused by the live loads and design loads on the most loaded beam of Bridge 1 and represented in the graph of Fig. 5.28

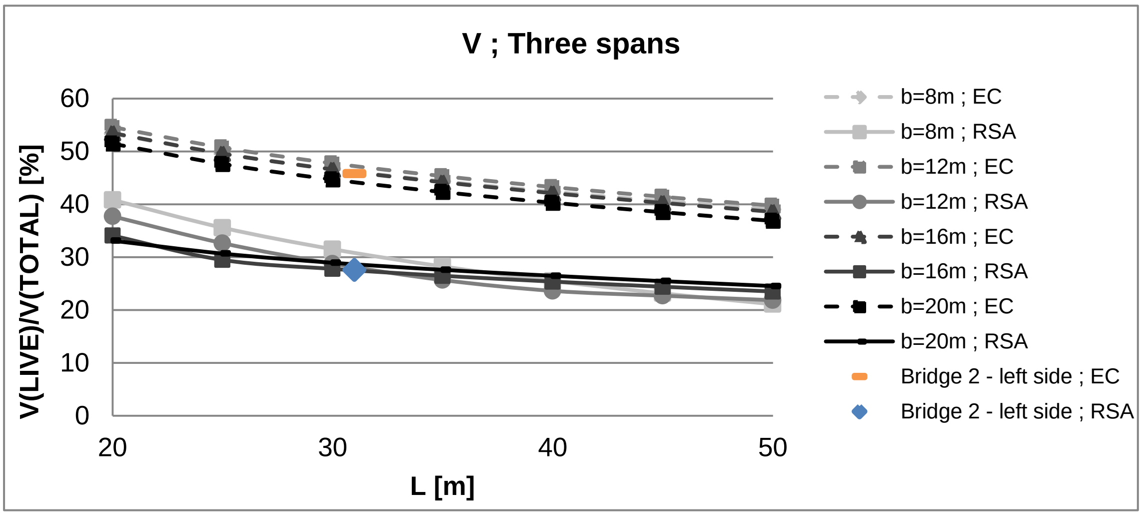

Figure 6.23 - Relation between the shear forces V caused by the live loads and design loads on the most loaded beam of Bridge 2 and represented in the graph of Fig. 5.27

It was verified that the results presented in Figures 6.15 to 6.20 allowed to obtain "good" results for both bridges analyzed and for each bridge internal force (M+, M- and V), even with the existence of some differences between the bridge models used to calibrate the presented graphs and the real cases.

It can therefore be concluded, based on the content of this chapter, that the results presented in Chapter 3 and 4 are sufficiently reliable to be applied, as an approximation, in a quick analysis of a wide range of bridges, in order to evaluate the differences in the structural response between the traffic actions of the RSA and the Eurocode Load Model 1.

CHAPTER 7

7. Conclusions and Future developments

7.1 Conclusions

The EN 1991-2 [2] establishes the new guidance towards the definition of loads to consider in bridge analysis and it will substitute the current Portuguese code (RSA) [3] in the near future.

This fact motivated a comparative evaluation between the results obtained from the application of both codes, which was performed for bridges with a slab-beam cross-section in a local and global context.

Regarding the local effects, the characteristics of the bridge deck cross-section were evaluated in Chapter 3 by using several transverse finite element analyses of the deck slab which allowed to conclude:

(i) The slab transverse bending moments over the longitudinal beams can be produced not only by loads acting on the overhangs but also by wheel and knife-edge loads acting on the internal panel;

(ii) For the evaluation of the transverse moments over the beams the wheel loads can be considered as point loads with sufficient accuracy;

(iii) The influence of the torsional and flexural stiffness of the longitudinal beams was neglected, being those considered with a null torsional stiffness and with an infinite flexural stiffness in all analyses performed;

(iv) Regarding the transverse moments due to cantilever loads, the influence of the relation between the cantilever span and the internal span is small for realistic deck dimensions, having been considered in the analyses a ratio $S_c/S = 0.5$. However, considerable differences were verified between the distributions obtained by considering the influence of the internal panel flexibility and by considering a full-fixed cantilever;

(v) Also for the transverse moments over the beams due to cantilever loads the existence of curbs and respective location were considered relevant, but for the moments due to internal panel loads the positioning of the curb was neglected;

(vi) Regarding the thickness variation of the internal slab in the form of brackets, the value of the variation t_1/t_3 was considered influent, although the size of the brackets was neglected, being always considered the ratio $c'/S = 0.2$;

(vii) The thickness variation of the cantilever slab t_1/t_2 was considered influent for the transverse moments over the beams due to both cantilever and internal panel loads;

(viii) In what concerns the transverse bending moments at the mid-span of the internal panel, Timoshenko's solution [4] (Eq. (3.15) and Eq. (3.16)) provided always conservative results. This method neglected the existence of overhangs, the presence of brackets on the internal panel and the torsional and flexural stiffness of the longitudinal beams. On the other hand it considered the influence of the internal span *S* and of the loads dimensions referred to the middle surface of the slab.

The transverse moments distribution curves due to cantilever loads were obtained in generic bridge deck models by using Bakht's methods presented in [10] and [14] and by using a finite element analysis. The results were compared and some differences for the cases when the load is closer to the clamped end of the overhang were verified.

In order to obtain the distribution curves for the transverse moments due to both cantilever and internal panel loads well-adjusted with the ones obtained by using a finite element analysis, two semi-analytical methods were developed in Chapter 3. The methods represented by Eq. (3.5) and by Eq. (3.17) consider a longitudinal distribution of an exponential type for the bending moments due to concentrated loads acting both on the overhangs and on the internal panel, respectively.

The influence of thickness variations of the cantilever slab, the existence of structural barriers (curbs) at the overhangs, the influence of the internal panel flexibility on the cantilever's supported edge, the load positioning and the existence of brackets in the internal panel were properly considered in the developed semi-analytical methods.

The methods consider four coefficients that were obtained from a set of non-linear equations that considered the solutions obtained by a finite element analysis (see Figures 3.21 and 3.57) in order to better adjust the transverse bending moments distributions.

In Chapter 4 the developed methods (Eq. (3.5) and Eq. (3.17)) and Timoshenko's solution [4] were used for a parametric analysis of bridges submitted to the loadings defined according with the Eurocode LM1 [2] and with the RSA [3]. The results obtained allow to conclude that the transverse moments obtained by applying the EN 1991-2 (LM1) are significantly higher than the moments due to the application of the RSA. In fact, the relation between the transverse moments $m_{y(RSA)}/m_{y(EC)}$ is within the range 0.4 – 0.6. If a "clamped cantilever model" is adopted for the evaluation of the moments due to the RSA, those increase and the ratio $m_{y(RSA)}/m_{y(EC)}$ takes values within the range 0.45 – 0.8.

It was also verified that with the introduction of brackets (thickness variation) in the internal panel the relation $m_{y(RSA)}/m_{y(EC)}$ decreases. This fact is due to the higher number of vehicles considered by the Eurocode LM1 in the internal panel, whose corresponding transverse moments over the beams are increased by the presence of brackets.

For the sagging transverse moments at the mid-span of the internal slab, evaluated by using Timoshenko's solution [4] (Eq. (3.15) and Eq. (3.16)), it was concluded that the moments due to the application of the RSA are about 40% to 50% of those due to the Eurocode LM1.

The evaluation of the internal forces due to the load definitions of EN 1991-2 [2] and RSA [3] in terms of the bridge longitudinal analysis was performed in Chapter 5.

The bridges structural systems were modeled by continuous beams for four sets of spans solutions: one, two, three and five spans (the case with one span was not considered for the hogging bending moments M-). The evaluation of the corresponding internal forces (bending moments and shear force) was made by considering the respective influence lines.

The results obtained allowed to conclude that the bridge internal forces increase significantly with the application of the Eurocode LM1 in comparison with the RSA. Generally, the internal forces obtained using the RSA correspond to 35% to 65% of the ones evaluated by considering the EN 1991-2.

The importance of the live loads, when compared with the dead loads, was evaluated inferring that traffic loads have more influence on the sagging bending moments and on the shear force than on the bending moments evaluated in the hogging region.

The analysis was performed for the loadings defined from both codes, being considered that:

(i) For the sagging maximum bending moments (M+), 35% to 70% of the total effects are due to the Eurocode LM1, while the RSA only represents between 20% and 60% of the moments produced.

(ii) Regarding the hogging maximum bending moments were verified values of the relation $M\text{-}_{(EC)}/M\text{-}_{(TOTAL)}$ between 27% and 45% were verified as well as values of $M\text{-}_{(RSA)}/M\text{-}_{(TOTAL)}$ between 15% and 30%.

(iii) In what concerns the maximum shear force (V), the Eurocode LM1 represents between 35% and 55% of the total effects while the relation $V_{(RSA)}/V_{(TOTAL)}$ has values within the range 18% - 40%.

In Chapter 6 two real bridges (Figures 6.1 and 6.2) were analyzed using the developed semi-analytical methods (Eq. (3.5) and Eq. (3.17)) and Timoshenko's solution (Eq. (3.15) and Eq. (3.16)) regarding the local effects and globally analyzed by using the respective influence lines adopted in Chapter 5, in order to verify the applicability by extrapolation of the results of the parametric analyses performed in Chapters 4 and 5.

Considering the results obtained for both real bridges and presented in Tables 6.2 to 6.7, it may be concluded that: (i) the methods adopted can be used towards an efficient evaluation of the internal forces due to any load model considering wheel and knife-edge loads and acting on slab-beam bridge decks with two longitudinal beams and (ii) the comparative values between the bridge deck internal forces due to the RSA and due to the Eurocode LM1, in a local and global analysis, can be easily extrapolated from the results graphically presented on Chapters 4 and 5 with a reasonable accuracy.

7.2 Future developments

Regarding possible developments of the work presented on this thesis, several issued can be approached:

(i) Since this work only focused on the transverse bending moments regarding the local analysis of the deck slab, the slab shear forces or even the longitudinal bending moments verified under the loads, both at the cantilever slab and at the mid-span of the internal panel could also be evaluated. This would represent a more complete local analysis of the deck slab, and therefore provide more information in what concerns the comparison between the Eurocode and the RSA.

(ii) The semi-analytical methods developed were calibrated by considering the most important parameters. However, these semi-analytical methods would provide better results with an extension of the tables containing the respective coefficients, or with the development of better adjusted interpolation formulas for these coefficients.

(iii) This work can also be used as reference for a comparison between other load codes besides the RSA and the EN 1991-2, since the semi-analytical methods developed in Chapter 3 can be applied to a wide range of two-beam bridge decks under wheel and knife-edge loads.

References

[1] C. O'Connor and P. Shaw, "Bridge Loads, an international perspective" (2000);

[2] CEN, "Eurocode 1: Actions on structures – Part 2: Traffic loads on bridges" (2003);

[3] "RSA - *Regulamento de Segurança e Acções para Estruturas de Edifícios e Pontes*", Diário da República, Portugal (1983);

[4] S. Timoshenko, "Theory of Plates and Shells", Second Edition (1959);

[5] Highways Agency, "Design Manual for Roads and Bridges", London (2006);

[6] Ontario Ministry of Transportation, "Ontario Highway Bridge Design Code" (1983);

[7] P. Cruz, "Inspecção, Diagnóstico, Conservação e Monitorização de pontes" (2006);

[8] M. Pipa, "Evolução da Regulamentação de Estruturas em Portugal", LNEC (2009);

[9] H. Westergaard, "Computation of stresses in bridge slabs due to wheel loads", Public Roads, 2(1), 1-23 (1930);

[10] A. Mufti, B. Bakht and L. Jaeger, "Moments in Deck Slabs Due to Cantilever Loads", Journal of Structural Engineering, Vol.119, No. 6 [ASCE], 1761-1777 (1993);

[11] F. Sawko and J. Mills, "Design of cantilever slabs for spine beam bridges. Developments in bridge design and construction", Proc. Cardiff Conf. Crosby Lockwood and Son Ltd., London, England (1971);

[12] B. Bakht and D. Holland, "A manual method for the elastic analysis of wide cantilever slabs of linearly varying thickness", Canadian Journal of Civil Engineering, 3(4), 523-530 (1976);

[13] W. Dilger, G. Tadros and J. Chebib, "Bending moments in cantilever slabs.", Developments in Short and Medium Span Bridges, Engineering'90, Vol. 1 [Canadian Society for Civil Engineers], 265-276 (1990);

[14] B. Bakht: "Simplified analysis of edge-stiffened cantilever slabs", Journal of the Structural Division, 103(3), 535-550 [ASCE] (1981);

[15] A. Pucher, "Influence Surfaces of Elastic Plates" (1964);

[16] E. Hambly, "Bridge Deck Behaviour", Second Edition (1991);

[17] A. Reis, "Dimensionamento de Estruturas", supporting document to the course "Design of Structures", IST (2001);

[18] A. Mufti, B. Bakht and L. Jaeger, Closure of "Moments in Deck Slabs Due to Cantilever Loads", Journal of Structural Engineering, Vol.120, No. 10 [ASCE], 3086-3088 (1994);

[19] A. Reis, "Pontes", supporting document to the course "Bridges", IST, Chapter 4, 32-39 (revision of 2006);

[20] F. Virtuoso, Personal notes (2012).

Annexes

Annex 1. Results provided by the semi-analytical method for cantilever loads (Eq. (3.5)) and by a finite element analysis

All the comparisons made between the results provided by the developed semi-analytical method for cantilever loads (Eq. (3.5)) and by a finite element analysis performed by using the software SAP2000® that are not represented in Chapter 3 are presented in this appendix.

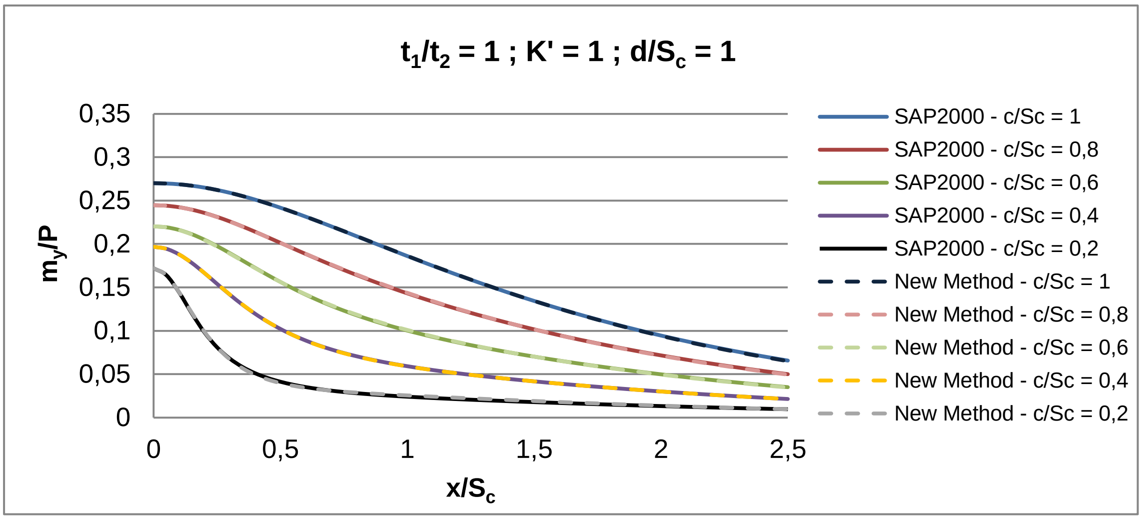

Figure A1.0.1 - Comparison between the results provided by the new semi-analytical method and by a finite element analysis for a cantilever with a ratio t_1/t_2 = 1, with a curb at d/S_c = 1 and with a factor K' = 1

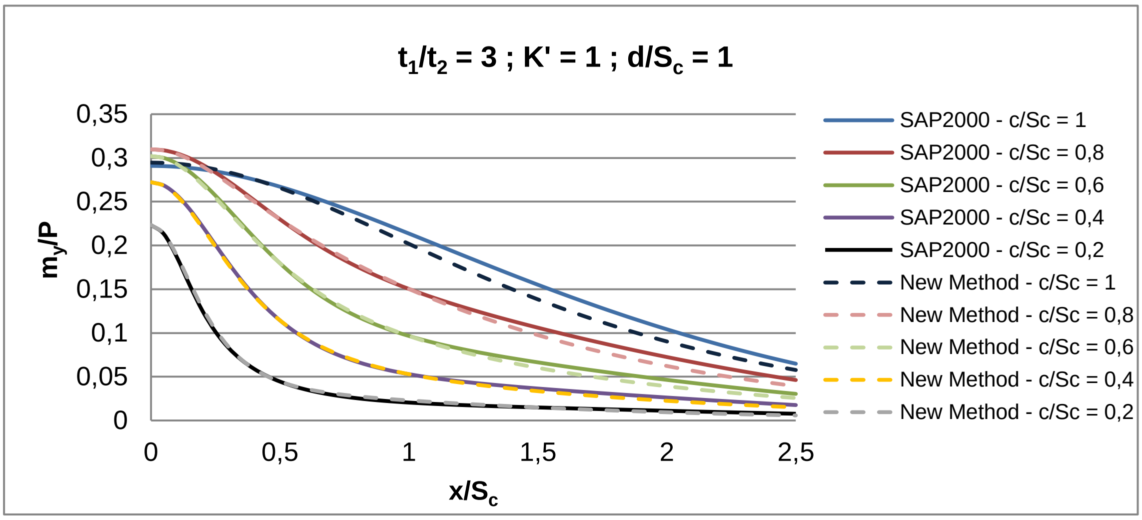

Figure A1.0.2 - Comparison between the results provided by the new semi-analytical method and by a finite element analysis for a cantilever with a ratio t_1/t_2 = 3, with a curb at d/S_c = 1 and with a factor K' = 1

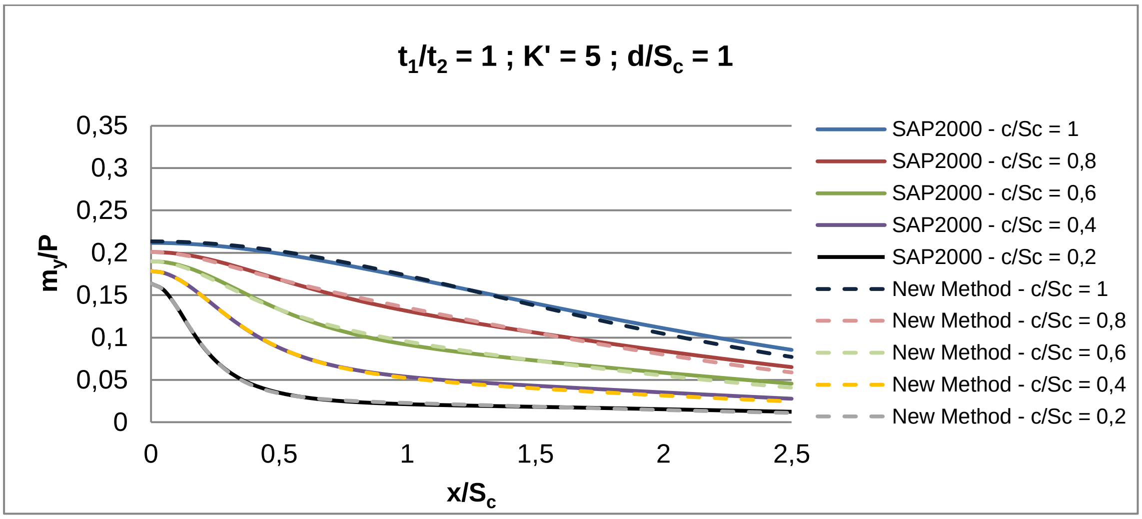

Figure A1.0.3 - Comparison between the results provided by the new semi-analytical method and by a finite element analysis for a cantilever with a ratio t_1/t_2 = 1, with a curb at d/S_c = 1 and with a factor K' = 5

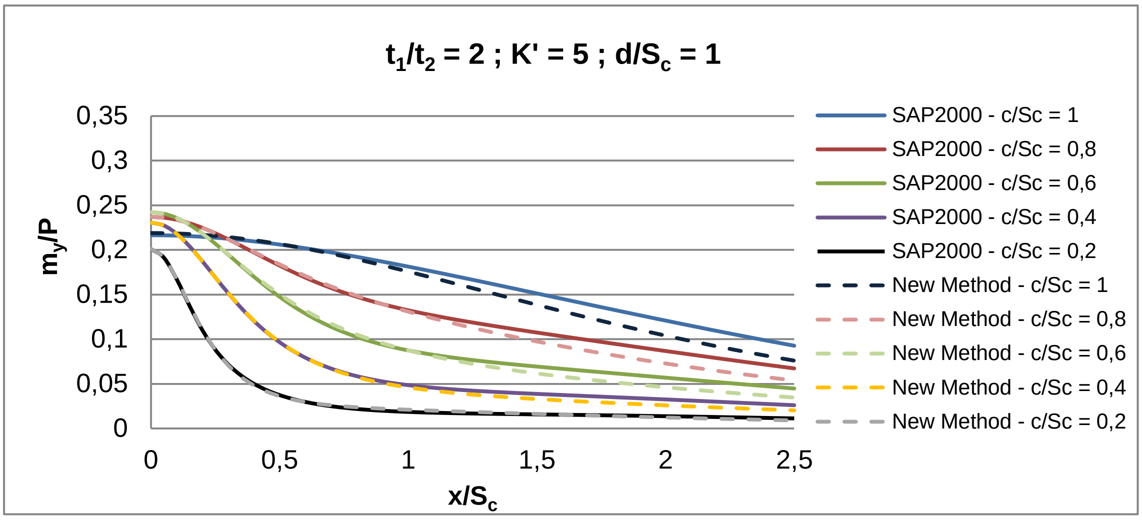

Figure A1.0.4 - Comparison between the results provided by the new semi-analytical method and by a finite element analysis for a cantilever with a ratio t_1/t_2 = 2, with a curb at d/S_c = 1 and with a factor K' = 5

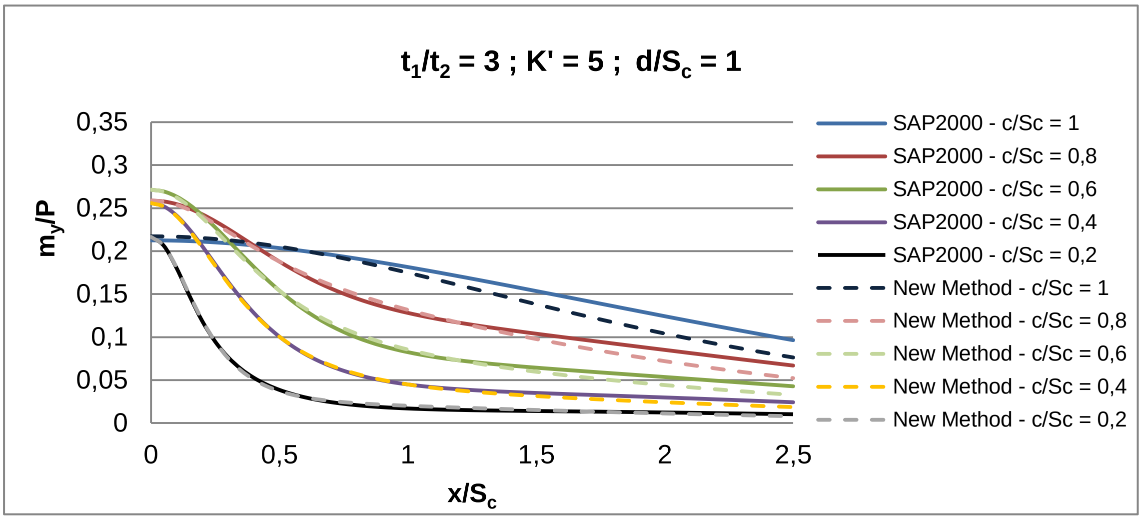

Figure A1.0.5 - Comparison between the results provided by the new semi-analytical method and by a finite element analysis for a cantilever with a ratio t_1/t_2 = 3, with a curb at d/S_c = 1 and with a factor K' = 5

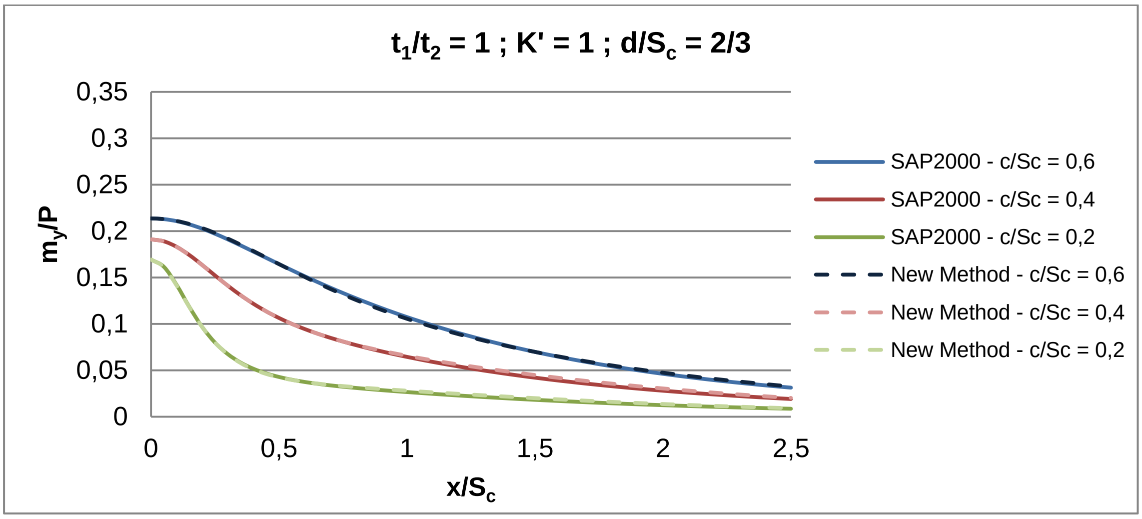

Figure A1.0.6 - Comparison between the results provided by the new semi-analytical method and by a finite element analysis for a cantilever with a ratio t_1/t_2 = 1, with a curb at d/S_c = 2/3 and with a factor K' = 1

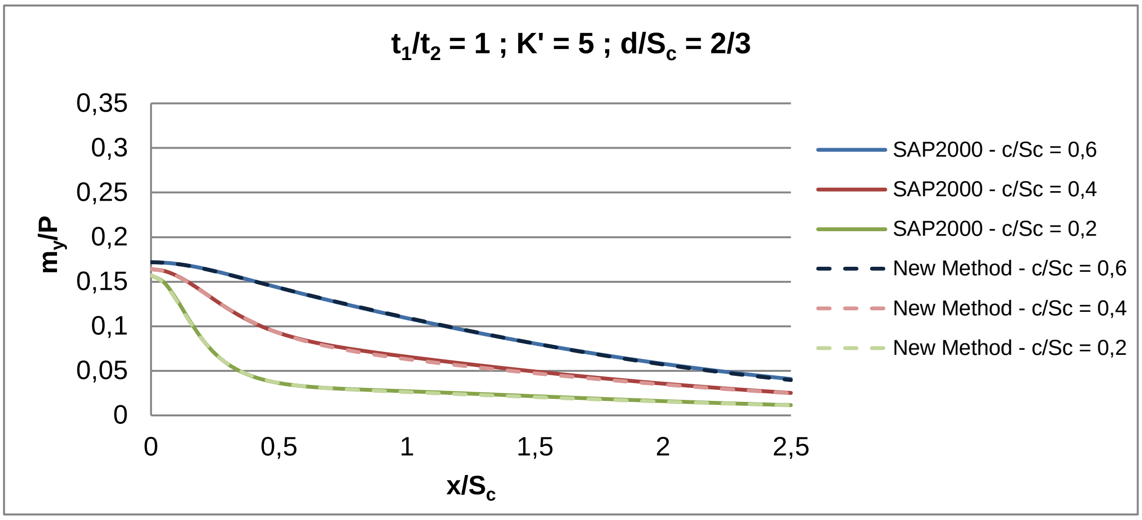

Figure A1.0.7 - Comparison between the results provided by the new semi-analytical method and by a finite element analysis for a cantilever with a ratio t_1/t_2 = 1, with a curb at d/S_c = 2/3 and with a factor K' = 5

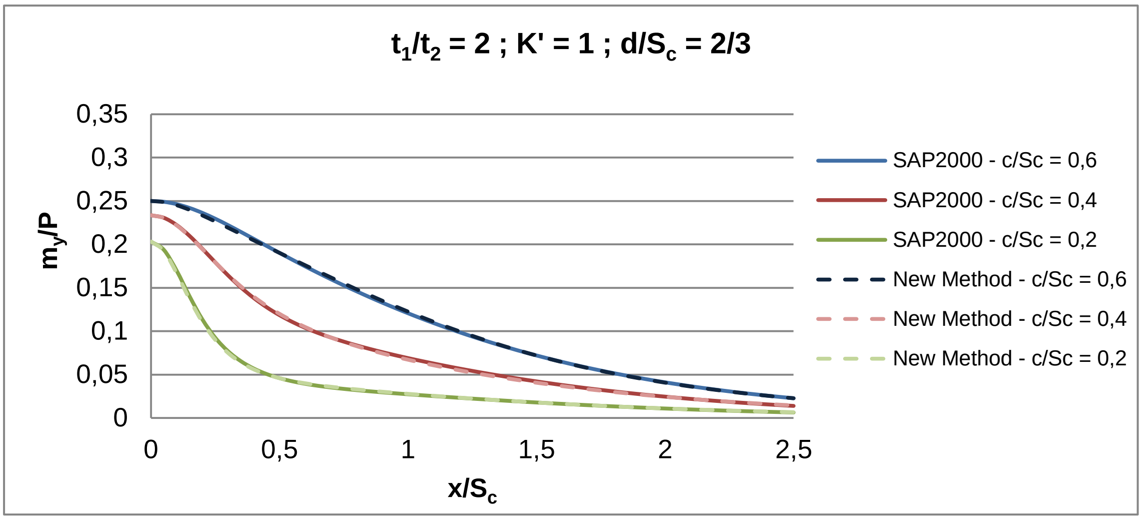

Figure A1.0.8 - Comparison between the results provided by the new semi-analytical method and by a finite element analysis for a cantilever with a ratio t_1/t_2 = 2, with a curb at d/S_c = 2/3 and with a factor K' = 1

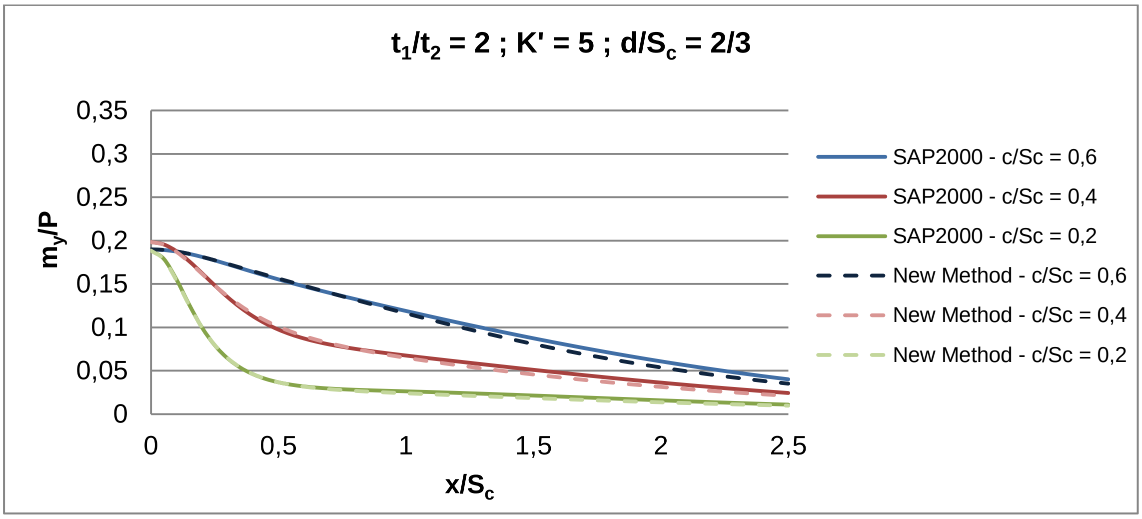

Figure A1.0.9 - Comparison between the results provided by the new semi-analytical method and by a finite element analysis for a cantilever with a ratio t_1/t_2 = 2, with a curb at d/S_c = 2/3 and with a factor K' = 5

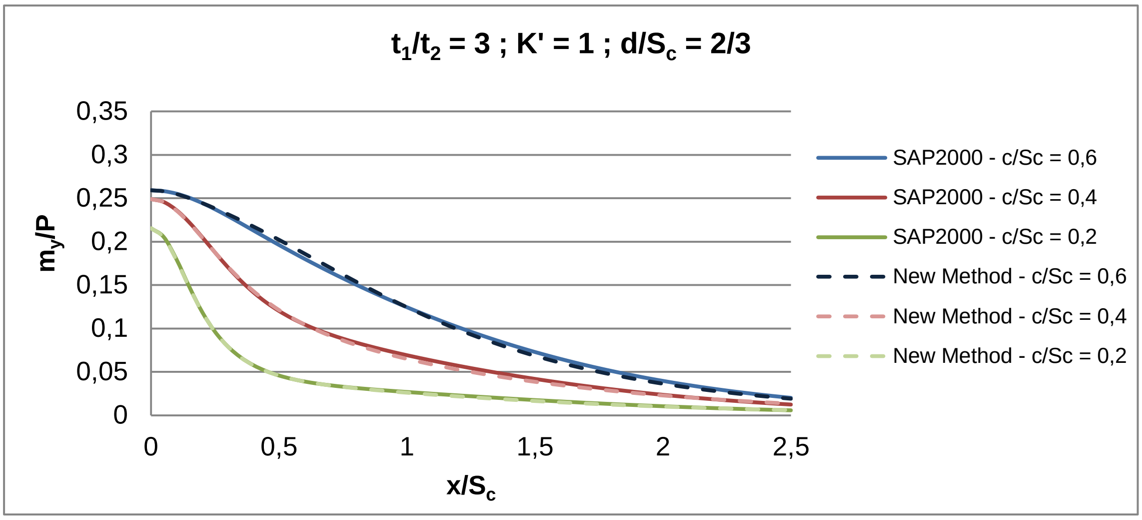

Figure A1.0.10 - Comparison between the results provided by the new semi-analytical method and by a finite element analysis for a cantilever with a ratio t_1/t_2 = 3, with a curb at d/S_c = 2/3 and with a factor K' = 1

Annex 2. Results provided by the semi-analytical method for internal panel loads (Eq. (3.17)) and by a finite element analysis

All the comparisons made between the results provided by the developed semi-analytical method for internal panel loads (Eq. (3.17)) and by a finite element analysis performed by using the software SAP2000® that are not represented in Chapter 3 are presented in this appendix.

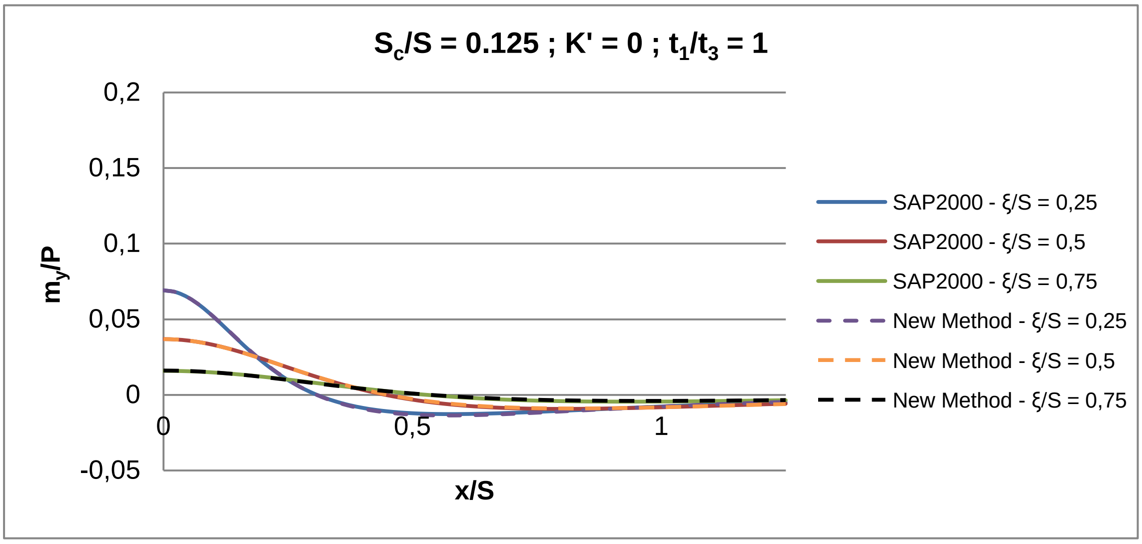

Figure A2.0.11 - Comparison between the results provided by the semi-analytical method and by a finite element analysis for a deck without edge-stiffening considering a ratio S_c/S = 0.125 and a ratio t_1/t_3 = 1

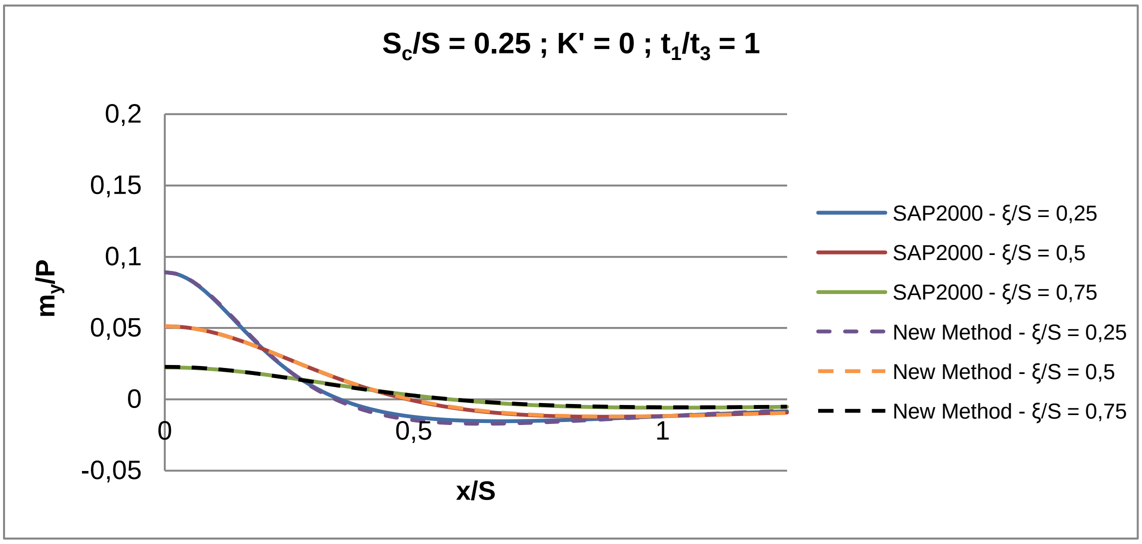

Figure A2.0.12 - Comparison between the results provided by the semi-analytical method and by a finite element analysis for a deck without edge-stiffening considering a ratio S_c/S = 0.25 and a ratio t_1/t_3 = 1

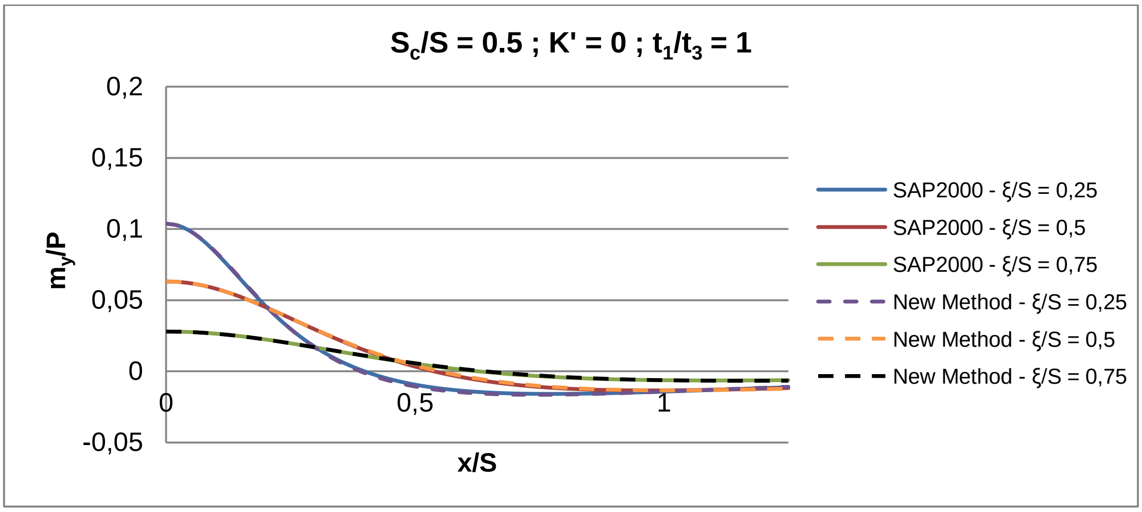

Figure A2.0.13 - Comparison between the results provided by the semi-analytical method and by a finite element analysis for a deck without edge-stiffening considering a ratio $S_c/S = 0.5$ and a ratio $t_1/t_3 = 1$

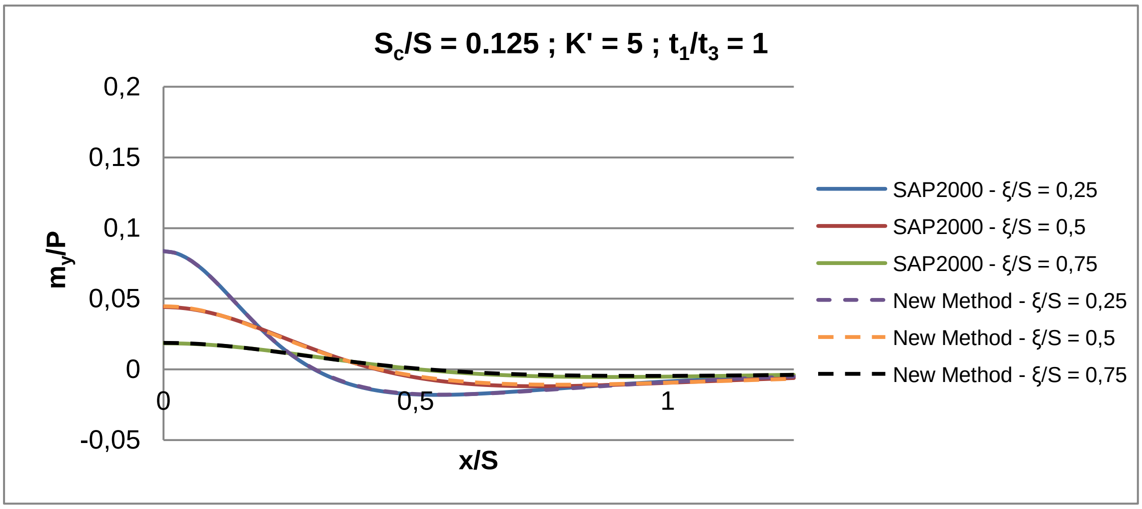

Figure A2.0.14 - Comparison between the results provided by the semi-analytical method and by a finite element analysis for a deck with edge-stiffening (K' = 5) considering a ratio $S_c/S = 0.125$ and a ratio $t_1/t_3 = 1$

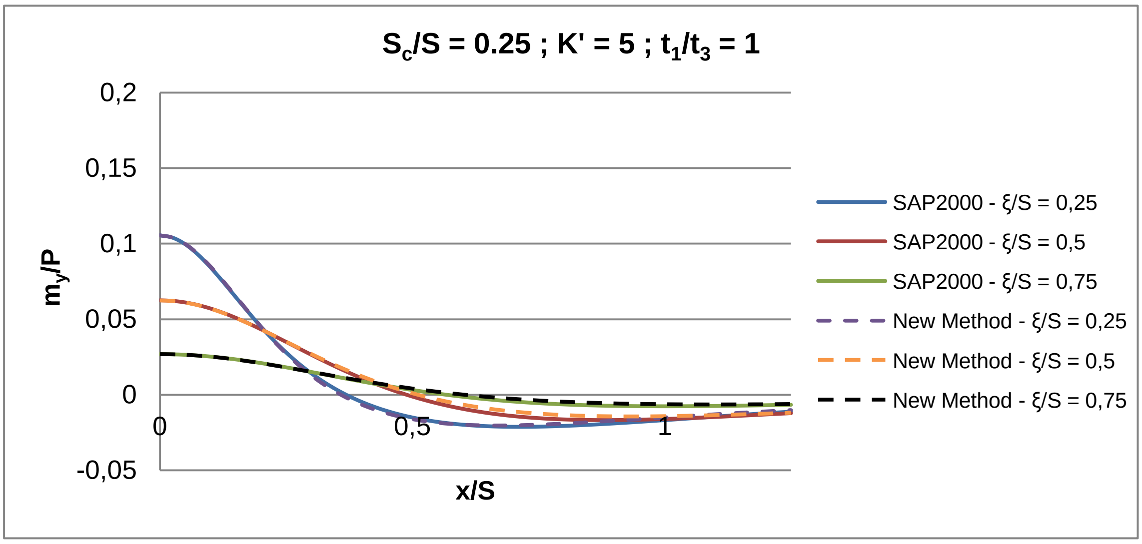

Figure A2.0.15 - Comparison between the results provided by the semi-analytical method and by a finite element analysis for a deck with edge-stiffening (K' = 5) considering a ratio $S_c/S = 0.25$ and a ratio $t_1/t_3 = 1$

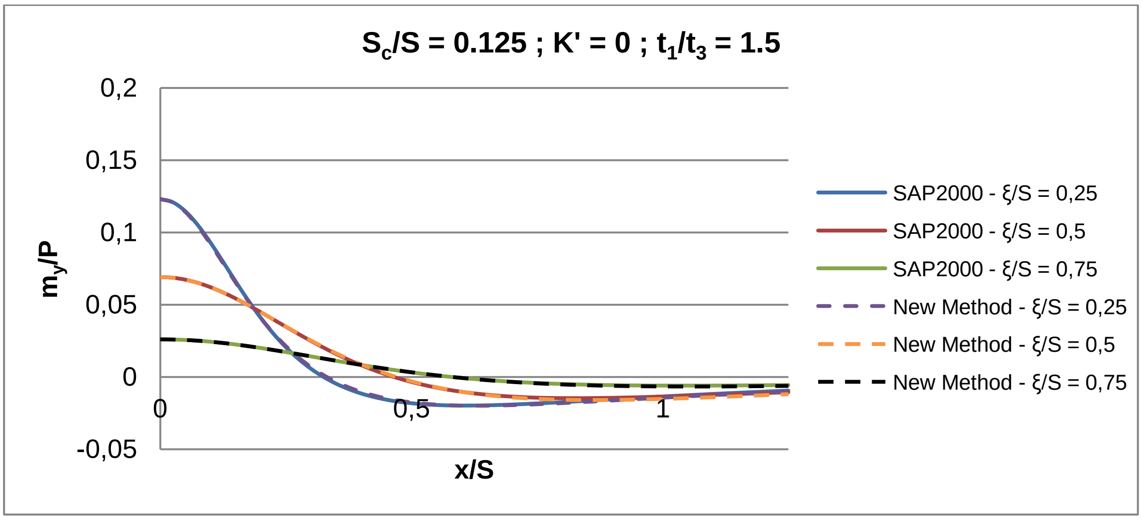

Figure A2.0.16 - Comparison between the results provided by the semi-analytical method and by a finite element analysis for a deck without edge-stiffening considering a ratio $S_c/S = 0.125$ and a ratio $t_1/t_3 = 1.5$

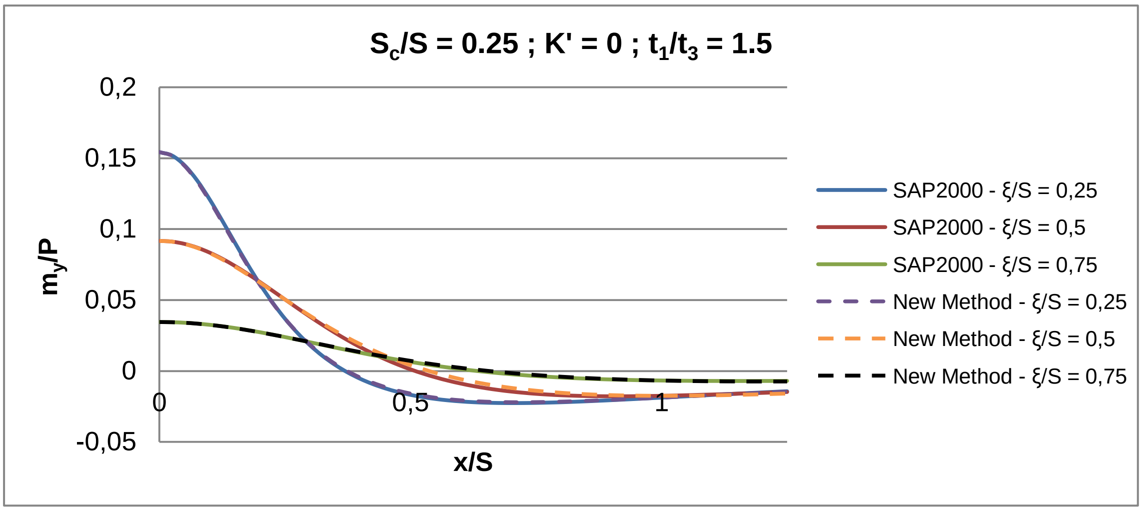

Figure A2.0.17 - Comparison between the results provided by the semi-analytical method and by a finite element analysis for a deck without edge-stiffening considering a ratio $S_c/S = 0.25$ and a ratio $t_1/t_3 = 1.5$

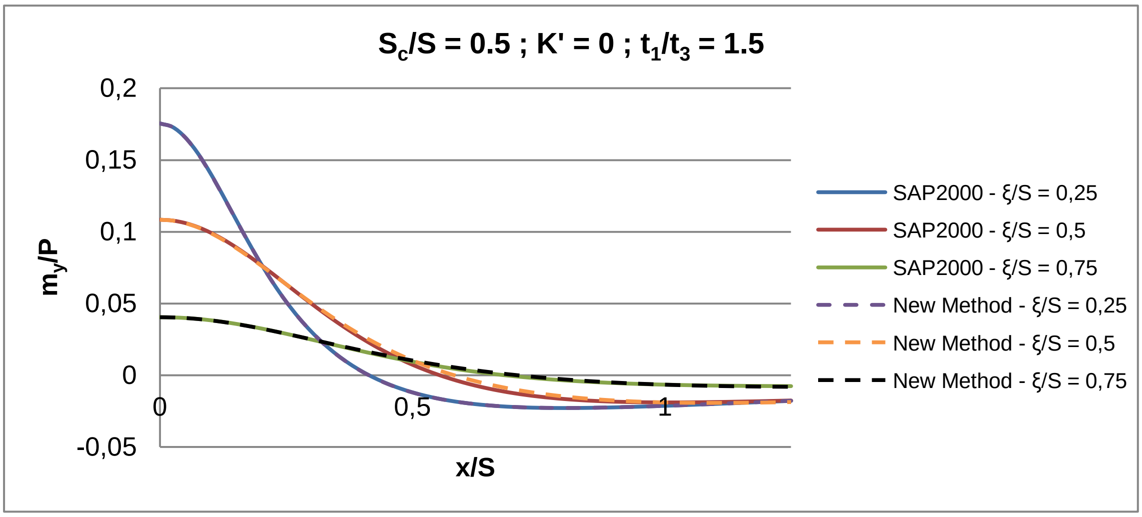

Figure A2.0.18 - Comparison between the results provided by the semi-analytical method and by a finite element analysis for a deck without edge-stiffening considering a ratio $S_c/S = 0.5$ and a ratio $t_1/t_3 = 1.5$

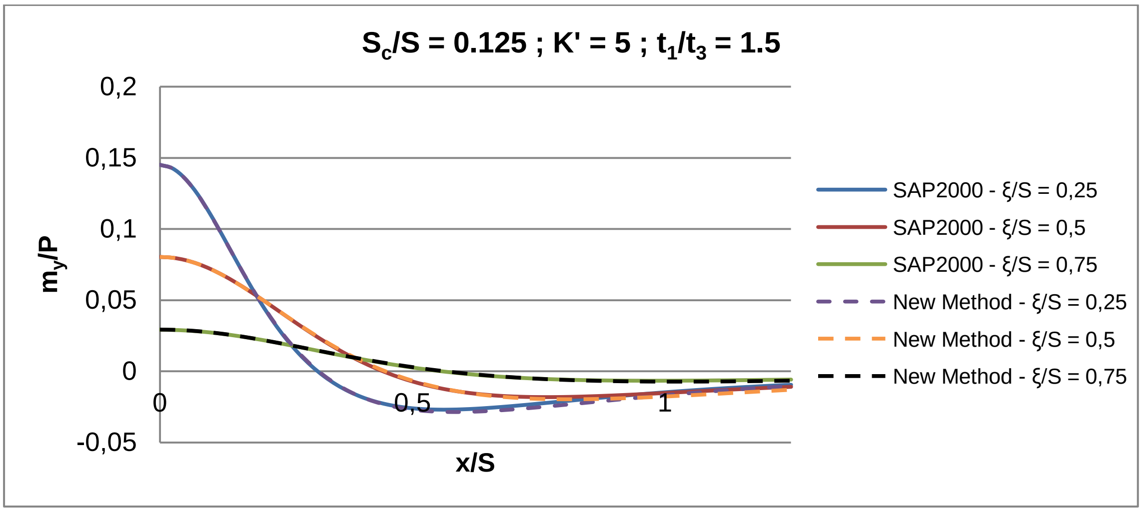

Figure A2.0.19 - Comparison between the results provided by the semi-analytical method and by a finite element analysis for a deck with edge-stiffening (K' = 5) considering a ratio $S_c/S = 0.125$ and a ratio $t_1/t_3 = 1.5$

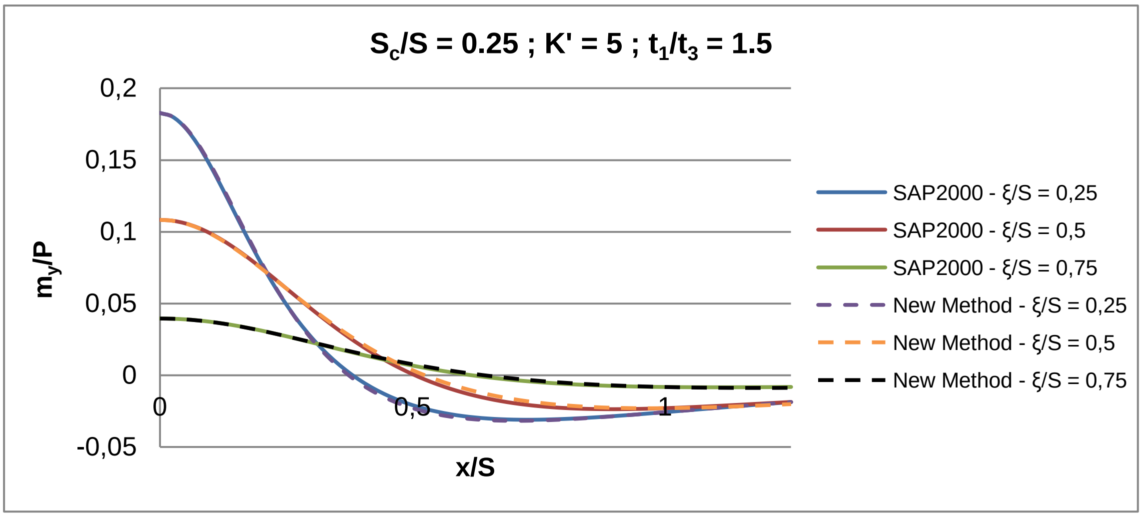

Figure A2.0.20 - Comparison between the results provided by the semi-analytical method and by a finite element analysis for a deck with edge-stiffening (K' = 5) considering a ratio $S_c/S = 0.25$ and a ratio $t_1/t_3 = 1.5$

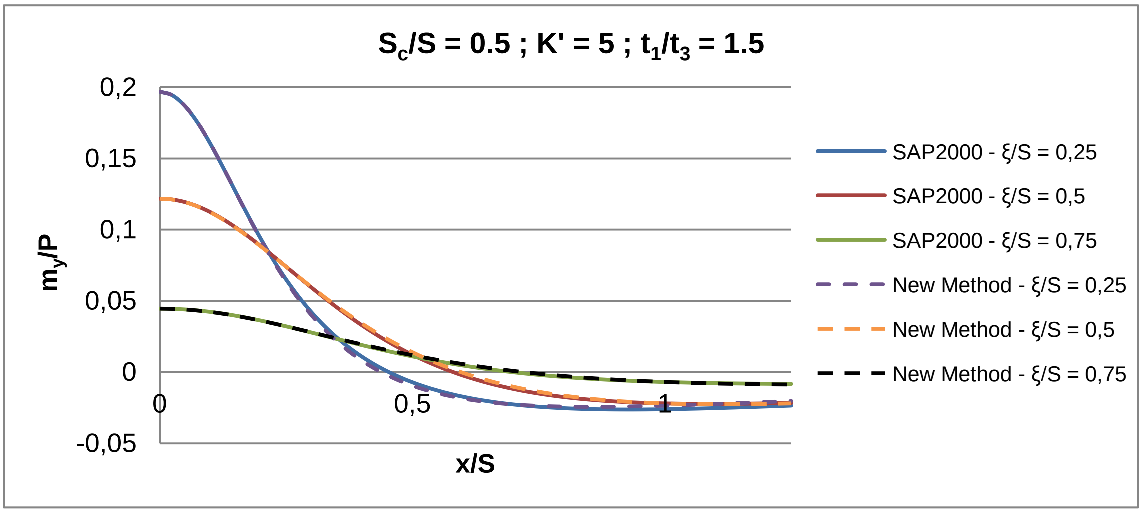

Figure A2.0.21 - Comparison between the results provided by the semi-analytical method and by a finite element analysis for a deck with edge-stiffening (K' = 5) considering a ratio $S_c/S = 0.5$ and a ratio $t_1/t_3 = 1.5$